PREDICTION OF LINEAR VISCOELASTIC RESPONSE OF THE LOSS SHEAR MODULUS OF POLYMER-MODIFIED BINDERS

James W. Bryant, Jr.

Thesis submitted to the faculty of Virginia Polytechnic Institute and State University in partial fulfillment of the requirements for

Master's Degree in Civil Engineering

(Civil Infrastructure Engineering)

Imad L. Al-Qadi, Chair

Toni Triani

Gerardo Flintsch

March 19, 1999
Blacksburg, Virginia

Keywords: polymer modified asphalt, shear modulus, viscoelasticity

PREDICTION OF LINEAR VISCOELASTIC RESPONSE OF THE LOSS SHEAR MODULUS OF POLYMER-MODIFIED BINDERS

by

James W. Bryant, Jr.

Abstract

Current mathematical models, developed on straight asphalt binders, are inadequate to characterize the frequency dependence of response of polymer-modified asphalt binders. In an earlier study at Virginia Tech, mathematical models were developed to predict the storage and loss shear moduli of polymer-modified binders. However the model developed for the loss shear moduli is limited at high frequency ($G'' \leq 10^{7.5}$ Pa). This thesis presents a statistical modeling of loss shear modulus of polymer (random copolymers and thermoplastic block copolymers) modified binder. Data from dynamic mechanical analysis on modified binders, at temperatures between 5 and 75°C and frequencies ranging from 0.06 to 0188.5 rad/s, were reduced to dynamic master curves of moduli, and used to develop the model. Twenty-one polymer-binder blends prepared and tested earlier at Virginia Tech where included in the study. Realistic characterization of loss shear moduli values was obtained using the Gompertz statistical model. The model was validated by using mean square error of prediction (MSEP) in which a second set of frequency data was input in the model to obtain the moduli values, which were compared to the measured data of the second set. Although this model was successfully tested for shear loss modulus prediction of polymer-modified binders, caution should be exercised when it is applied, as such a model should be able to predict the storage modulus for a known phase angle.

Acknowledgments

I thank GOD for leading me to Virginia Tech for graduate school. I am extremely grateful to Dr. Al-Qadi, who gave me the opportunity to work on this project. I would like to thank the other committee members, Dr. Triani and Dr. Flintsch , for their comments and support.

I would like to thank Fariborz Gahvari, a former graduate student, for the original work on which this research is built upon.

Finally I would like to thank my family and my church for their support throughout this process.

TABLE OF CONTENTS

LIST OF FIGURES

LIST OF TABLES

Chapter 1. Introduction

1.1 Background

The ability of our nation's infrastructure to provide necessities such as shelter, transportation, water and waste disposal, is vital to our quality of life. Highways play a major role in our infrastructure system. Over 94% of the surfaced roads in the United States are covered with flexible pavement (FHWA, 1990), hot-mix asphalt(HMA). Part of the flexible pavement highways fail prematurely due to increases in traffic, axle load and higher tire pressure. The volume of truck traffic doubled from 1974 to 1989 (Nahas, *et al.*, 1989). It is estimated that nearly 50% of all funds spent in the transportation area go directly to construction, maintenance and rehabilitation of pavements (Lytton, 1991).

Hot-mix asphalt (HMA) is composed of both mineral aggregate and asphalt binder. Although its performance is a function of both materials, the binder controls specific failure modes, including fatigue cracking and low temperature cracking. The performance of the binder, which is a viscoelastic material, is highly influenced by temperature and rate of loading (Lewandowski, 1994).

There are three main types of distress that flexible pavement surfaces undergo: (1) high temperature permanent deformation; (2) load-associated fatigue cracking; and (3) low temperature cracking. The binder properties play a significant role in each type of distress. Types of permanent deformation include rutting, distortion, and shoving. The progressive movement of HMA materials under repeated loads causes rutting. It usually occurs along the wheel path in the traffic direction. An asphalt binder that has a low viscosity at intermediate to high temperatures is more likely to rut because of its inability to respond elastically to the applied stresses. Fatigue (or alligator) cracking is caused by cyclic stress on a pavement over an extended period of time. Stiff binder and/or low

binder content also cause this type of distress. Low temperature cracking occurs when the binder becomes too brittle and it looses the ability to deform elastically.

The behavior of asphalt binder is complicated, because it is a viscoelastic material. At intermediate to high temperatures, asphalt behaves like a viscous fluid, while at low temperatures, it acts like a brittle elastic solid. A new and more complex material is formed when polymeric modifiers are added to asphalt binder.

In an effort to improve flexible pavement durability, different types of asphalt additives have been investigated. Modifications of asphalt binders using various types of polymeric materials have been promoted as an attractive technique to improve binder properties and the overall performance of flexible pavements (Lewandowski, 1994; Bonemazzi *et al*., 1996; Fleckenstein *et al*., 1992).

One researcher suggests that there are at least 22 benefits attributed to the addition of polymers to asphalt binder (Lewandowski, 1994). It has been suggested that the use of polymer additives in HMA reduces rutting and fatigue cracking, while maintaining an acceptable binder viscosity at medium to high service temperatures (Bonemazzi *et al*., 1996). In addition to being less susceptible to low temperature cracking, polymer modified asphalts are also more resistant to freeze thaw damage (Fleckenstein *et al*., 1992).

There is no consensus among researchers on the effectiveness of polymer modification on the performance of asphalt binder. A number of investigators agree that significant improvement in the resistance to permanent deformation is obtained when polymer modified binders are used in flexible pavements (Fleckenstein *et* al., 1992; Srivastave *et al*., 1992; Little, 1992; Collins *et al*., 1992; Ponniah *et al*., 1996; Maccarrone *et al*., 1997). Polymer modifiers have also been found to increase the fatigue life of flexible pavements (Maccarrone *et al*., 1997). However, there is discussion on the effectiveness of polymer additives as it pertains to improved low temperature properties. Some researchers find polymeric modification of asphalt binder beneficial (King *et al*.,

1993; Stock *et al.*1992), while others state its effect to be negligible (Anderson *et al.*, 1992; Bonemazzi *et al.*, 1996; Gahvari 1995; Freeman *et al.*, 1997).

1.2 Problem Statement

Characterizing the viscoelastic behavior of asphalt binder requires obtaining the response of the material over a wide range of temperatures and frequencies (i.e., loading time). Several researchers have produced models that mathematically describe the temperature and the time dependency of straight asphalt binders (Jongepier and Kuilman, 1969; Dobson, 1969; Dickinson and Witt, 1974; Christensen and Anderson, 1992; Stastna *et al.*, 1996). These models were not developed for predicting the viscoelastic response of modified binders; consequently, they have been found to produce considerable discrepancies with experimental data (Gahvari, 1995). Few researchers have proposed mathematical describing the response of polymer-modified binder (Gahvari, 1995; Stastna *et al.*, 1996, Marasteanu and Anderson, 1999).

The model presented by Gahvari is the most practical model proposed to date. However, there are certain limitations inherent in each model. The proposed model for storage modulus is valid only for moduli below 10^8 Pa; above this value, the moduli tend to be overestimated. The proposed loss modulus model is symmetrical in shape with respect to the peak point and therefore must be restricted to a specified range (Gahvari, 1995).

1.3 Objectives

The objective of this study was to develop a model to describe the frequency dependence of the response of polymer modified binders, over the entire range of temperatures and frequencies. The developed model was compared to the data collected from previous experiments at conducted Virginia Tech.

1.4 Scope

Characterization of the linear viscoelastic response of the polymer-modified binder is generally made possible by interpretation of dynamic master curves. At Virginia Tech, experimental research was conducted to characterize the complex moduli of polymer modified asphalt binders using a Dynamic Shear Rheomoter. Dynamic mechanical analysis was conducted on 21 binder-polymer blends at frequencies between 0.06 to 188.5 rad/s and temperatures ranging from 5° to 75°C. The mixes were prepared using one viscosity graded binder and seven different polymer modifiers. Each polymeric additive was blended with asphalt binder at three different concentration levels. The modifiers were thermoplastic block copolymers and random copolymers, which are commonly used in industry. The polymers selected represented a wide range of chemical structures and mechanical and physical properties. The study also investigated the effect of short term aging on rheological properties of the modified blends.

The linear viscoelastic range of response was established by performing stress sweeps over the entire range of temperatures at the desired frequencies. Isothermal graphs of dynamic moduli data verses frequency were obtained as a result of frequency sweeps. Master curves were developed for the dynamic moduli over several decades of reduced frequency by the application of time-temperature superposition. These master curves were used in order to characterize the response of the material. Two mathematical models were proposed to discuss the frequency dependence of the response and presented in earlier studies (Gahvari, 1995; Gahvari and Al-Qadi, 1996).

Using the collected isothermal data, time superposition has been employed to reconstruct the dynamic master curves of all 21 polymer-binder blends (using seven polymers, each at three levels of concentration). The shifted moduli data was used to derive model constants by use of nonlinear regression analysis.

Statistical analysis was performed comparing experimental data against data generated by the suggested model to determine its' level of accuracy. In addition, the

model accuracy was compared to that of the previous model developed during the original Virginia Tech Experiment.

This thesis contains Five chapters. Chapter 2 is an overview of binder types, rheological properties, polymeric modifiers, linear viscoelastic theory, time-temperature superposition, and current research on the modeling of straight and modified binders. Chapter 3 presents the research program including the materials and specimen preparation, data collection and previous analyses. Chapter 4 describes the model development, where a new statistical model is introduced to describe the frequency dependency of the loss shear modulus and the evaluation and validation of the suggested model. Chapter 5 presents the summary, findings and conclusions, as well as recommendations for future research.

Chapter 2. Literature Review

2.1 Introduction

Asphalt binder is one of the oldest engineering materials used by man. The waterproofing and adhesive qualities of asphalt make it suitable for use as roofing and paving materials. The first use of asphalt as a paving material occurred during the 1800's. Hot-mix asphalt (HMA) is a composite mixture consisting of a number of interfaces and phases, and is used to construct flexible pavements. Asphalt binder is a viscoelastic material; therefore, at high temperatures it behaves like a viscous fluid and at low temperature it behaves like an elastic solid. Therefore, behavior of HMA is highly dependent on the binder properties as temperature and rate of loading are varied.

Modifiers, such as polymers, are added to asphalt binder to enhance its properties. The result of this modification increases the complexity of the material structure. Since the binder plays such an important role in the behavior of HMA, it is imperative to understand the behavior of asphalt binder, its components and their interaction. This chapter provides an overview of the nature of asphalt binder, the tests used to characterize it, types of polymers used in asphalt binder, asphalt-polymer interaction, linear viscoelastic theory, and current research on straight and polymer-modified binder characterization.

2.2 Asphalt Cement Types and Properties

The composition of asphalt binder is very diverse. It is composed of nonpolar saturated hydrocarbons and polar aromatic molecules (heteroatoms). Small amounts of heavy metals are also found in asphalt binder (Table 2-1)

Table 2-1. Elemental Analyses of Representative Petroleum Binders (After Roberts, *et al.*, 1996).

Composition (%)				
Element	**Mexican**	**Arkansas-Louisiana**	**Boscan**	**California**
Carbon	83.77	85.78	82.90	86.77
Hydrogen	9.91	10.19	10.45	10.93
Nitrogen	0.28	0.26	0.78	1.10
Sulfur	5.25	3.41	5.43	0.99
Oxygen	0.77	0.36	0.29	0.20
Vanadium (ppm)	180	7	1380	4
Nickel (ppm)	22	0.4	109	6

The chemical composition and binder morphology influence the rheological properties of asphalt binder, which in turn affects the pavement performance. The current asphalt morphological model divides the many different asphalt molecules into two classes: polar and non-polar. The polar molecules associate through hydrogen bonding, forming a weak network within the non-polar medium. The weak network of hydrogen bonds dissociate under increased heat or loading. The non-polar molecules act as the matrix for the polar network and predominately affect the low temperature stiffness (Mckay *et al.*, 1995).

Three integrated phases or fractions are used in order to characterize asphalt: (1) asphaltenes; (2) resins; and (3) oils. Asphaltenes, the primary component of asphalt, are multi-ring, polar, aromatic compounds that give asphalt its structure. They are surrounded by moderately polar aromatic molecules and dispersed in the continuous non-

polar oily phase. Resins are intermediate molecular weight materials that contain more side chains than asphaltenes. They are semi-solid fractions that act as peptizing agents, which keep the asphaltene molecules from coagulation (Kerbs and Walker, 1971). Oils yield asphaltene and resin molecules upon oxidation. They are soluble in most solvents and have both paraffinic and naphthenic structures.

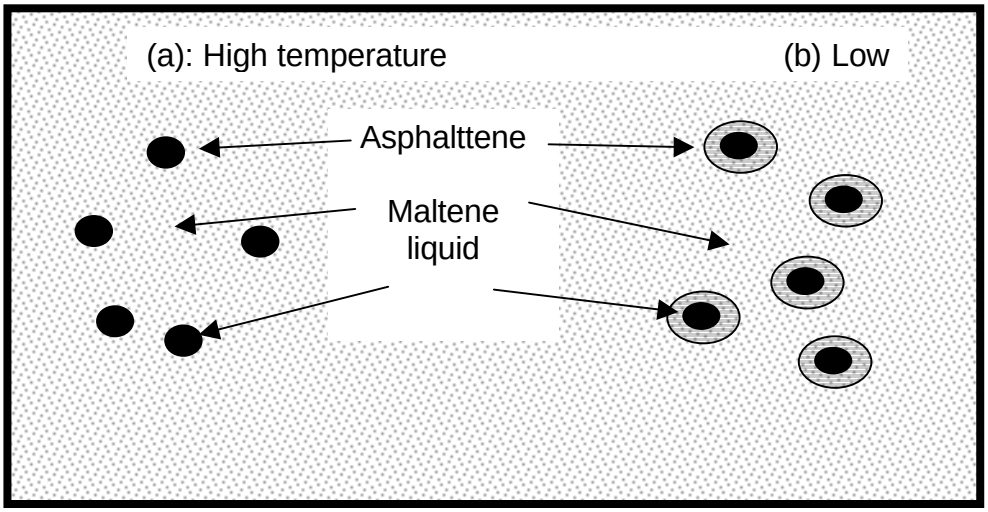

Figure 2-1. Current morphological model for asphalt binder.

The physical properties of asphalt binder are a function of the relative proportion of the integrated fractions: asphaltenes, resins and oils. Newtonian behavior is generally exhibited by binders containing a high degree of peptized asphaltenes, while binders with low dispersed asphaltenes exhibit non-Newtonian flow. Figure 2-1 depicts the current morphological model used for asphalt binder. Other morphological models exist but Figure 2-1 is the most widely accepted.

2.3 Binder Tests and Evaluation

Traditionally, a variety of test methods have been used to characterize the consistency, aging, and physical properties of asphalt binder. The penetration and viscosity tests are used to characterize temperature susceptibility. Asphalt binder specifications were developed around these physical tests. These tests are empirical in

nature, which place certain limitations on the results that they provide. Pavement performance experience is required before the test results yield meaningful information. The relationships between the test results and the performance may not be accurate because the tests do not take into account the mechanistic properties i.e. stresses and strains.

In recent years, it became apparent that new test methods were needed, both for use in specifications and in developing correlation between physical and chemical properties for binder characterization. Fundamental material properties expressed in engineering units are needed in order to accurately develop relationships between the properties of asphalt binder and HMA. These fundamentally sound relationships are used to develop models that relate binder properties to mixture properties and finally to pavement performance. The Strategic Highway Research Program (SHRP) proposed a new system for binder specification. These new binder specification tests are performance based, expected to be better correlated to field results, and take into account both rheological and mechanistic failure modes. The following section summarizes the conventional consistency tests for asphalt binder and Superpave Binder Specification tests.

2.3.1 Consistency Tests

Consistency describes the degree of fluidity of asphalt binder at any given test temperature. Since asphalt binder is a viscoelastic material, its consistency varies with temperature. It is essential to measure the consistency of different binders at the same temperature and loading rate if comparisons between binders are to be made.

Penetration Test

The penetration test is an empirical measure of the consistency of an asphalt binder and is measured in accordance with ASTM D 5 (Annual Book of ASTM Standards, 1996). The test is performed by measuring how far a stainless steel needle penetrates a specimen of asphalt binder when loaded with 100 g for 5 s at a temperature of 25°C

(77°F) (Annual Book of ASTM Standards, 1996). The farther the needle penetrates the "softer" the binder. For binders used in the United States, the typical penetration number range is 60-100, which represents a penetration range of 15- 25 mm (0.6 – 1 in).

Viscosity Tests

Absolute viscosity is measured in accordance with ASTM D 2171 (Annual Book of ASTM Standards, 1996) using a U-shaped capillary tube viscometer. An asphalt binder sample is heated to temperature of 60°C and is poured into the viscometer. Under the action of a vacuum the binder rises (flows) and passes through timing marks. The measured time of flow between two successive timing marks on the capillary tube is multiplied by the calibration factor (provided by the manufacturer) of the viscometer. The result of this test yields the viscosity of the binder in units of poise. Paving grade asphalts are classified into six groups based on the viscosity grading system: AC-2.5, AC-5, AC-10, AC-20, AC-30 and AC-40. The digital number represents the viscosity of the binder in 100 poise.

The kinematic viscosity is performed at 135°C. It is measured in accordance with ASTM D 2170 (Annual Book of ASTM Standards, 1996) using a cross-armed viscometer. Here the binder flows under the force of gravity rather than vacuum application. The procedure is similar to the absolute viscosity test and results are usually defined in units of centistokes.

These tests do not provide information about binder properties over the entire range of typical in-place pavement temperatures. The standard test temperatures of 60°C and 135°C may provide information about the higher temperature viscous behavior. However, the binder behavior at low temperatures cannot be realistically determined from data obtained from the viscosity tests.

2.3.2 SuperPave™ Tests

Rotational Viscometer

This test method is used in order to determine the viscosity of asphalt binder at high temperatures, usually above 100°C. This information is needed to determine the pumping and mixing temperatures. This test method is performed in accordance to AASHTO TP 48. The rotational viscosity is determined by measuring the torque required to maintain a constant rotational speed (20 RPM) of a special spindle in an asphalt binder sample at a constant temperature. The SuperPave™ binder specifications limit the viscosity to 3 Pa·s at 135°C.

Dynamic Shear Rheometer (DSR)

The Dynamic Shear Rheometer (DSR) is used to measure rheological properties, such as the linear viscoelastic moduli of binders at intermediate to upper service temperatures. The DSR is used for specification purposes to measure the complex modulus and the phase angle of asphalt binders at a frequency of 10 rad/s, where the complex modulus is approximately 10 Mpa or greater. The DSR can be used to determine the time (frequency) dependency of the modulus. In order to construct thermorheologically simple linear viscoelastic master curves, time-temperature superposition can be applied to data obtained from the DSR.

Figure 2-2 illustrates the testing setup for the DSR. In general, the asphalt binder sample is placed between two plates; the bottom plate being fixed, while the upper plate oscillates. The centerline of the plate, point A, moves to point B as the plate oscillates. The centerline then passes through point A and moves to point C, after which the centerline returns to point A. This test is performed on both aged and unaged binder specimen.

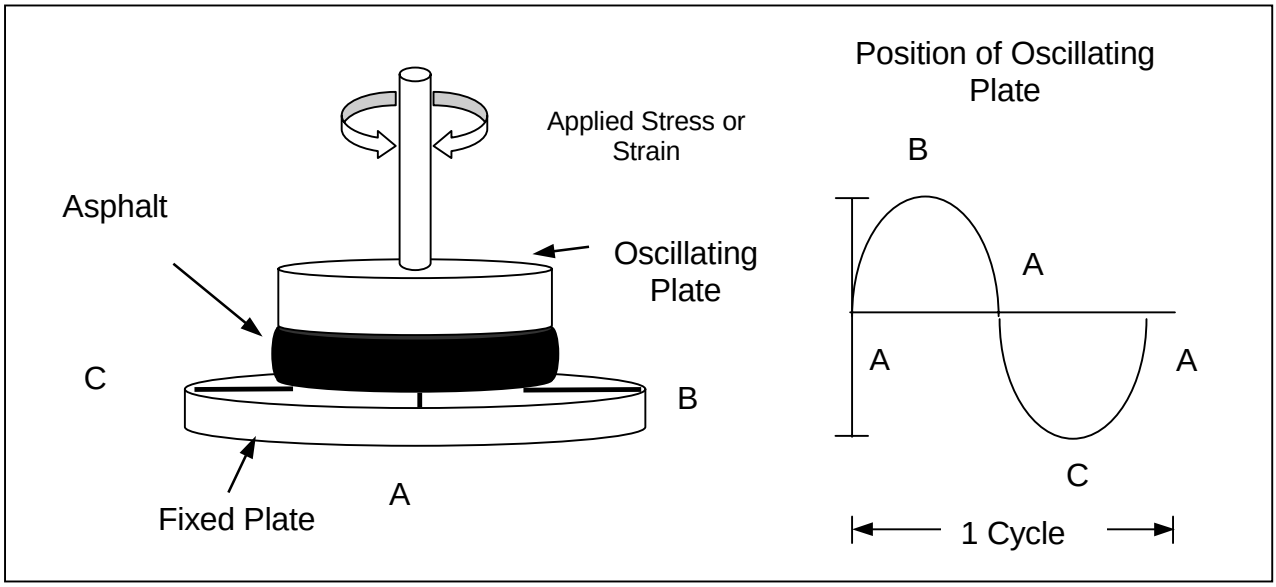

Figure 2-2. Testing setup for DSR.

Bending Beam Rheometer (BBR)

The Bending Beam Rheometer (BBR) test the properties of asphalt binders at low service temperatures (below 5°C) to determine its' susceptibility to thermal cracking. The testing procedure is given by AASHTO TP1. The BBR measures stiffness using a transient creep load, applied in bending mode, to load a beam specimen constructed with asphalt binder held at a constant low temperature.

Rolling Thin Film Oven (RTFO)

The Rolling Thin Film Oven (RTFO) test simulates the short term aging of asphalt binder, which usually takes place in the mixing plant and during hauling and construction of HMA. This test is performed in accordance to ASTM D2872 (Annual Book of ASTM Standards, 1996). A certain amount of asphalt is poured into a bottle and placed on a rotating rack inside an oven maintaining a temperature of 163°C. The rack rotates while a hot air jet with a specified discharge is blown into the sample. This test takes approximately 75 to 85 minutes.

Pressure Aging Vessel (PAV)

The Pressure Aging Vessel (PAV) test exposes the binder to high pressure and temperatures to simulate the effects of long term aging. The pressure vessel is designed to operate under a pressure of 2070 kPa and temperature conditions ranging from 90° – 110°C. The sample rack is placed in a preheated unpressurized PAV. When the vessel temperature is within 2°C of the desired temperature, the pressure is applied and the timing for the aging process begins. After 20 hours, the pressure is gradually removed. This test is performed on binder that has been aged using the RTFO method.

2.4 Polymers

Polymers are large molecules constructed from a number of smaller structural units called monomers. These monomers are covalently bonded in any conceivable pattern. Monomers have two or more bonding sites, through which they can be linked to another monomers to form a polymer chain. Homopolymers (or simply polymers) occur when only one species of monomer is used to construct a macromolecule. If the macromolecule consists of two types of monomer units, it is referred to as a copolymer.

Polymers can be grouped into three major categories: plastics, fibres and elastomers. There is no defining line that separates polymer groups. One method of defining a member of these categories is to observe the load-deformation behavior. Fibres and rigid plastics are resistant to deformation and are characterized by a high modulus and low percentage elongation. Elastomers exhibit behavior similar to that of a rubber band, i.e., increasing tensile strength with increased elongation and the ability to recover to the initial state after removal of the load (King and King, 1986).

As it pertains to asphalt binders, the major elastomeric modifiers include styrene-butadiene-styrene (SBS), styrene-isoprene-styrene (SIS), styrene-ethylene/butadiene-styrene (SEBS), and styrene-butadiene rubber. The plastomeric modifiers are ethylene-vinyl-acetate (EVA), polyvinylchloride (PVC), and polyethylene/polypropylene. As

compared to plastomeric modifiers, elastomeric modifiers are more commonly used in the modification of asphalt binder.

The thermoplastic elastomeric modifiers used in this study mainly consisted of random copolymers and block copolymers. The following section discusses their mechanical properties and molecular structure.

2.4.1 Random Copolymers

Random copolymers are synthesized by statistical placement of monomer units along a polymer chain backbone (Nosky and McGrath, 1977). They are homogeneous systems that exhibit characteristics between the two extremes of the reacting monomers. Unlike block copolymers, random copolymers do not form polymer networks and have a single-phase morphology. Styrene-butadiene rubber (SBR) is an example of a random copolymer.

2.4.2 Thermoplastic Block Copolymers

Thermoplastic block copolymers are formed through the process of reacting monomers together. The three general structures for block copolymers are tri-block linear, radial (or branched) systems and linear diblock structures. Tri-block linear structures are denoted as A-B-A, where A is a thermoplastic end-block, such as polystyrene and B is a rubbery mid-block, such as polybutadiene or polyisoprene. Styrene-butadiene-styrene (SBS) and styrene-isoprene-styrene (SIS) are examples of tri-block copolymers. Styrene-ethylene/butadiene-styrene and styrene-ethylene/propylene-styrene are formed by hydrogenation of the rubbery mid-block, therefore creating another version of these copolymers. This structure represents a two-phase system in which the rubbery mid-block forms a continuous phase of three-dimensional elastomeric network containing the dispersed end-block phase (Holden *et al.*, 1969). Radial (or branched) systems are of the $(A\text{-}B)_n$ type. Examples of this system include $(SB)_n$ and $(SI)_n$. Diblock linear structures are depicted by A-B; examples include SB, SEP, and SEB.

Block copolymers can be synthesized in three ways: (1) ionic initiators, where an active site is kept alive on the end of the initial block, which is then capable of initiating chain growth of the second monomer on the end of the first chain; (2) coupling of different blocks with functional terminal units, either directly or through a reaction involving a small intermediate molecule; and (3) bifunctional radial initiators, where a second potential active site is incorporated at the one end of the first chain grown, which can initiate at a later stage a new chain from the macro-radial produced (Cowie, 1991).

Inherent thermodynamic incompatibilities exist in thermoplastic copolymers between the end block and the rubbery mid-block. End-blocks, such as polystyrene, act as physical cross-links connected by rubbery springs forming a three dimensional rubbery system at temperatures below T_g, the glass transition temperature. At temperatures above T_g, the cross-linked network becomes less rigid and softens in the presence of shear. It is at this stage that polymers can be incorporated into asphalt. This process is reversed upon cooling therefore the rigid domains and the network reform and imparts elasticity and tensile strength to the polymer-asphalt blend.

2.5 Polymerized Asphalt

For a polymer to be effective in HMA, it should blend with the binder and improve its resistance to vehicular and environmental loading. There is a complex relationship between the chemical composition and morphology of an asphalt binder and its physical and rheological properties. Critical to the process of polymer modification of asphalt binder is the compatibility of the system. In modifying asphalt binder with polymeric materials, a change in its chemical composition and structure occurs, which in turn affects its properties. The polymer modification or blending process of asphalt binder may result in one of three type mixtures: (1) heterogeneous; (2) totally homogenous; and (3) micro-heterogeneous. A heterogeneous mixture is one in which phase separation occurs, meaning that the binder and polymer are incompatible. In a totally homogeneous mixture the polymer is completely soluble in the oils of the binder, which inhibits any intermolecular interactions. This creates a stable binder, while only slightly improving the

binder properties. A micro-heterogeneous mixture is made up of two distinct finely interlocked phases. In this system, the polymer swells, absorbing some of the nonasphatlene fraction of the binder forming a network composed of both a polymer and binder phase (Brule, 1997).

In binders containing SBS and SEBS, a polymeric network is formed which leads to the enhanced performance of the binder, especially at elevated temperatures. The modulus has been found to be temperature independent at higher temperatures; consequently the material exhibits more elastic behavior at higher temperatures (Bouldin and Collins, 1992).

Block copolymers have been shown to form a continuous network within asphalt binder at polymer concentrations as low as five percent by weight. Polymer modification reduces the effects of oxidative aging. This may be caused by molecules in the binder, that are chemically active and bound to oxidize, to undergo micro-structural interactions with the modifier and prevent the molecules from picking up an oxygen molecule (Srivastave, *et al.,* 1992).

2.6 Linear Viscoelastic Theory

The response of viscoelastic materials is intermediate between the behavior of an elastic solid and a viscous fluid. In an elastic material, the strain response to an arbitrary stress is not time dependent. When loaded in creep, this material deforms immediately to a constant strain. When the load is removed, the material instantaneously returns to its initial shape. Under the application of a load, viscous materials deform at a constant rate, continuing until the load is removed. Unlike elastic materials, there is no recovery of deformation, i.e. it does not return to its initial state.

The behavior of viscoelastic materials is time dependent and includes both elastic and viscous components. When loaded, viscoelastic materials do undergo some immediate deformation, which corresponds to the elastic component of response. This deformation

is followed by a gradual time dependent deformation that can be divided into two components, delayed elastic and viscous. When the load is removed, the delayed elastic deformation is recovered. This recovery does not occur instantaneously as seen in a purely elastic response. As stated earlier, there is no recovery of this deformation.

2.6.1 Dynamic Response

Dynamic mechanical analysis is one of the best tools used to characterize viscoelastic material. These tests are performed in either stress or strain controlled modes. In the stress controlled mode, a sinusoidal stress is applied to the sample and the resulting strain is monitored as a function of frequency. In the strain controlled mode, a sinusoidal strain is applied and the stress is monitored with respect to time.

Considering the strain controlled mode, the applied strain is defined as the real part of a complex strain,

$$\varepsilon^* = \hat{\varepsilon}\, e^{i\omega t} = \hat{\varepsilon}\,(\cos \omega t + i \sin \omega t) \qquad (2.1)$$

$$\varepsilon(t) = \hat{\varepsilon} \cos \omega t \qquad (2.2)$$

where,

ε^* = complex strain,

$\varepsilon(t)$ = applied strain,

$\hat{\varepsilon}$ = applied strain amplitude,

t = time, s, and

ω = frequency, rad/s

The stress output can also be considered as the real part of a complex stress:

$$\sigma^* = \hat{\sigma}\, e^{i(\omega t + \delta)} = \hat{\sigma}\,[\cos(\omega t + \delta) + i \sin(\omega t + \delta)] \quad (2.3)$$

$$\sigma(t) = \hat{\sigma}\, \cos(\omega t + \delta) \quad (2.4)$$

where,

σ^* = complex stress,

$\sigma(t)$ = stress output, Pa,

$\hat{\sigma}$ = stress output amplitude, Pa,

δ = phase angle, rad.

In an elastic material, the applied strain and resulting stress are always in phase, therefore, $\delta = 0$ rad. In a viscous material, the strain lags behind stress by $\pi/2$ rad ($\delta = \pi/2$ rad). For a viscoelastic material the phase angle, δ, is always between 0 and $\pi/2$.

The dynamic complex modulus can be defined as the ratio of complex stress to complex strain:

$$E^*(i\omega) = \sigma^*/\varepsilon^* = \frac{\hat{\sigma}}{\hat{\varepsilon}} e^{i\delta} \quad (2.5)$$

The dynamic complex modulus can be resolved into two components:

$$E^*(i\omega) = E'(\omega) + iE''(\omega) \quad (2.6)$$

where,

$E'(\omega)$ = dynamic storage modulus, Pa,

$E''(\omega)$= dynamic loss modulus, Pa.

The “in phase” and “out of phase” components of the complex modulus are represented by E' (ω) and E''(ω), respectively. Furthermore, the absolute value of the complex modulus can be computed as

$$|E^*(i\omega)| = \sqrt{[E'(\omega)]^2 + [E''(\omega)]^2} = \frac{\hat{\sigma}}{\hat{\varepsilon}} \quad (2.7)$$

Through simple mathematical manipulation the following relationships exist:

$$E' = |E^*| \cos \delta \quad (2.8)$$

$$E'' = |E^*| \sin \delta \quad (2.9)$$

$$\tan \delta = E''/E' \quad (2.10)$$

where tan δ is called the loss tangent and is a measure of relative energy dissipation.

In shear mode, dynamic mechanical analysis yield moduli values represented by G^*, G' and G'', which correspond to complex, storage and loss dynamic shear moduli. Figure 2-3 shows the schematic of a typical dynamic mechanical analysis along with the related equations.

Figure 2-3 shows, that at high frequencies (short loading times) the storage modulus is the major contributing component to the complex modulus. At low frequencies (corresponding to high temperatures), the complex modulus is approximately equal to the loss modulus ($|G^*| \cong G''$). Here it is observed that the slope of the complex modulus curve approaches unity and viscous behavior is exhibited by the binder.

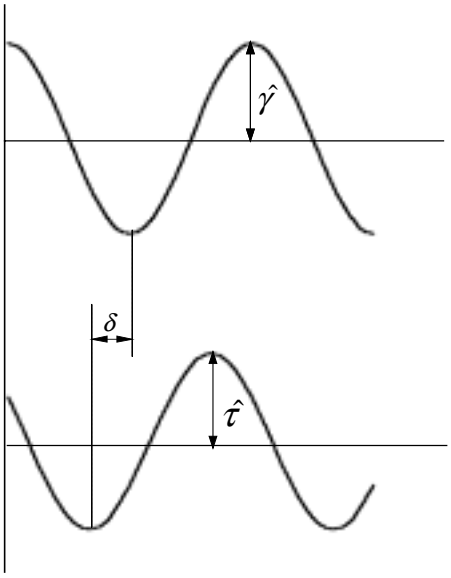

STRAIN INPUT : $\gamma(t) = \hat{\gamma}\cos\omega t$

STRESS RESPONSE : $\tau(t) = \hat{\tau}\cos(\omega t + \delta)$

COMPLEX MODULUS : $|G^*| = \dfrac{\hat{\tau}}{\hat{\gamma}}$

Figure 2-3. Schematics of a typical dynamic mechanical analysis in shear mode.

Dynamic mechanical analysis provides insight into the behavior of viscoelastic materials. The elastic and viscous components of response reflect the material's behavioral variations. These variations are due to changes in the material's microstructure, temperature or frequency. Dynamic moduli master curves are constructed in order to view the response of the material over a broad range of frequencies or temperatures. The construction of these curves is contingent upon the applicability of the principle of time-temperature superposition. The next section describes time-temperature superposition, as it pertains to the construction of master curves.

2.7 Time-Temperature Superposition

The modulus of a viscoelastic material is both time (frequency) and temperature dependent. In viscoelastic experiments, moduli can be measured as a function of temperature with constant time (frequency). The complete modulus-temperature behavior extends over several decades of frequency. It is not practical to perform

dynamic mechanical test over wide ranges of frequency. Through time-temperature superposition the frequency scale can be extended to encompass the entire modulus-temperature behavior for a viscoelastic measurement performed over a limited frequency range.

Leaderman (1943) observed that the viscoelastic response curves, for a wide variety of amorphous polymers obtained at different temperatures, were identical in shape and differed only in their location along the frequency (time) axis. Tobolosky and Eyring (1943) made similar observations leading to the introduction of the time-temperature superposition principle (Andrews *et al.,* 1948; Tobolosky, 1956). According to this principle, viscoelastic data at any temperature can be translated to another temperature by a simple multiplicative transformation of the time scale or an additive factor to the log time-scale.

Time-temperature superposition is applicable to thermorheologically simple materials (Schwarzl and Staverman, 1952). Thermorheologically simple materials are a special class of viscoelastic materials whose temperature dependence of mechanical properties is particularly responsive to analytical description (Haddad, 1995). These materials, which include a number of non-crystalline homopolymers and homogeneous copolymers, generally make up the simplest and most realistic viscoelastic constitutive equation for which response under constant temperature is used to predict the response under transient temperatures. Although asphalt binder is complex in nature, it has been found to exhibit the behavior of a thermorheologically simple material (Brodnyan *et al.,* 1960; Wada and Hirose, 1960; Dickenson and Witt, 1974).

In a thermorheologically simple material, a change in temperature results in a change in the rate of molecular motion. The sequence of molecular events is unchanged. The rate of molecular motion, as well as the sequence of molecular processes, is affected by changes in temperature for a thermorheologically complex material. For thermorheologically simple materials the relaxation times are assumed to be equally

effected by changes in temperature (Schwarzl and Stavemen, 1952). This assumption is the underlying principle behind time-temperature superposition.

In thermorheologically complex materials the mechanical response curves cannot be superimposed to form a master curve by a simple transition along the frequency axis. The shift factor for this class of material is a function of both temperature and frequency (Fesko and Tschoegl, 1971). Superposition may be applied to these types of materials but only by a point by point basis.

Mathematically time-temperature superposition principle may be expressed as follows (Aklonis and MacKnight, 1983):

$$F(T_1, \omega) = F(T_2, \omega/a_T) \qquad (2.11)$$

where,

$F(T_1, \omega)$ = value of a viscoelastic function at temperature T_1 and frequency ω,

$F(T_2, \omega/a_T)$ = value of viscoelastic function at temperature T_2 and frequency ω/a_T,

a_T = horizontal shift factor (which is a function of T_1 and T_2.

In order to apply time-temperature superposition, dynamic mechanical tests must be performed at several temperatures over a limited frequency range. The entire range of data, for a viscoelastic function (compliance, modulus, or loss tangent) is then plotted against frequency. A reference temperature is selected and the remaining curves are shifted along the frequency axis, partially overlapping, forming a continuous smooth master curve. The master curve extends over a wide range of frequencies. The amount to shift for each isothermal set of data is a measure of the temperature dependency of response. Figure 2-4 presents a graphical illustration of time-temperature superposition.

Three conditions must exist for time-temperature superposition to be applicable (Ferry, 1980). The response curves should have the same shape; shift factors for all

viscoelastic functions should be unique; and the variations of shift factors with temperature should follow a rational pattern.

2.8 Models Developed For Frequency Dependence of Asphalt Binder

The use of asphalt-polymer blends has been documented as early as 1902, when a French rubberized asphalt company laid rubberized asphalt roads (Thompson, 1979). In the 1930's, a number of rubberized asphalt test roads were constructed by both the British and French (Lewandowski, 1994).

In recent years, there has been an increased interest in the use of polymer modifiers in flexible pavements. During the past three decades there have been a number of studies investigating the cost effectiveness, application, behavior and the performance of polymer-modified asphalt binders. Several studies have addressed the performance of polymer modified binders and mixes under field conditions (Al Dhalaan, *et al.,* 1992; Collins *et al., 1992;* Fleckenstein *et al.,* 1992; Little, 1992; Maccarrone *et al.,* 1997; Oliver *et al.,* 1997; Ponniah *et al.,* 1996; Seerfass *et al.,* 1992; Stock and Arand 1992; Tayebali *et al.,* 1992; Thomas *et al.*, 1996; Zhou *et al.;* 1994). Research has also been done in the area of polymer-asphalt compatibility, microstructure, and polymer-asphalt interaction (Collins *et al.,* 1991; King and King, 1986; Shuler *et al.,* 1987). Other studies have concentrated on the effect of aging on the temperature susceptibility and rheological behavior of modified binders (Anderson *et al.,* 1992; Bonemazzi *et al.,* 1996; Collins and Bouldin, 1992; Gahvari, 1995; Gahvari and Al-Qadi, 1996; Huang *et al.,* 1996; Oliver *et al.,* 1997; Srivastava *et al.,* 1992).

Many of the aforementioned studies used dynamic mechanical analysis in the characterization of polymer-modified binders. Characterizing the viscoelastic behavior of asphalt binder requires obtaining the response of the material over a wide range of temperatures and frequencies (loading time).

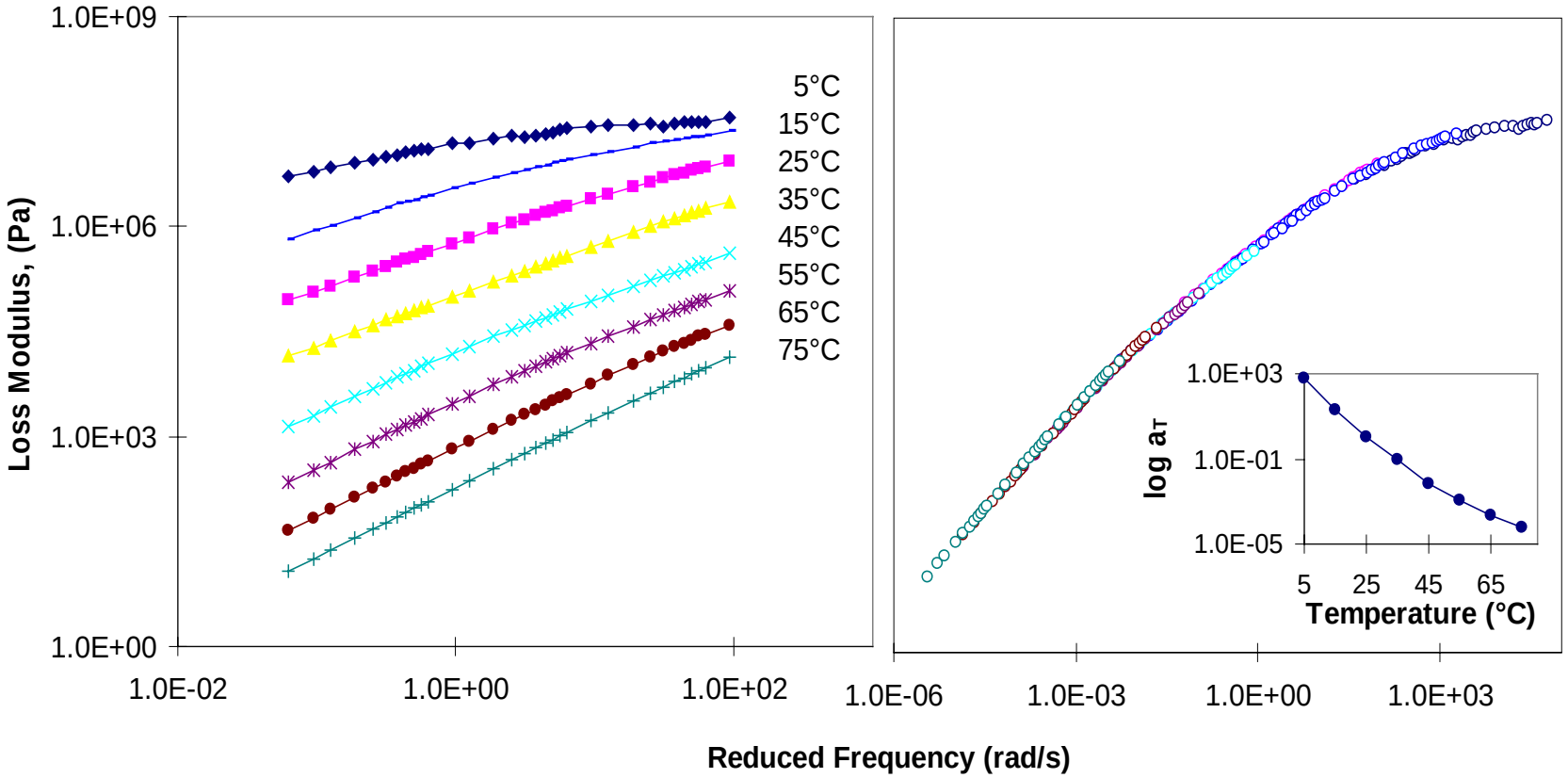

Figure 2-4. Graphical presentation of time-temperature superposition (data from Virginia Tech 1994 experiment, with reference temperature 25°C).

Several researchers have produced models that mathematically describe the temperature and the time dependency of straight asphalt binders (Jongepier and Kuilman, 1969; Dobson, 1969; Dickinson and Witt, 1974; Christensen and Anderson, 1992). These models are not adequate in predicting the linear viscoelastic response of polymer modified binders. Until recently, no effort had been made to reduce the dynamic mechanical data on a wide variety of modified binders into the framework of mathematical models.

Anderson *et al.* (1992) studied rheological properties of asphalt emulsions modified with SBS, SBR, and neoprene. Master curves were constructed from dynamic mechanical tests performed at temperatures ranging from –35 to 60 ° C. Anderson concluded that the addition of polymer extends the relaxation process to longer times. In order to form smooth continuous curves of viscoelastic functions, both horizontal and vertical shift factors were used. The significance of the vertical shift factors is not certain. Moreover, no quantitative measure of shift in the relaxation spectra was established. The Williams Landel Ferry (WLF) equation (Williams *et al.,* 1955) and the Arrhenius function was used in order to describe the temperature dependency above and below the T_g, respectively.

Stock and Arrand (1993) investigated the rheological properties of six different polymer modified binders. Plastomeric and elastomeric modifiers were used in their study. Dynamic mechanical tests were performed on the modified binders over a limited range of frequencies (0.1 to 10 Hz) and temperatures (40 to –10 ° C). The model proposed by Dobson (1969) was used to describe the frequency dependency of the response.

As stated earlier, there has been very little effort to reduce the dynamic mechanical data on a wide range of modified binders into the framework of mathematical models. Two researchers have produced models that can, with some degree of accuracy, predict the dynamic response of polymer modified binders (Gahvari, 1995, Stastna *et al.*, 1996, Marasteanu Anderson, 1999).

Gahvari and Al-Qadi (1996) conducted dynamic mechanical analysis on 21 asphalt-polymer blends at frequencies between 0.06 to 188.5 rad/s temperatures ranging from 5° to 75° C. The mixes were prepared using one viscosity graded asphalt binder and seven different polymer modifiers. Each polymeric additive was blended with asphalt binder at three different concentration levels. The modifiers were thermoplastic block copolymers and random copolymers. The effect of short term aging on rheological properties of the modified blends was also investigated. Master curves were developed for the dynamic moduli over several decades of reduced frequency. Two mathematical models, for G' and G" respectively, were proposed to discuss the frequency dependence of the response. The WLF equation was found to adequately describe the temperature dependency of all modified binders used in that study.

Stastna *et al.* (1996) performed dynamic mechanical analysis on five asphalt-polymer blends. The five modified binders were divided into two groups. Group 1 used a SBS modifying agent and Group 2 contains binder that was modified with PE and EVA.

A fractional model of complex modulus, based on the general principles for a linear response function, is used to depict the frequency dependency of the response. The model considers the polar form of G^*, $G^* = |G^*| \exp(i\delta)$. The values $|G^*|$ are slightly underestimated in the region of the T_g.

Marasteneanu and Anderson (1999) proposed a modified version of the model developed by Christensen and Anderson. Testing was performed on 38 plain and modified binders. As compared to the original Christensen and Anderson model, the degree of precision was found to be greater.

A brief description of previous models used to describe the dynamic response of both modified and unmodified binders is presented in the remaining part this section.

2.8.1 Jongepier and Kuilman's Model

Jongepier and Kuilman (1969) derived models for various rheological functions based on the assumption that the relaxation spectra is approximately log normal in shape. This model is expressed mathematically using a relatively complex set of mathematical equations. The relaxation spectrum is given by:

$$H(\tau) = \frac{G_g}{\beta\sqrt{\pi}} \exp - \left(\frac{\ln \tau / \tau_m}{\beta} \right)^2 \qquad (2.12)$$

where,

β = width of the distribution function,

τ = relaxation time, s,

τ_m = time constant, s, defined by $\frac{\eta_0}{G_g} e^{-\frac{\beta^2}{4}}$,

η_0 = Newtonian viscosity, Pa·s,

G_g = Glassy modulus, Pa.

The glassy modulus, G_g, is defined as the limiting value of storage modulus at extremely high frequencies and is expressed by:

$$G_g = \int_{-\infty}^{+\infty} H(\tau) d \ln \tau . \qquad (2.13)$$

In order to mathematically describe the loss and storage modulus, the following transformations were applied:

$$u = \ln \omega\tau \text{ , and } x = \frac{2}{\beta^2} \ln \omega_r \qquad (2.14)$$

where,

ω_r is a dimensionless reduced frequency defined by

$$\omega_r = \frac{\omega \eta_0}{G_g} \tag{2.15}$$

The mathematical expressions for storage and loss moduli are given as:

$$G'(x) = \frac{G_g}{\beta\sqrt{\pi}} \exp -\left[\frac{\beta(x-1/2)}{2}\right]^2 \times \int_0^\infty \exp -\left(\frac{u}{\beta}\right)^2 \frac{\cosh(x+1/2)u}{\cosh u} du, \tag{2.16}$$

$$G''(x) = \frac{G_g}{\beta\sqrt{\pi}} \exp -\left[\frac{\beta(x-1/2)}{2}\right]^2 \times \int_0^\infty \exp -\left(\frac{u}{\beta}\right)^2 \frac{\cosh(x-1/2)u}{\cosh u} du, \tag{2.17}$$

Jongepier and Kuilman (1969) developed a set of master curves for complex modulus and phase angle for a wide variety of asphalt binders by integrating the above equations 2.16 and 2.17 for a range of β values. The authors concluded that the variations in the relaxation spectra resulted from changes in the width parameter β. Comparisons were made between experimental data and data generated by the model. It was discovered that the accuracy of the model for binders with small β was greater than that of binders with large β values. It was reported that the response of binders with larger β values is less frequency dependent.

The WLF equation (Williams *et al.,* 1955) was used in order to describe the temperature dependency of the response:

$$\log a_T = -\frac{C_1(T - T_R)}{C_2 + (T - T_R)} \quad (2.18)$$

where,

a_T = shift factor,

T_R = reference temperature, °K or °C,

C_1 and C_2 = experimental constants.

Jongepier and Kuilman stated that in order for the interpretation of constants C_1 and C_2 to be meaningful, T_R should be selected to have a physical significance. However, through dylatometric glass transition temperature (T_g) measurements, they realized that use of T_g as the reference temperature does not result in a universal set of constants in the WLF equation. The authors concluded that the glass transition temperature is not an appropriate parameter to describe the temperature dependence of asphalt cement. Defining T_R as an equi-viscous temperature (a temperature at which asphalts have a certain viscosity), resulted in varying sets of C_1 and C_2 constants for different asphalt types.

Although this model is theoretically sound, it is not suitable for practical use, because of the mathematical complexity of the equations developed for frequency dependence.

2.8.2 Dobson's Model

Dobson (1969) developed a model for frequency dependence of asphalt binders based on describing the complex modulus and loss tangent master curves as a function of frequency. The proposed model by Dobson relating complex modulus and reduced frequency is given by:

$$\log \omega_r = \log G_r - \frac{1}{b}\left[\log(1 - G_r^b) + \frac{20.5 - G_r^{-b}}{230.3}\right] \qquad \text{for } G_r > 10^{-\frac{1.02}{b}}, \tag{2.19}$$

where,

$$\omega_r = \frac{\eta_0 \omega a_T}{G_g}, \tag{2.20}$$

$$G_r = \frac{|G^*|}{G_g}, \tag{2.21}$$

b = a parameter describing the width of relaxation spectrum.

The other parameters were previously defined. Although *b* is defined as the width parameter for relaxation spectrum, no further explanation has been made on it and it is not clear what type of distribution function it refers to. The author states that *b* can be looked upon as a shear susceptibility parameter and is related to the penetration index.

Dobson also used the WLF equation to describe the temperature dependency of the response of asphalt binders. He found that for $T - T_R > -20$, the WLF, with universal constants, can be used to fit the shift factor data. This agreed with the previous findings by Brodnyan (1960). At lower temperatures, it was found that the WLF equation overestimates the shift factors. Therefore, Dobson's version of the WLF equation consists of two pairs of constants for temperatures below and above the reference temperature:

$$\log a_T = \frac{-12.5(T - T_R)}{142.5 + (T - T_R)}, \qquad T - T_R < 0, \tag{2.22}$$

$$\log a_T = \frac{-8.86(T - T_R)}{101.6 + (T - T_R)}, \qquad T - T_R > 0, \tag{2.23}$$

Dobson did not specify a certain reference temperature, but like Jongepier and Kuilman stated that T_R should be an equi-viscous temperature for asphalts.

2.8.3 Dickenson and Witt's Model

Dickinson and Witt (1974) developed analytical expressions for the complex modulus and phase angle in terms of frequency. These expressions were derived from dynamic mechanical data from 14 different asphalt binders. The master curves for complex modulus and phase angle were treated mathematically as hyperbolas. The equation presented for complex modulus is given by:

$$\log G_r = \frac{1}{2}\left[\log \omega_r - \sqrt{(\log \omega_r)^2 + (2\beta)}\right], \qquad (2.24)$$

G_r and ω_r have been previously defined. This equation represents one arm of a hyperbola whose asymptotes, log G_r = log ω_r and log G_r = 0. The values of the asymptotes indicate the viscous and elastic extremes of response, respectively. The parameter β corresponds to shear susceptibility and is equal to the distance between the origin of hyperbola and the master curve on the $\log G_r$ scale.

The mathematical expression for phase angle is:

$$\delta = \delta' + \frac{\pi - 2\delta'}{4}\left[1 - \frac{\log \omega_r}{\sqrt{(\log \omega_r)^2 + (2\beta)^2}}\right], \qquad (2.25)$$

where, δ' is a very small angle (less than 3°), which is assigned to the glassy modulus.

Based on these two equations, Dickinson and Witt computed the values of storage and loss moduli and developed the relaxation spectra. They observed that the spectra were not symmetrical with respect to the maximum value; concluding that the spectra were not consistent with Jongepier and Kuilman's assumption of log normal distribution for relaxation times.

Dickinson and Witt used the Dobson's version of WLF equation to describe the temperature dependency of their experimental data. Based on the two sets of constants proposed by Dobson, they evaluated the reference temperature for the range of studied asphalts.

2.8.4 Christensen and Anderson's Model

Christensen and Anderson (1992) developed several master curves of complex modulus and loss tangent for eight SHRP core asphalts. The frequency dependence of the response was describe by a mathematical model based on a modified logistic distribution function for the resulting relaxation spectra. Complex modulus and phase angle in terms of frequency were described by the following:

$$\left|G^*(\omega)\right| = G_g\left[1+\left(\frac{\omega_c}{\omega}\right)^{\frac{\log 2}{R}}\right]^{-\frac{R}{\log 2}}, \qquad (2.26)$$

$$\delta(\omega) = \frac{90}{1+\left(\frac{\omega}{\omega_c}\right)^{\frac{\log 2}{R}}}, \qquad (2.27)$$

where,

ω_c = crossover frequency, rad/s,

R = rheological index defined by $\log\left(\frac{G_g}{|G^*(\omega)|}\right)\Big|_{\omega=\omega_c}$. (2.28)

The remaining parameters are as previously defined. In this model, parameters ω_c and R have considerable physical significance. The rheological index, *R,* is a shape parameter for the master curve and represents the width of relaxation spectrum. Asphalts characterized by larger R values exhibit wider relaxation spectrum. The crossover frequency, ω_c, represents the frequency at which $\delta = 45°$. Several empirical observations have confirmed that the crossover frequency usually coincides with the intersection of glassy and viscous asymptotes of the complex modulus master curve. Therefore, it can be regarded as a location parameter on the master curve.

Through comparison between the experimental data and data generated by the model, Christensen and Anderson observed some discrepancies for moduli below approximately 10^5 Pa. Moduli values below this range represent higher temperatures or loading times. Therefore, use of the Christensen and Anderson model is strictly suitable for characterizing the response of asphalt binders from low to intermediate temperatures.

To describe the temperature dependency of shift factors, both the WLF and the Arrhenius function were used. At temperatures lower than a certain limit (designated by a defining temperature), an Arrhenius function, defined by the following equation, was used to characterize the temperature dependency of asphalt:

$$\log a_T = \frac{H_a}{2.303\,\mathrm{R}}\left(\frac{1}{T} - \frac{1}{T_d}\right), \quad (2.29)$$

where,

H_a = activation energy for flow below T_d, J/mol,

R = ideal gas constant, 8.304 J/mol.°K,

T_d = defining temperature, °K or °C.

At temperatures above T_d, the WLF equation yielded reasonable values for shift factors. A strong correlation between T_d and T_g was suggested, however, no explicit relationship between the two was ever established.

2.8.5 Gahvari's Model

Gahvari performed dynamic mechanical analysis on 21 asphalt-polymer blends. A dynamic shear rheometer was used to test original asphalt-polymer blends as well as their RTFO residue. Models for storage and loss modulus were developed in order to discuss the frequency dependence of response. The model for storage modulus is given by:

$$\log G' = \log G_g [1 - e^{-p(\log \omega + I)}] \qquad (2.30)$$

where,

G'(ω) = storage modulus,

G_g = glassy modulus,

p= proportionality factor,

I = location parameter for the master curve = $\log 1/\omega\big|_{G'=1}$.

Gahvari observed that the variation of the storage modulus between the two asymptotic extremes followed an exponential pattern, which can be described by Mitcherlich's law of diminishing returns (1909). This law states that the rate of increase in value of certain functions is proportional to the difference between the maximum asymptotic and actual values of the function. The model proposed by Gahvari, for storage modulus, adequately characterized the frequency dependence of the material for moduli below 10^8 Pa. Above this limiting value, this model tends to overestimate the modulus.

The model proposed for characterizing the frequency dependence of loss modulus is a hyperbolic equation given by:

$$\log G''(w) = (\log G''_{max} + d) - \sqrt{(\log \omega - \log \omega_d)^2 + d^2} \qquad (2.31)$$

where,

G"(ω) = loss modulus Pa,

ω = reduced frequency, rad/s,

G''_{max} = peak value of the loss modulus, Pa,

d = half length of the transverse axis, Pa, and

ω_d = location parameter for the master curve, rad/s = $\omega\big|_{G''= G''max}$

This equation represents one arm of a rectangular hyperbola centered at ($\log\omega_d$, $\log G''_{max}$+d) on the $\log\omega$ - logG'' coordinate system. At low frequencies, the hyperbola approaches an asymptote whose equation is given by:

$$\log G''(\omega) = (\log\omega - \log\omega_d) + (\log G''_{max} + d) \qquad (2.32)$$

This equation represents the viscous asymptote of response, and is given by a line with a slope of unity on the same coordinate system. It was observed that the value of ω_d varied with polymer type. Higher ω_d values were observed for binders modified with block copolymers as compared to those modified with SBR. It was also found that ω_d increased with increasing polymer content. However, with constant polymer content, aging treatment caused the value of ω_d to shift backward.

The parameter *d*, defined as a shape factor, is similar to the constant β in Dickinson and Witt's Model. With equal polymer concentration levels, the asphalt-polymer blends containing block copolymers exhibited considerably higher *d* values than those modified with random copolymers. Short term aging of the binder resulted in a significant increase in the value of *d*.

G''_{max}, the peak value of loss modulus, was found to be a characteristic of the base asphalt. This parameter was not appreciably influenced by the addition of polymer or aging treatment. The value of G''_{max} was measured to be approximately $10^{7.5}$ Pa.

The model for frequency dependence of the loss modulus fit the experimental data over the entire range of reduced frequencies. However, there was no experimental data available to demonstrate the behavior of the model above ω_d. The proposed model is hyperbolic and is symmetric to the line $\log\omega = \log\omega_d$. The shape of the loss modulus master curve is not symmetrical in shape with respect to the peak point; therefore, the use of this model is restricted to the specified range of moduli values less than or equal to $10^{7.5}$ Pa.

The temperature dependency of the shift factors was found to follow the WLF equation with universal constants.

2.8.6 Stastna's Model

Stastna, *et al.* (1996) proposed a simple model of the complex modulus and phase angle based on a generalization of the Maxwell model. Dynamic mechanical analysis was performed on five modified and some 19 different unmodified asphalt binders. The proposed equation for complex modulus is given by:

$$\left|G^{*}\omega)\right| = i\eta_0\omega\left\{\frac{\prod_{1}^{m}[1+(\omega\mu_k)^2]}{\prod_{1}^{n}[1+(\omega\lambda_k)^2]}\right\}^{1/(n-m)} \tag{2.33}$$

$$\delta(\omega) = \frac{\pi}{2} + \beta\left[\sum_{1}^{m}\arctan(\mu_k\omega) - \sum_{1}^{n}\arctan(\lambda_k\omega)\right] \tag{2.34}$$

where,

$m < n$, $\mu_k > 0$, $\lambda_k > 0$, $\eta_0 > 0$;

μ_k and λ_k represent relaxation times; and

η_0 represents the zero-shear viscosity.

Equations (2.33) and (2.34) were able to model the response of polymer modified asphalts with a limited number of parameters (between 10 to 15). Each parameter is binder specific and must be determined through regression analysis and experimental data. When applied to a typical experimental data set, the model lacks statistical vitality, because the number of unknown parameters approaches the degrees of freedom in the data (Marasteanu and Anderson, 1999).

2.8.7 Marasteanu and Anderson Model

Marasteanu and Anderson (1999) modified the model developed by Christensen and Anderson (1992) in order to accomadate modified binders. The researchers applied the Havriliak and Negami model to the |G*|, resulting in the following equation:

$$\left|G^*(\omega)\right| = G_g[1+(\omega_c/\omega)^v]^{-\frac{v}{w}} \quad (2.35)$$

$$\delta(\omega) = \frac{90}{1+\left(\frac{\omega}{\omega_c}\right)^v} \quad (2.36)$$

where,

v = log2/R, and

ω_c = describes the slope of the phase angle curve.

This model was applied to 38 plain and modified binders, and the degree of precision of the improved equation was found to be greater than the original model.

All of the aforementioned models were developed based on experimental dynamic mechanical data from straight asphalt binders, with the exception of those presented by Gahvari and Al-Qadi (1996), Stastna *et al.* (1996), and Marasteanu and Anderson (1999). The frequency dependence models are successful in describing the overall shape of the master curves but they are either mathematically complex or have some aforementioned limitations in the range of application.

Chapter 3. Research Program

The experimental plan, conducted in earlier research at Virginia Tech, consisted of the measurement of the complex moduli of 21 asphalt-polymer blends at frequencies between 0.06 to 188.5 rad/s and temperatures ranging from 5 to 75°C. The mixes were prepared using a conventional AC-20 paving grade asphalt binder and seven different elastomeric polymer modifiers. Each polymeric additive was blended with asphalt binder at three different concentration levels. The modifiers used were thermoplastic block copolymers and random copolymers, which are commonly used in industry and represent a wide range of chemical structures, and mechanical and physical properties. The study also investigated the effect of short-term aging on the rheological properties of the polymer-modified asphalt blends.

3.1 Materials and Specimen Preparation

All tested samples were prepared at the Structures and Materials Laboratory at Virginia Tech (Gahvari, 1995). The base asphalt was a grade AC-20 asphalt that was supplied by Amocco Oil Company. Table 3-1 shows the conventional test results for the asphalt used. Seven different elastomeric polymers were used in this study: two styrene-butadiene-rubber (SBR) random copolymers, two styrene-butadiene-styrene (SBS) block copolymers, two styrene-butadiene/butylene-styrene (SEBS) linear block copolymers, and one $(SB)_n$ branched copolymer. Typical properties for these copolymers are presented in Tables 3-2 and 3-3. The tables also indicate the designation adopted to identify the copolymers during experimentation.

The two SEBS linear block copolymers were supplied by the manufacturer in the form of a fine uniform powder, which is suitable for mixing with asphalt due to the high surface area of particles.

Table 3-1. AC-20 Properties.

Specimen Condition	Unaged	(RTFO)
Specific Gravity	1.037	(N/A)
Penetration at 25°C (0.01 mm)	66	40
Absolute Viscosity at 60°C (poise)	2054	4232
Kinematic Viscosity at 135°C (cSt)	4437	(N/A)

Table 3-2. Typical properties of the random modifiers.

Designation	P	C
Physical Form	Emulsion	Emulsion
Solid Content	68	68
Specific Gravity	.95	.95
pH	10	10
Brookfield Viscosity, cps	1300	1300
Styrene Butadiene Ratio	24/76	24/76

Table 3-3. Typical properties of the thermoplastic block copolymer modifiers at 23°C.

Designation	**S**	**D**	**G**	**X**	**N**
Structure	Linear SBS	Linear SBS	Linear SEBS	Linear SEBS	Radial (SB)n
Physical Form	Porous Pellet	Porous Pellet	Powder	Powder	Porous Pellet
Plasticizer Oil Content (%w)	0	29	0	0	0
Specific Gravity	.94	.93	.91	.92	.94
Brookfield Viscosity at 25°C (cps)	4000	1000	1350	5370	20000
Tensile Strength, Pa (ASTM D 412)	31700	19000	31050	24150	27600
300% Modulus, Pa (ASTM D 412)	2760	1720	4830	6210	5520
Elongation , % (ASTM D 412)	880	1300	500	700	820
Styrene/Butadiene Ratio	31/69	31/69	29/71	31/69	30/70

The linear block copolymers (SBS) and the branched copolymer $(SB)_n$ were reduced using a laboratory granulator, because the particle size was too large to assure proper mixing. The grounded polymers were passed through a 1.19mm sieve to obtain a fine and uniform mix.

Blending was performed using a Lightnin Labmaster laboratory mixer. All polymers were blended with the asphalt binder at three different concentration levels. For the random copolymer designated as C, the concentration levels were 2, 3, and 4% by weight of asphalt. All other polymers were blended at 3, 4, and 5%. Depending on the polymer type, the mixing temperature ranged from 163° to 177°C. With the mixer operating at a low speed, the binder was heated to the desired temperature. Once this temperature was reached, the polymer was added slowly in order to avoid agglomeration of the polymeric particles. The main mixing cycle started at an increased speed after the addition of polymer, and continued for a one to 10 hr period, depending on the polymer type and content. The beaker was then transferred to an oven maintained at 163°C and allowed to stay for approximately one hr. If no obvious signs of phase separation between polymer and binder were observed, the blend was poured in several small containers. These containers were sealed, marked for identification, and stored at room temperature for further testing.

Immediately after blend preparation, samples of each modified asphalt were aged in accordance with the rolling thin film oven test (RTFOT) procedure, ASTM D 2872 (Annual Book of Standards, 1991). The aged samples were then transferred to smaller containers, marked for identification, sealed, and stored at room temperature.

A four-character code was used to designate each polymer-asphalt combination. The first character, A, refers to the type of asphalt, Amoco AC-20. The second character describes the aging condition of the binder, U for unaged and R for RTFO residue. The polymer type and concentration percentage is given by the third and fourth characters, respectively. For example, a blend of unaged asphalt with 5% polymer N (radial SB_n) is designated as ARN5.

3.2 Data Collection and Analysis

The binders were tested using a Bohlin stress-controlled dynamic shear rheometer (DSR) with parallel plate configuration. Measurement temperatures ranged from 5° to

75°C with increments of 10°C. The 8-mm plate was used for performing tests at temperatures of 5° to 35°C, and the 25-mm plate was used for tests at 35° to 75°C. Specimens were completely immersed in a temperature-controlled water bath with forced circulation in order to maintain the specified constant temperature during testing. The 25-mm-diameter binder specimens were prefabricated using a silicon rubber mold, and the 8-mm-diameter specimens were poured directly between the two plates and trimmed to the desired geometry.

The linear viscoelastic range was determined for each binder-polymer blend in both aged and unaged conditions by performing stress sweeps over the entire range of temperatures and specified frequencies. Limiting strains were determined from the stress sweeps and then reduced to a uniform range for all binders, which were later used as target strains in performing frequency sweeps. The target strains for 5, 15, 25, 35, and 45°C were 0.8, 1, 2, 3, and 6.5%, respectively. For temperatures above 55 °C, the target strain was was found to be 9%. These strains are well within the linear range of response as established by the stress sweeps, and are below the values stated by AASHTO TP5 (AASHTO Provisional Standards, 1994) for straight binders. Frequency sweeps were then performed on all samples over the entire range of temperatures. Thirty-four frequencies ranging from 0.063 to 188.5 rad/s were used. Two replicate specimens were tested for each binder.

3.3 Comparison of Recent and Previous Data Analysis

The experimental data for dynamic moduli functions were obtained from the original frequency sweeps. The principle of time-temperature superposition was found to be applicable. For each polymer asphalt combination, isothermal graphs of complex, storage, and loss moduli data were plotted against frequency on a log-log scale.

Generally it is accepted to use either the loss or storage modulus in determining the amount of translation along the frequency axis in the construction of master curves. Figures 3-1 and 3-2 show the isothermal plots for storage and loss moduli for the sample

designated as ARG3. The storage modulus measurements tend to yield erroneous readings at high temperatures (very low frequencies on the translated frequency axis). This is expected, because at very high temperatures, the complex shear modulus is almost entirely composed of the loss modulus. The shapes of these curves are skewed and are not suitable for use in developing a smooth master curve over the entire range of frequencies. For this research, master curves for the dynamic moduli were prepared using the time-temperature superposition principle based on the loss modulus measurements. Two sets of dynamic moduli master curves were constructed for each polymer-asphalt blend using the replicate specimen data. Figures 3-3 and 3-4 show the dynamic loss and storage moduli, as well as the loss tangent master curve for ARG3.

The isothermal curve corresponding to 25°C was used as the reference temperature for construction of the master curves. All other segments were translated along the frequency axis to obtain a smooth unique curve. The translation was accomplished using a spreadsheet and visual inspection of corresponding graphs to find the best possible fit. The same shift factors derived from the loss moduli apply to the remaining viscoelastic functions.

Dynamic loss modulus master curves, shift factor, and isothermal graphs are presented in Appendix A.

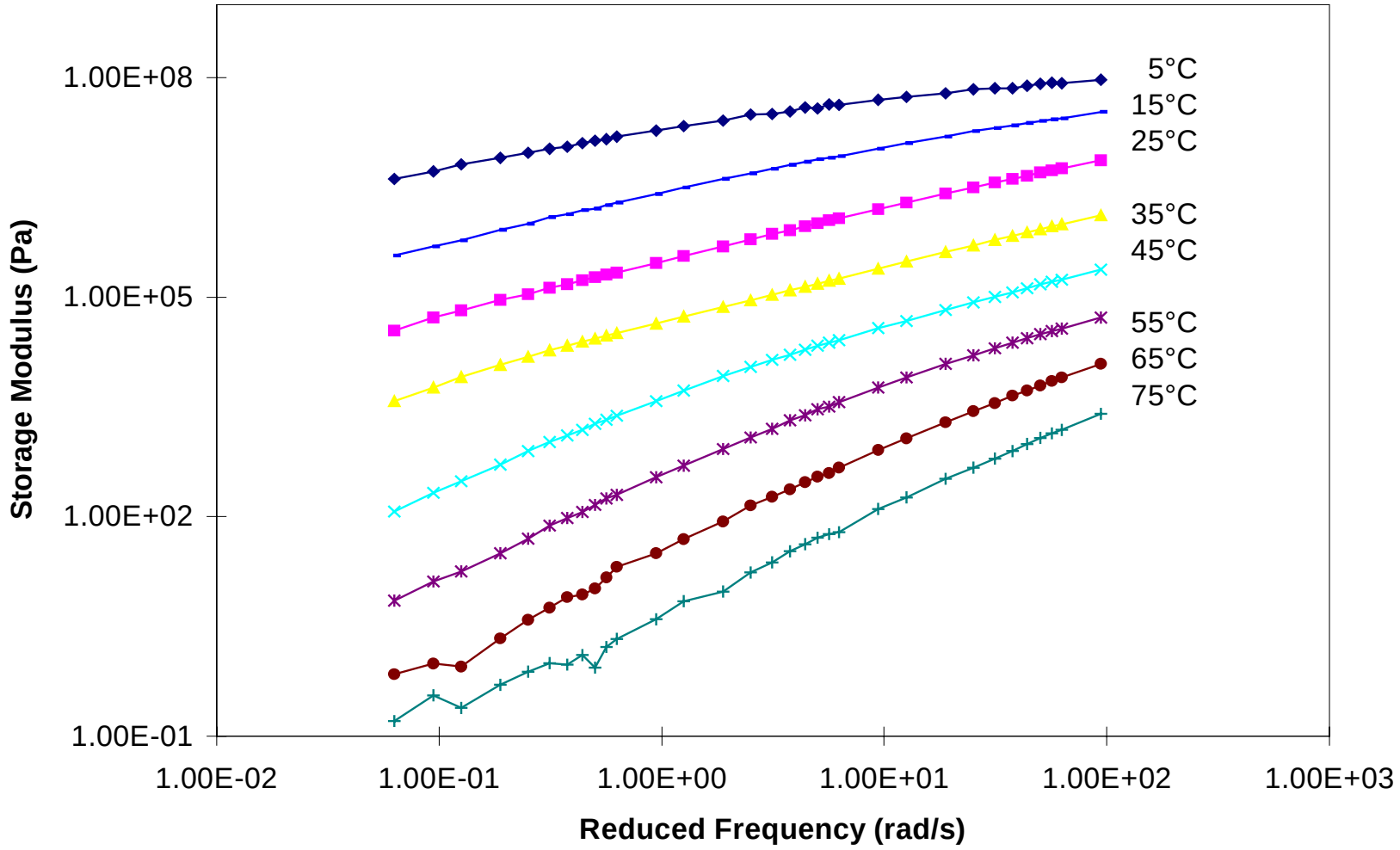

Figure 3-1. Dynamic storage modulus versus frequency at eight test temperatures for ARG3.

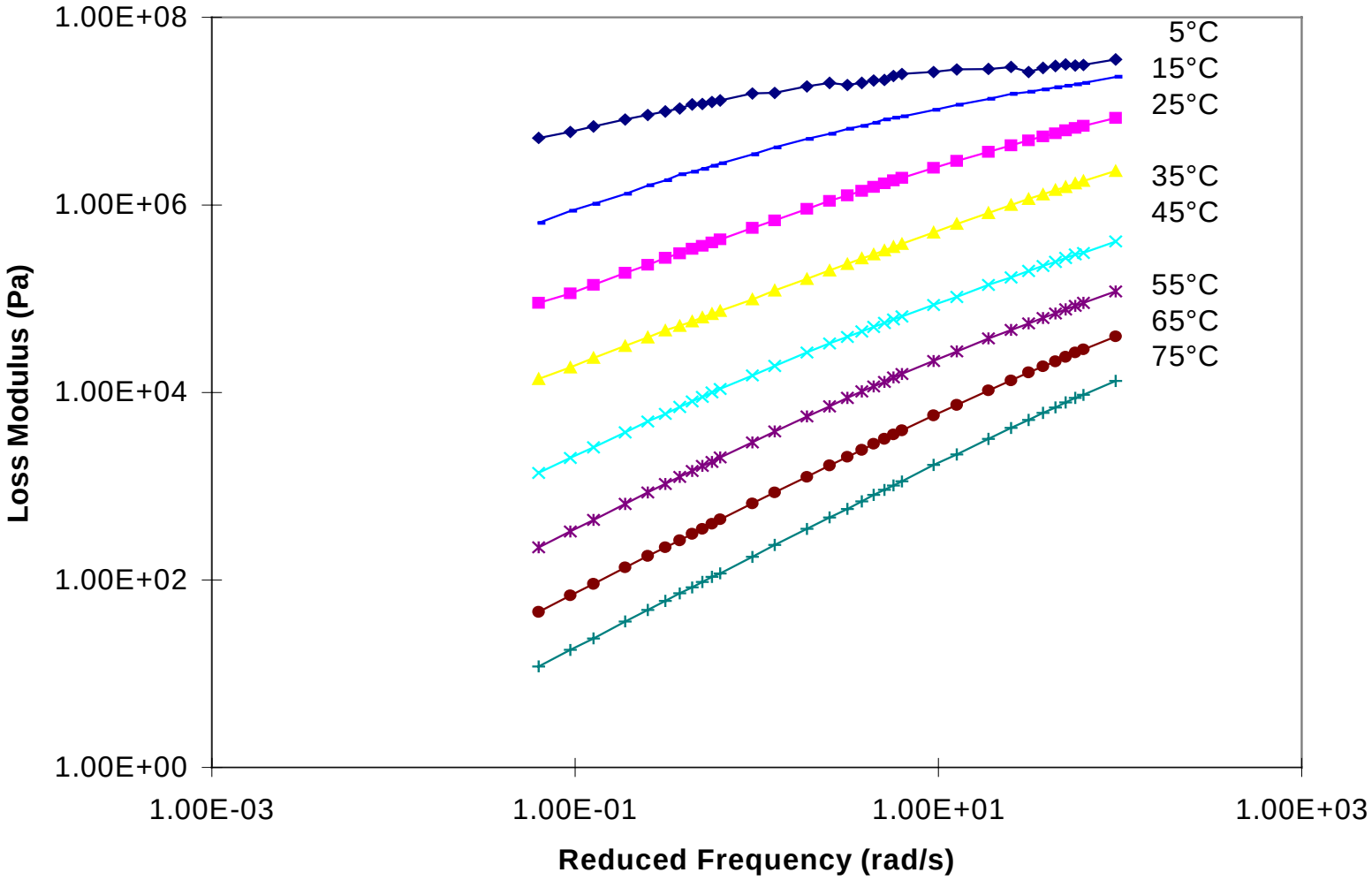

Figure 3-2. Dynamic loss modulus versus frequency at eight test temperatures for ARG3.

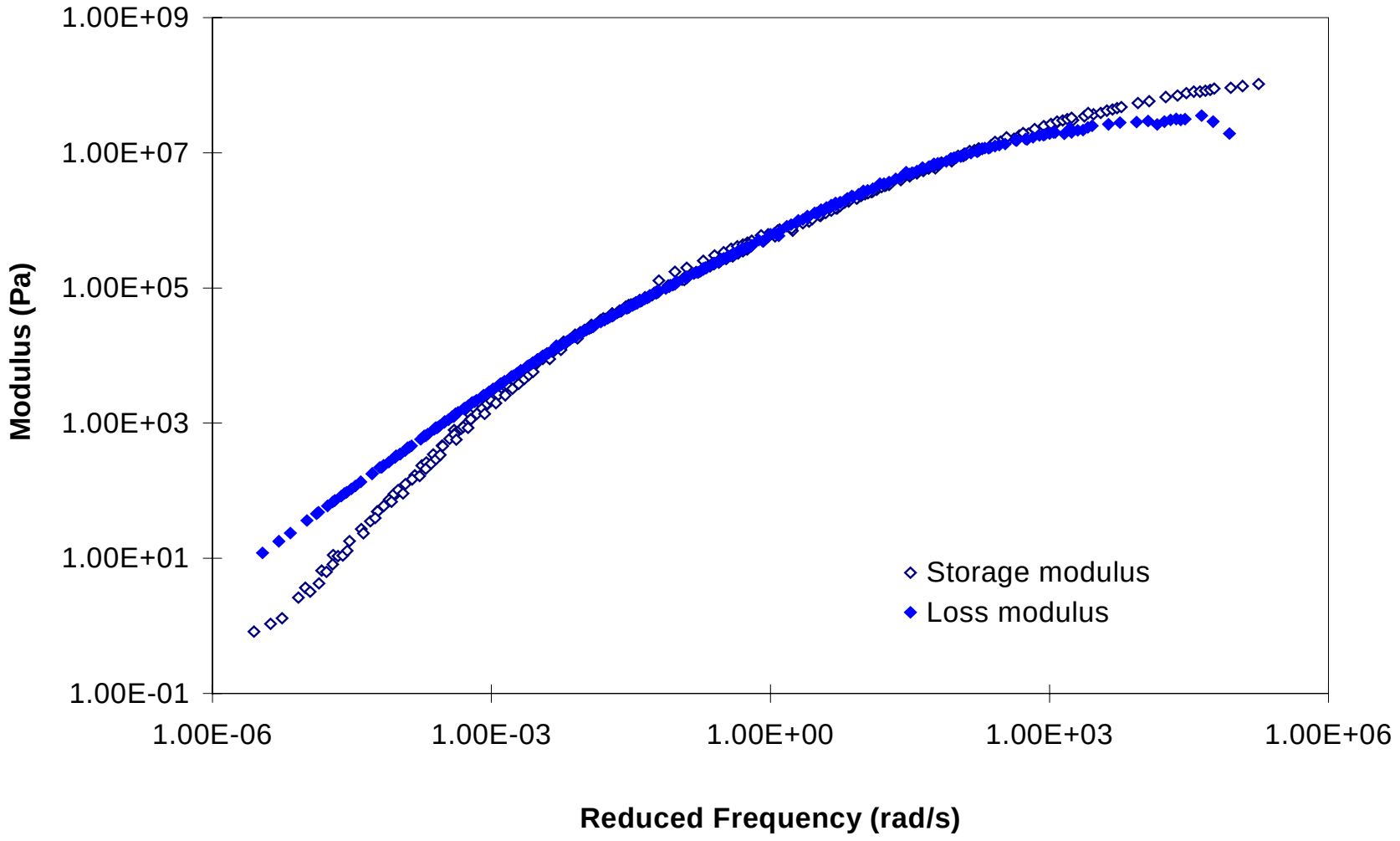

Figure 3-3. Dynamic storage modulus and loss modulus master curves for ARG3 (reference temperature 25°C).

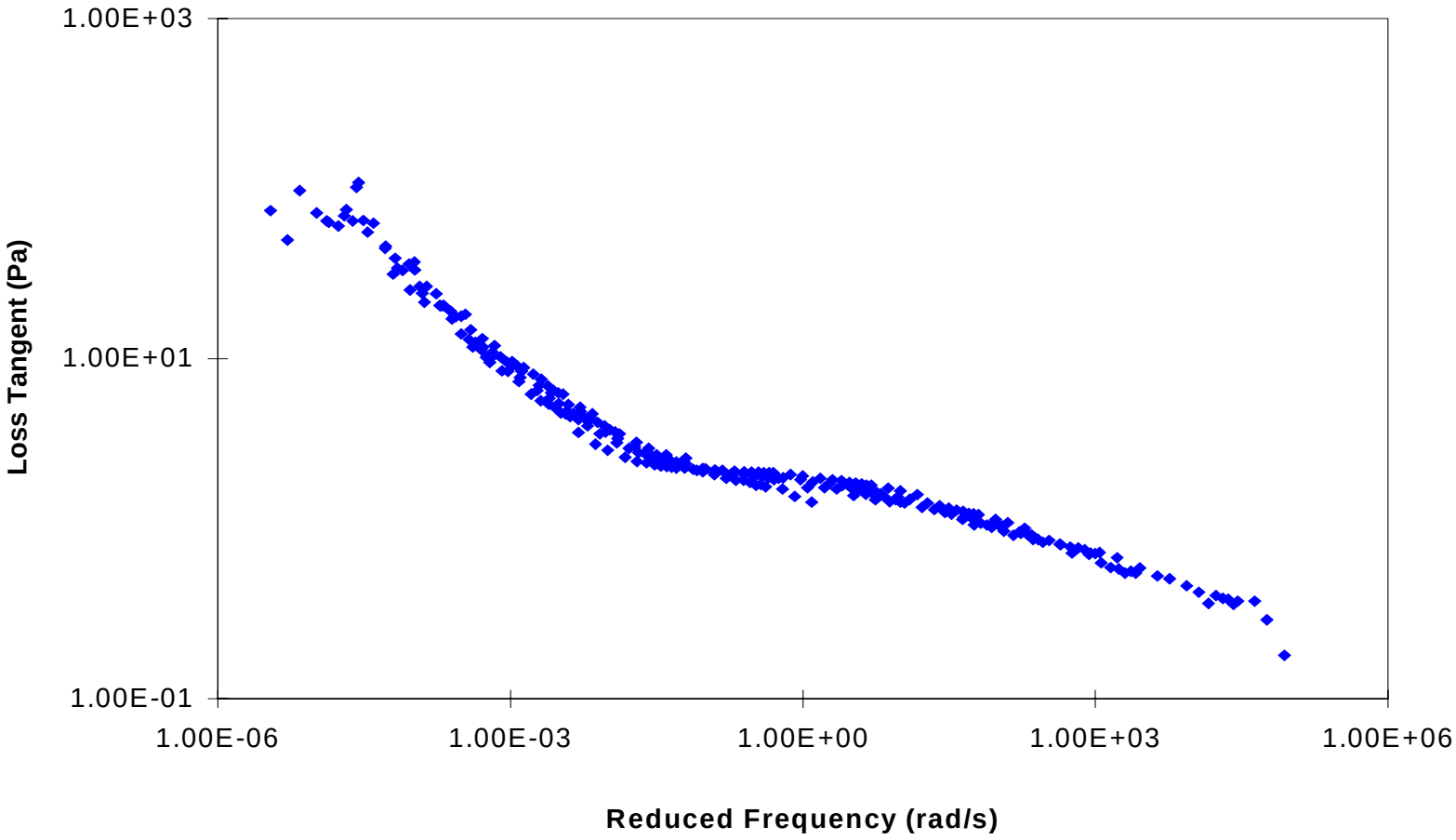

Figure 3-4. Loss tangent master curve for ARG3 (reference temperature 25°C).

Chapter 4. Model Development for Frequency Dependency of Loss Moduli

4.1 Background

During the primary analysis of the experimental data, several Master Curves were constructed for the purpose of developing a model to predict the frequency response of the loss modulus. It is previously noted that the models described in Chapter 2 for predicting the frequency response of straight asphalt binders are not applicable to polymer-modified binders (Gahvari, 1995). In most cases, considerable discrepancies were observed between the experimental results and data generated by the mathematical models for straight binders.

Gahvari (1995) attempted to fit the complex modulus data to a number of sigmodal functions. The Weibull distribution function, logistic equation, Gompertz growth model, and Mitcherlich's equation were among the different models used for this purpose. None of these models were successful in predicting the response of the complex modulus.

Similar results were encountered when applying the aforementioned models to the dynamic loss moduli data. Figure 4-1 compares the experimental data for loss moduli with data generated from the logistic model. The logistic model provides a relatively good fit for loss moduli values above 10^5 Pa. Below this value, a moderately good fit is obtained until 10^2 Pa is reached, at which point the model overestimates the experimental data. However, the Gompertz growth model was successfully used to characterize the loss moduli data over the entire range of reduced frequencies.

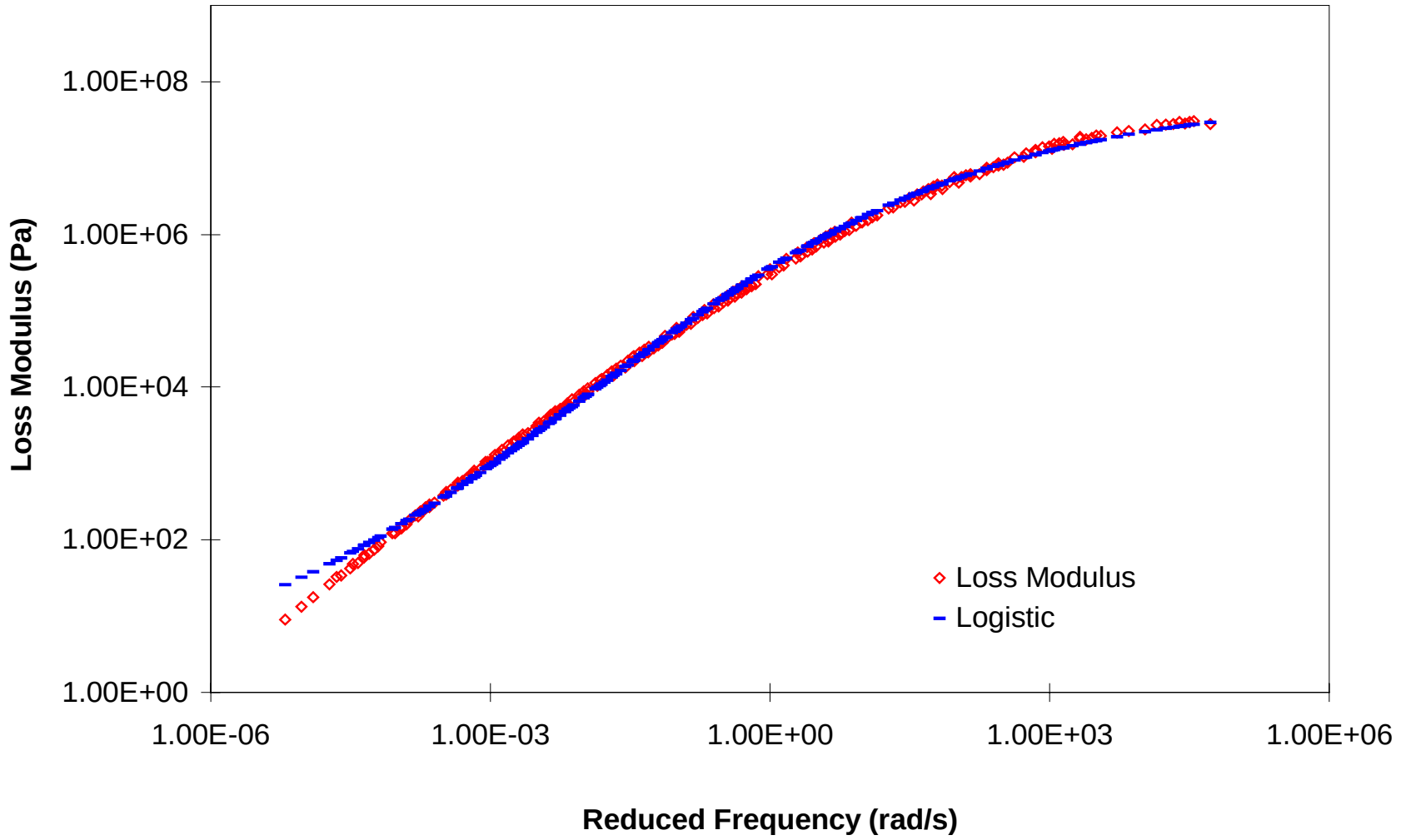

Figure 4-1. Comparison between measured dynamic loss modulus for ARC4 and results obtained from the logistic model.

4.2 Gompertz Model

The Gompertz distribution function is a sigmoidal or "S-shaped" growth curve that is widely used in biology, agriculture, and economics (Ratkowski, 1983). It is ideal for applications where growth is not symmetrical about the point of inflection. Gompertz introduced the basis for this model in 1825, and Wright (1926) used it as a growth rate model. Medawar (1940) derived it as a growth model for the heart of a chicken. The growth rate is given by:

$$\frac{df}{dx} = \gamma f(\log \alpha - \log f) \qquad (\gamma>0,\ \alpha>0) \qquad (4.1)$$

where,

f = The function in question,

γ = Proportionality factor, and

α = Maximum value of the function.

The relative growth rate declines with log (size). From the above equation, the following expression is derived:

$$f(x) = \alpha \exp[-\exp(-\gamma(x-k))] \qquad (4.2)$$

Another form of equation 4.2 is given by:

$$f(x) = \alpha \exp[-\exp(\beta - \gamma x)] \qquad (4.3)$$

where,

$\beta = \gamma k$ (from equation 4.2)

Using the log scale version of equation 4.3 to model the frequency response of the loss modulus for modified binders, did not yield adequate results. However, it was able to predict the response successfully when using an extension of equation 4.3. The model proposed to fit the loss modulus is given by:

$$\log G''(\omega) = \delta + \alpha \exp[-\exp(\beta - \gamma \log \omega)] \qquad (4.4)$$

where

δ = maximum asymptotic value of logG"(ω),

β = reparameterization variable (from Equation 4.3),

γ = proportionality factor, and

$\delta+\alpha$ = minimum asymptotic value for log G"(ω).

A graphical representation of the model constants is shown in Figure 4-2. A brief derivation of the model's behavior follows.

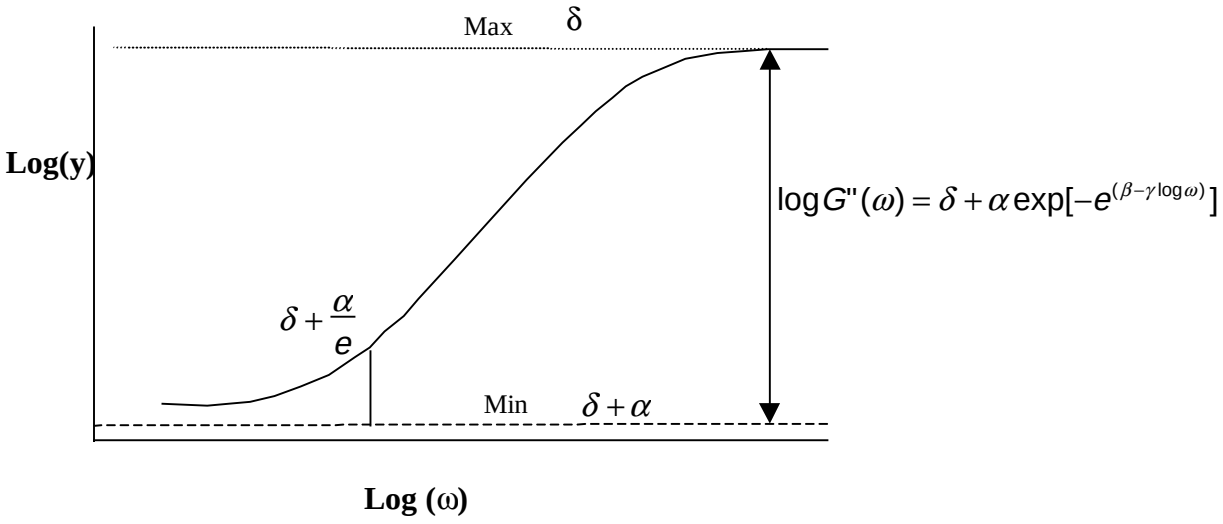

Figure 4-2. A graphical representation of proposed model for loss modulus.

The maximum value of equation 4.4 occurs as log (ω) $\rightarrow \infty$, the entire expression of (β-γlogω) $\rightarrow \infty$ and equation 4.4 is transformed into the following expression:

$$\log G''_{max}(\omega) = \delta + \alpha \exp[-\exp \infty] \quad (4.5)$$

Solving equation 4.5 yields,

$$\log G''_{max}(\omega) = \delta \quad (4.6)$$

Similarly, the expression for the minimum asymptotic value is derived when log (ω) $\rightarrow$ -∞

$$\log G''_{min}(\omega) = \delta + \alpha \quad (4.7)$$

The following expression given for the inflection point is derived when γlogω = β:

$$f = \delta + \alpha/e \quad (4.8)$$

When analyzing the data presented in chapter 3, values for model parameters were obtained by using the nonlinear regression procedure of the SAS software. A sample SAS input and out file can be found in appendixes B and C respectively. A high coefficient of determination (R^2) value for model parameters was obtained in all cases. The value of model parameters and their corresponding statistical data are presented in Table 4-1. Although a high R^2 value is an indication of how well a model is able to fit the original data, it does not give any indication of how well the model will perform in predicting the values of an independent data set. This issue is investigated in Section 4.3, using the replicate data as an independent data set.

The parameter β was higher for binders modified with block copolymers as compared to binders modified with random copolymers. For all samples, β increased with aging treatment. All polymer-modified blends, with the exception of those modified with polymer D and G, showed decreases in the value of β with increases in polymer content. β behaves as a location parameter on the y- axis, as seen in Figure 4-3.

Table 4-1. Estimated parameters for the current proposed loss modulus model based on Least Squares Analysis (Gompertz Growth Model).

Binder	α	s(α)	β	S(β)	δ	s(δ)	γ	s(γ)	r^2	MSE	DF	*n**
Auc2	-14.625	0.208	0.522	0.005	7.915	0.019	-0.177	0.002	0.999973	0.00064	254	256
Auc3	-14.095	0.357	0.509	0.009	7.906	0.035	-0.180	0.004	0.999911	0.00214	255	256
Auc4	-14.214	0.254	0.508	0.007	7.922	0.025	-0.178	0.003	0.999961	0.00935	255	256
Arc2	-16.202	0.353	0.664	0.007	7.904	0.022	-0.157	0.003	0.999963	0.00095	254	256
Arc3	-15.347	0.223	0.640	0.005	7.854	0.015	-0.168	0.002	0.999981	0.00048	254	256
Arc4	-15.010	0.303	0.634	0.007	7.794	0.020	-0.166	0.003	0.999966	0.00088	254	256
Aup3	-14.380	0.199	0.544	0.005	7.896	0.018	-0.179	0.002	0.999975	0.00062	254	270
Aup4	-14.362	0.177	0.578	0.004	7.816	0.014	-0.181	0.002	0.999985	0.00048	254	264
Aup5	-14.390	0.201	0.587	0.005	7.767	0.016	-0.178	0.002	0.999977	0.00056	254	270
Arp3	-14.956	0.199	0.673	0.005	7.779	0.018	-0.170	0.002	0.999980	0.00054	255	270
Arp4	-14.890	0.283	0.651	0.007	7.807	0.019	-0.168	0.003	0.999967	0.00087	255	270
Arp5	-14.925	0.201	0.672	0.005	7.756	0.016	-0.169	0.002	0.999982	0.00048	255	270
Aud3	-16.978	0.488	0.604	0.010	8.075	0.035	-0.150	0.004	0.999944	0.00137	254	270
Aud4	-19.002	0.673	0.644	0.012	8.151	0.042	-0.136	0.004	0.999950	0.00124	254	270
Aud5	-25.439	1.797	0.770	0.023	8.354	0.068	-0.108	0.005	0.999928	0.00182	254	270
Ard3	-18.708	0.590	0.743	0.010	7.956	0.027	-0.139	0.003	0.999959	0.00109	254	270
Ard4	-18.801	0.640	0.739	0.011	7.963	0.030	-0.136	0.003	0.999959	0.0011	255	270
Ard5	-20.054	0.905	0.754	0.015	8.015	0.039	-0.126	0.004	0.999950	0.00135	255	270
Aug3	-18.061	0.544	0.692	0.010	7.998	0.028	-0.148	0.003	0.999944	0.00146	255	270
Aug4	-21.315	1.139	0.787	0.017	8.021	0.042	-0.125	0.005	0.999924	0.00206	255	270
Aug5	-20.531	3.670	0.783	0.040	8.055	0.088	-0.121	0.007	0.999861	0.004	255	270
Arg3	-16.840	0.561	0.765	0.011	7.769	0.024	-0.153	0.004	0.999933	0.00189	269	270
Arg4	-19.172	0.777	0.829	0.013	7.849	0.026	-0.137	0.004	0.999945	0.00161	269	270
Arg5	-37.964	5.073	1.062	0.038	8.093	0.056	-0.085	0.006	0.999915	0.00255	269	269

Table 4-1. Estimated parameters for the current proposed loss modulus model based on Least Squares Analysis (Continued).

Binder	α	s(α)	β	s(β)	δ	s(δ)	γ	s(γ)	r^2	MSE	DF	*n**
Aun3	-18.113	0.750	0.653	0.014	8.120	0.046	-0.137	0.004	0.999930	0.00178	255	270
Aun4	-12.954	0.299	0.556	0.008	7.841	0.026	-0.169	0.003	0.999955	0.00121	255	270
Aun5	-11.229	0.240	0.544	0.008	7.699	0.023	-0.182	0.004	0.999953	0.00129	255	270
Arn3	-17.881	0.875	0.751	0.016	7.928	0.041	-0.137	0.005	0.999909	0.00252	255	270
Arn4	-17.839	0.970	0.770	0.017	7.881	0.041	-0.133	0.005	0.999914	0.00244	255	270
Arn5	-13.416	0.401	0.688	0.010	7.748	0.024	-0.158	0.004	0.999951	0.00144	255	270
Aus3	-16.437	0.483	0.650	0.011	7.913	0.029	-0.152	0.004	0.999942	0.00153	269	270
Aus4	-17.707	0.670	0.682	0.013	8.014	0.036	-0.140	0.004	0.999935	0.00174	269	270
Aus5	-14.987	0.523	0.637	0.013	7.822	0.034	-0.152	0.004	0.999925	0.00203	269	270
Ars3	-17.086	0.574	0.765	0.011	7.813	0.025	-0.147	0.004	0.999946	0.00155	269	270
Ars4	-17.368	0.678	0.755	0.013	7.863	0.029	-0.139	0.004	0.999940	0.00171	269	270
Ars5	-14.943	0.644	0.705	0.015	7.796	0.034	-0.148	0.005	0.999909	0.00263	269	270
Aux3	-13.180	0.225	0.555	0.006	7.891	0.019	-0.175	0.003	0.999965	0.00093	268	270
Aux4	-13.822	0.361	0.617	0.009	7.851	0.026	-0.166	0.004	0.999941	0.00163	269	270
Aux5	-12.323	0.295	0.578	0.009	7.796	0.024	-0.177	0.004	0.999935	0.00181	269	270
Arx3	-17.813	0.722	0.778	0.013	7.874	0.030	-0.142	0.004	0.999930	0.00203	269	270
Arx4	-19.810	1.393	0.822	0.022	7.979	0.044	-0.126	0.006	0.999883	0.00346	269	270
Arx5	-18.856	1.220	0.815	0.020	7.942	0.044	-0.130	0.006	0.999879	0.0036	269	270

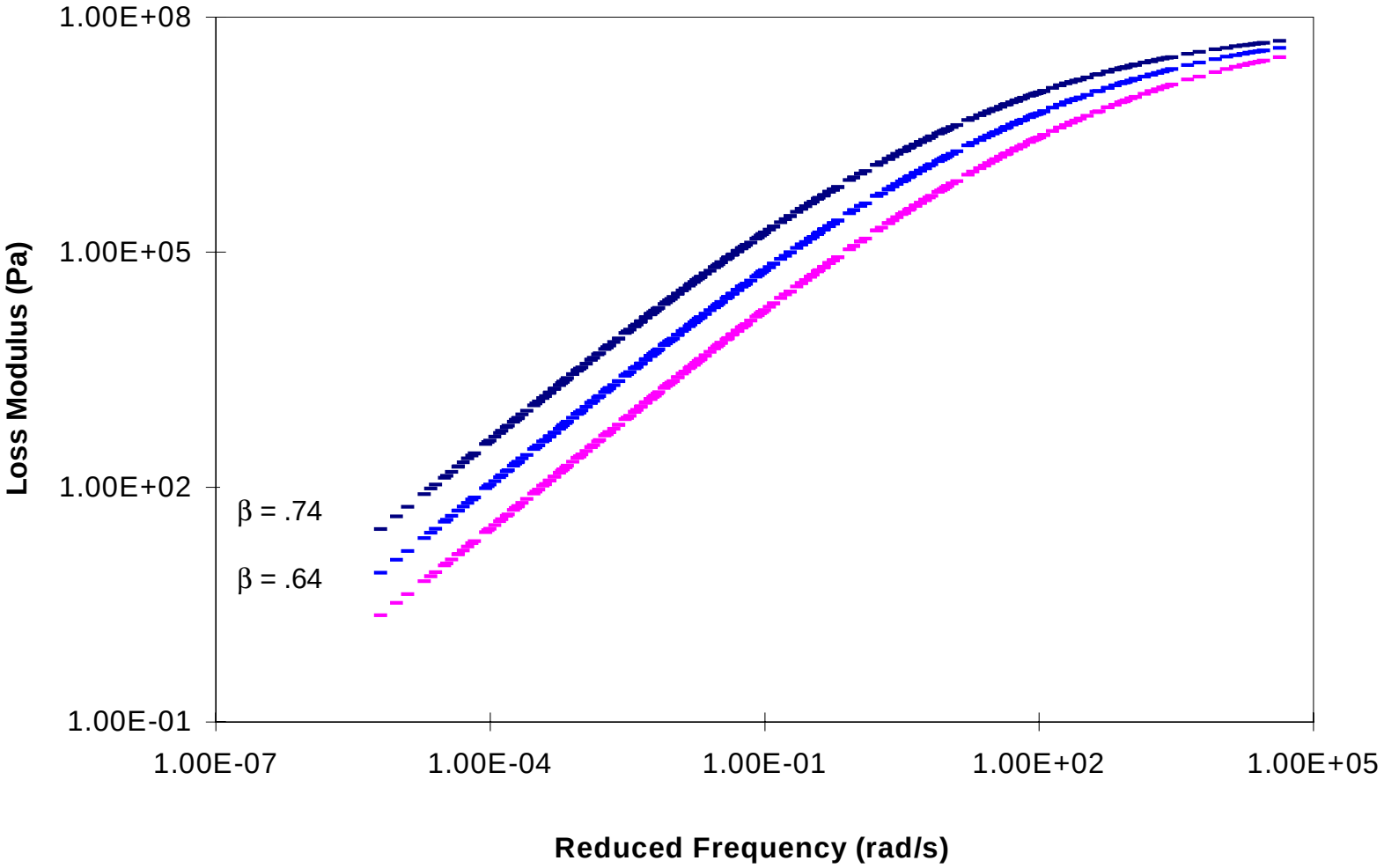

Figure 4-3. Effect of β on the location of Gompertz distribution model for ARC3.

The maximum value of δ for random copolymers and for block copolymers was approximately 8 and 8.4, respectively (i.e. $G''_{max} = 10^8$ and $10^{8.4}$). For all asphalt polymer blends, δ decreased with aging treatment. The value of δ for SBR modified binders was lower, as compared to binders that were modified with block copolymers. With the exception of polymer D and G, δ decreases with increasing polymer content. Similarly, a slight increase in α and γ with increasing polymer content was noted, with the exception of D and G. Generally, the effects of aging treatment decreased α and increased γ.

The four-parameter Gompertz model fits the experimental data throughout the entire range of reduced frequency. Figure 4-4 shows both the experimental data and results obtained from the Gompertz model for sample AUD3. In some cases, the proposed model slightly overestimates the value of the loss modulus at high frequencies, i.e. low temperatures. Comparison between experimental data and the Gompertz models for all polymer-modified blends is presented in Appendix D. The next section compares and evaluates both the Gompertz distribution function and the hyperbolic model proposed by Gahvari (1995) for characterization of the response of the dynamic loss modulus. Table 4-2 presents the values of model parameters for the hyperbolic model. These values were obtained by using the aforementioned nonlinear regression procedure of the SAS software.

4.3 Model Validation and Comparison

4.3.1 Validation

In the estimation of the model constants, only the first replica of data was used. The second set of data was used for model validation through mean squared error of prediction (MSEP). Model validation requires assessing how effective the model would be against future observations. Results from regression analysis alone cannot describe how well the model will agree with future data sets. Mean squared error of prediction incorporates both bias and variance and is a measure of the predictive capability of the model (Rawlings, 1988).

Table 4-2. Estimated parameters for the hyperbolic model proposed by Gahvari (1995) for loss modulus based on Least Squares Analysis.

Binder	D	s(d) (Pa)	log ω_d	s(log ω_d) (Pa)	LogG"$_{max}$	s(logG"$_{max}$)	r^2	MSE	DF	*n**
Auc2	3.012	0.029	4.332	0.026	7.428	0.009	0.999957	0.00101	254	256
Auc3	3.163	0.044	4.371	0.039	7.437	0.014	0.999913	0.00207	255	256
Auc4	3.268	0.028	4.439	0.025	7.439	0.009	0.999968	0.00076	255	256
Arc2	3.984	0.045	4.338	0.036	7.457	0.012	0.999929	0.00182	254	256
Arc3	3.561	0.037	4.175	0.030	7.441	0.010	0.999941	0.00153	254	256
Arc4	4.093	0.040	4.401	0.031	7.402	0.010	0.999948	0.00135	254	256
Aup3	3.102	0.026	4.242	0.023	7.441	0.008	0.999966	0.00082	254	270
Aup4	3.085	0.036	4.115	0.030	7.414	0.011	0.999932	0.00162	254	264
Aup5	3.389	0.038	4.230	0.032	7.375	0.011	0.999934	0.00162	254	270
Arp3	3.820	0.041	4.115	0.031	7.432	0.010	0.999931	0.00182	255	270
Arp4	4.010	0.040	4.267	0.031	7.434	0.010	0.999944	0.00147	255	270
Arp5	3.970	0.039	4.175	0.029	7.406	0.009	0.999945	0.00147	255	270
Aud3	3.800	0.042	4.592	0.036	7.484	0.013	0.999941	0.00146	254	270
Aud4	3.975	0.047	4.650	0.040	7.444	0.014	0.999939	0.00149	254	270
Aud5	4.763	0.072	4.885	0.059	7.468	0.020	0.999904	0.00253	254	270
Ard3	4.353	0.051	4.340	0.039	7.440	0.012	0.999923	0.00206	254	270
Ard4	4.642	0.052	4.472	0.039	7.431	0.012	0.999936	0.00173	255	270
Ard5	5.286	0.057	4.746	0.043	7.429	0.013	0.999943	0.00153	255	270
Aug3	3.685	0.050	4.324	0.039	7.505	0.013	0.999888	0.00293	255	270
Aug4	4.846	0.063	4.561	0.046	7.445	0.014	0.999902	0.00269	255	270
Aug5	5.926	0.088	4.891	0.061	7.505	0.018	0.999882	0.00337	255	270
Arg3	4.500	0.050	4.238	0.035	7.497	0.011	0.999906	0.00266	269	270
Arg4	4.953	0.060	4.233	0.040	7.452	0.012	0.999903	0.00283	269	270
Arg5	7.046	0.107	4.790	0.065	7.461	0.017	0.999857	0.00427	269	269

Table 4-2. Estimated parameters for the hyperbolic model proposed by Gahvari (1995) for loss modulus based on Least Squares Analysis (Continued).

Binder	d	S(d) (Pa)	log ω_d	s(log ω_d) (Pa)	logG"$_{max}$	s(logG"$_{max}$)	r^2	MSE	DF	*n**
Aun3	4.655	0.050	4.810	0.041	7.496	0.014	0.999947	0.00135	255	270
Aun4	5.869	0.050	5.199	0.031	7.536	0.012	0.999970	0.00081	255	270
Aun5	6.940	0.082	5.391	0.057	7.532	0.017	0.999946	0.00149	255	270
Arn3	5.353	0.064	4.573	0.045	7.456	0.013	0.999922	0.00215	255	270
Arn4	6.004	0.071	4.691	0.048	7.433	0.014	0.999929	0.00202	255	270
Arn5	6.887	0.054	4.910	0.035	7.473	0.010	0.999970	0.00086	255	270
Aus3	4.309	0.041	4.602	0.032	7.462	0.010	0.999945	0.00143	269	270
Aus4	4.842	0.049	4.756	0.038	7.493	0.012	0.999944	0.00149	269	270
Aus5	6.018	0.057	5.083	0.041	7.453	0.012	0.999954	0.00125	269	270
Ars3	4.904	0.049	4.333	0.034	7.436	0.010	0.999935	0.00153	269	270
Ars4	5.775	0.054	4.634	0.037	7.455	0.011	0.999943	0.00162	269	270
Ars5	6.417	0.066	4.884	0.043	7.458	0.012	0.999942	0.00168	269	270
Aux3	4.905	0.029	4.875	0.022	7.576	0.007	0.999982	0.00491	268	270
Aux4	5.287	0.041	4.796	0.030	7.522	0.009	0.999968	0.00089	269	270
Aux5	5.843	0.051	4.982	0.036	7.547	0.011	0.999960	0.00113	269	270
Arx3	5.004	0.055	4.360	0.038	7.469	0.011	0.999923	0.00221	269	270
Arx4	5.873	0.078	4.584	0.052	7.511	0.015	0.999894	0.00314	269	270
Arx5	5.931	0.075	4.540	0.049	7.506	0.014	0.999901	0.00291	269	270

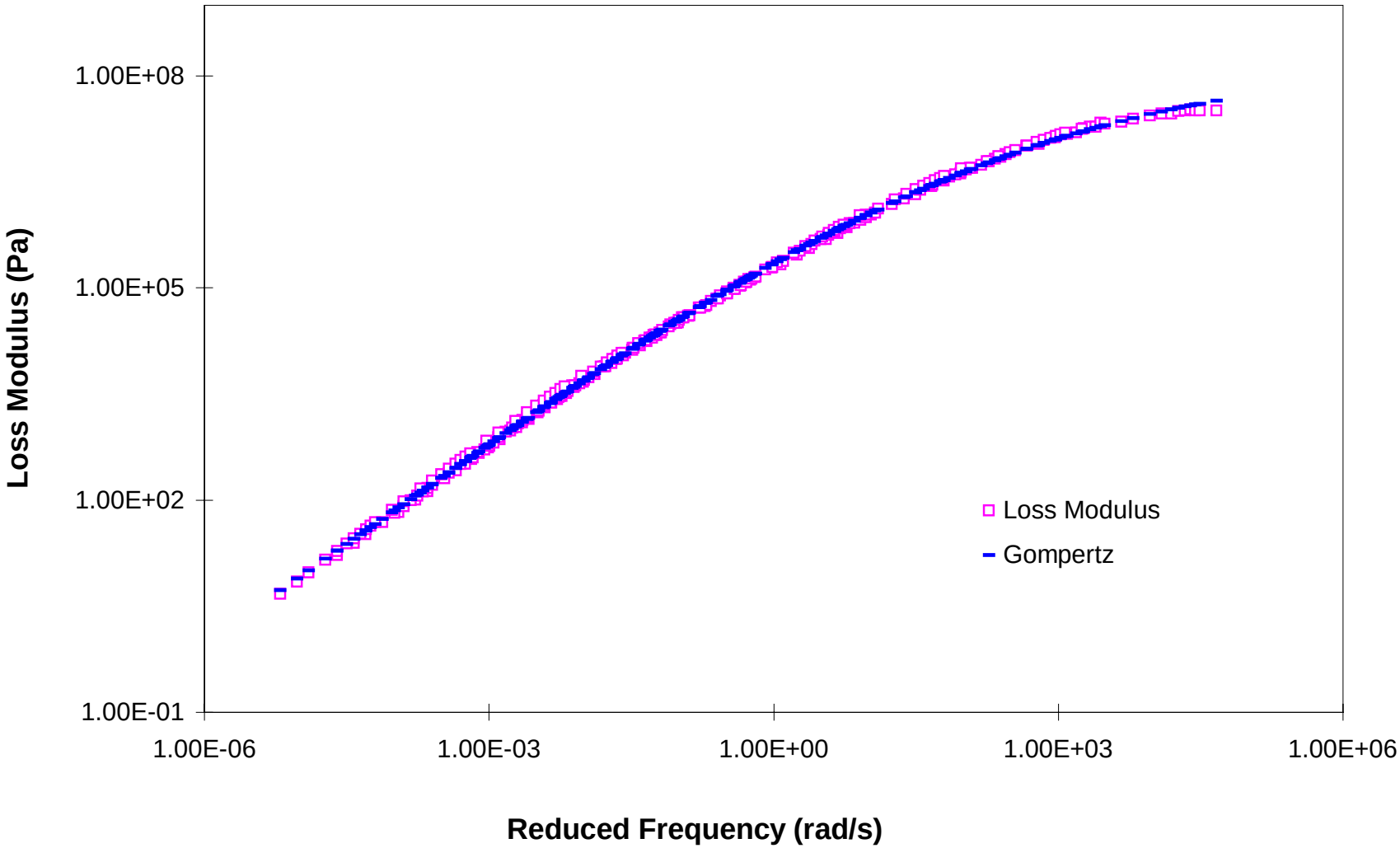

Figure 4-4. Comparison between measured dynamic loss modulus for AUD3 and results obtained from the Gompertz Growth model.

Mean squared error of prediction can be defined as the average squared difference between independent observations and the model-generated data sets. The equation for MSEP can be given by:

$$MSEP = \frac{\sum \delta_i^2}{n} \tag{4.9}$$

where,

δ_i = difference between independent observations and predicted values for the ith validation case; and

n = number of observations in the independent data set.

To validate the models, values of model parameters presented in Equations (2.31) and (4.4) were determined using the first data set. The second data set was considered to be the independent or validation data set. The model parameters from the first data set were used to predict loss moduli values with the frequency (x-axis) input being that of the independent data set. The predicted loss moduli values were compared with the experiment data obtained from the replicate set.

The computed MSEP are included in Table 4-3. The resulted small values for MSEP indicate that both models are probably valid for other data sets, within the specified moduli and frequency range.

4.3.2 Model Comparison

The Gompertz distribution model and the Hyperbolic model are both able to fit and predict the frequency response of the of loss moduli for all modified binders used in this study. This is evident by the resulted small values of MSEP (Table 4-3) and MSE. The R^2 values are close to one for all parameters (as presented in Tables 4-1 and 4-2). The MSE values indicate no preference to either model in its capability of fitting the original data from which its constants were derived. The Gompertz distribution model generally

yields lower MSEP values, indicating that it is more suitable for predicting the values of future data sets.

Figure 4-5 presents the experimental data for AUD3 and the results obtained from the hyperbolic model. Although the model fits the data well, its application is restricted to moduli values below $10^{7.5}$. As stated in Section 2.8.5, since the model is hyperbolic, it is symmetric about the line $\log\omega = \log\omega_d$. However, the shape of the loss modulus master curve is not symmetrical in shape with respect to the peak point. Figure 4-6 shows the behavior of both, the hyperbolic and the Gompertz distribution model, when the frequency axis is extended (i.e., extremely cold and hot conditions). The experimental data window, shown in Figure 4-6, is small compared to the overall behavior of both the hyperbolic and the Gompetz distribution model. It is noted that the Gompertz distribution model extends to an asymptotic value equal to the parameter δ. The lower asymptote occurs at extremely low frequencies. At high frequencies, the Gompertz distribution model is able to more accurately represent the behavior of polymer-modified binders.

4.4 Model Limitations

It is clearly recognized that the loss modulus does not adequately describe the frequency dependence of modified asphalt binders. As noted in section 2.6, the complex modulus, G* consists of two parts: the storage modulus, G', and the loss modulus, G". Simple mathematical manipulation can be used to show that both G' and G" are functions of G* and δ, the phase angle. It is also clear that any combination of G" or G' and δ can be used to describe the complex modulus. Therefore, any model developed to predict G" should be able to accurately predict G' for a given δ. The two values G' and G" are interdependent and thus any model development should be applied to both parameters. Due to several factors including time constraints, further analysis could not be accomplished at this time for the completion of this thesis.

Table 4-3. Evaluation of Mean Squared Error Prediction for both current and previous proposed models for loss modulus.

Binder	MSEP		n*	Binder	MSEP		n*
	Gompertz	Hyperbolic			Gompertz	Hyperbolic	
Auc2	0.000645	0.002733	256	**Arg3**	0.001895	0.003316	270
Auc3	0.002137	0.002310	256	**Arg4**	0.001610	0.003593	270
Auc4	0.009350	0.000953	256	**Arg5**	0.002548	0.014697	269
Arc2	0.000950	0.004955	256	**Aun3**	0.001784	0.002131	270
Arc3	0.000485	0.001124	256	**Aun4**	0.001206	0.001483	270
Arc4	0.000881	0.001348	256	**Aun5**	0.001291	0.002255	270
Aup3	0.000618	0.000985	270	**Arn3**	0.002522	0.007312	270
Aup4	0.000485	0.001276	264	**Arn4**	0.002444	0.002781	270
Aup5	0.000560	0.001977	270	**Arn5**	0.001441	0.001372	270
Arp3	0.000543	0.005398	270	**Aus3**	0.001533	0.002313	270
Arp4	0.000872	0.004986	270	**Aus4**	0.001740	0.002532	270
Arp5	0.000476	0.002951	270	**Aus5**	0.002029	0.003133	270
Aud3	0.001373	0.002922	270	**Ars3**	0.001550	0.001703	270
Aud4	0.001240	0.002590	270	**Ars4**	0.001714	0.005651	270
Aud5	0.001817	0.005592	270	**Ars5**	0.002628	0.002530	270
Ard3	0.001092	0.002217	270	**Aux3**	0.000928	0.000746	270
Ard4	0.001096	0.002411	270	**Aux4**	0.001633	0.001599	270
Ard5	0.001352	0.003973	270	**Aux5**	0.001814	0.001204	270
Aug3	0.001465	0.004018	270	**Arx3**	0.002027	0.004217	270
Aug4	0.002061	0.002708	270	**Arx4**	0.003460	0.002962	270
Aug5	0.003998	0.003389	270	**Arx5**	0.003599	0.004062	270

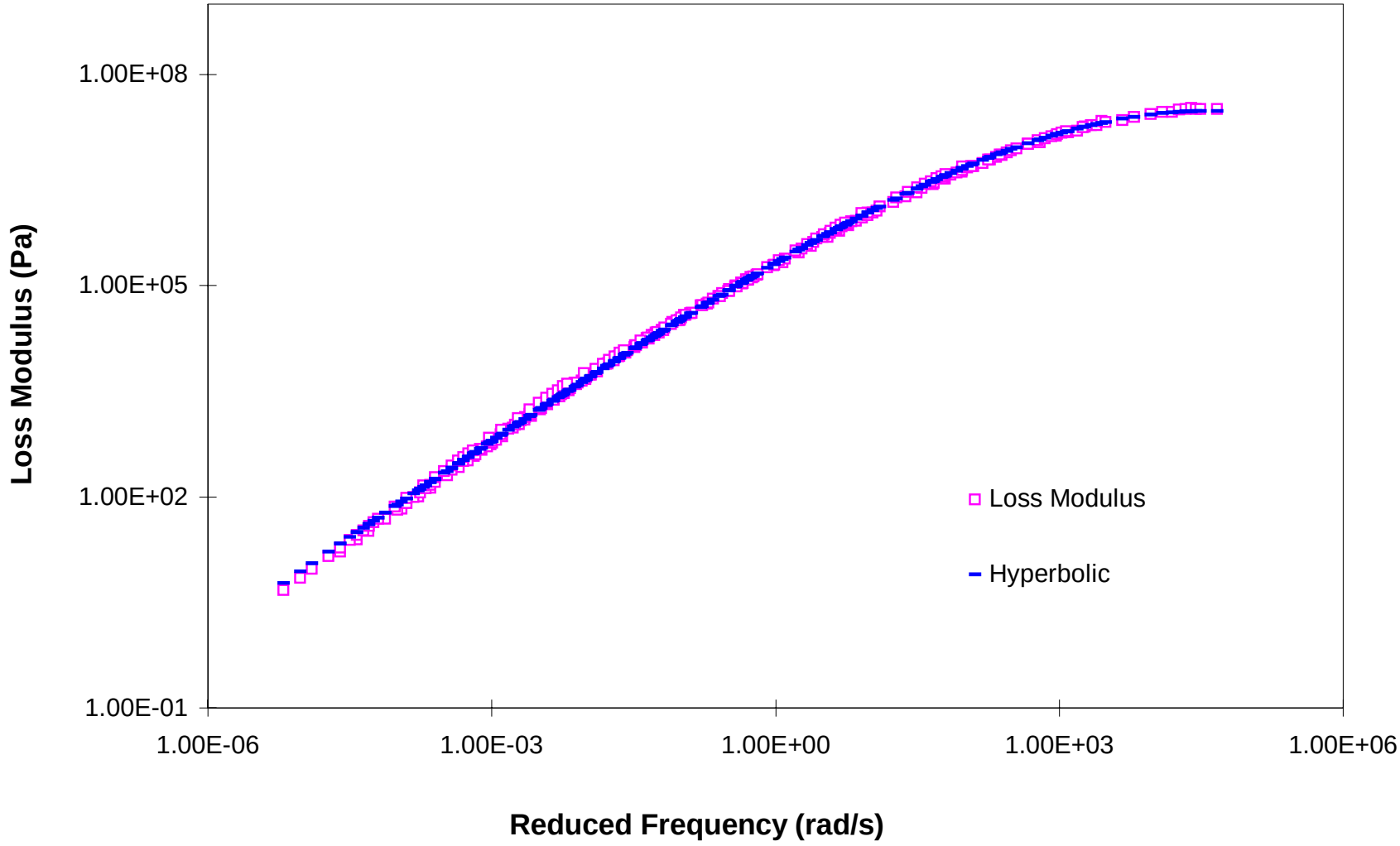

Figure 4-5. Comparison between measured dynamic loss modulus for AUD3 and results obtained from the hyperbolic model.

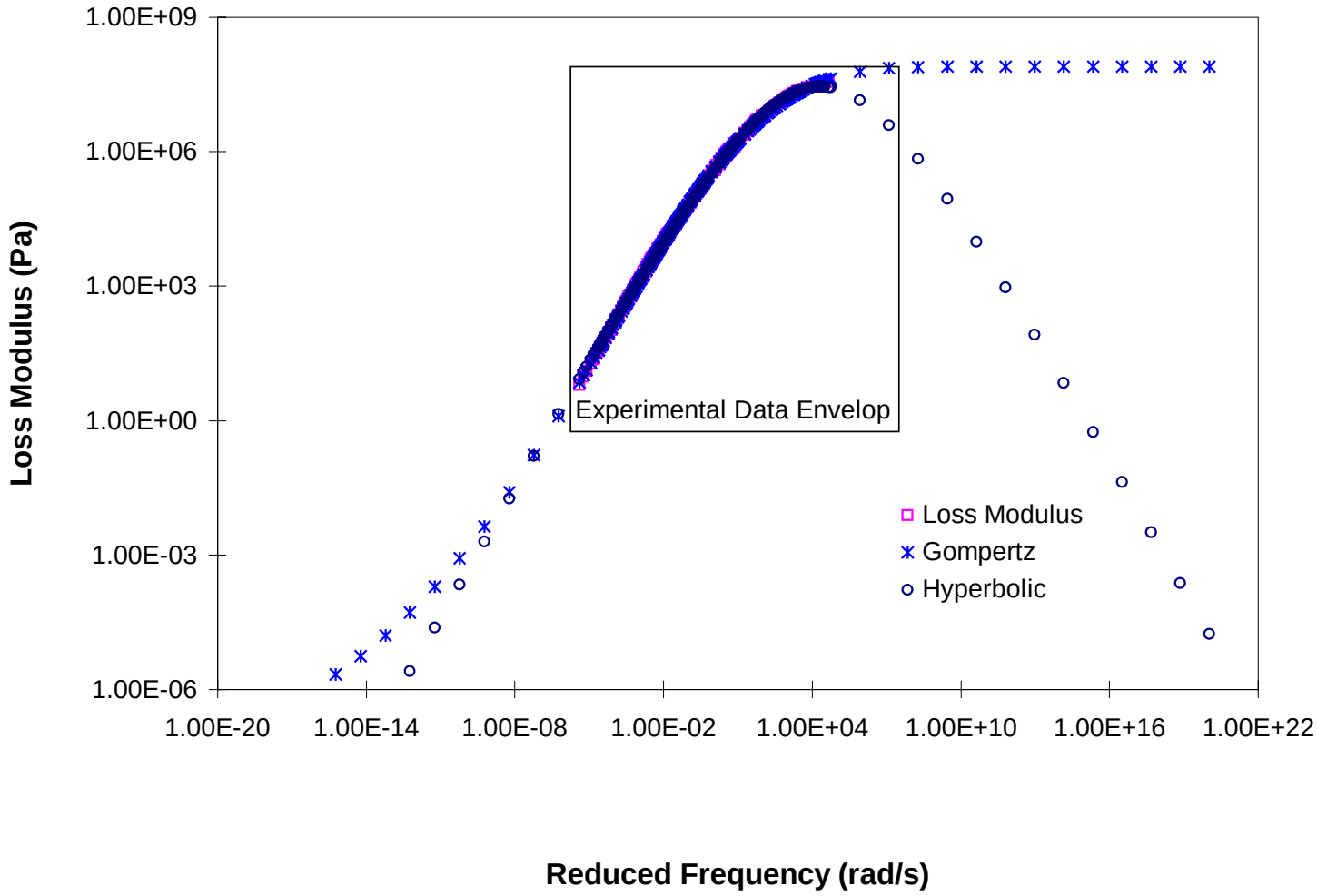

Figure 4-6. Hyperbolic and Gompertz distribution models with an extended frequency range.

Chapter 5. Summary, Findings, Conclusions, and Recommendations

5.1 Summary

The goal of this study was to develop a model that could accurately predict the linear viscoelastic response of polymer-modified binders. Data from dynamic mechanical analysis on modified binders at temperatures between 5 and 75°C and frequencies ranging from 0.06 to 0188.5 rad/s, were reduced to dynamic master curves of moduli. Two sets of dynamic moduli master curves were constructed, one for the development of a model, the other for model validation. A statistical model was developed to predict the linear viscoelastic response of the loss modulus of polymer-modified binders over the entire frequency range. The developed model is a four parameter Gompertz distribution model. Model parameters were derived using the non-linear regression function of the SAS software program. The developed model was statistically compared to a hyperbolic model proposed by Gahvari (1995). Mean Squared Error of prediction was used to measure how effective both the developed model and the hyperbolic model were in predicting future data sets. The limitations and appropriate situations for use associated with the developed model were also assessed.

5.2 Findings

Simple time-temperature superposition was found to be applicable to polymer-modified asphalts. This is in agreement with the previous research performed at Virginia Tech (Gahvari and Al-Qadi, 1996). On a log-log scale, for the frequency range used in this study, the loss modulus was found to exhibit the behavior of a sigmoidal growth curve. It was confirmed that the hyperbolic model proposed by Gahvari (1995) to predict loss shear moduli values was limited to $G'' \leq 10^{7.5}$ Pa. A four-parameter Gompertz

Distribution model is able to predict the dynamic loss modulus with a slightly higher degree of accuracy as compared to the hyperbolic model. However, both models are statistically developed and could not predict G' for a known δ.

5.3 Conclusions

Mathematical models for frequency dependence of unmodified binders are generally not applicable to the characterization of polymer-modified binders. The hyperbolic model proposed by Gahvari in 1995 was found to fit an experimental data, generated at Virginia Tech in 1994, over the entire range of the reduced frequencies up to G" $\leq 10^{7.5}$ Pa. However, it is hyperbolic and symmetric to the line $\log\omega = \log\omega_d$. Therefore, a new model was developed to predict the frequency dependence of response of polymer-modified binders at intermediate to high service temperatures. The model is based on Gompertz distribution. The model was found to have a high prediction capability over the entire range of reduced frequencies. However, it is noted that the model is statistically developed and thus G' may not be accurately determined if δ is known.

5.4 Recommendations

Based on the findings and conclusions of the present study, the following guidelines for further research is recommended:

- Development of a model for G' and G" that is able to accurately predict G* and is a function of δ.
- Investigation into the effects of long term aging of polymer-modified binders as it pertains to the previously mentioned models developed at Virginia Tech.
- Applicability of the developed models in the prediction of dynamic moduli response of binders modified with polymers or other additives dissimilar to those used in this study.

References

AASHTO Designation TP5, “Standard Test Method for Determining the Rheological Properties of Asphalt Binder Using a Dynamic Shear Rheometer (DSR),” 1994 AASHTO Provisional Standards.

Aklonis, J. J. and MacKnight, Intorduction to Polymer Viscoelasticity, John Wiley & Sons, Inc., 1983.

Amoco Oil Company, *Technical Data Sheets, 1995.*

Anderson, D. A., Christensen, D. W., and Bahia, H., “Physical Properties of Asphalt Cement and the Development of Performance Related Specifications,” *Proceedings of the Association of Asphalt Paving Technologists, V. 60,* 1991,pp. 437-475.

Anderson, D. A., Christensen, D. W., Roque, R., and Robyak, R. A., "Rheological Properties of Polymer-Modified Emulsion Residue,” Polymer Modified Asphalt Binders, STP 1108, Wardlaw, K. R. and Shuler, S., Editors, ASTM, Philadelphia, PA, 1992, pp. 21-34.

Andrews, R. D., Hofman-Bang, N., and Tobolosky, A. V., “Elastovicous Properties of Polyisobutylene. I. Relaxation of Stress in Whole Polymers of Different Moleculsr Weights at Eleavated Temperatures,” *Journal of Polymer Science, V. 3,* No. 5, pp. 669-692.

ASTM D 1754-87, “Standard Test Method for Effect of Heat and Air on Asphaltic Materials (Thin-Film Oven Test),” *1991 Annual Book of ASTM Standards, V. 04.03*, ASTM, Philadelphia, PA, pp. 231-233.

ASTM D 2170-85, (1991), “Standard Test Method for Kinematic Viscosity of Asphalts (Bitumens),” *1991 Annual Book of ASTM Standards, V. 04.03*, ASTM, Philadelphia, PA, pp. 260-268.

ASTM D 2171-88, (1991), “Standard Test Method for Viscosity of Asphalts by Vacuum Capillary Viscometer,” *1991 Annual Book of ASTM Standards, V. 04.03*, ASTM, Philadelphia, PA, pp. 269-275.

ASTM D 2872-88, (1991), “Standard Test Method for Effect of Heat and Air on a Moving Film of Asphalt (Rolling Thin Film Oven Test),” *1991 Annual Book of ASTM Standards, V. 04.03*, ASTM, Philadelphia, PA, pp. 315-318.

ASTM D 5-86, (1991), “Standard Test Method for Penetration of Bituminous Materials,” *1991 Annual Book of ASTM Standards, V. 04.03*, ASTM, Philadelphia, PA, pp. 71-73.

Bonemazzi, F., Barga, V., Corrieri, R., Giavarini, C., and Sartori, F., “Characteristics of Polymers and Polymer-Modified Binders,” Transportation Research Record No. 1535, Transportation Research Board, National Academy Press, Washington, 1996, pp. 36-47.

Bouldin, M. G. and Collins, J. H., "Influence of Binder Rheology on Rut Resistance of Polymer Modified and Unmodified Hot-Mix Asphalt”, Polymer Modified Asphalt Binders, STP 1108, Wardlaw, K. R. and Shuler, S., Editors, ASTM, Philadelphia, PA, 1992, pp. 50-60.

Brodnyan, J. G., Gaskins, F. H., Philippoff, W., and Thelen, E., “The Rheology of Asphalt, III. Dynamic Mechanical Properties of Asphalt,” *Transactions of the Society of Rheology, V. 4*, 1960, pp. 279-296.

Brule, B., “Polymer-Modified Asphalt Cemenets Used in the Road Construction Industry: Basic Principles,” Transportation Research Record No. 1535, Transportation Research Board, National Academy Press, Washington, 1996, pp. 48-53.

Christensen, D. W. and Anderson, D. A., “Interpretation of Dynamic Test Data for Paving Grade Asphalt Cements,” Transportation Research Record No. 1535, Transportation Research Board, National Academy Press, Washington, 1996, pp. 54-60.

Christensen, D. W., and Anderson, D. A., “Interpretation of Dynamic Mechanical Test Data for Paving Grade Asphalt Cements,” Proceedings of the Association of Asphalt Paving Technologists, *V. 61*, 1992, pp. 67-115.

Collins, J. H., and Bouldin, M. G., “Stability of Straight and Polymer Modified Asphalts,” Asphalt and Asphalt Additives, Transportation Research Record No. 1342, Transportation Research Board, National Academy Press, Washington, D.C., 1992, pp. 92-100.

Collins, J. H., and Mikols, W. J., “Block Copolymer Modification of Asphalt intended for Surface Dressing Applications,” *Proceedings of the Association of Asphalt Paving Technologists, V. 54*, 1985, pp. 1-17.

Collins, J. H., Bouldin, M. G., Gelles, R., and Berker, A., “Improved Performance of Paving Asphalts by Polymer Modification,” Proceedings of the Association of Asphalt Paving Technologists, *V. 60*, 1991, pp. 43-79.

Dhalaan, M. A, Balghumain, Dhubaib, I. A., and Noureldin, S. A., “Field Trails with Polymer Modidied Asphalts in Suadi Arabia,” Polymer Modified Asphalt Binders, STP 1108, Wardlaw, K. R. and Shuler, S., Editors, ASTM, Philadelphia, PA, 1992, pp. 202-223.

Dickinson, E. J., and Witt, H. P., “The Dynamic Shear Modulus of Paving Asphalts as a function of Frequency,” Transactions of the Society of Rheology, 1974, *V. 18*, No. 4, pp. 591-606.

Dobson, G. R., “The Dynamic Mechanical Properties of Bitumen,” Proceedings of the Association of Asphalt Paving Technologists, *V. 38*, 1969, pp. 123-139.

Federal Highway Administration, Highway Statistics, U.S. Department of Transportation, Washington, D.C., 1990

Ferry, J. D., Viscoelastic Properties of Polymers, 2nd Edition, John Wiley & Sons, 1970.

Fesko, D. J. and Tschpegl, N. W., “Time-Temperature Superposition in Thermorheologically Complex Materials,” *Journal of Polymer Science,* Part C, No. 35, Viscoelastic Relaxation in Polymers, 1971, pp. 51-69.

Fleckenstein, J. L., Mahboub, K., and Allen D. L., "Performance of Polymer Modified Asphalt Mixes in Kentucky,” Polymer Modified Asphalt Binders, STP 1108, Wardlaw, K. R. and Shuler, S., Editors, ASTM, Philadelphia, PA, 1992, pp. 173-185.

Freeman, R. B., Newman, K. J., and Ahlirich, R. C., "Effect of polymer Modifiers on Dense-Graded, Heavy-Duty Pavement Mixtures,” Proceedings of the 8th International Conference on Asphalt Pavements, International Society for Asphalt Pavements, Seattle, WA, 1997, pp. 1289-1307.

Gahvari, F., Modeling of The Linear Viscoelastic Response of Polymer Modified Asphalt Binders at Intermediate and High Temperatures, Ph.D. Dissertation, The Via Department of Civil Engineering, Virginia Polytechnic Institute and State University, Blacksburg, VA, 1995.

Holden, G., Bishop, E. T., and Legge, N. R., “Thermoplastic Elastomers,” *Journal of Polymer Science,* Part C, No. 26, 1969, pp. 37-57.

Huang, S., Huh, D., Robertson, R. E., Tia, M.,”Aging Effects on Temperature Susceptibility of Pollymer Modified Asphalts,” Materials for the New Millienium, K. P. Chaung, Ed., ASCE, V. 2 , 1996, pp. 1366-1378.

Jongepier, R., and Kuilman, B., “Characteristics of the Rheology of Bitumen,” Proceedings of the Association of Asphalt Paving Technologists, *V. 38*, 1969, pp. 99-122.

King, G. N., and King, H. W., “Polymer Modified Asphalts, an Overview,” *Solutions for Pavement Rehabilitation Problems,* ASCE, New York, NY, 1986, pp. 240-254.

King, G. N., King, H. W., Harders O., Aradnd W., and Planche, P., "Influence of Asphalt Grade and Polymer Concentration on the Low Temperature Performance of Polymer Modified Asphalt", Proceedings of the Asphalt Paving Technologists, V*. 62*, 1993, pp. 1-22.

Krebs, R. D., and Walker, R. D., Highway Materials*,* Mc-Graw Hill, 1971.

Leaderman, H. “Elastic and Creep Properties of Filamentous Materials and Other High Polymers,” *The Textile Foundation Inc.,* Washington, D. C., 1943, p. 175.

Lewandowski, L. H., "Polymer Modification of Paving Asphalt Binders", Rubber Chemistry and Technology, V. 67, No. 3, 1994, pp. 447-480.

Little, D. N., "Analysis of The influence of Low Density Polyethylene Modification (Novaphalt) of Asphalt Concrete on Mixture Shear Strength and Creep Deformation Potential,” Polymer Modified Asphalt Binders, STP 1108, Wardlaw, K. R. and Shuler, S., Editors, ASTM, Philadelphia, PA, 1992, pp. 187-202.

Lytton, R. L., “Infrastructure: Back to Cadbury or on to Camelot,” Presented at Texas A&M University, College station, TX, 1991.

Maccarrone, S., Ky, A. V., and Gnanaseelan, G. P., “Permanent Deformation and Fatigue Properties of Polymer Modified Asphalt Mixes,” Proceedings of the 8th International Conference on Asphalt Pavements, International Society for Asphalt Pavements, Seattle, WA, 1997, pp. 1545-1554.

Marasteanu, M. O. and Anderson, D. A., “Improved Model for Butimens Rheological Characterization,” Submitted to the Eurobitume Workshop on Performance Related Properties for Bituminous Binders, Luxembourg, 1999.

McKay, K. W., Gross, W. A., Diehl, C. F., "The Influence of Styrene-Butadiene Diblock Copolymer on Styrene-Butadiene-Styrene Triblock Copolymer Viscoelastic Properties

and Product Performance," Journal of Applied Polymer Science, V. 56, May 1995, pp. 947-958.

Nahas, N. C., Bardet J., Bernard E., and Siano, D. B., “Polymer Modified Asphalts for High Performance Hot Mix Pavement Binders,” Proceedings of the Asphalt Paving Technologists, *V. 59*, 1990, pp. 509-525.

Ninomya, K., and Ferry, J. D., “Some Approximate Equations Useful in the Phenomenological Treatment of Linear Viscoelastic Data,” *Journal of Colloid Science,* Vol. 14, 1959, pp. 36-48.

Oliver, J. W., and Tredrea, P. F., “The Change in Properties of Polymer Modified Binders with Simulated Field Exposure,” Proceedings of the Asphalt Paving Technologists, *V. 66*, 1997, pp. 570-603.

Ponniah, J. and Gerhard K., “Polymer-Modified Asphalt Pavements in Ontario: Performance and Cost-Effectiveness” Transportation Research Record No. 1545, Transportation Research Board, National Academy Press, Washington, 1996, pp. 151-160.

Ratkowsky, D. A., Handbook of Linear Regression Models, Marcel Dekker, Inc., New York, NY, 1990.

Ratkowsky, D. A., Nonlinear Regression Models, Marcel Dekker, Inc., New York, NY, 1983.

Rawlings, J. O., Applied Regression Analysis: A Research Tool, Wadsworth & Brooks/Cole Advanced Books & Software, Pacific Grove, CA, 1988.

Roberts, F. L., Kandhal, P. S., Brown, E. R., Lee, D. Y., and Kennedy, T. W., Hot Mix Asphalt, Mixture Design and Construction, NAPA Education Foundation, 1996.

Schwarl, F. and Sraverman, A. J., “Time-Temperature Dependence of Linear Viscoelastic Behavior,” *Journal of Applied Physics, V. 23,* No. 8, 1952, pp.838-843.

Seber, G. F. and Wild, C. J., Nonlinear Regression Modeling, John Wiley & Sons, New York, NY, 1989.

Serfass, J. P., Joly, A., and Sammons, J., “SBS-Modified Asphalt for Surface Dressing - A Comparison Between Hot-Applied and Emulsified Binders,” Polymer Modified Asphalt Binders, STP 1108, ASTM, Philadelphia, PA, 1992, pp. 281-308

Shell Chemical Company, (1992), *Kraton Thermoplastic Rubber, Typical Properties.*

Shuler, T. S., Collins, J. H., and Kirkpatrick, J. P., “Polymer Modified Asphalt Properties Related to Asphalt Concrete Performance,” Asphalt Rheology, Relationship to Mixture, STP 941, ASTM, Philadelphia, PA, 1987, pp. 179-193.

Srivastava, A., Hopman, P. C., Molenaar, A. A., "SBS Polymer Modified Asphalt Binder and Its Implications on Overlay Design,” Polymer Modified Asphalt Binders, STP 1108, Wardlaw, K. R. and Shuler, S., Editors, ASTM, Philadelphia, PA, 1992, pp. 309-329.

Stastna, J., Zanzotto, L., and Kennepohl G., “Dynamic Material Functions and the Structure of Asphalts,” Transportation Research Record No. 1535, Transportation Research Board, National Academy Press, Washington, 1996, pp. 3-9.

Stock, A. F. and Arand W., "Low Temperature Cracking in Polymer Modified Binders,” Proceedings of the Asphalt Paving Technologists, *V. 62*, 1993, pp. 23-53.

Tayebali, A. H., Goodrich, J. L., Sousa, J. B., and Monismith, C. L., “Influence of the Rheological Properties of Modified Asphalt Binders on the Load Deformation Characteristics of the Binder-Aggregate Mixtures,” Polymer Modified Asphalt Binders, STP 1108, Wardlaw, K. R. and Shuler, S., Editors, ASTM, Philadelphia, PA, 1992, pp. 77-98.

Thomas, K. P., Harnsberger, P. M., Robertson, R. E., Lukens, L. A. and Peters, V. J., "Comparative Field Evaluation of Shale Oil-Modified Asphalts with Polymer-Modified Asphalts," Transportation Research Record No. 1545, Transportation Research Board, National Academy Press, Washington, 1996, pp. 120-125

Thompson, D. C., Bituminous Materials: Asphalt Tars and Pitches, Robert Krieger Publishing Company, *V. 1*., 1979

Tobolosky, A. V., "Stress Relaxation Studies of the Viscoelastic Properties of Polymers," *Journal of Applied Physics, V. 27,* No. 7, 1956, pp. 673-685.

Wada, Y., and Hirose, H., "Glass Transition Phenomena and Rheological Properties of Petroleum Asphalt," Journal of Physical Society of Japan*, V. 15*, No. 10, 1960, pp. 1885-1894.

Williams, M. L., Landel, R. F., and Ferry, J. D., "The Temperature Dependence of Relaxation Mechanism in Amorphous Polymers and Other Glass-Forming Liquids," Journal of the American Chemical Society*, V. 77*, 1955, pp. 3701-3706.

Zhou, H., Nodes, S. E., and Nichols, J. E., "Evaluation of Three Polymer Modified Asphalt Concretes," Transportation Research Record No. 1454, Transportation Research Board, National Academy Press, Washington, 1994, pp. 181-192.

Appendix A. Dynamic Moduli isothermal, master curve (with reference temperature of 25°C), and shift factor, a_T

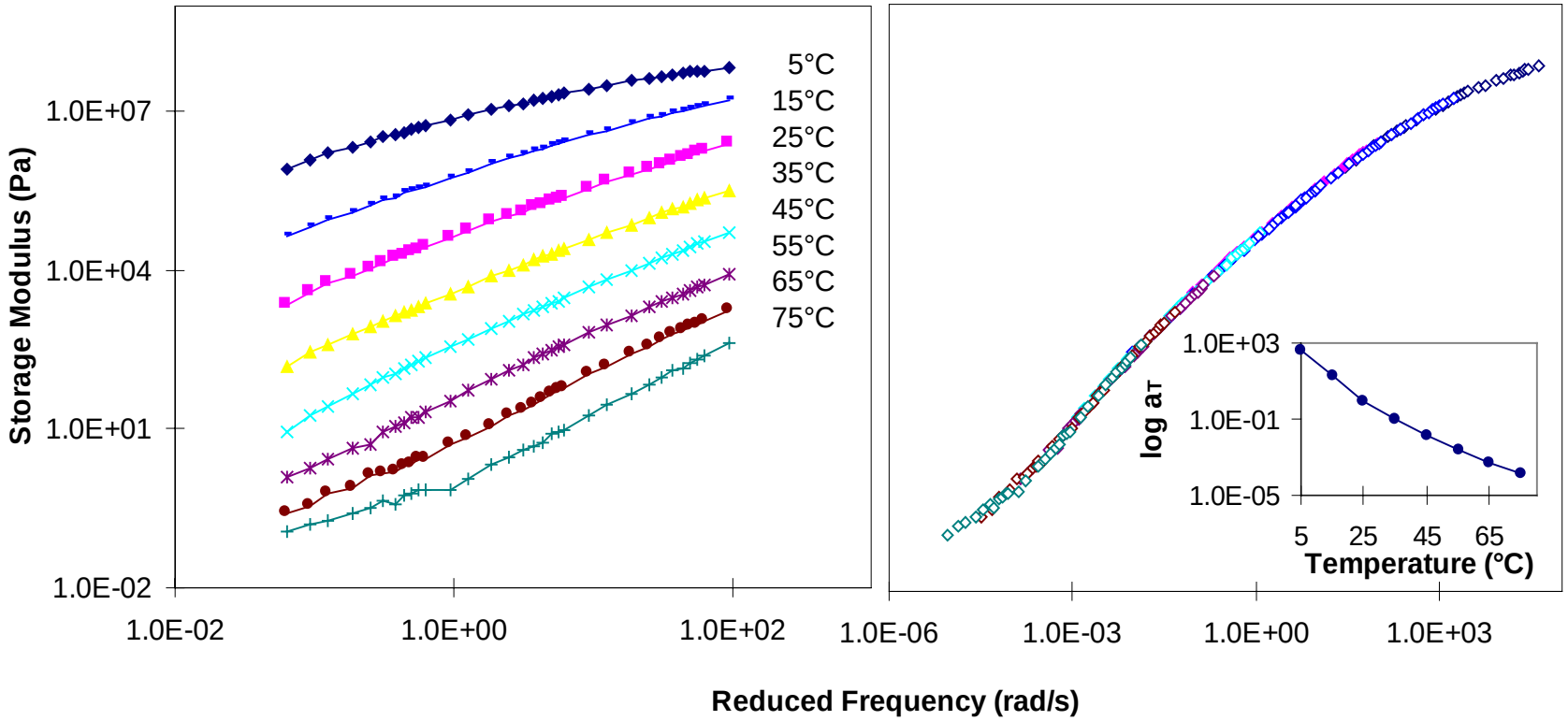

Figure A-1. Dynamic storage modulus isothermal, master curve (with reference temperature of 25°C), and shift factor, a_T , for AUC2.

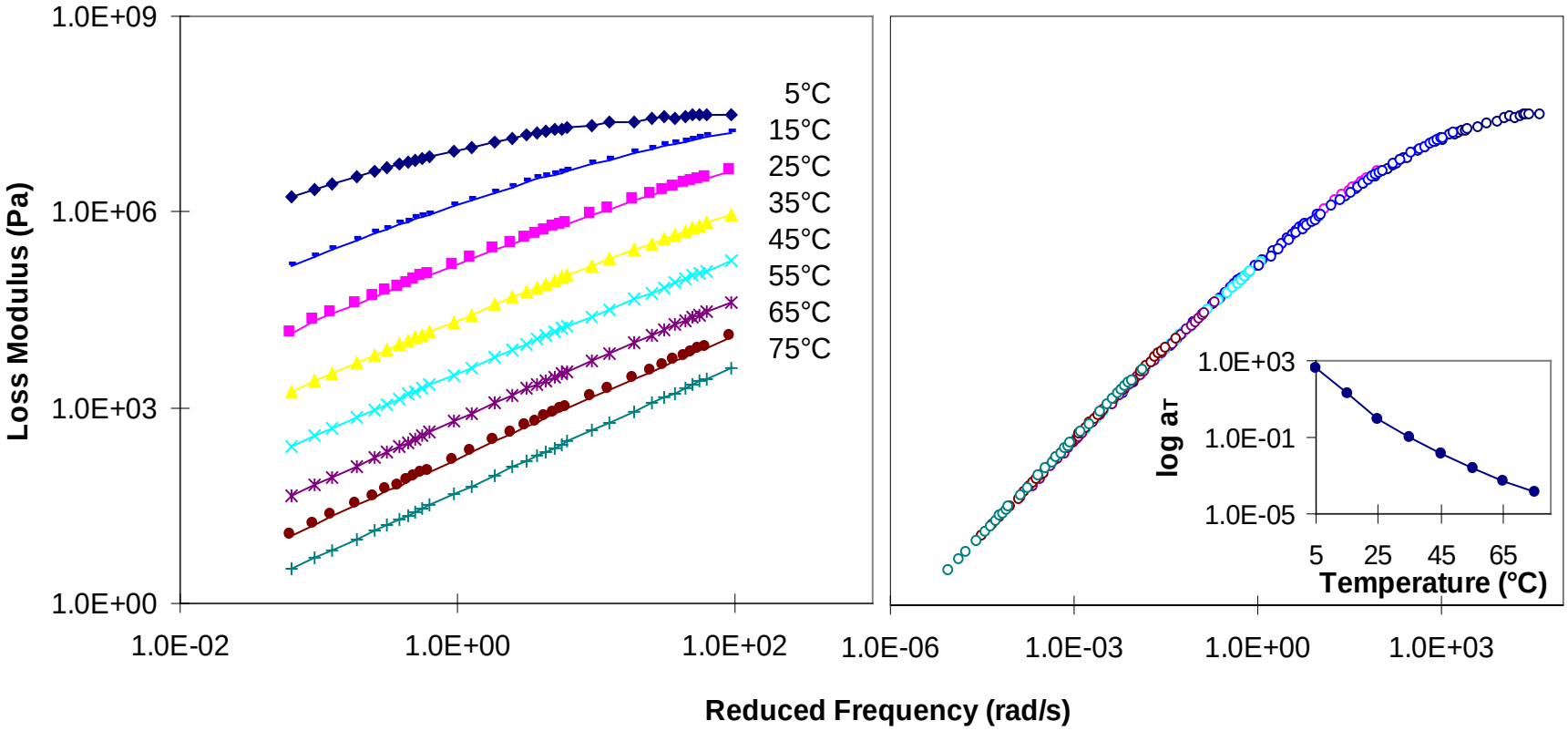

Figure A-2. Dynamic loss modulus isothermal, master curve (with reference temperature of 25°C), and shift factor, a_T , for AUC2.

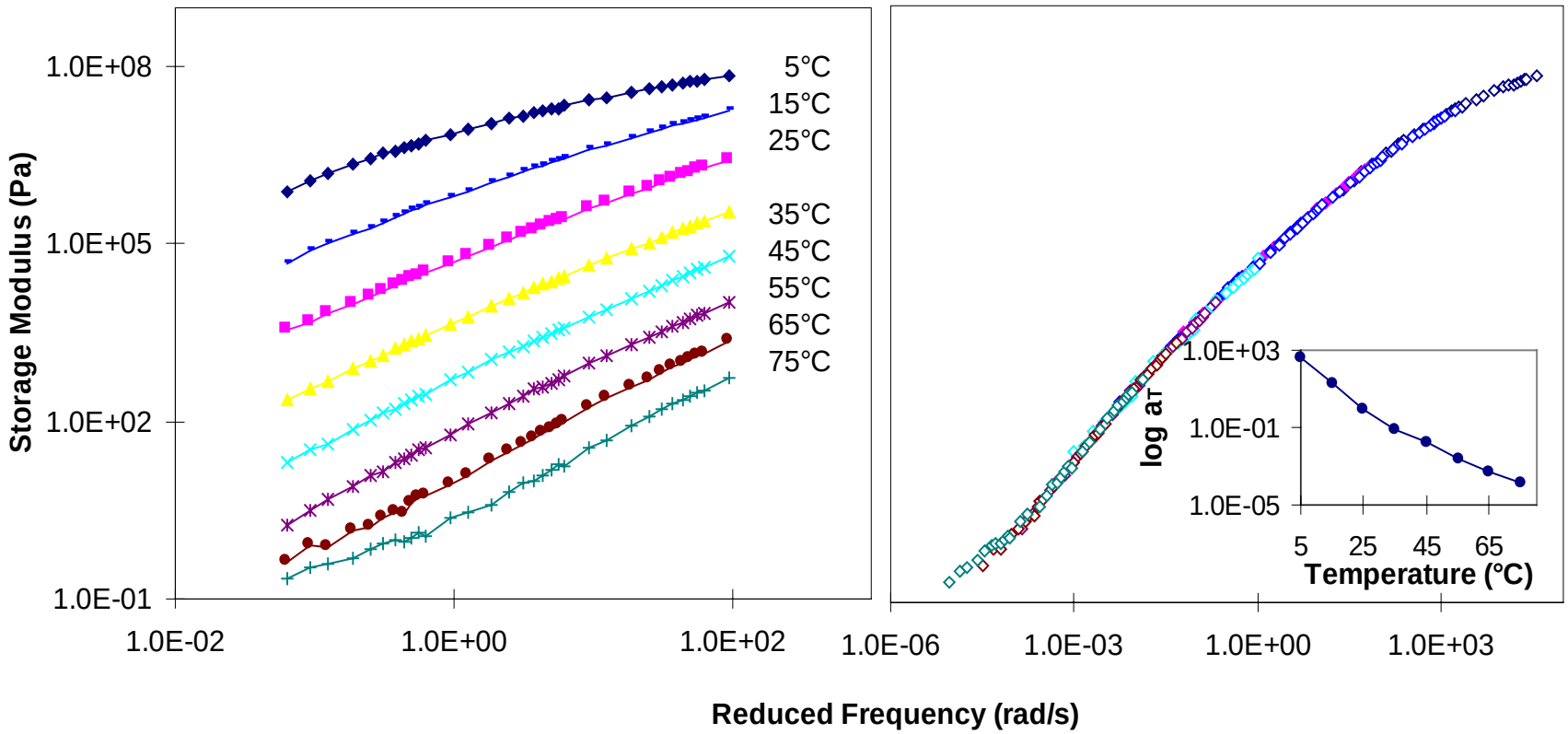

Figure A-3. Dynamic storage modulus isothermal, master curve (with reference temperature of 25°C), and shift factor, a_T, for for AUC3.

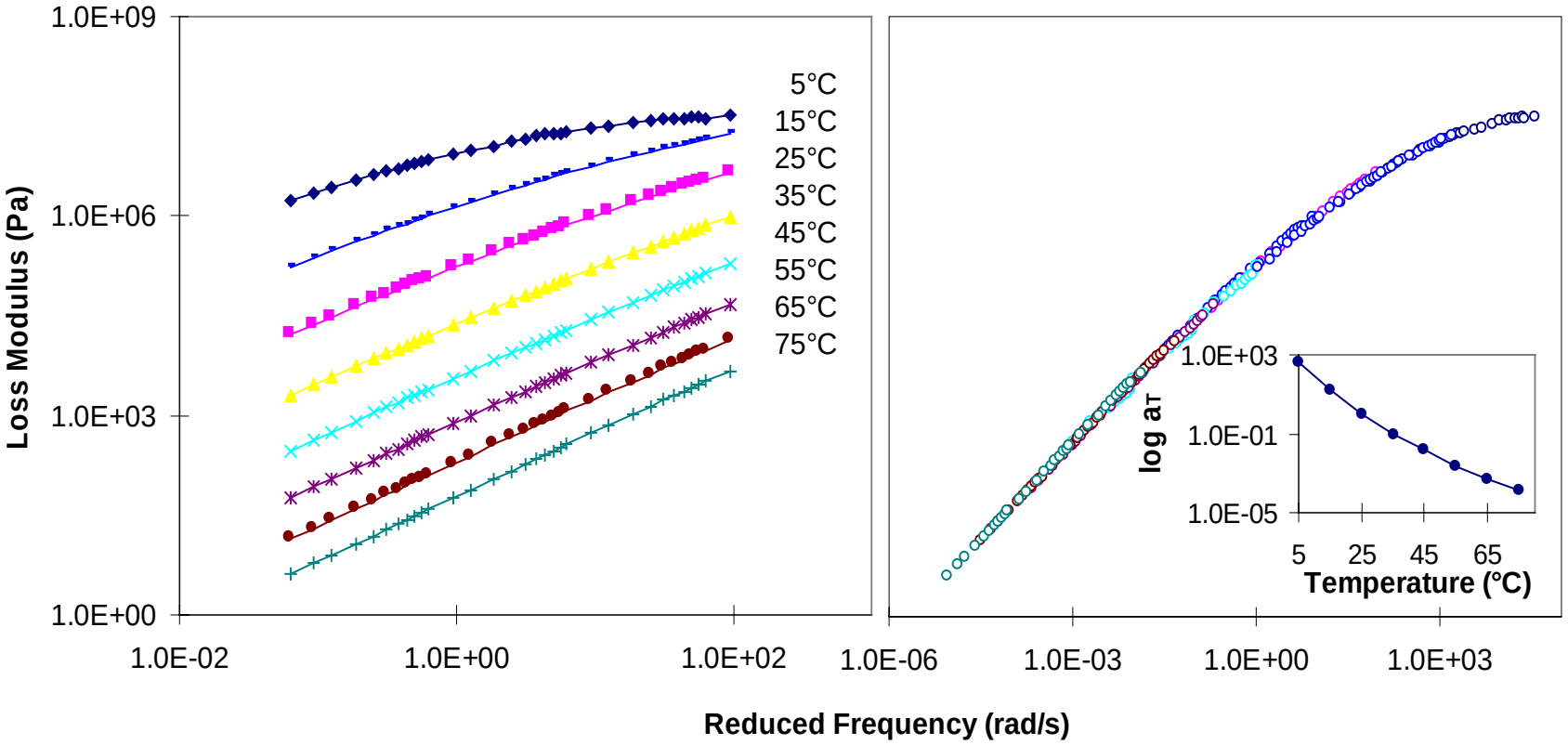

Figure A-4. Dynamic loss modulus isothermal, master curve (with reference temperature of 25°C), and shift factor, a_T , for AUC3.

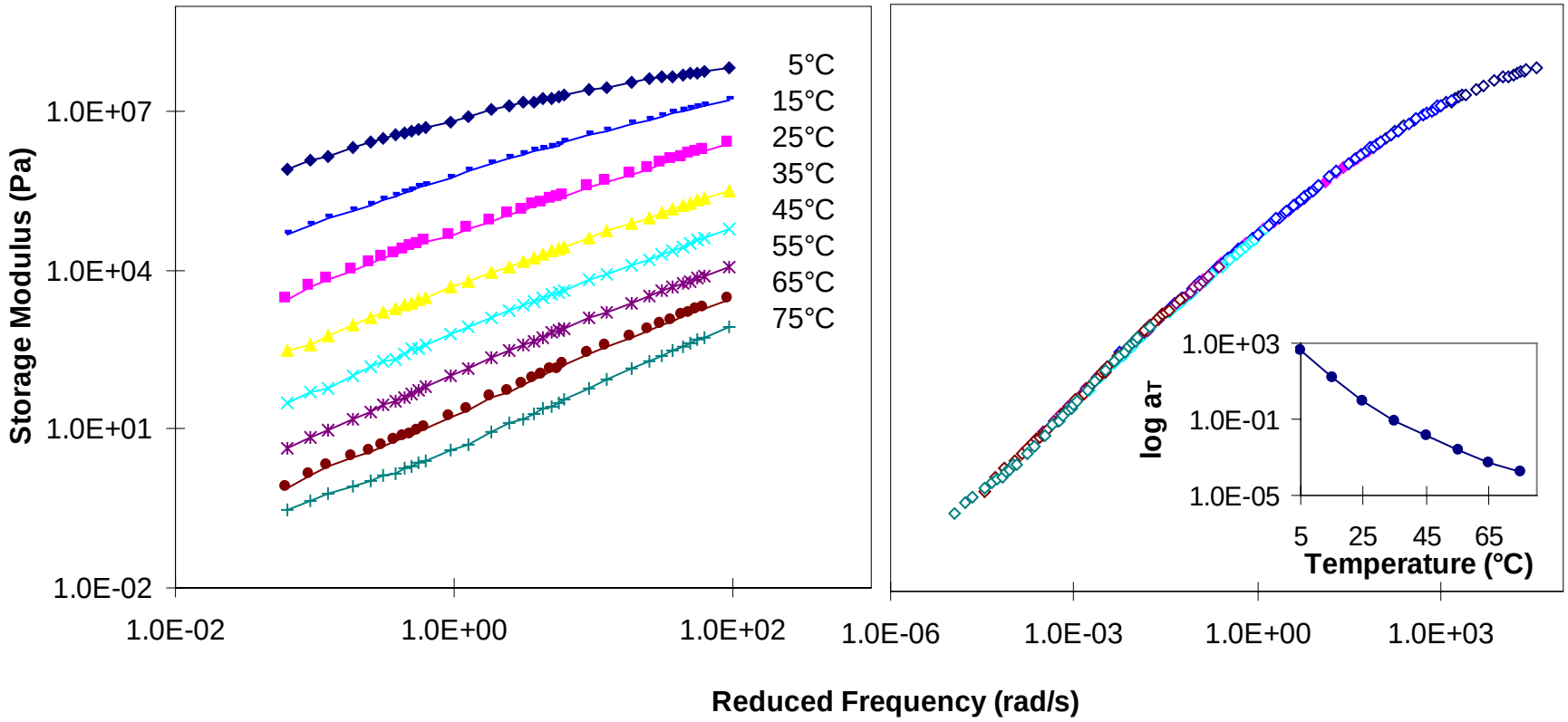

Figure A-5. Dynamic storage modulus isothermal, master curve (with reference temperature of 25°C), and shift factor, a_T, for AUC4.

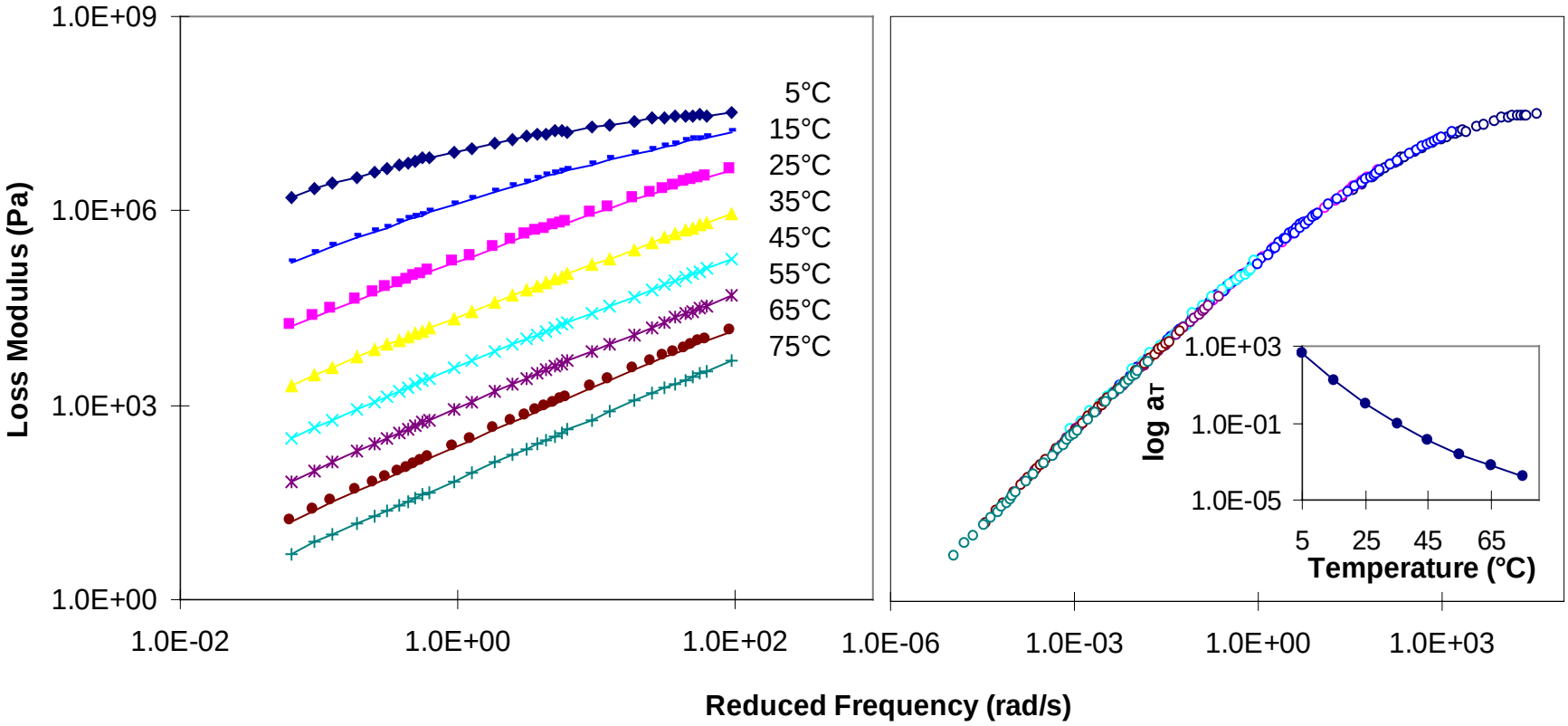

Figure A-6. Dynamic loss modulus isothermal, master curve (with reference temperature of 25°C), and shift factor, a_T , for AUC4.

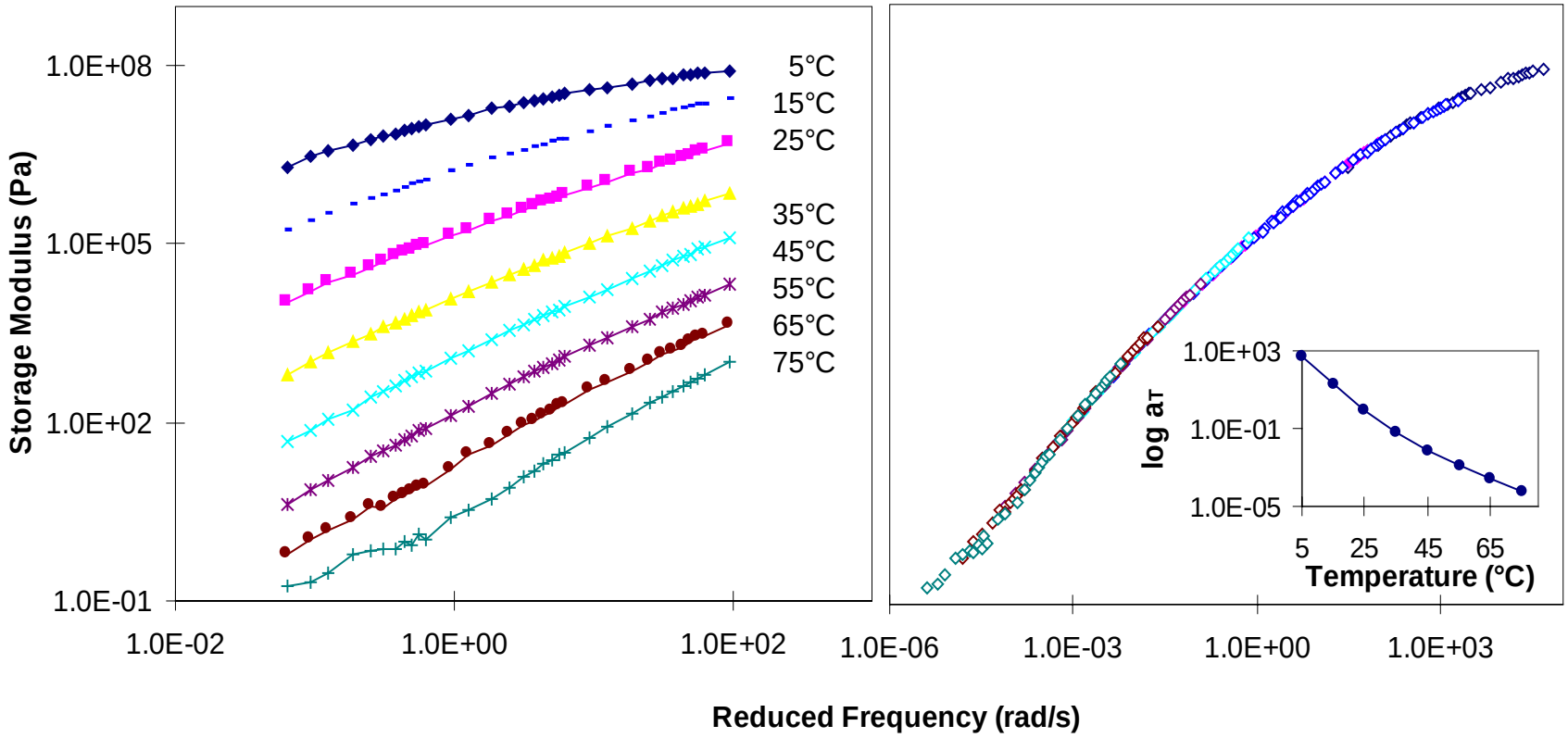

Figure A-7. Dynamic storage modulus isothermal, master curve (with reference temperature of 25°C), and shift factor, a_T, for ARC2.

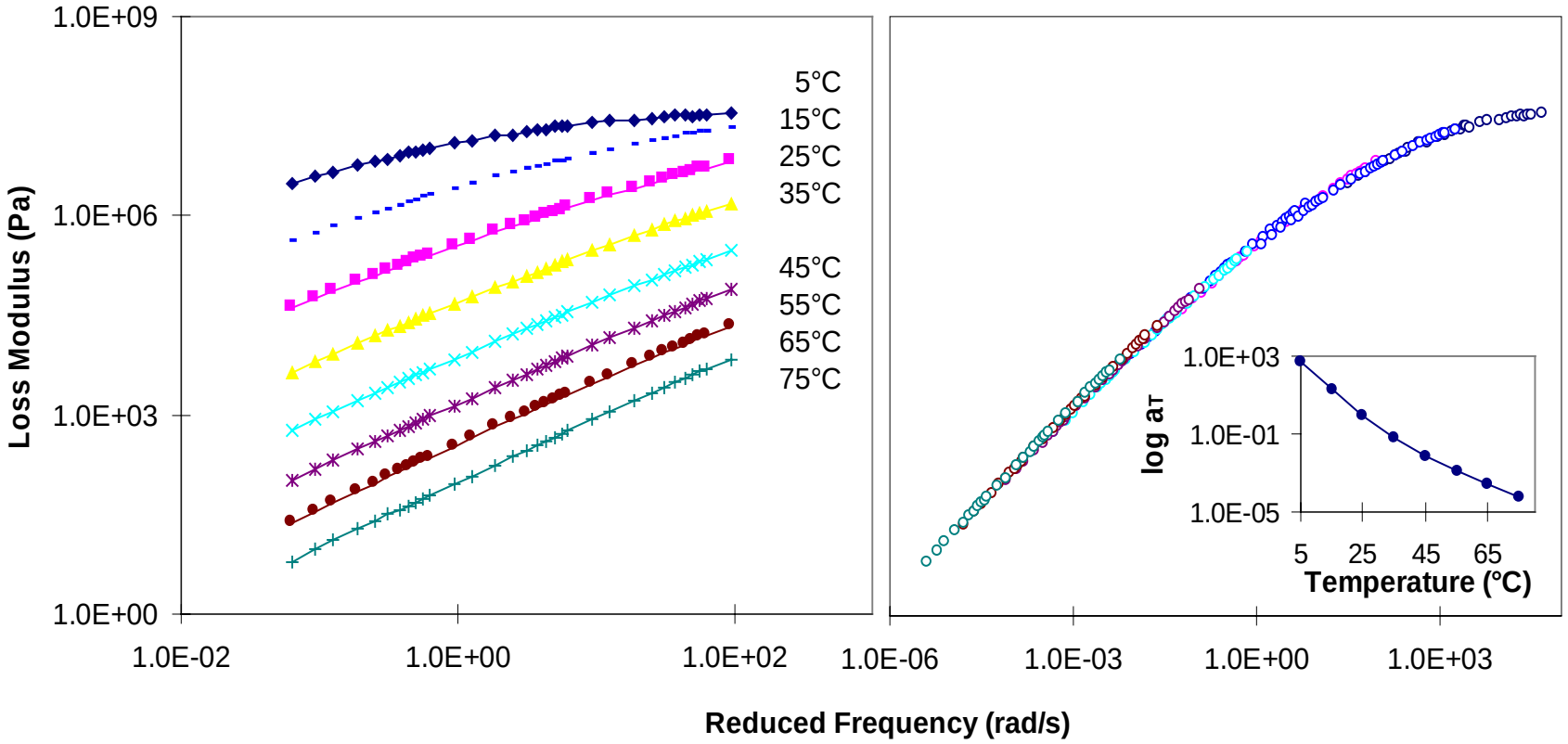

Figure A-8. Dynamic loss modulus isothermal, master curve (with reference temperature of 25°C), and shift factor, a_T, for ARC2.

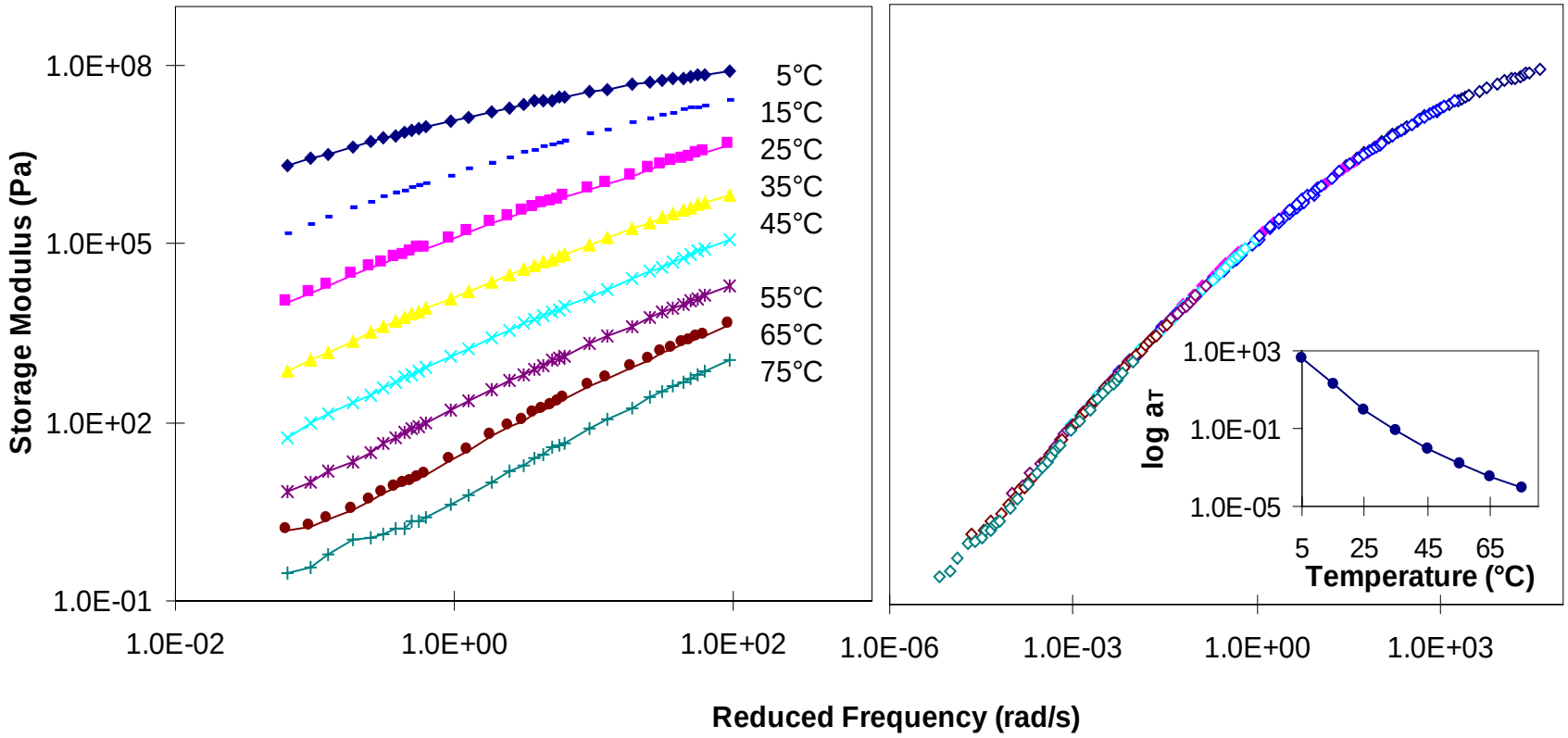

Figure A-9. Dynamic storage modulus isothermal, master curve (with reference temperature of 25°C), and shift factor, a_T, for ARC3.

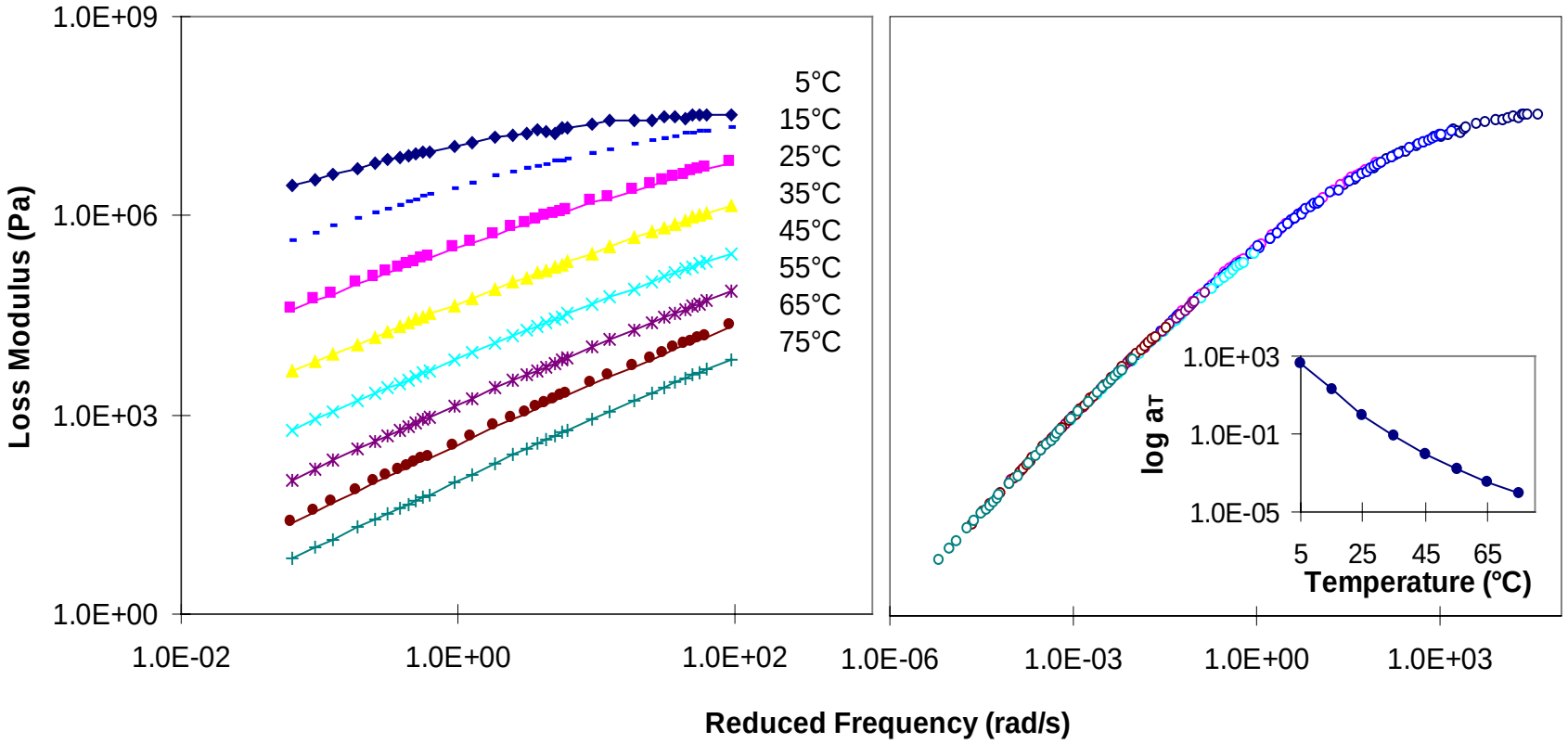

Figure A-10. Dynamic loss modulus isothermal, master curve master curve (with reference temperature of 25°C), and shift factor, a_T, for ARC3.

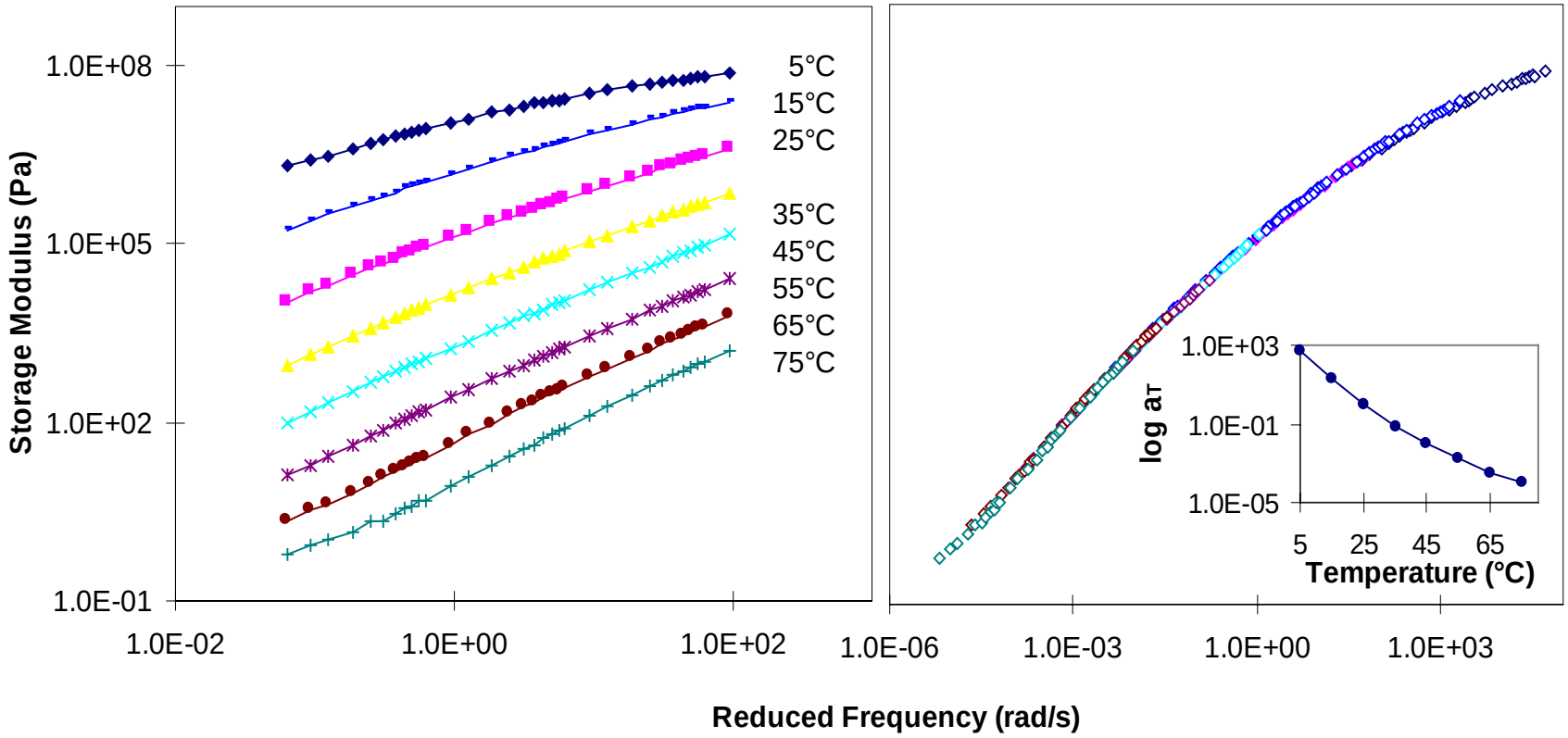

Figure A-11. Dynamic storage modulus isothermal, master curve (with reference temperature of 25°C), and shift factor, a_T,ARC4.

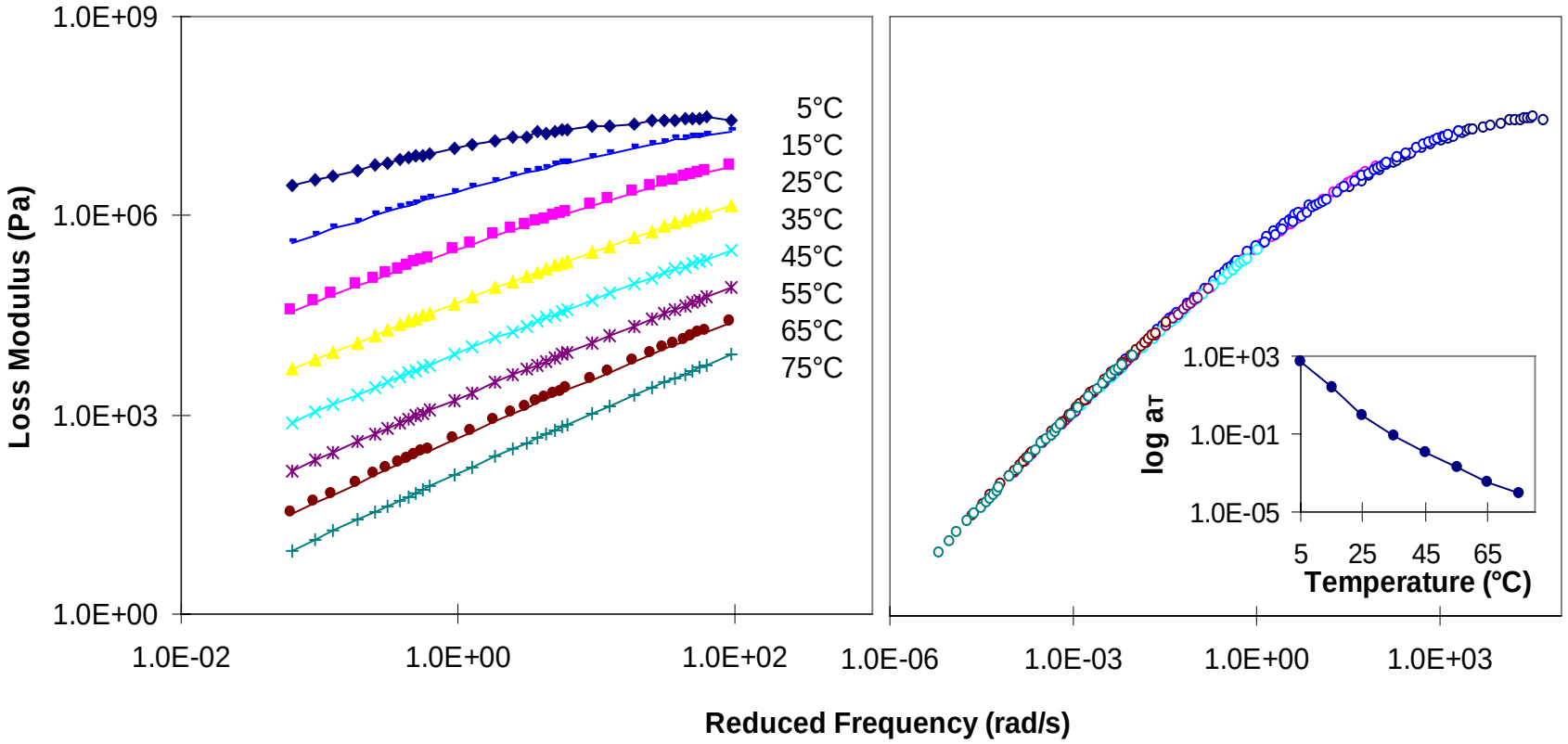

Figure A-12. Dynamic loss modulus isothermal, master curve master curve (with reference temperature of 25°C), and shift factor, a_T, for ARC4.

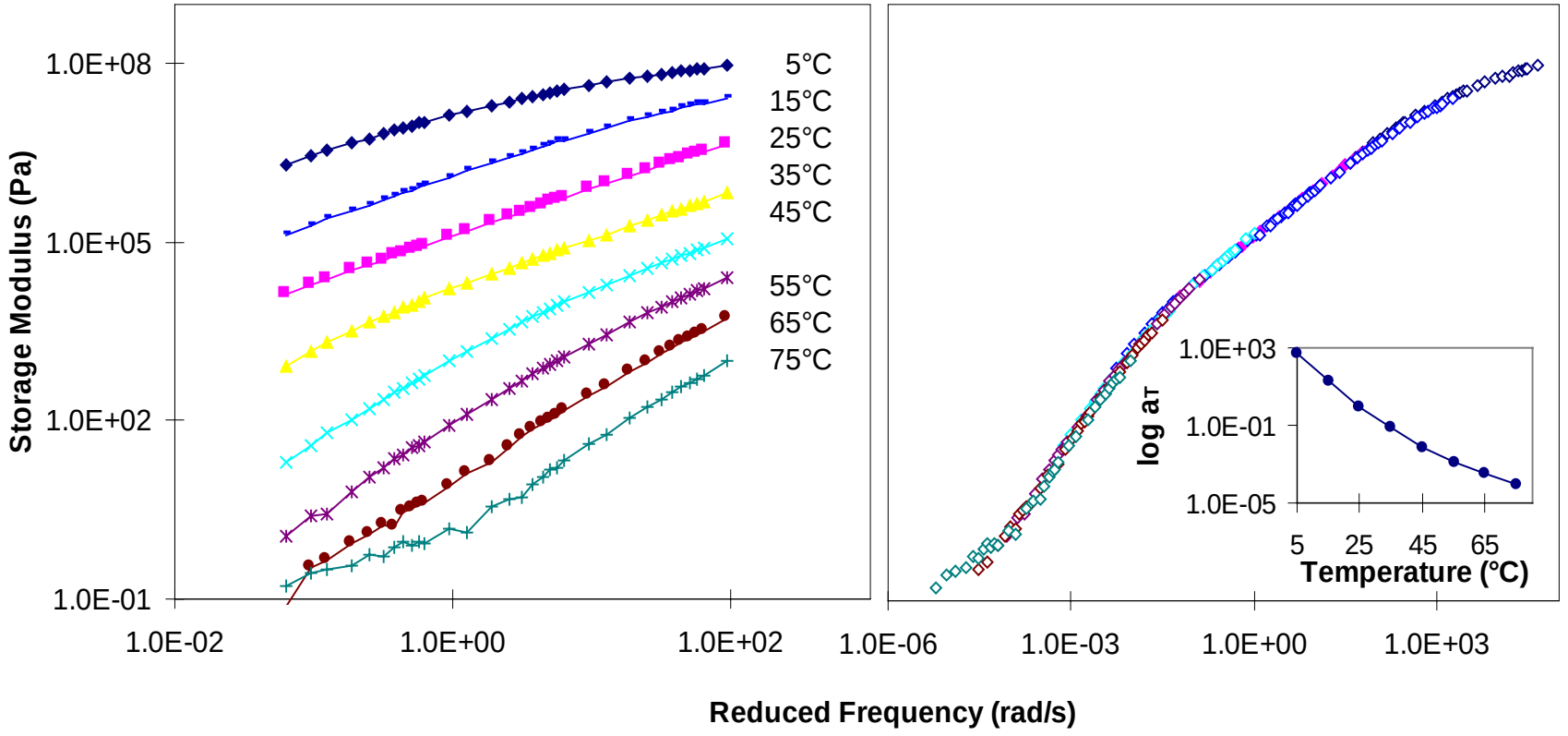

Figure A-13. Dynamic storage modulus isothermal, master curve (with reference temperature of 25°C), and shift factor, a_T, for AUG3.

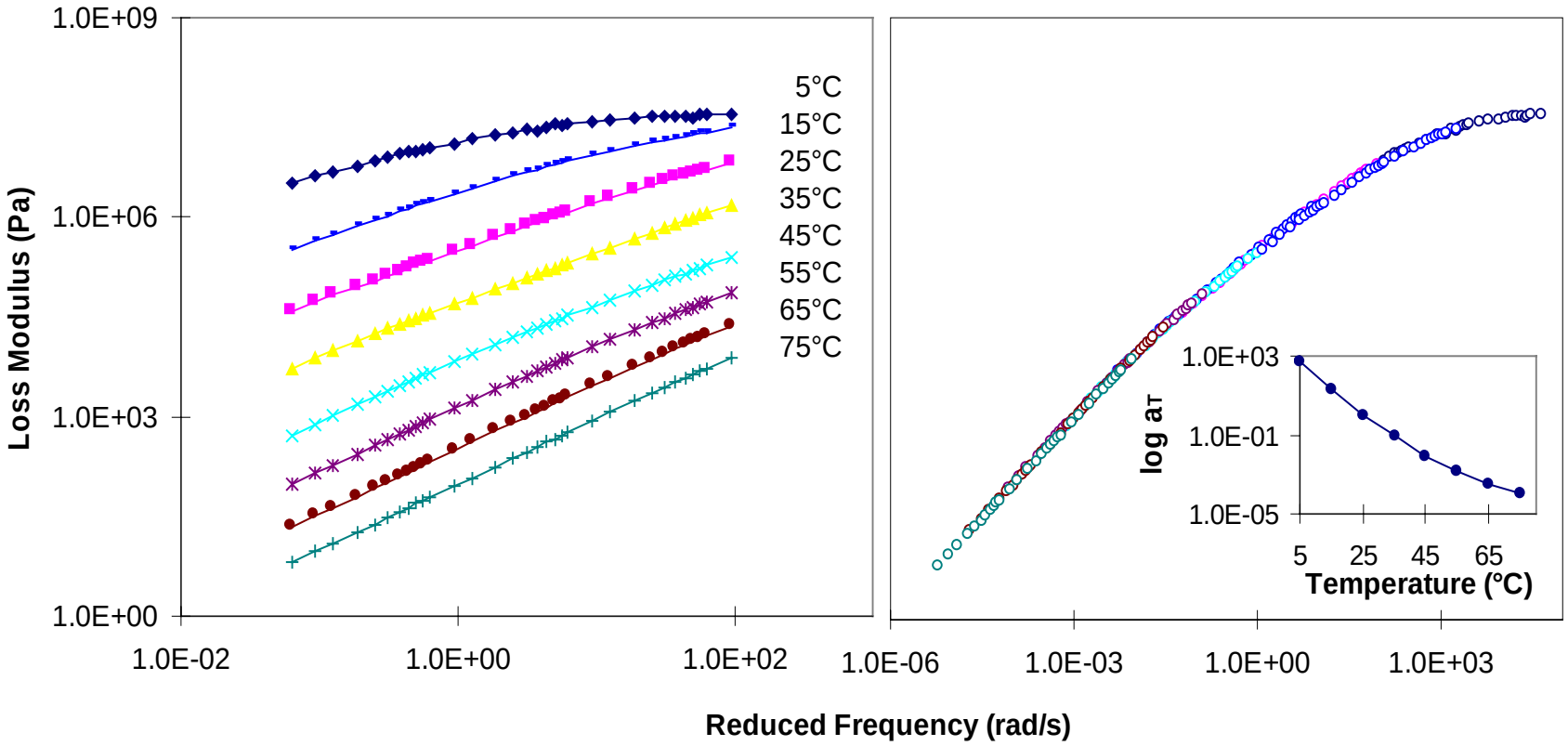

Figure A-14. Dynamic loss modulus isothermal, master curve (with reference temperature of 25°C), and shift factor, a_T , for AUG3.

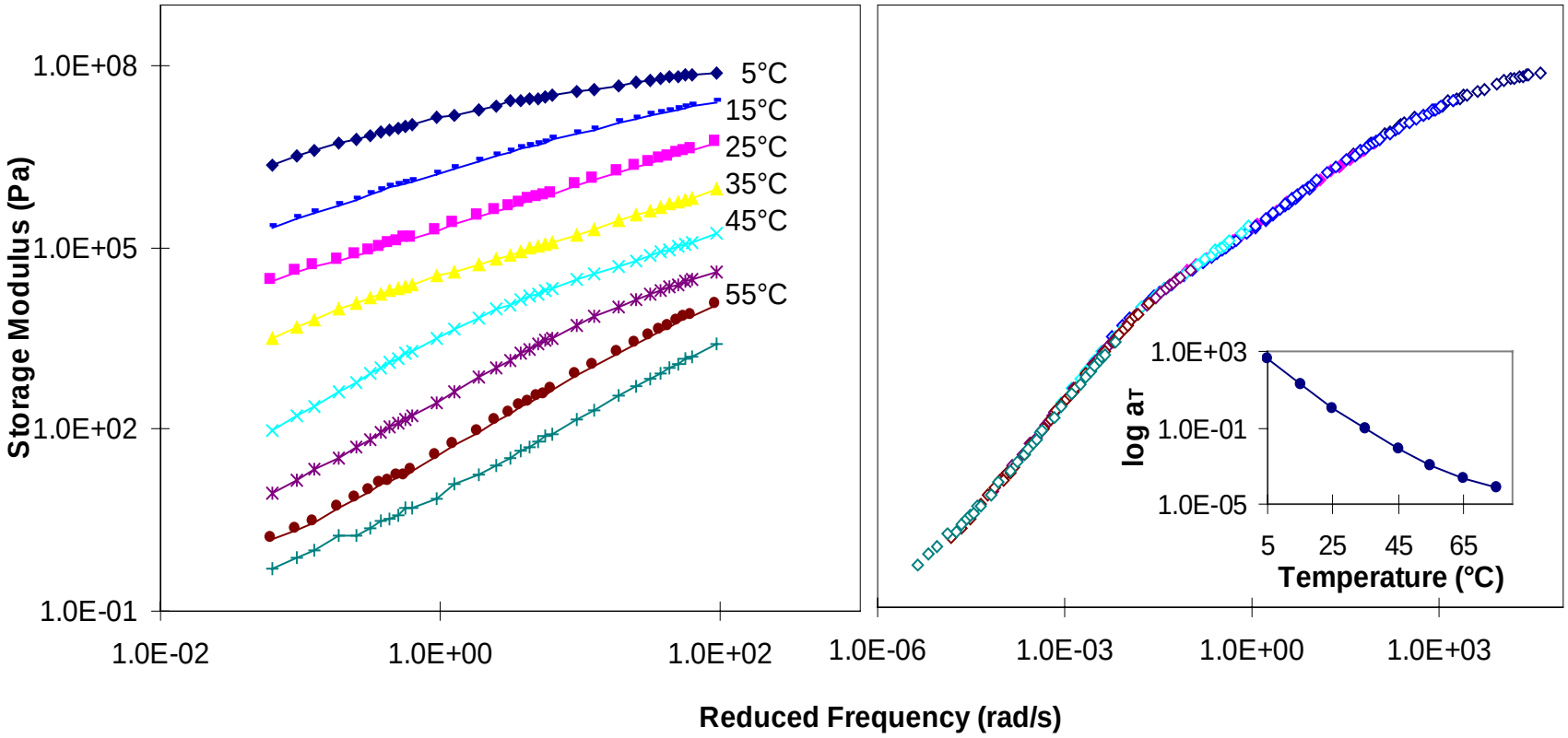

Figure A-15. Dynamic storage modulus isothermal, master curve (with reference temperature of 25°C), and shift factor, a_T, for AUG4.

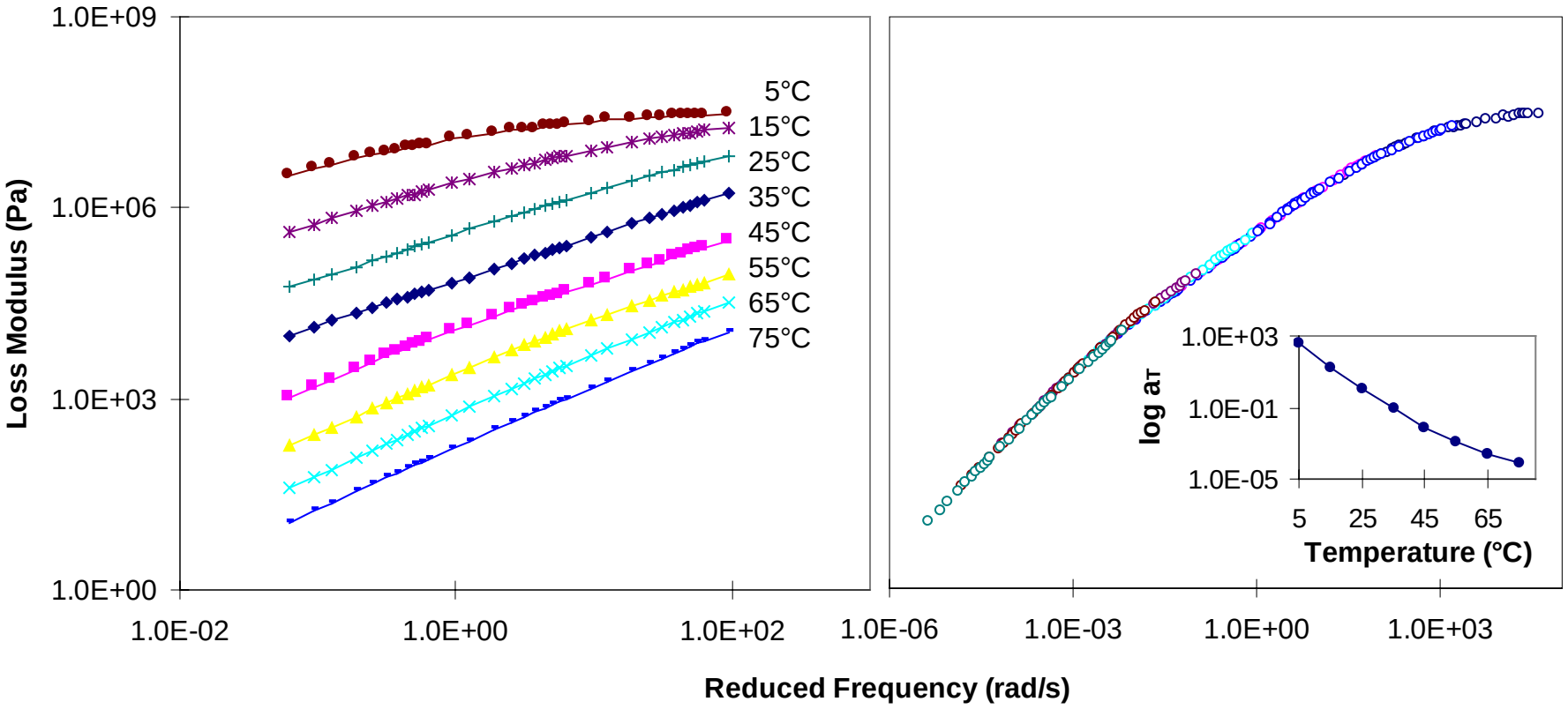

Figure A-16. Dynamic loss modulus isothermal, master curve (with reference temperature of 25°C), and shift factor, a_T , for AUG4.

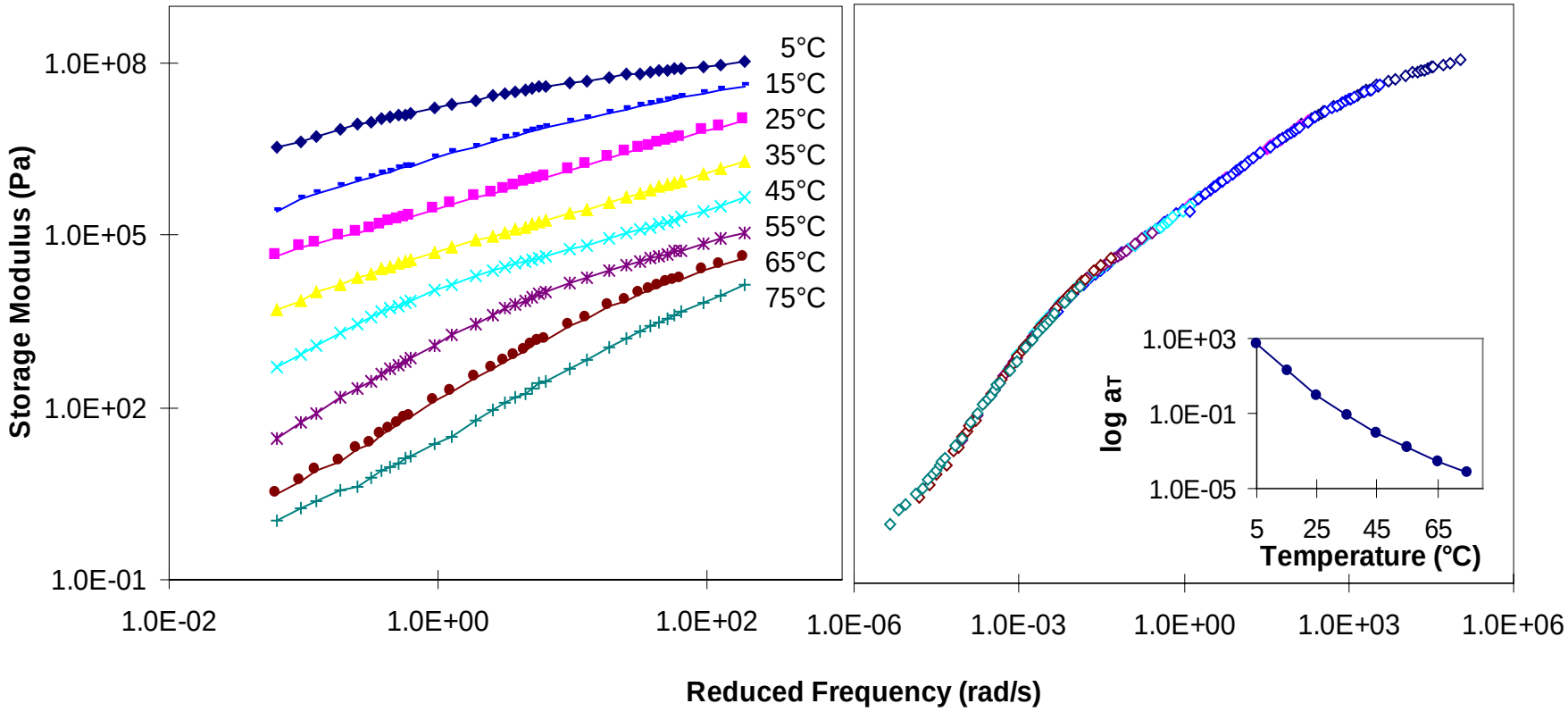

Figure A-17. Dynamic storage modulus isothermal, master curve (with reference temperature of 25°C), and shift factor, a_T, for AUG5.

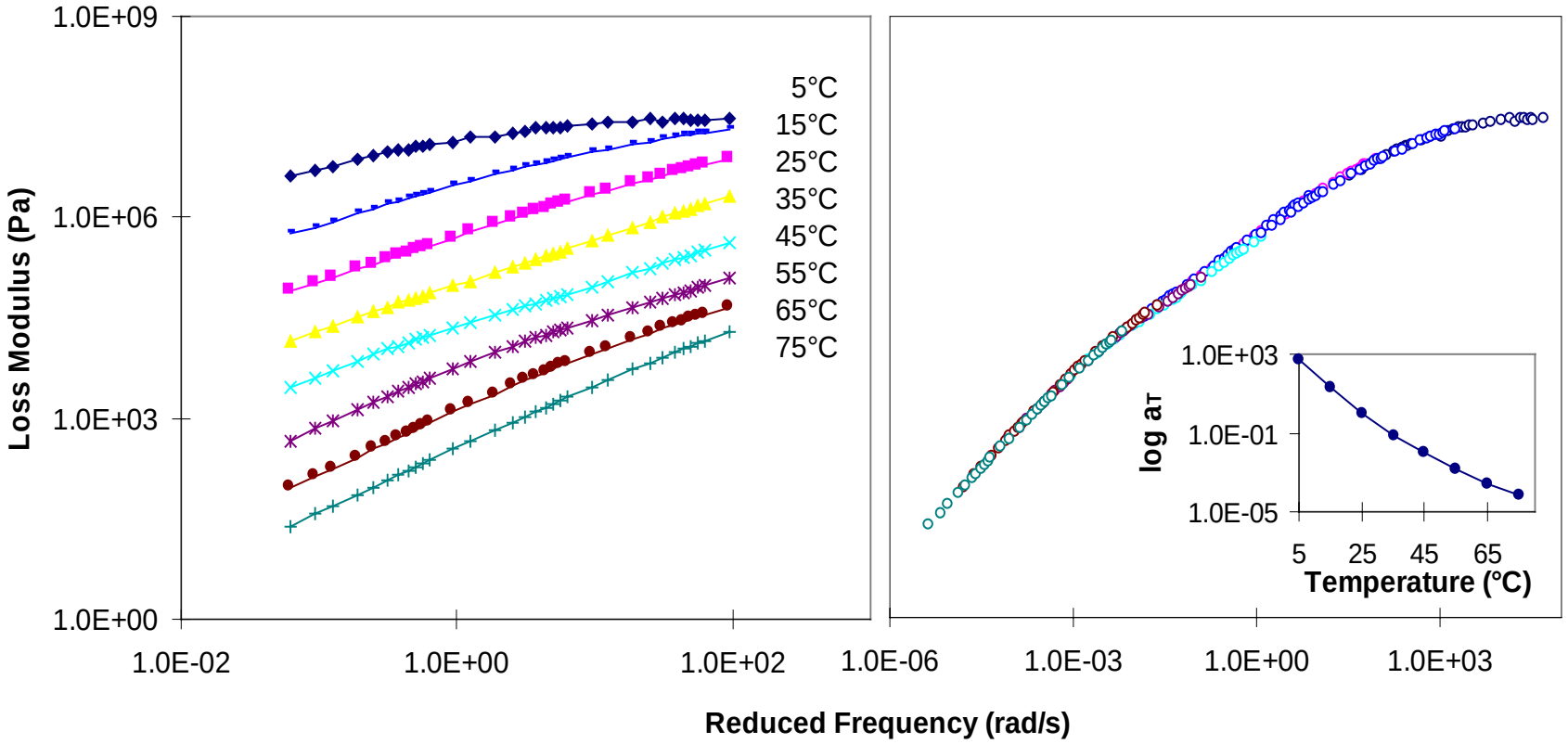

Figure A-18. Dynamic loss modulus isothermal, master curve (with reference temperature of 25°C), and shift factor, a_T , for AUG5.

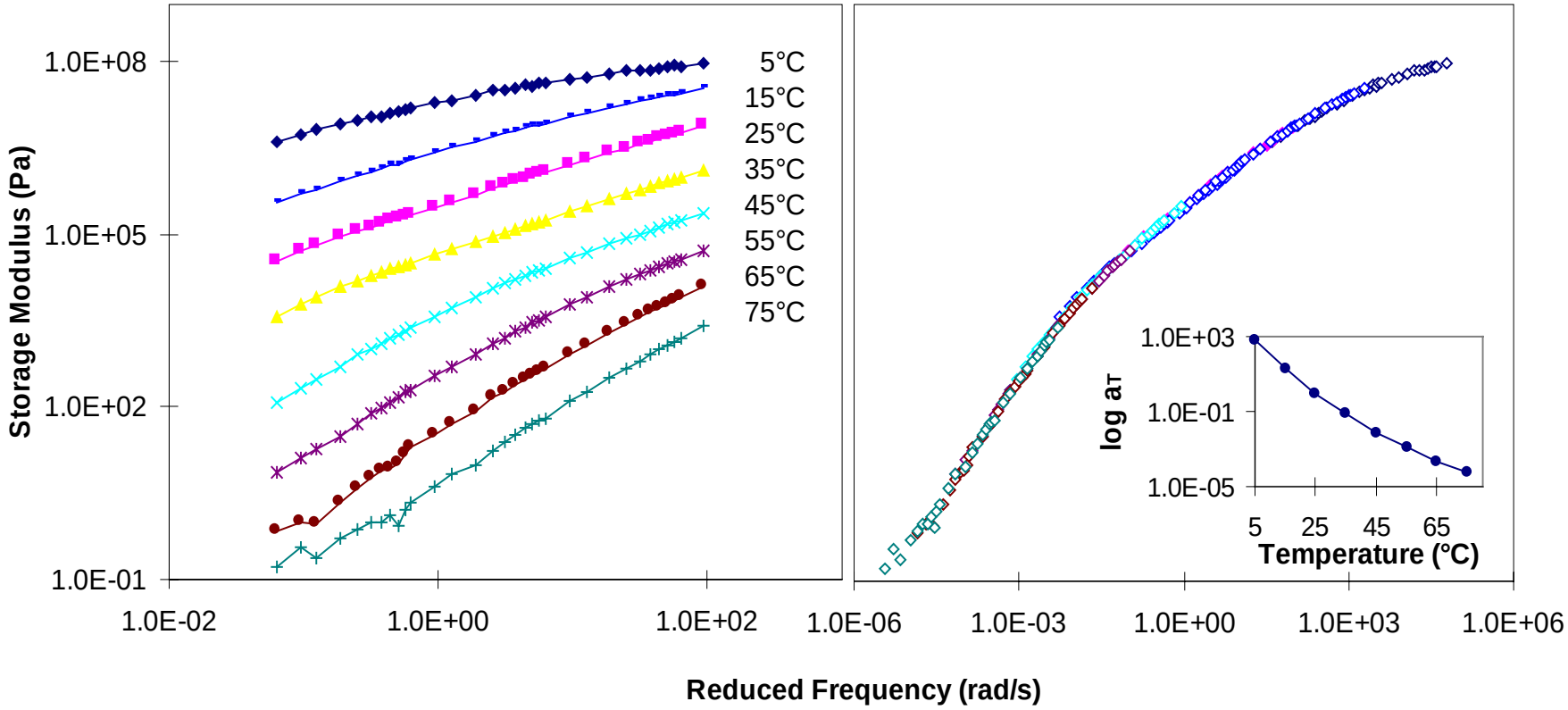

Figure A-19. Dynamic storage modulus isothermal, master curve (with reference temperature of 25°C), and shift factor, a_T, for ARG3.

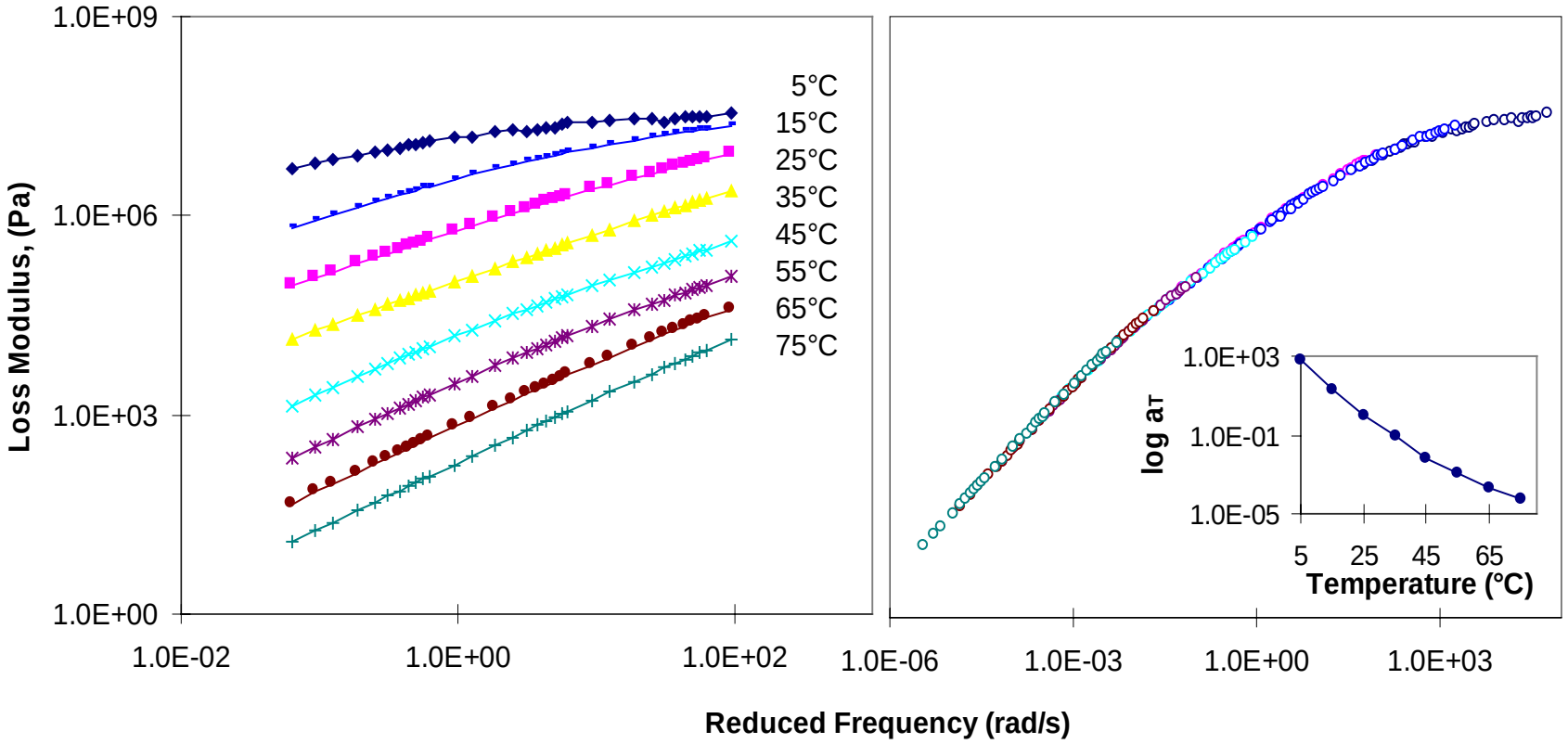

Figure A-20. Dynamic loss modulus isothermal, master master curve (with reference temperature of 25°C), and shift factor, a_T, for ARG3.

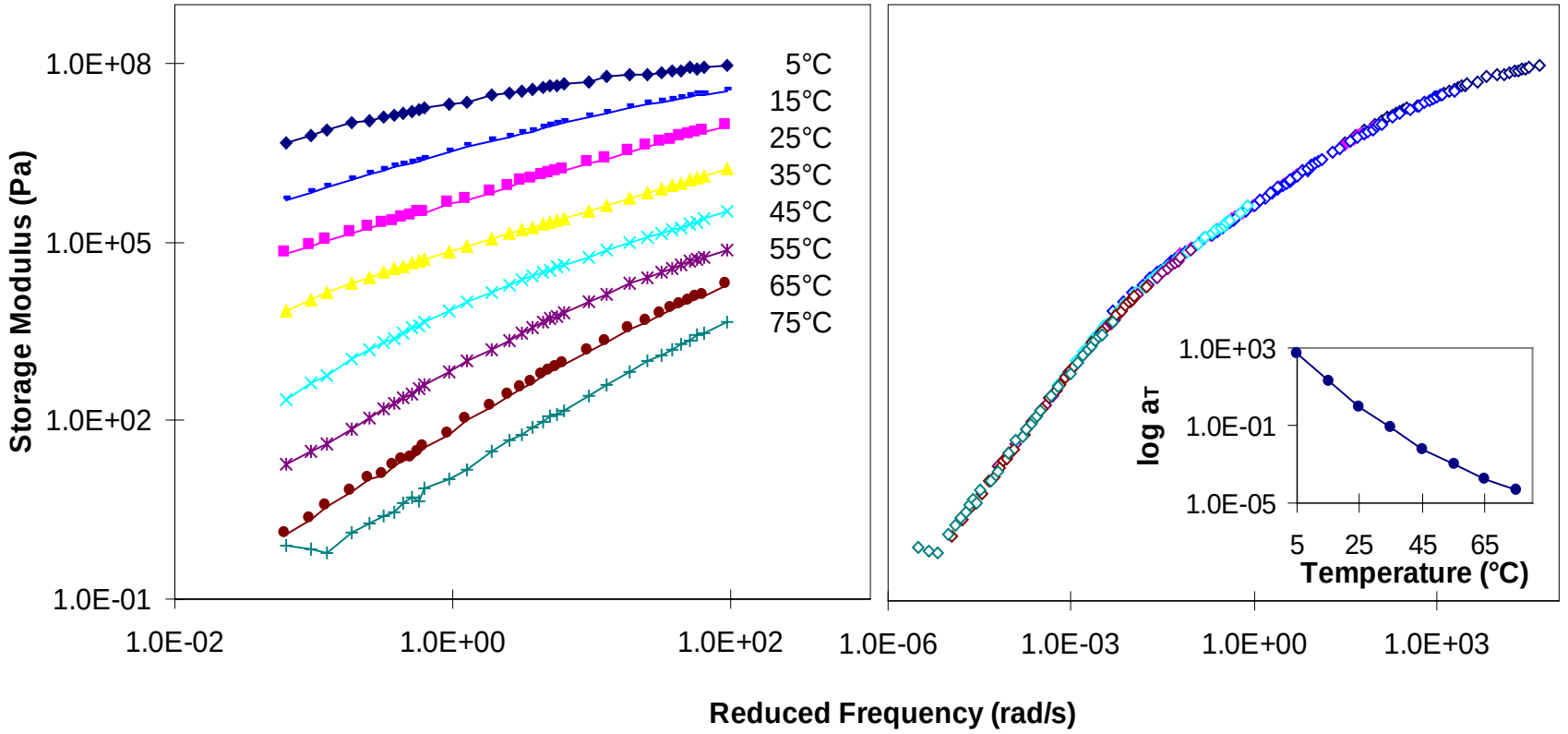

Figure A-21. Dynamic storage modulus isothermal, master curve (with reference temperature of 25°C), and shift factor, a_T, for ARG4.

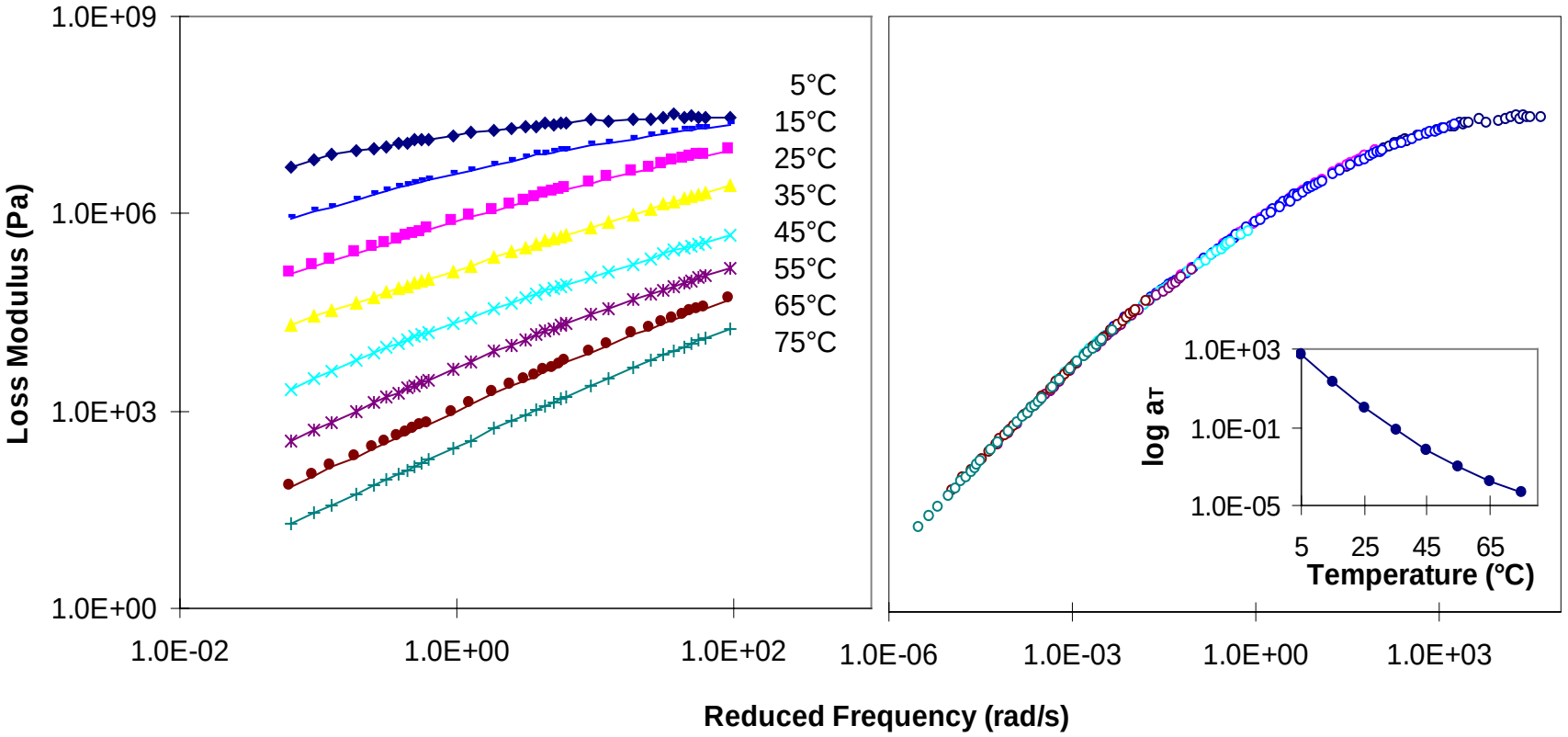

Figure A-22. Dynamic loss modulus isothermal, master curve (with reference temperature of 25°C), and shift factor, a_T, for ARG4.

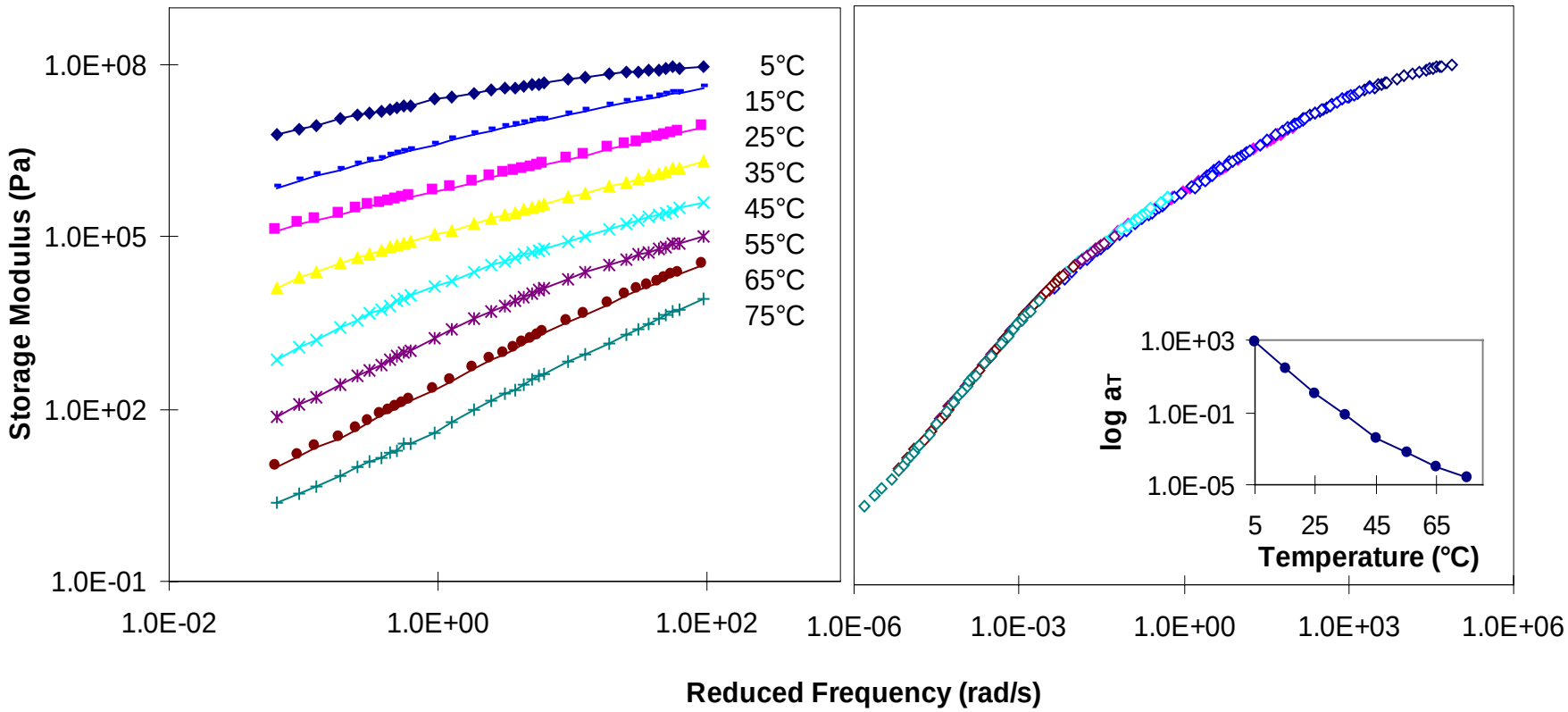

Figure A-23. Dynamic storage modulus isothermal, master curve (with reference temperature of 25°C), and shift factor, a_T, for ARG5.

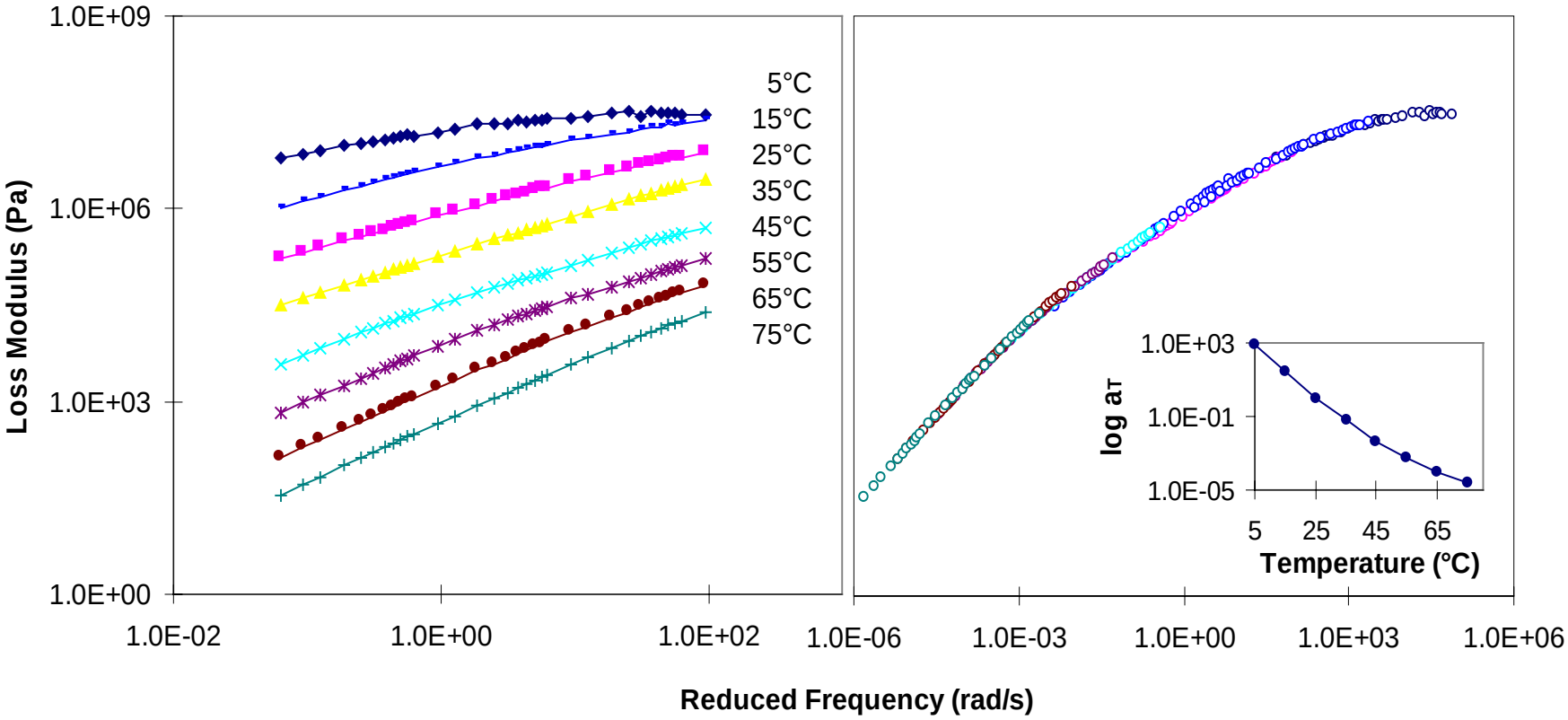

Figure A-24. Dynamic loss modulus isothermal, master curve (with reference temperature of 25°C), and shift factor, a_T, for ARG5.

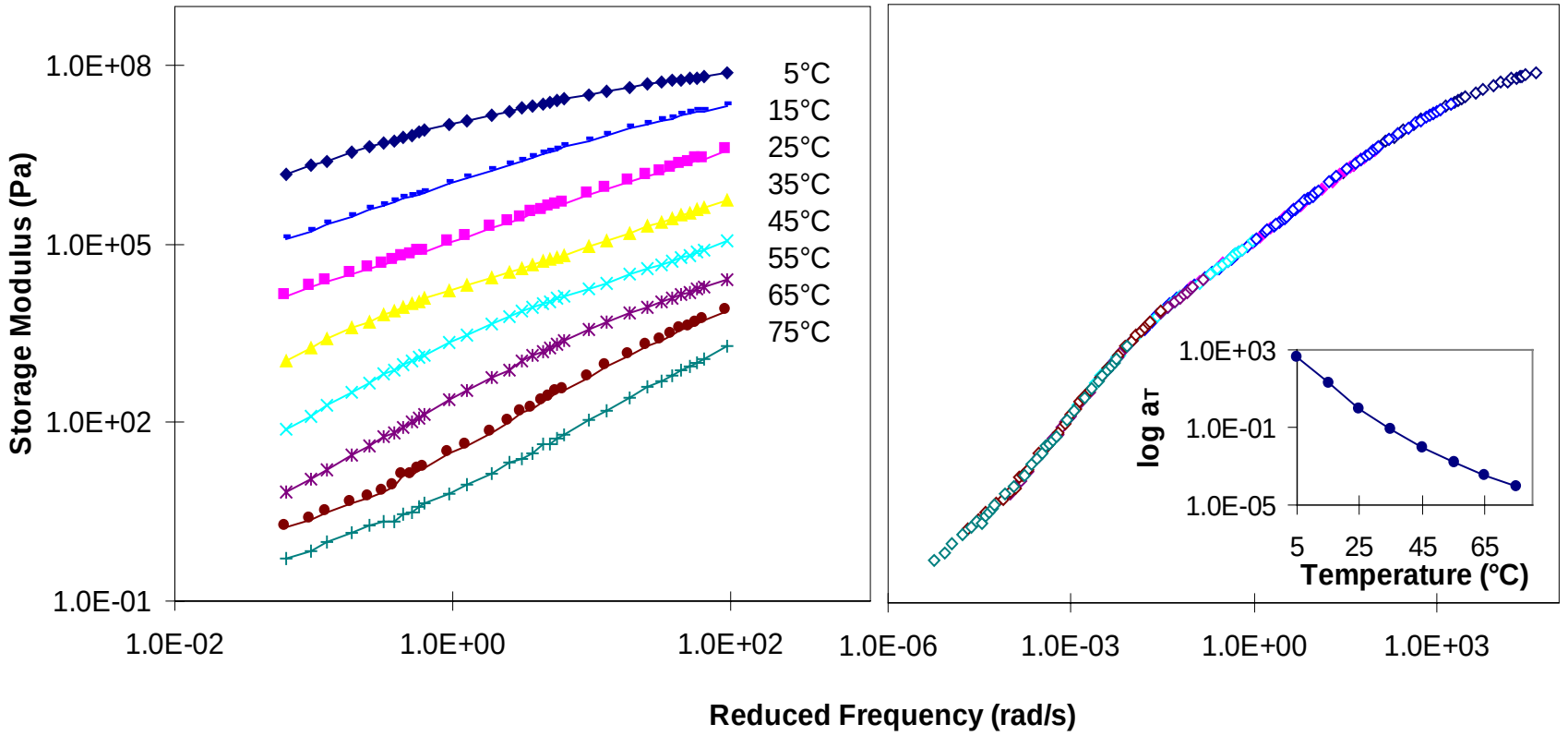

Figure A-25. Dynamic storage modulus isothermal, master curve (with reference temperature of 25°C), and shift factor, a_T, for AUN3.

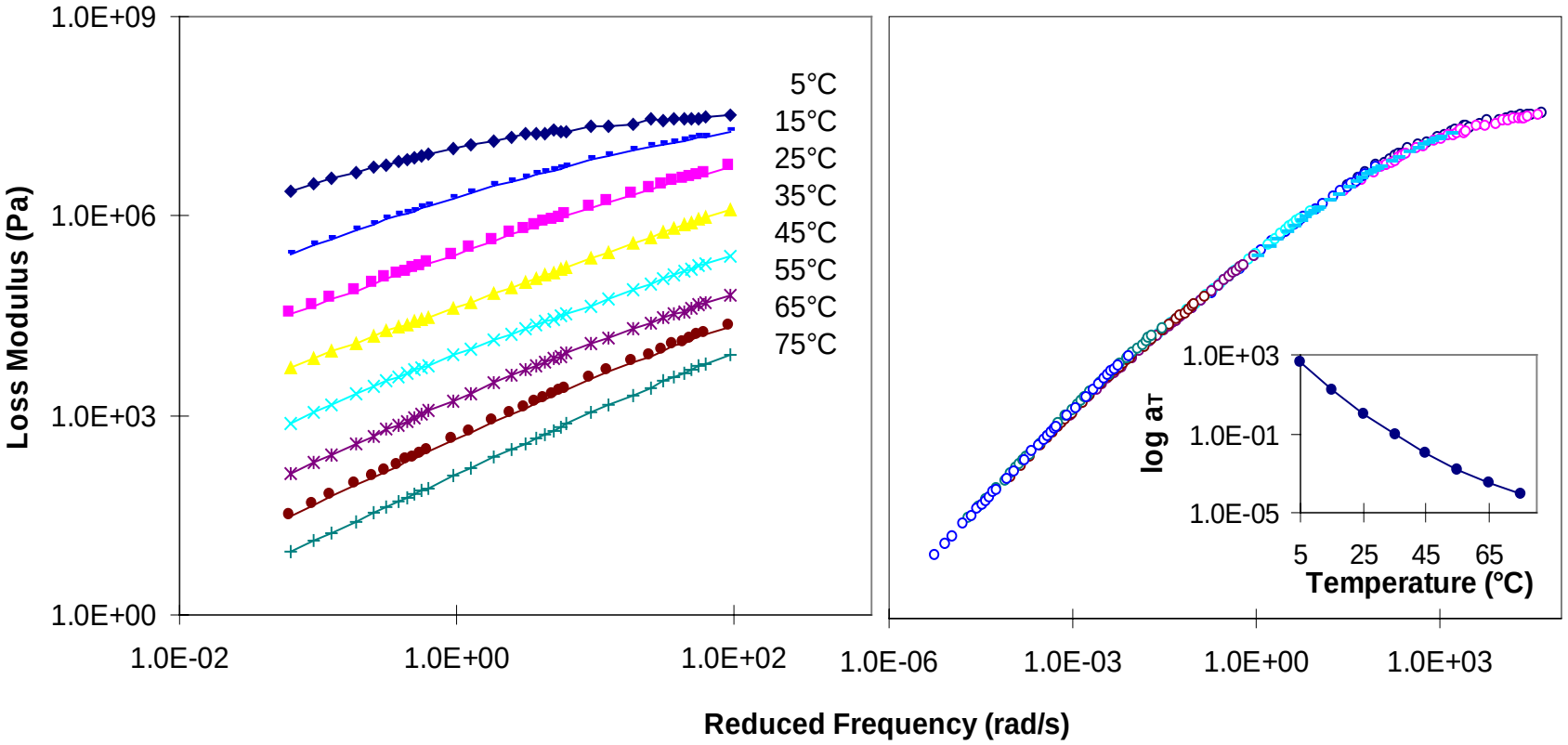

Figure A-26. Dynamic loss modulus isothermal, master curve (with reference temperature of 25°C), and shift factor, a_T, for AUN3.

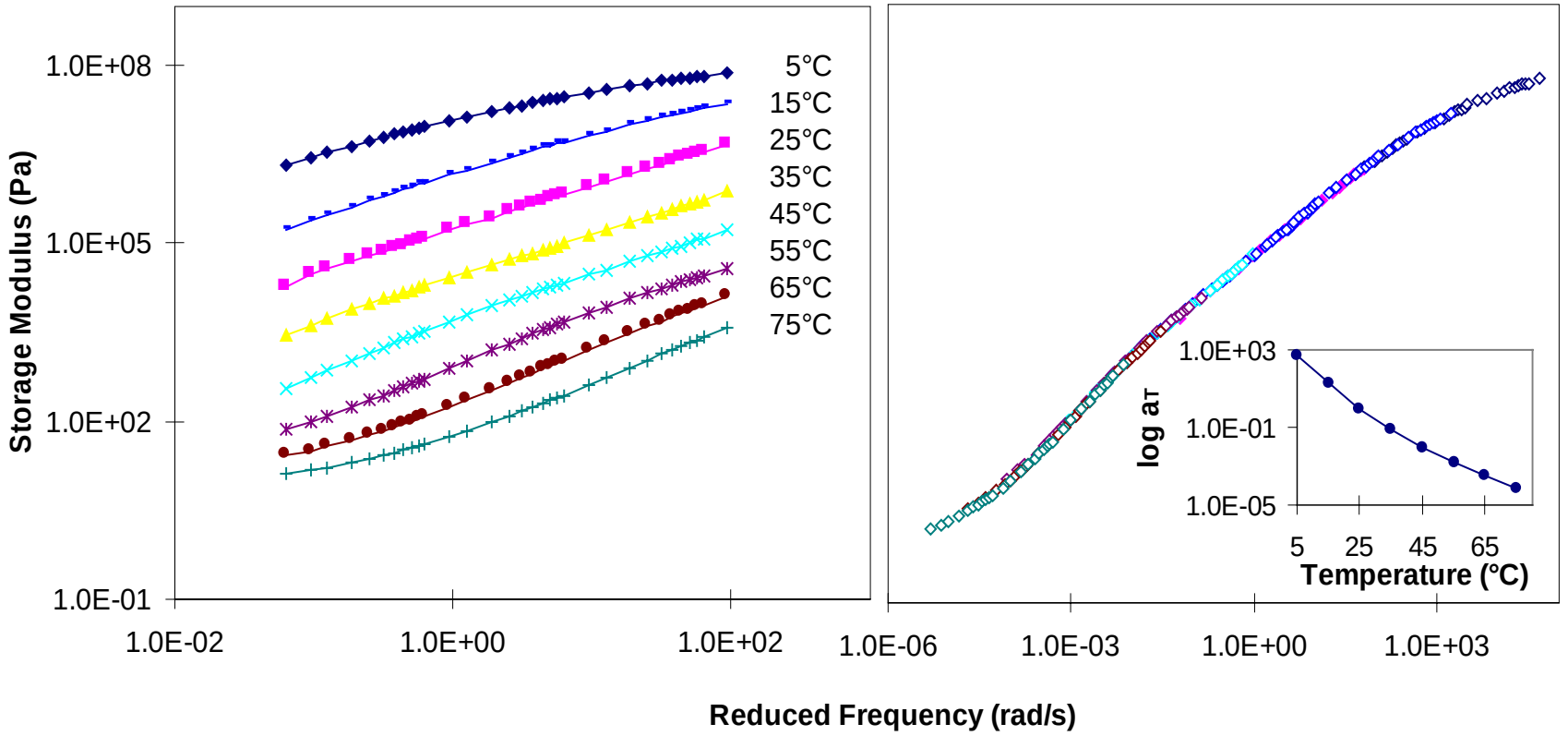

Figure A-27. Dynamic storage modulus isothermal master curve (with reference temperature of 25°C), and shift factor, a_T, for AUN4.

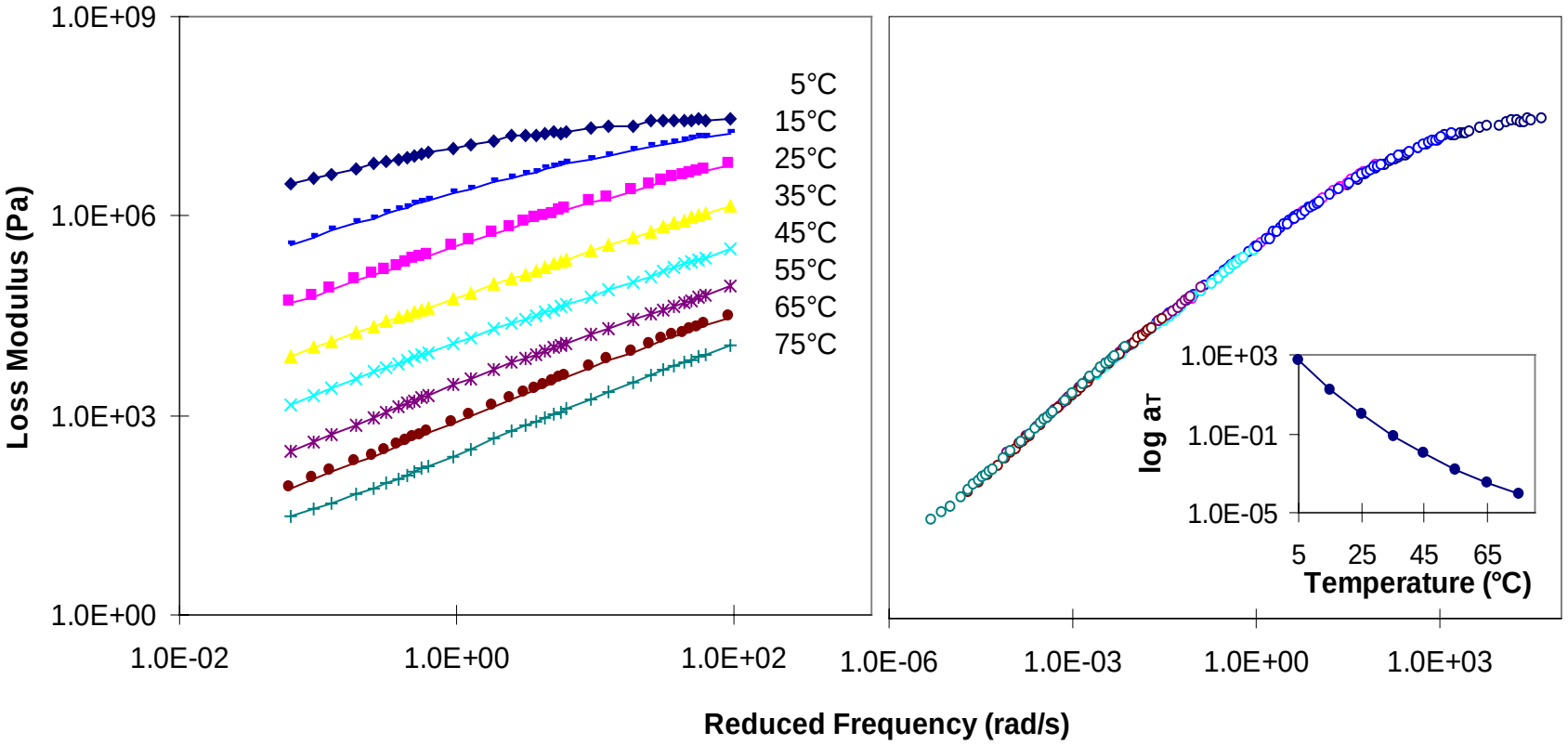

Figure A-28. Dynamic loss modulus isothermal master curve (with reference temperature of 25°C), and shift factor, a_T, for AUN4.

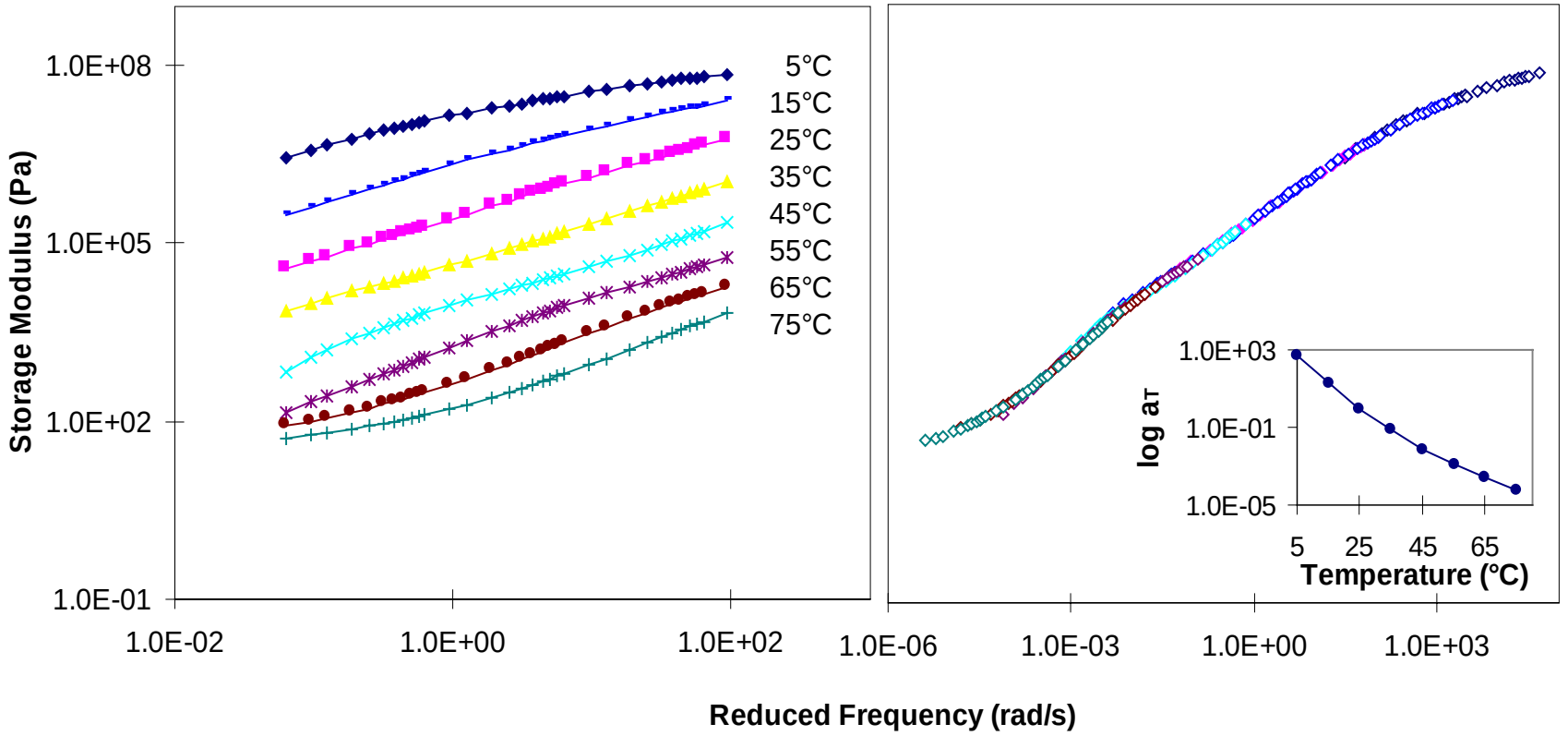

Figure A-29. Dynamic storage modulus isothermal, master curve (with reference temperature of 25°C), and shift factor, a_T, for AUN5.

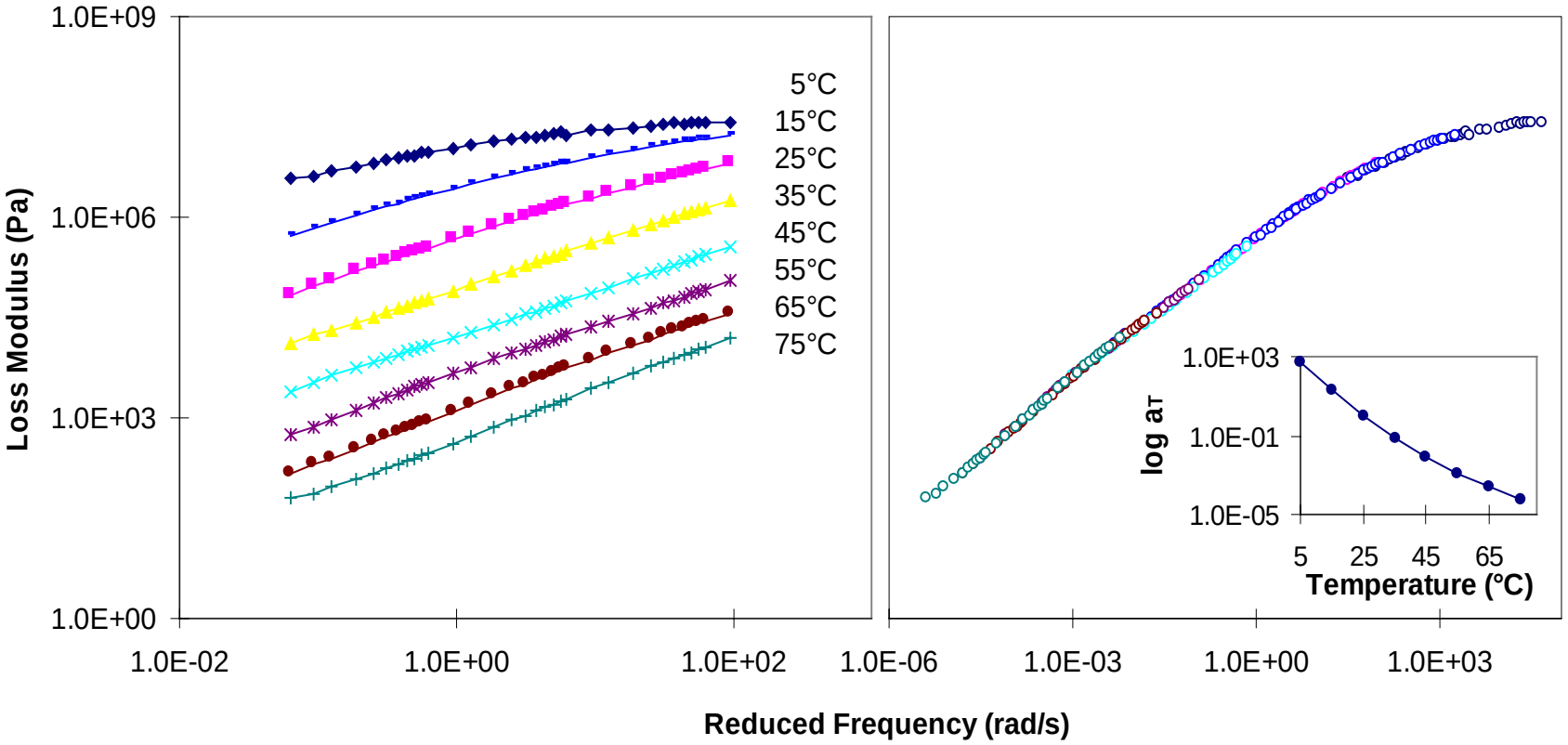

Figure A-30. Dynamic loss modulus isothermal, master curve (with reference temperature of 25°C), and shift factor, a_T, for AUN5.

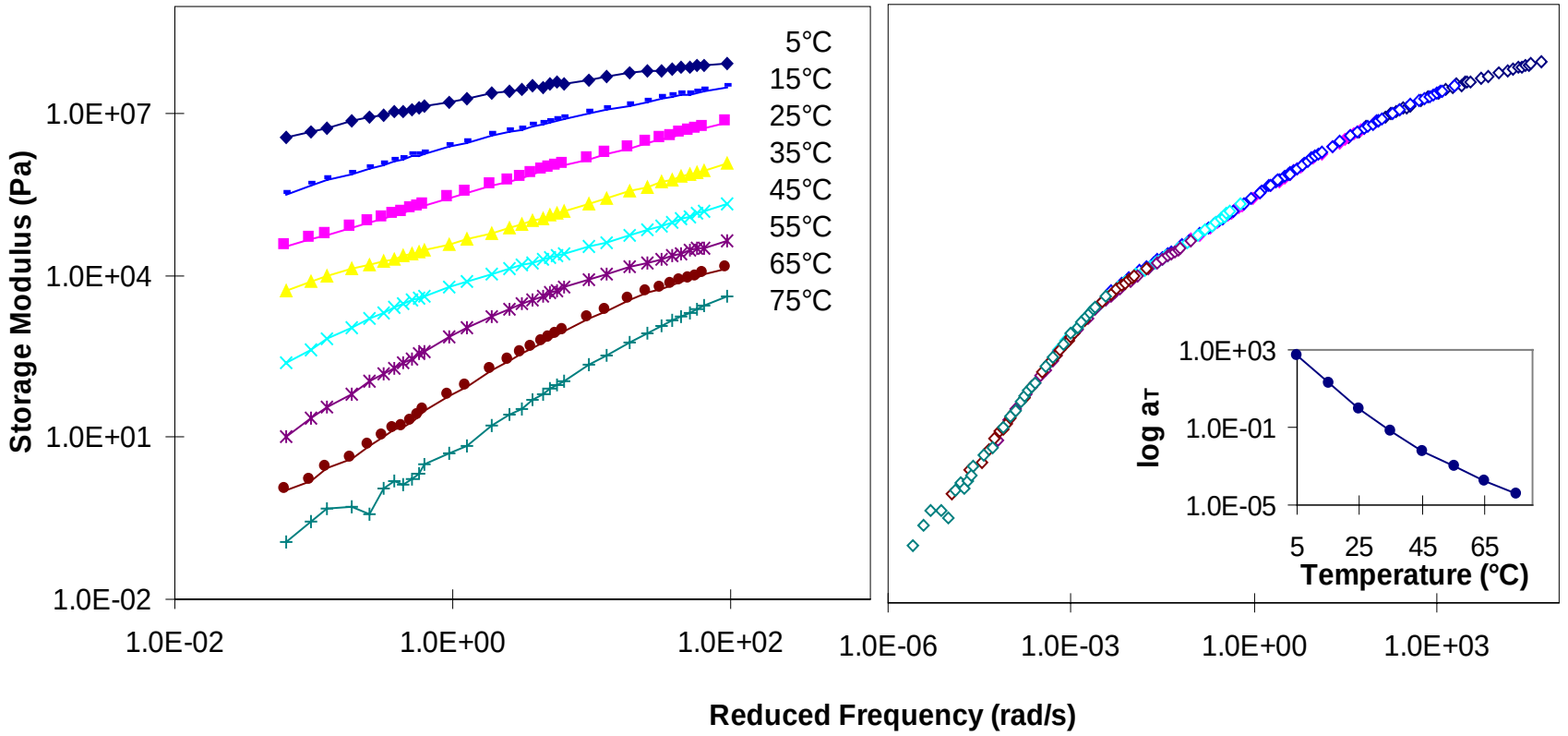

Figure A-31. Dynamic storage modulus isothermal, master curve (with reference temperature of 25°C), and shift factor, a_T, for ARN3.

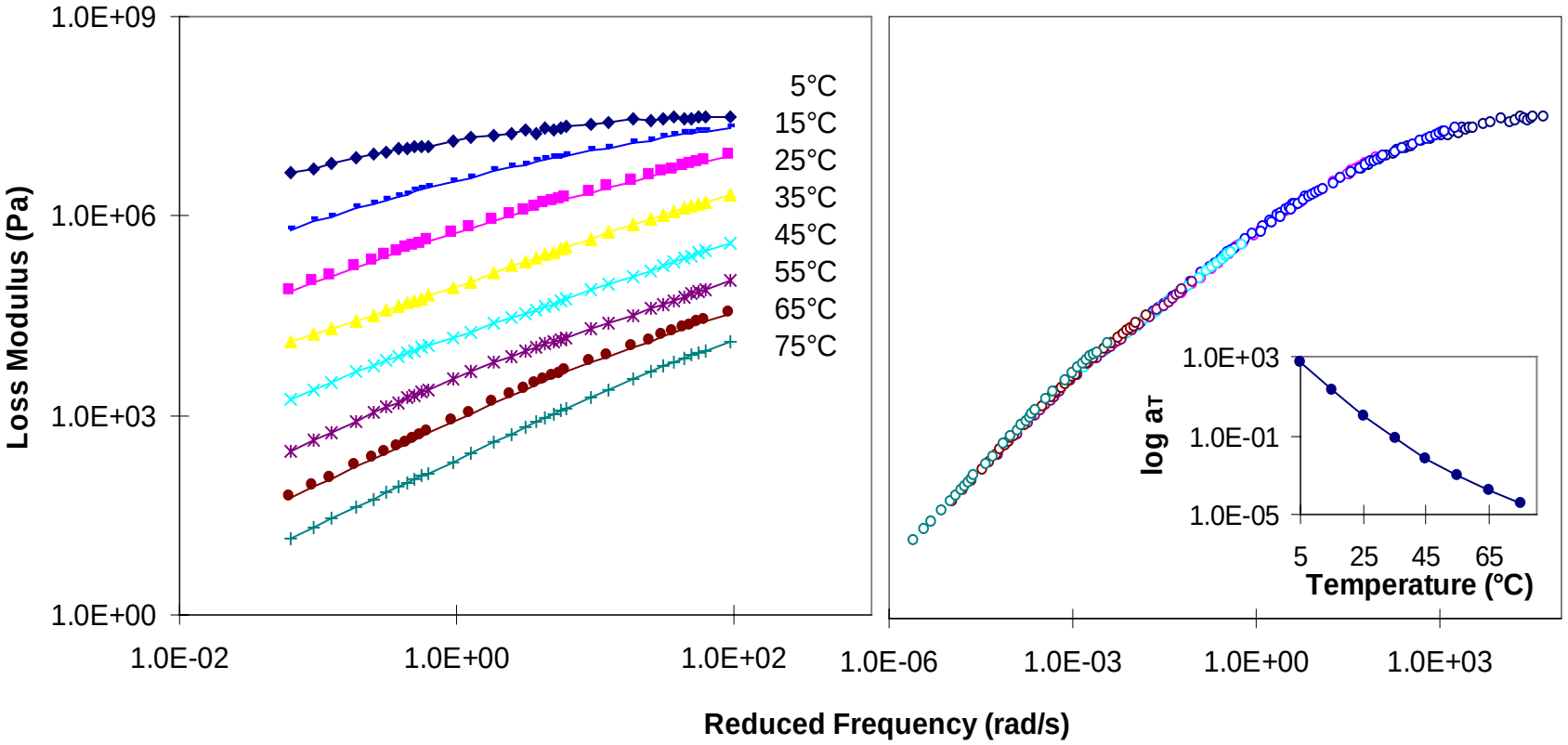

Figure A-32. Dynamic loss modulus isothermal, master curve (with reference temperature of 25°C), and shift factor, a_T, for ARN3.

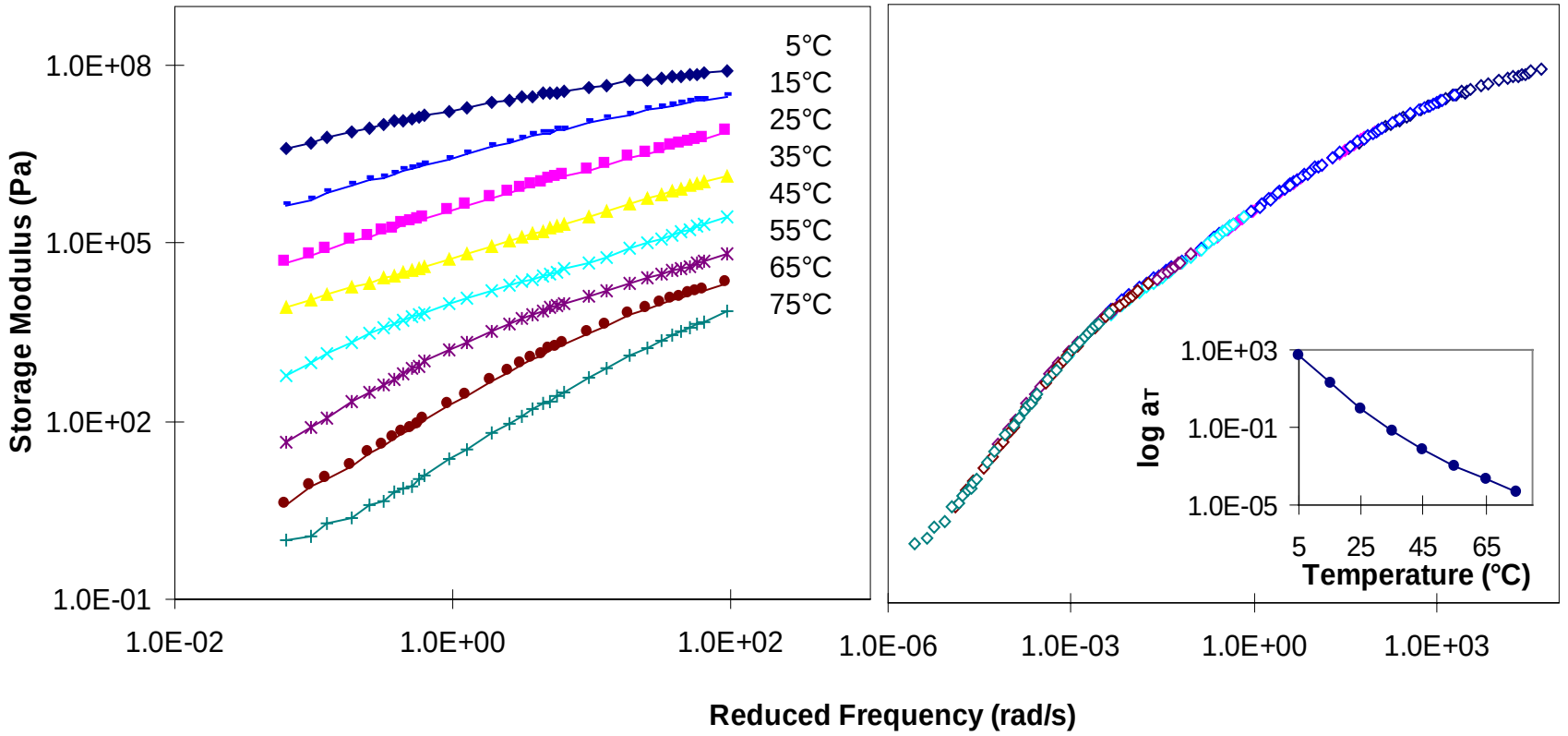

Figure A-33. Dynamic storage modulus isothermal, master curve (with reference temperature of 25°C), and shift factor, a_T, for ARN4.

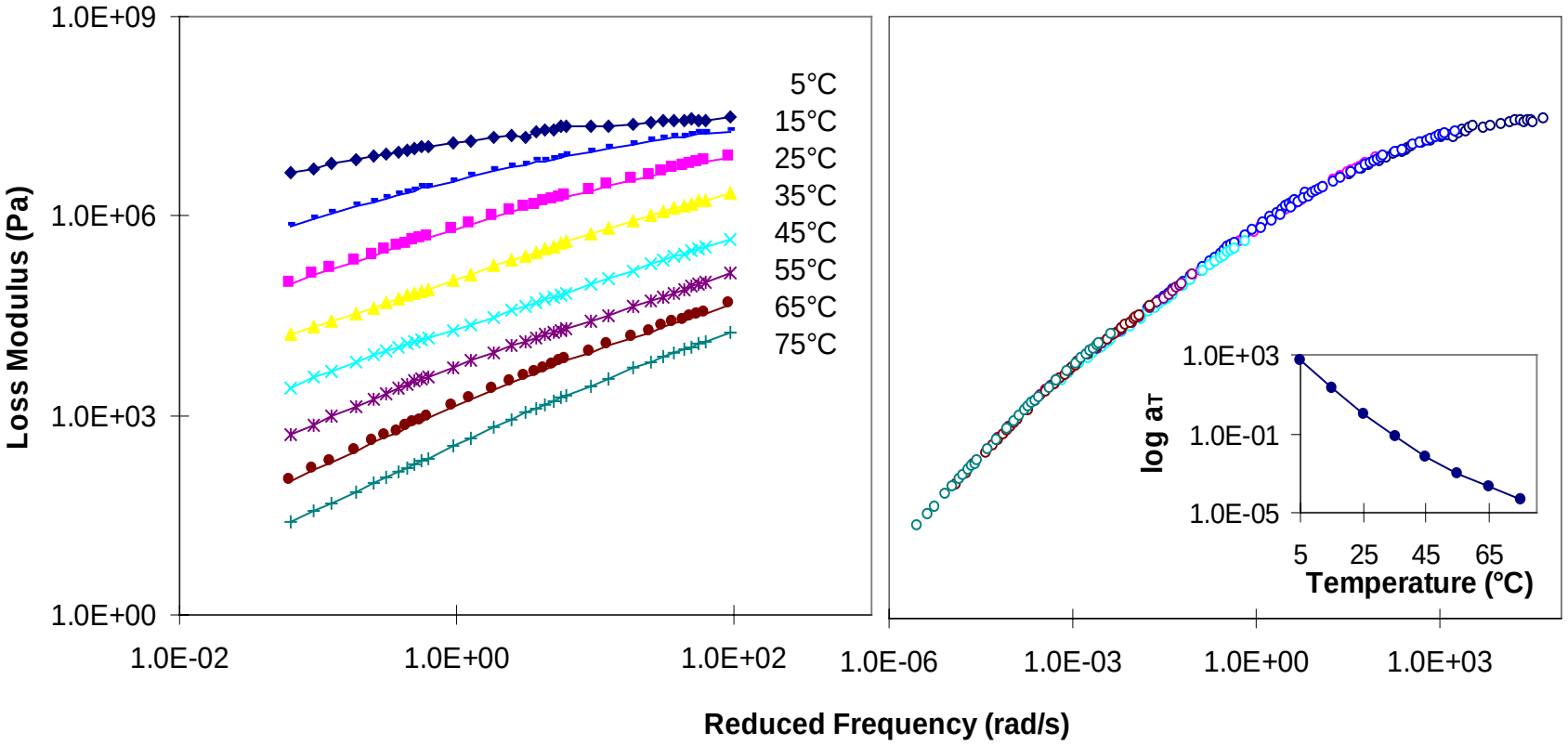

Figure A-34. Dynamic loss modulus isothermal, master curve (with reference temperature of 25°C), and shift factor, a_T, for ARN4.

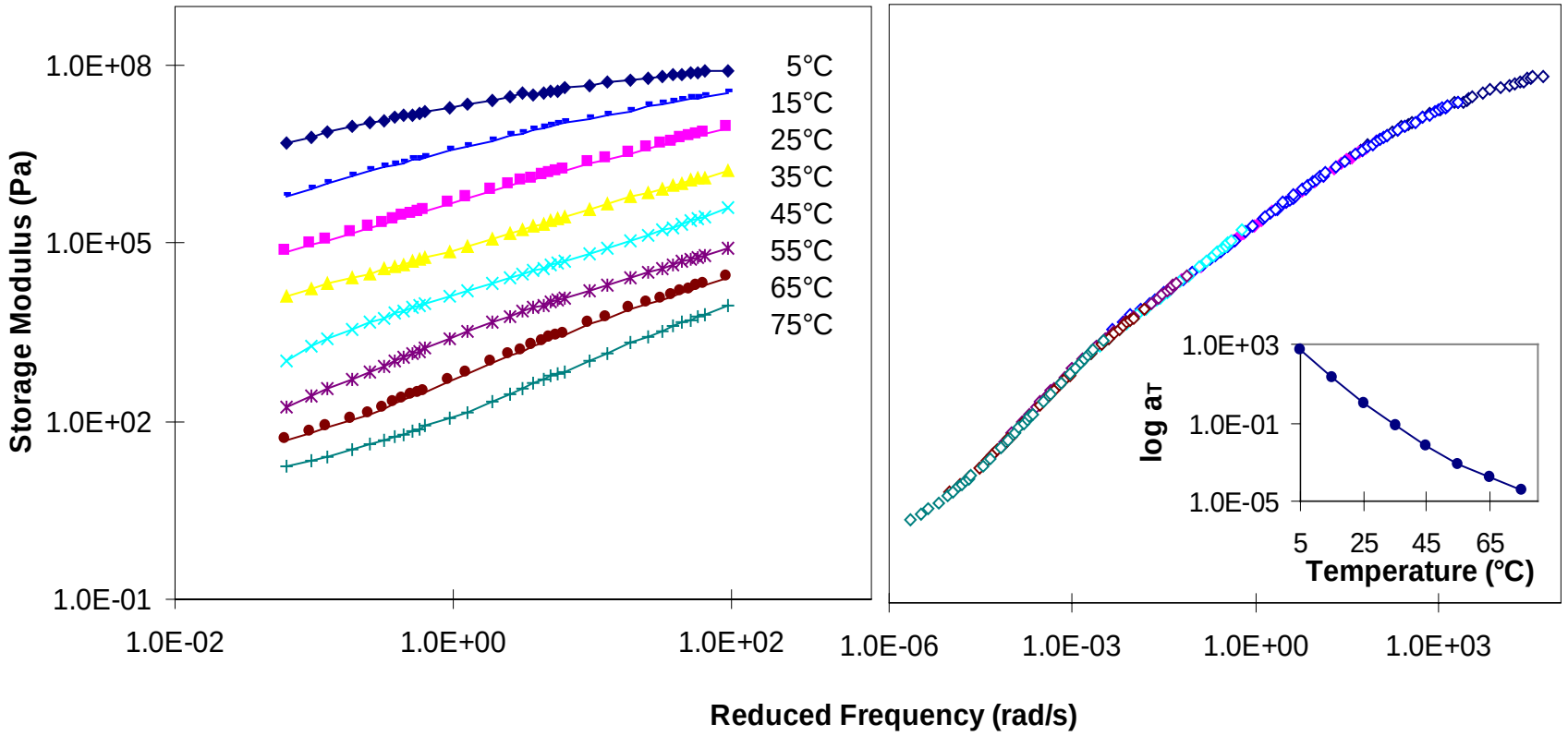

Figure A-35. Dynamic storage modulus isothermal master curve (with reference temperature of 25°C), and shift factor, a_T, for ARN5.

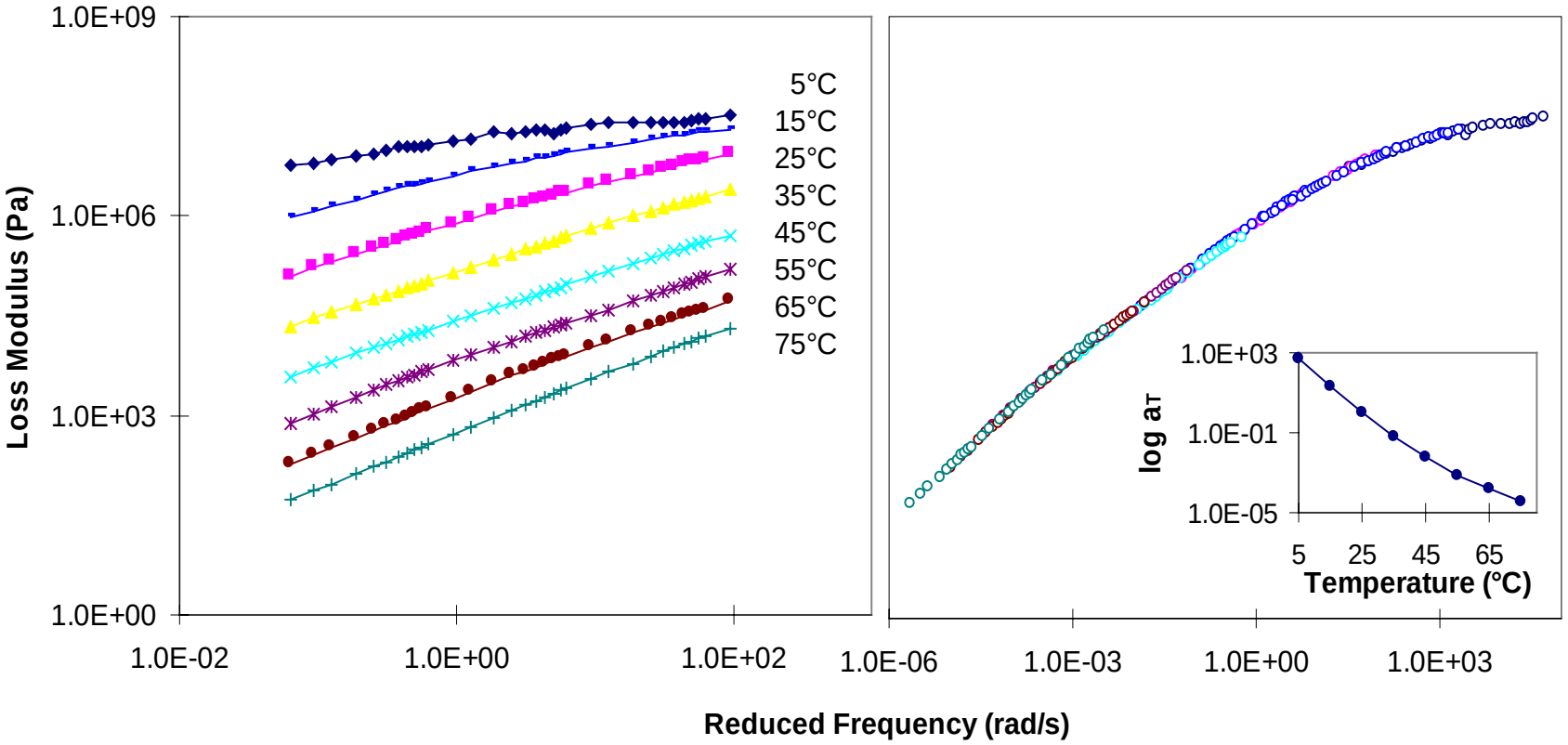

Figure A-36. Dynamic loss modulus isothermal, master curve (with reference temperature of 25°C), and shift factor, a_T, for ARN5.

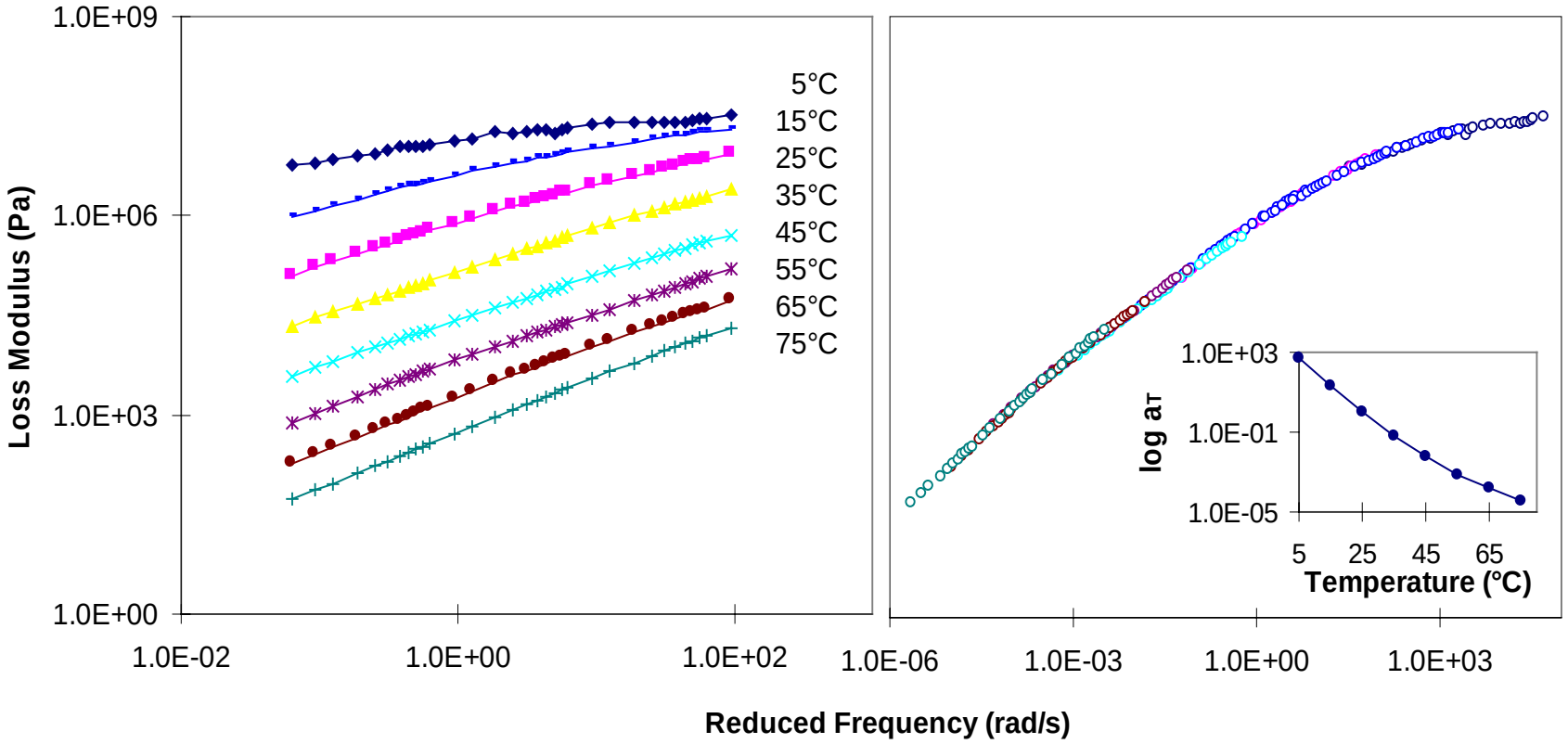

Figure A-37. Dynamic storage modulus isothermal, master curve (with reference temperature of 25°C), and shift factor, a_T, for AUP3.

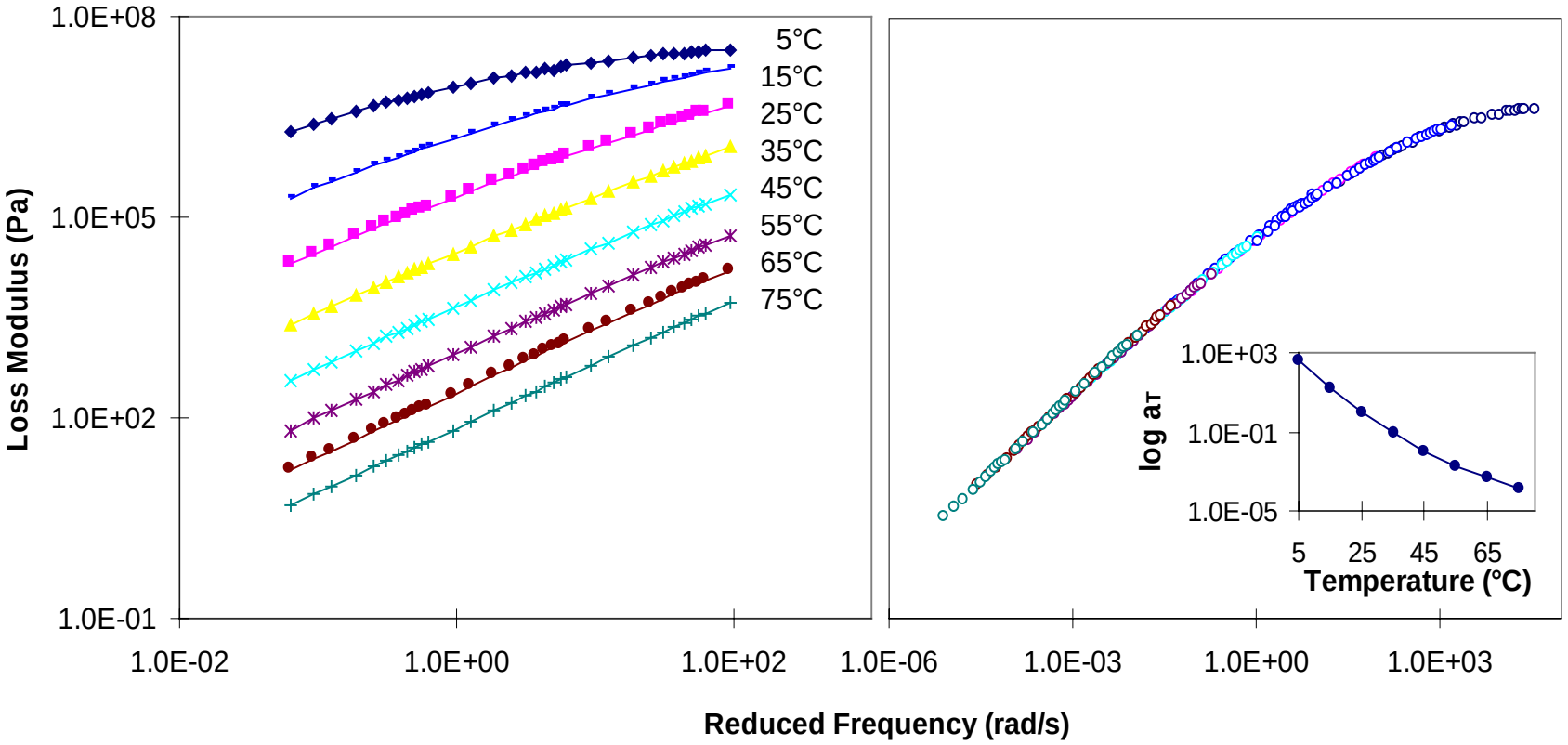

Figure A-38. Dynamic loss modulus isothermal, master curve (with reference temperature of 25°C), and shift factor, a_T, for AUP3.

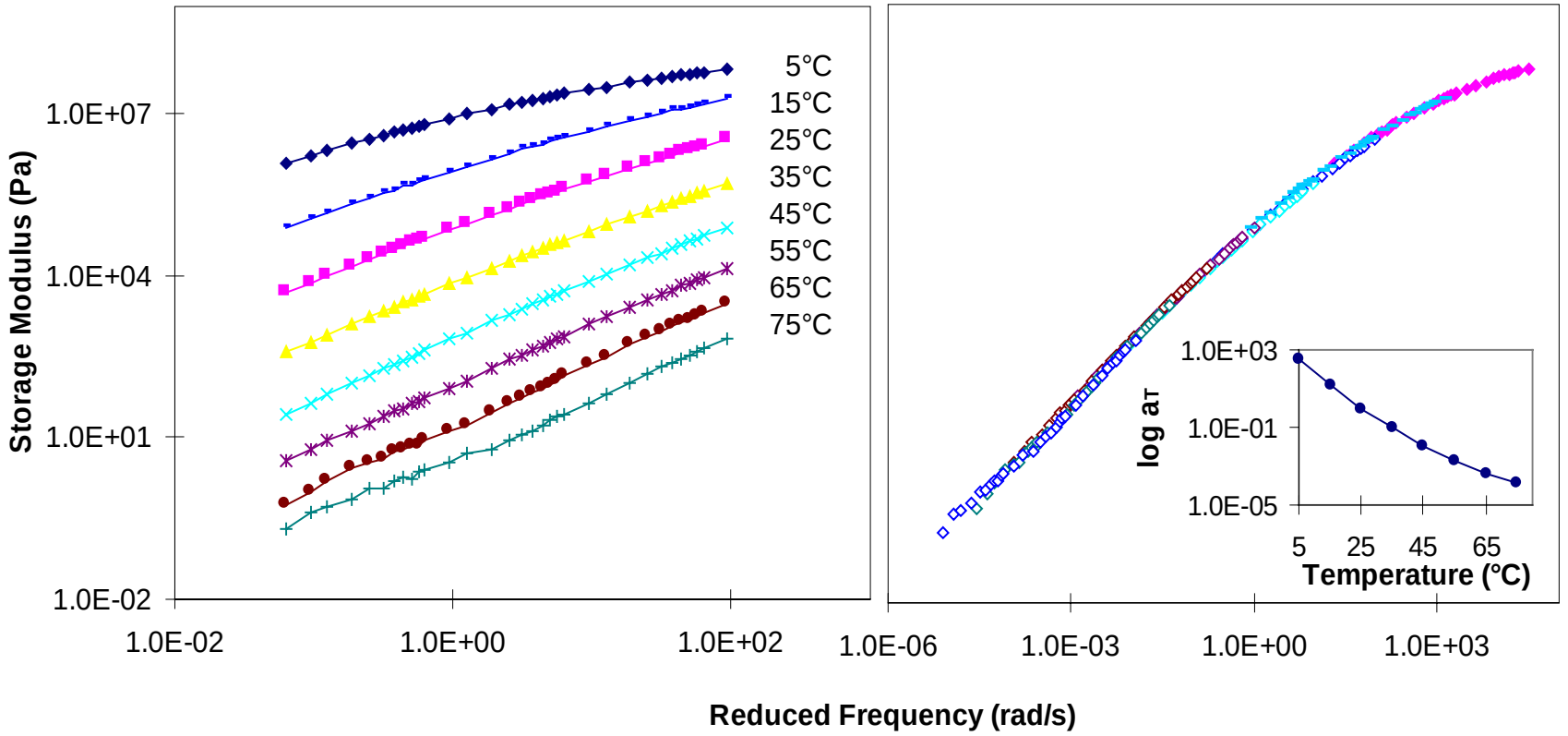

Figure A-39. Dynamic storage modulus isothermal, master curve (with reference temperature of 25°C), and shift factor, a_T, for AUP4.

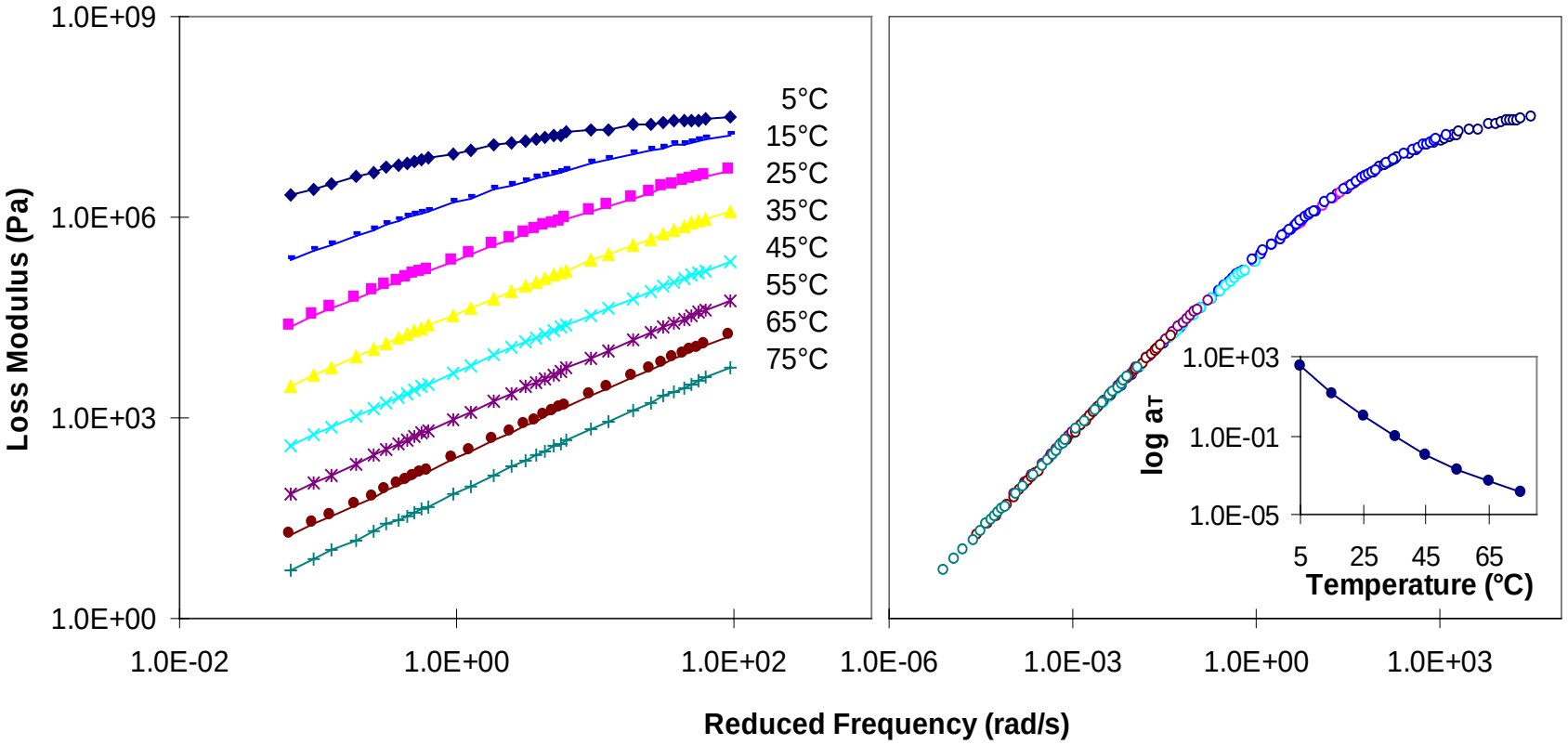

Figure A-40. Dynamic loss modulus isothermal, master curve (with reference temperature of 25°C), and shift factor, a_T, for AUP4.

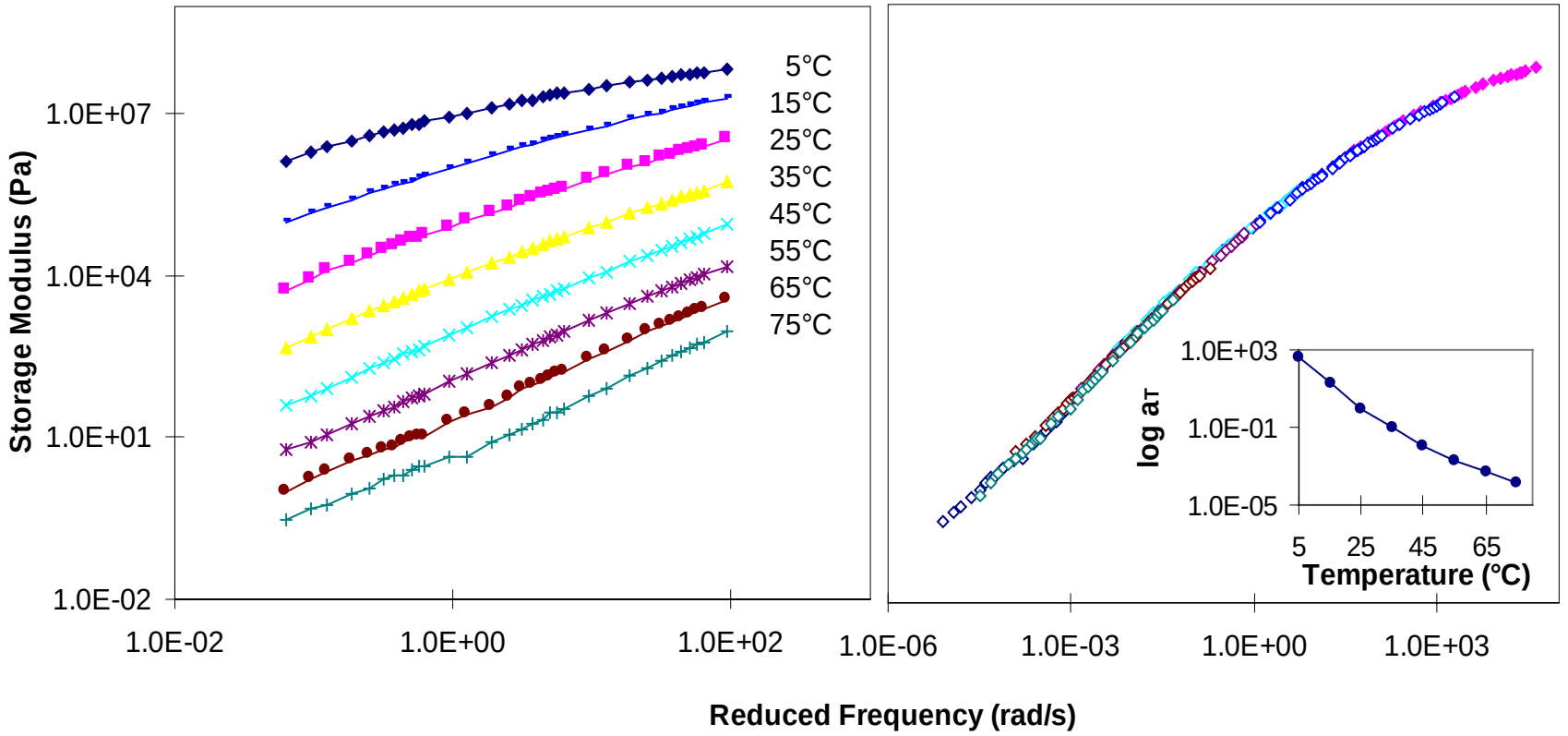

Figure A-41. Dynamic storage modulus isothermal master curve (with reference temperature of 25°C), and shift factor, a_T, for AUP5.

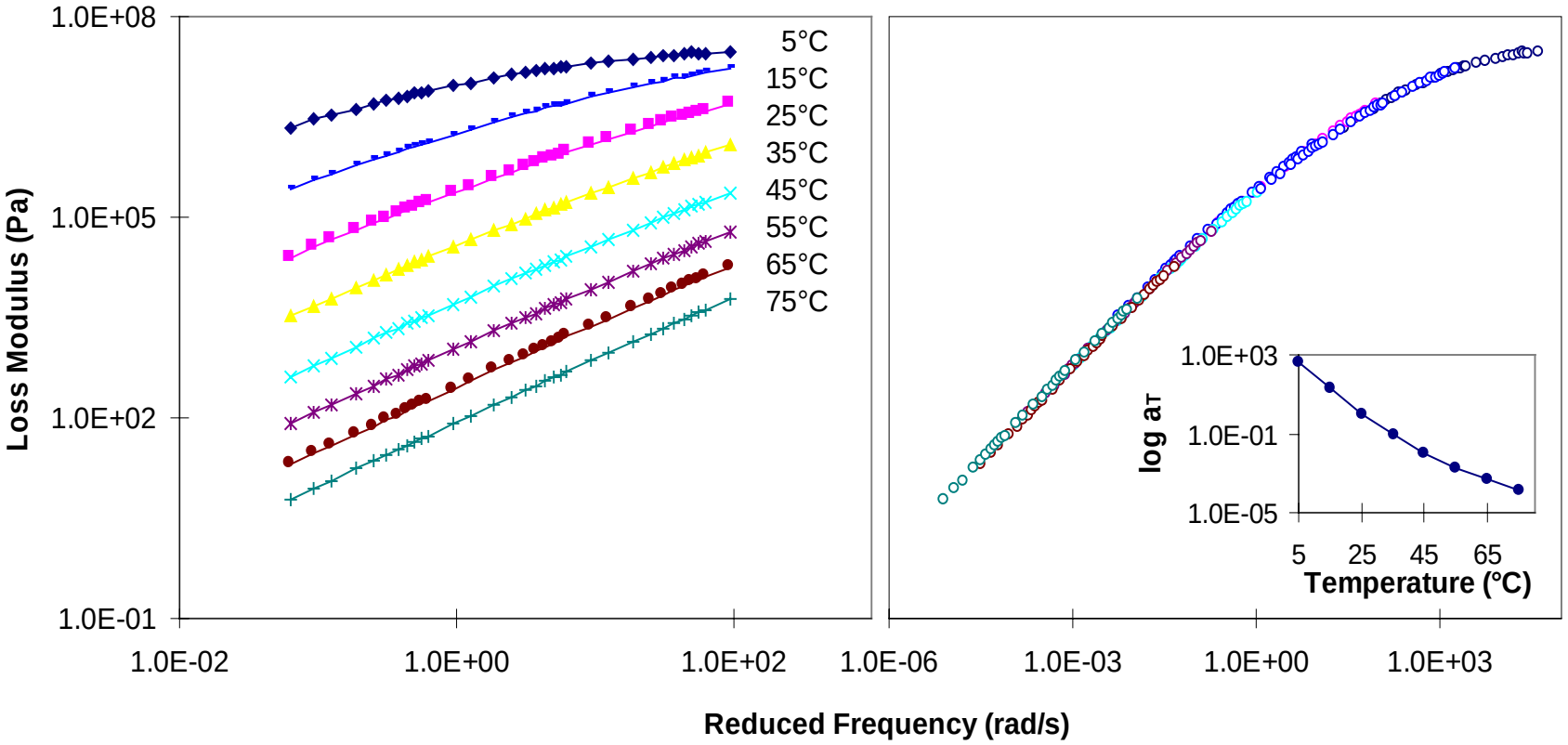

Figure A-42. Dynamic loss modulus isothermal, master curve (with reference temperature of 25°C), and shift factor, a_T, for AUP5.

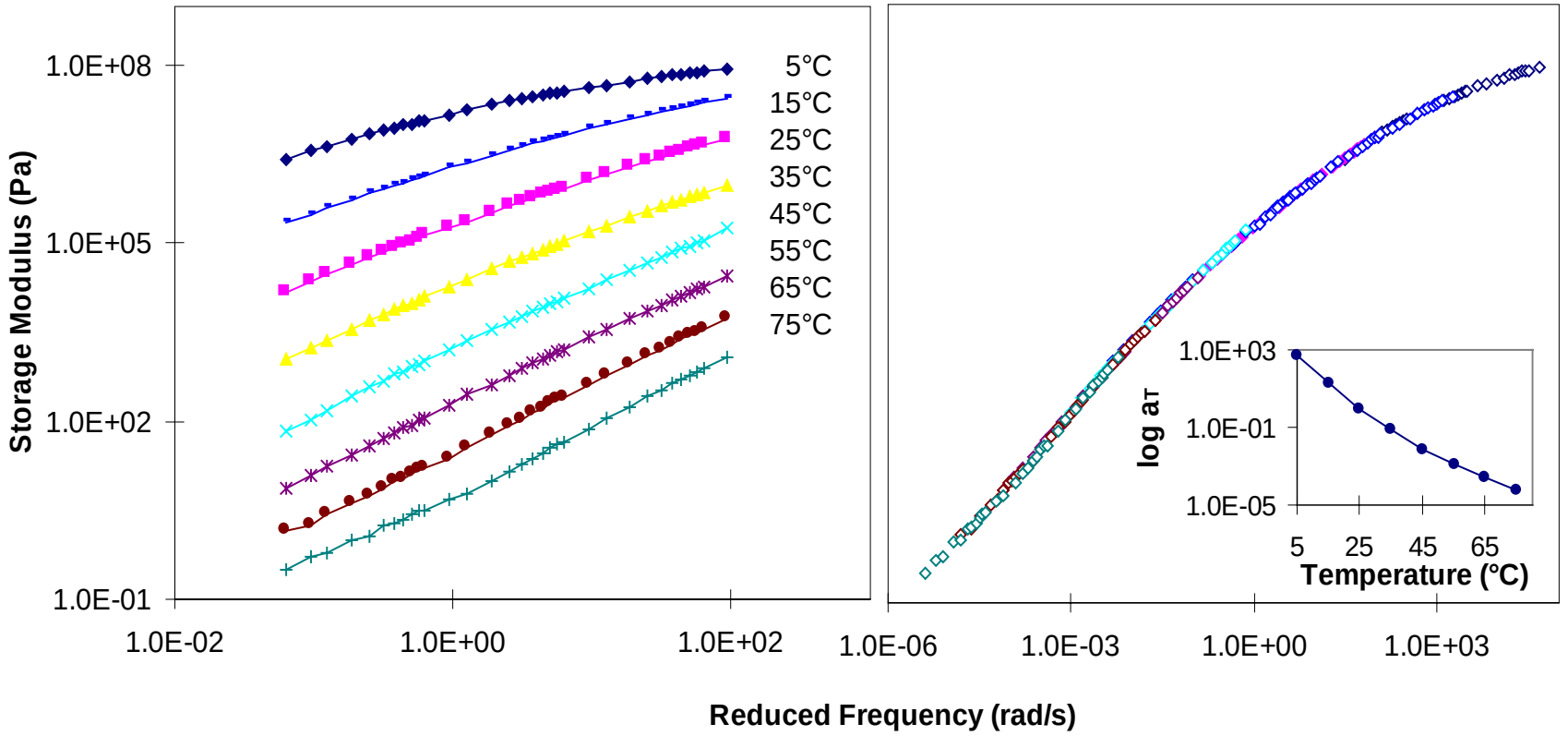

Figure A-43. Dynamic storage modulus isothermal, master curve (with reference temperature of 25°C), and shift factor, a_T, for ARP3.

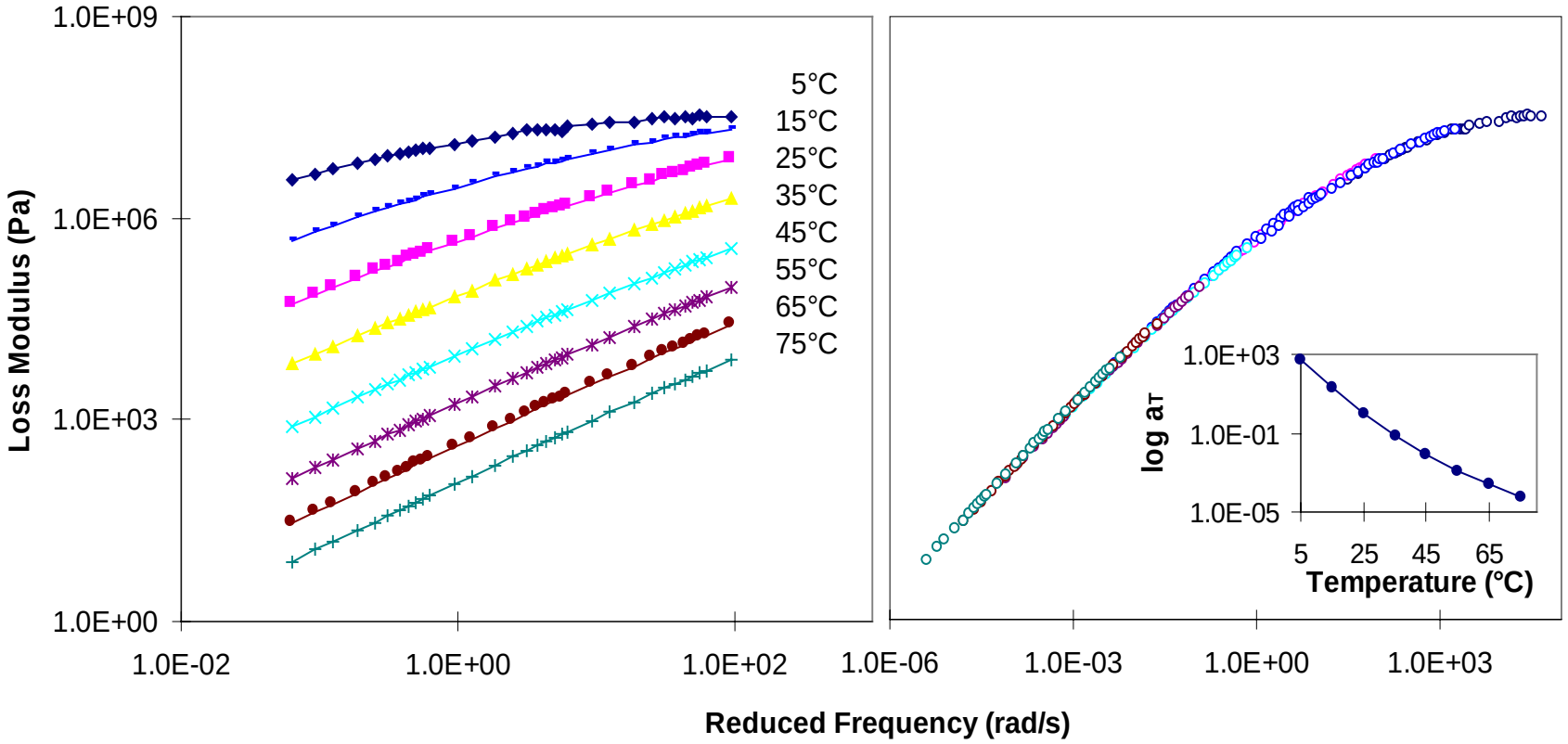

Figure A-44. Dynamic loss modulus isothermal, master curve (with reference temperature of 25°C), and shift factor, a_T, for ARP3.

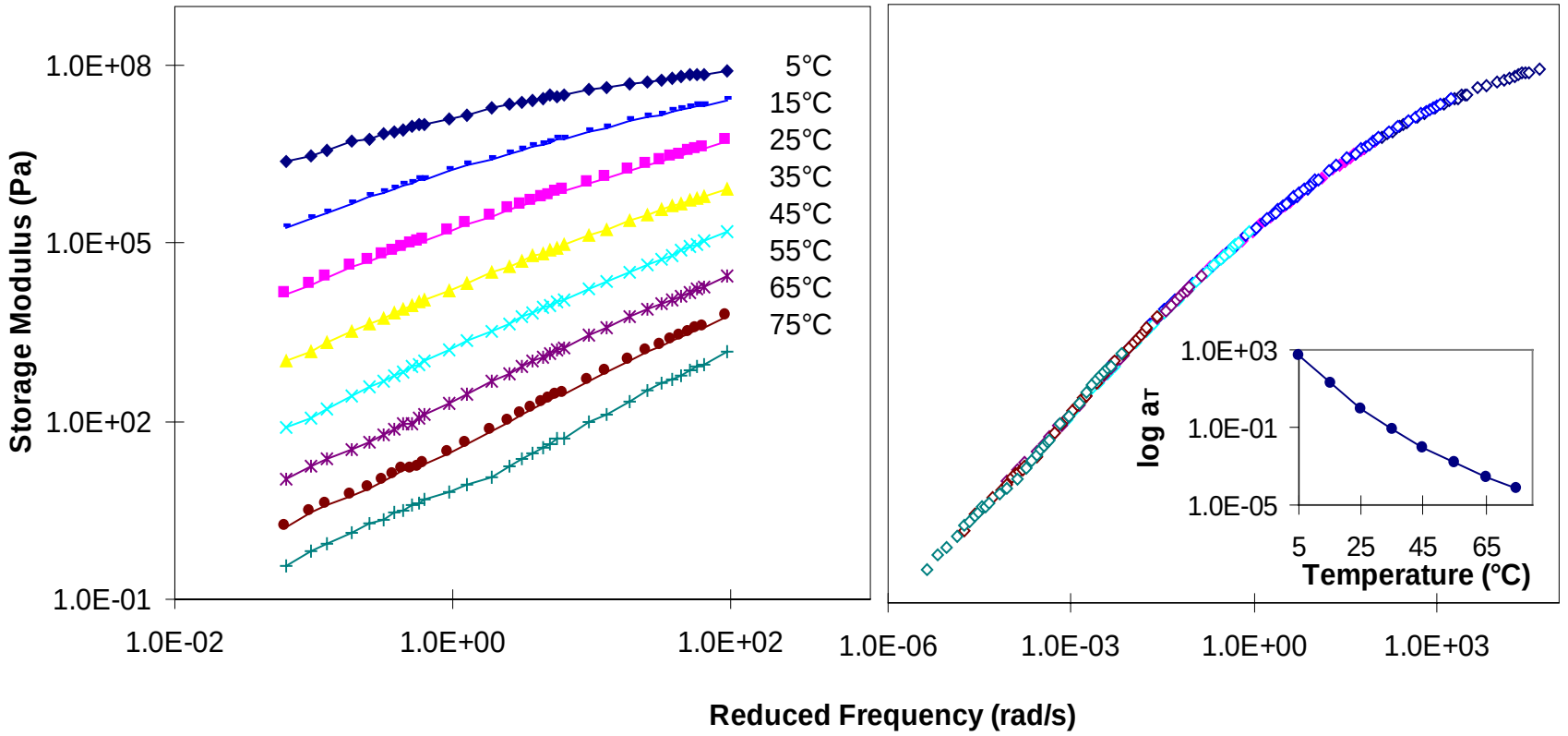

Figure A-45. Dynamic storage modulus isothermal, master curve (with reference temperature of 25°C), and shift factor, a_T, for ARP4.

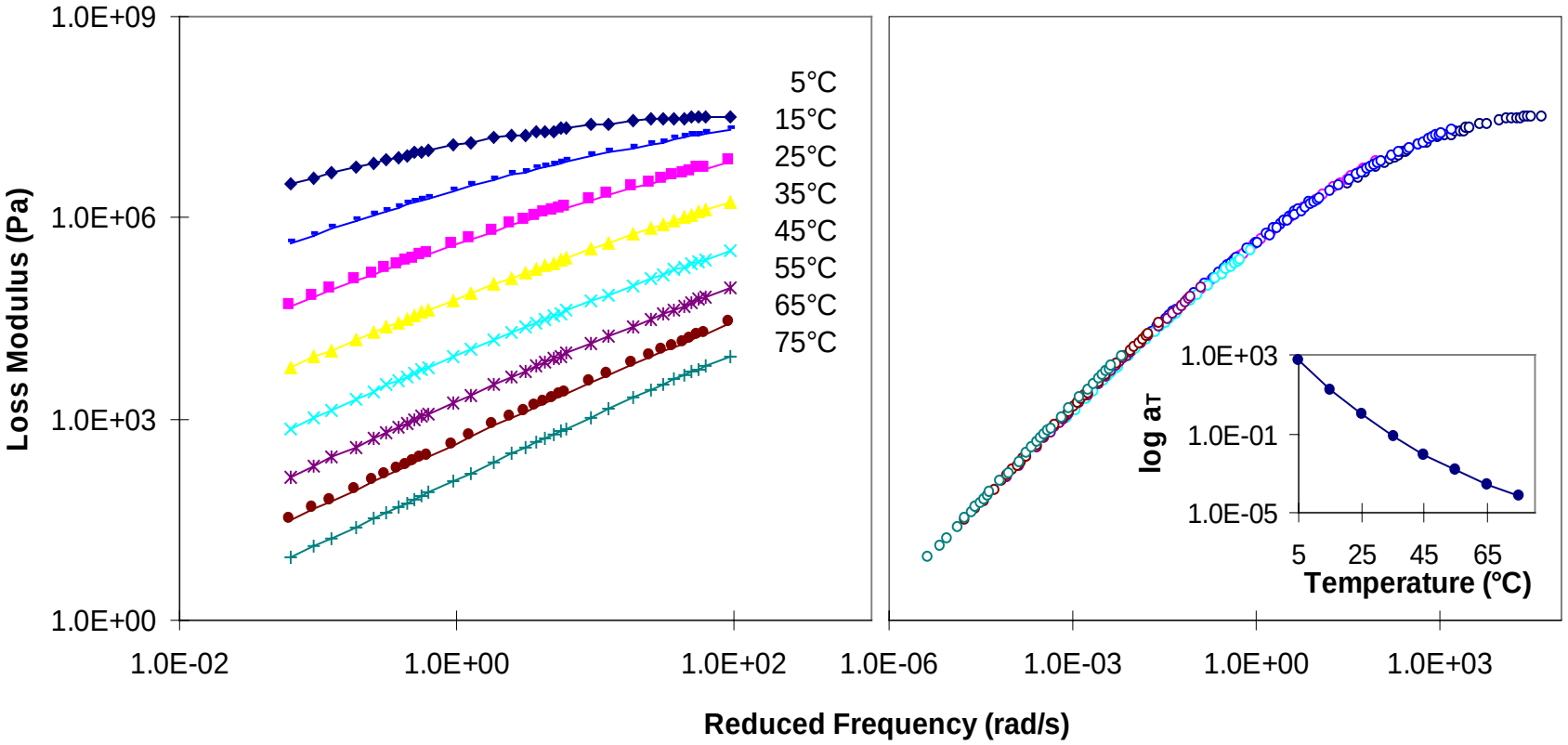

Figure A-46. Dynamic loss modulus isothermal, master curve (with reference temperature of 25°C), and shift factor, a_T, for ARP4.

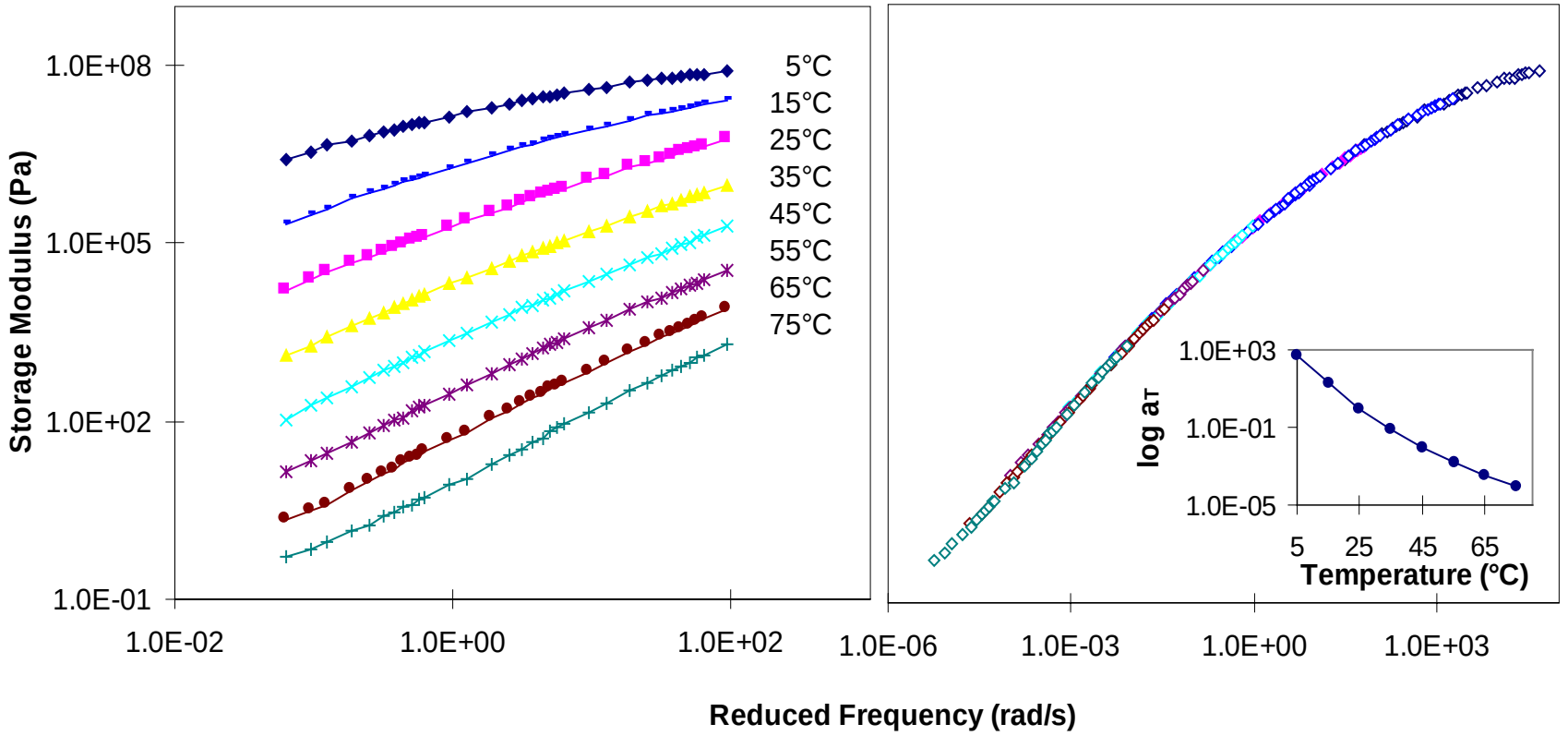

Figure A-47. Dynamic storage modulus isothermal master curve (with reference temperature of 25°C), and shift factor, a_T, for ARP5.

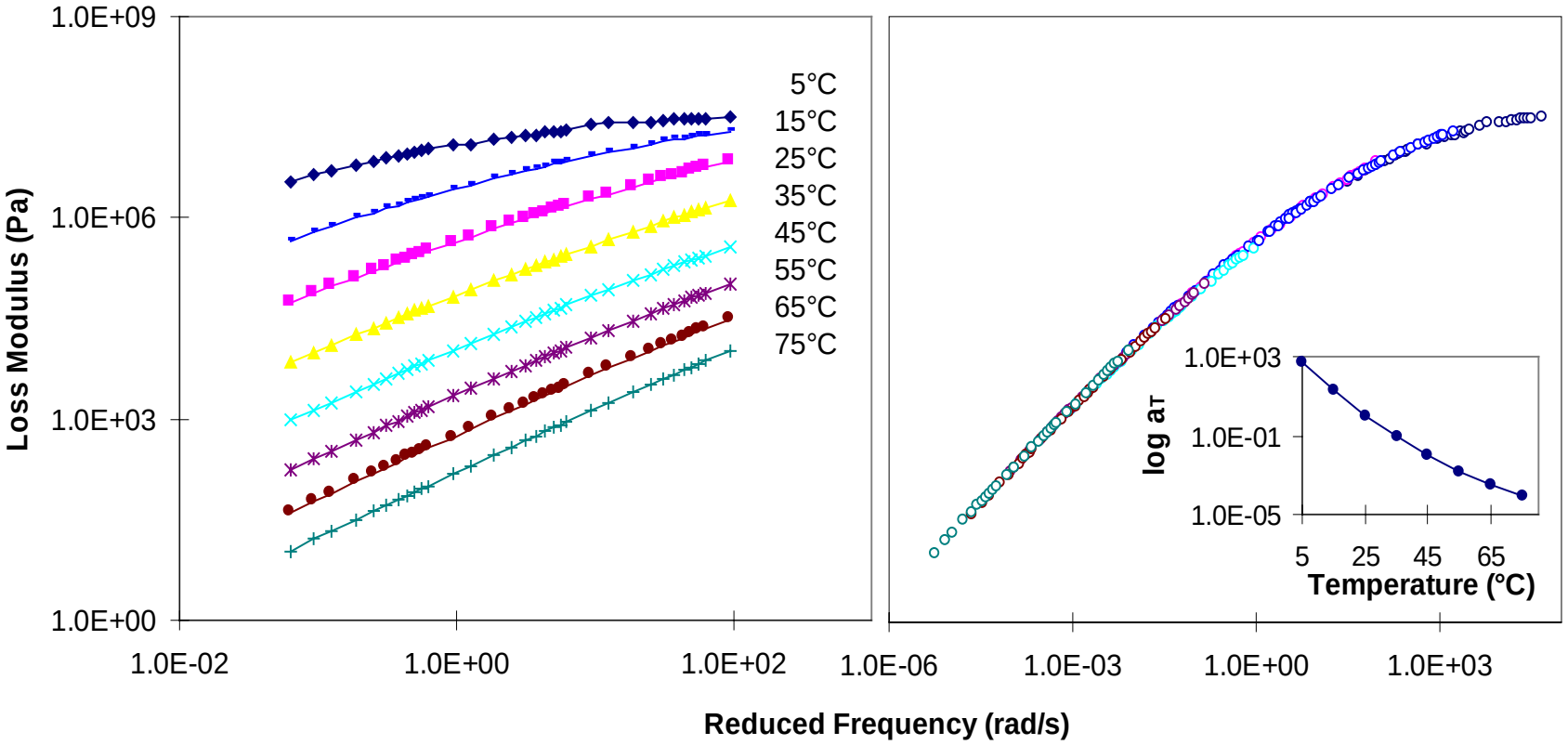

Figure A-48. Dynamic loss modulus isothermal, master curve (with reference temperature of 25°C), and shift factor, a_T, for ARP5.

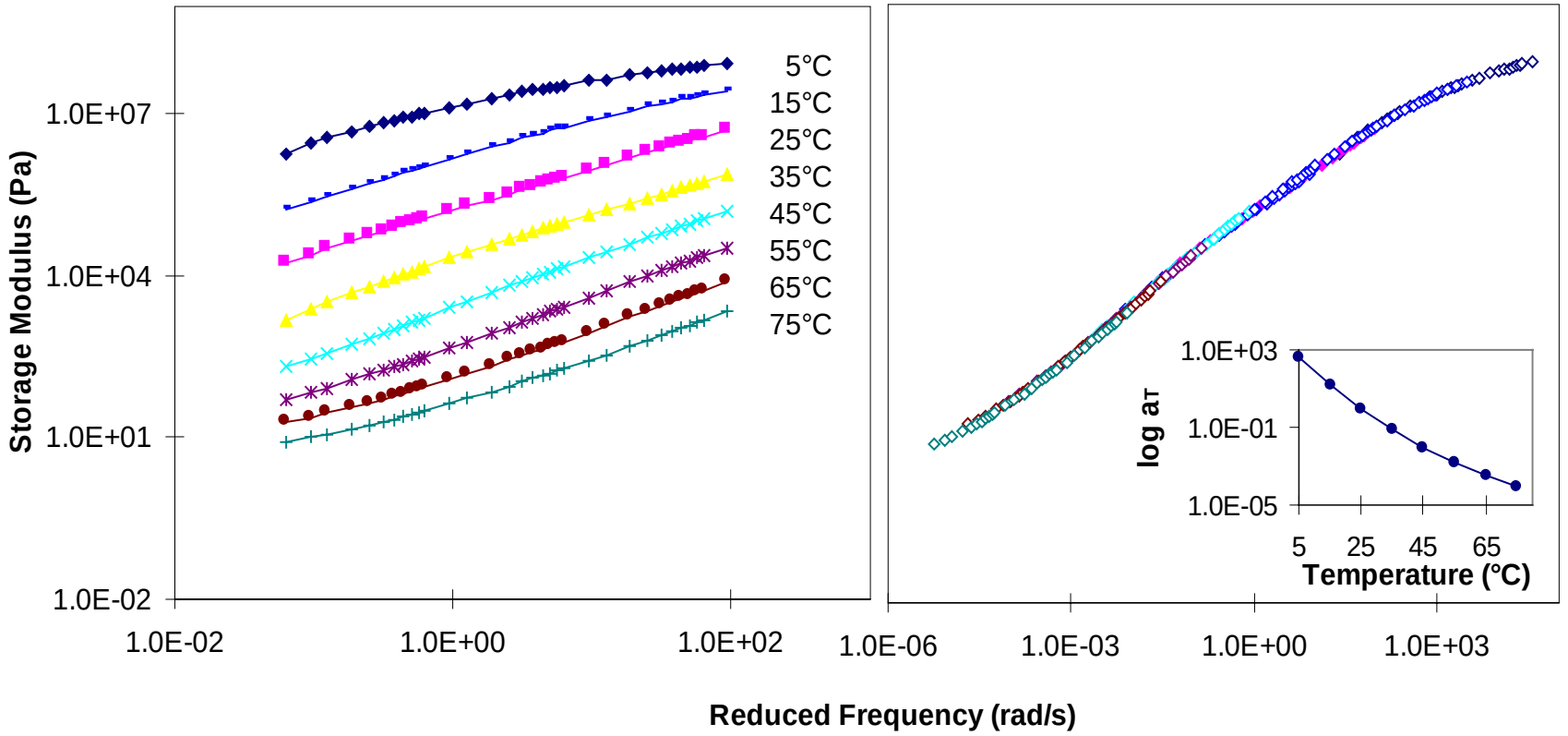

Figure A-49. Dynamic storage modulus isothermal, master curve (with reference temperature of 25°C), and shift factor, a_T, for AUX3.

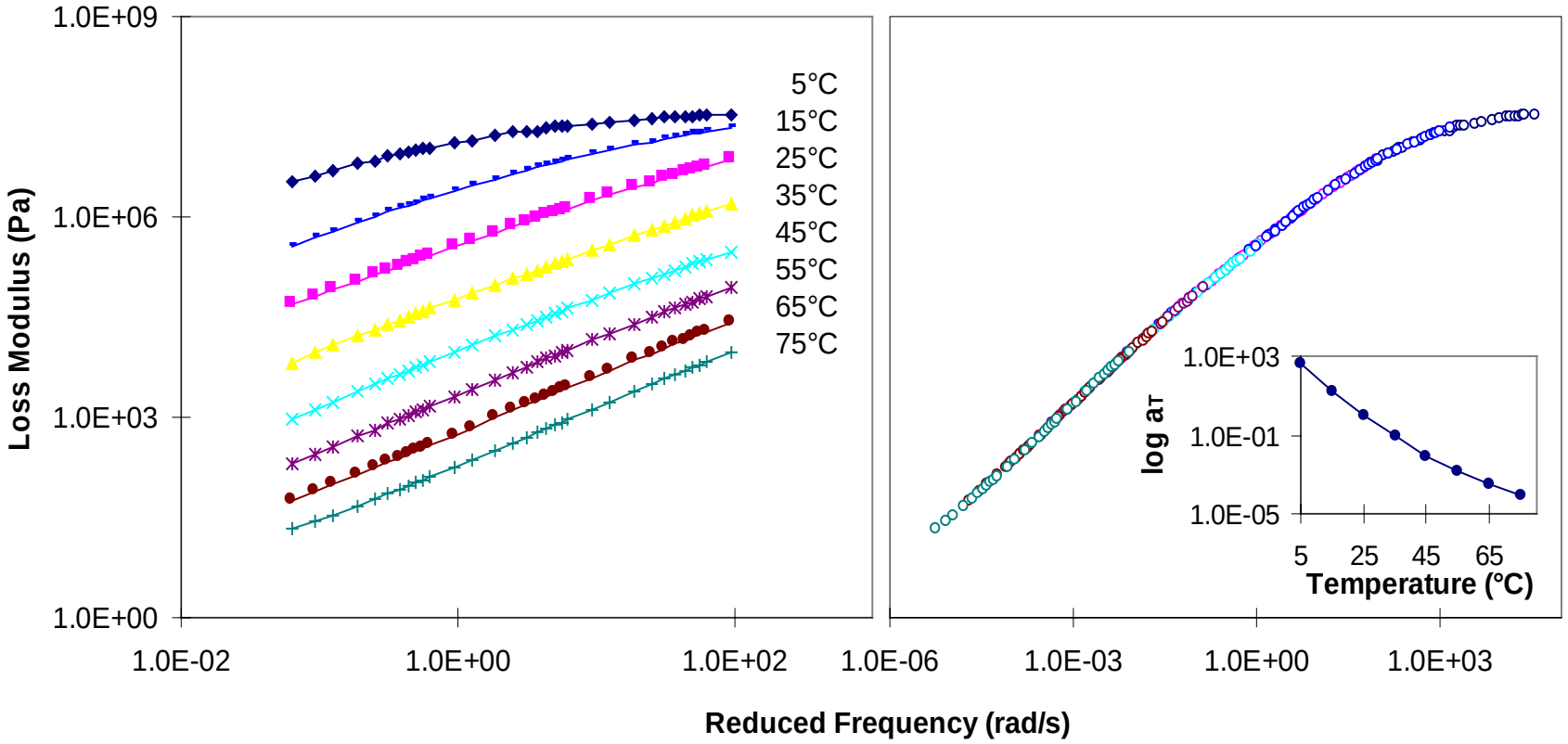

Figure A-50. Dynamic loss modulus isothermal master curve (with reference temperature of 25°C), and shift factor, a_T, for AUX3.

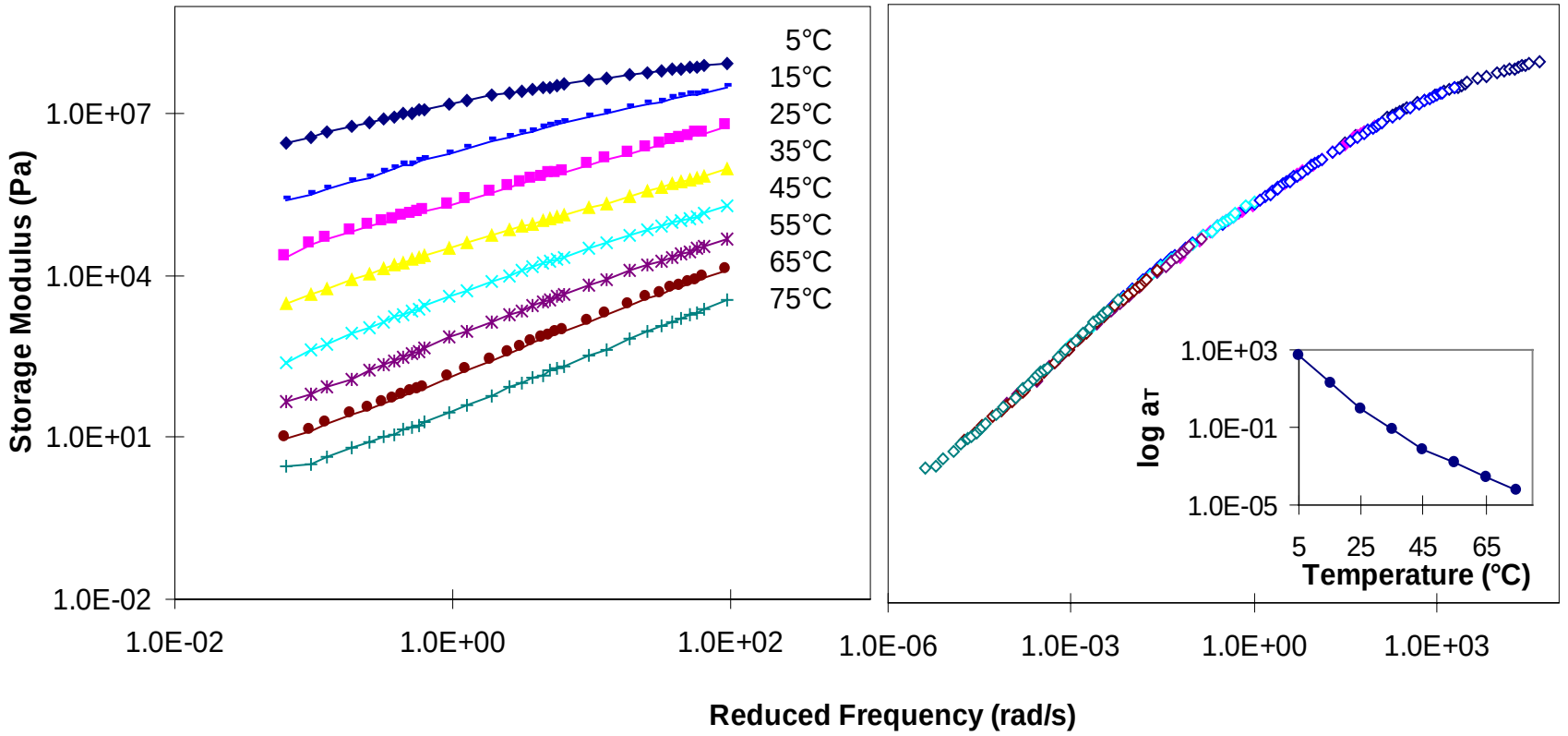

Figure A-51. Dynamic storage modulus isothermal, master curve (with reference temperature of 25°C), and shift factor, a_T, for AUX4.

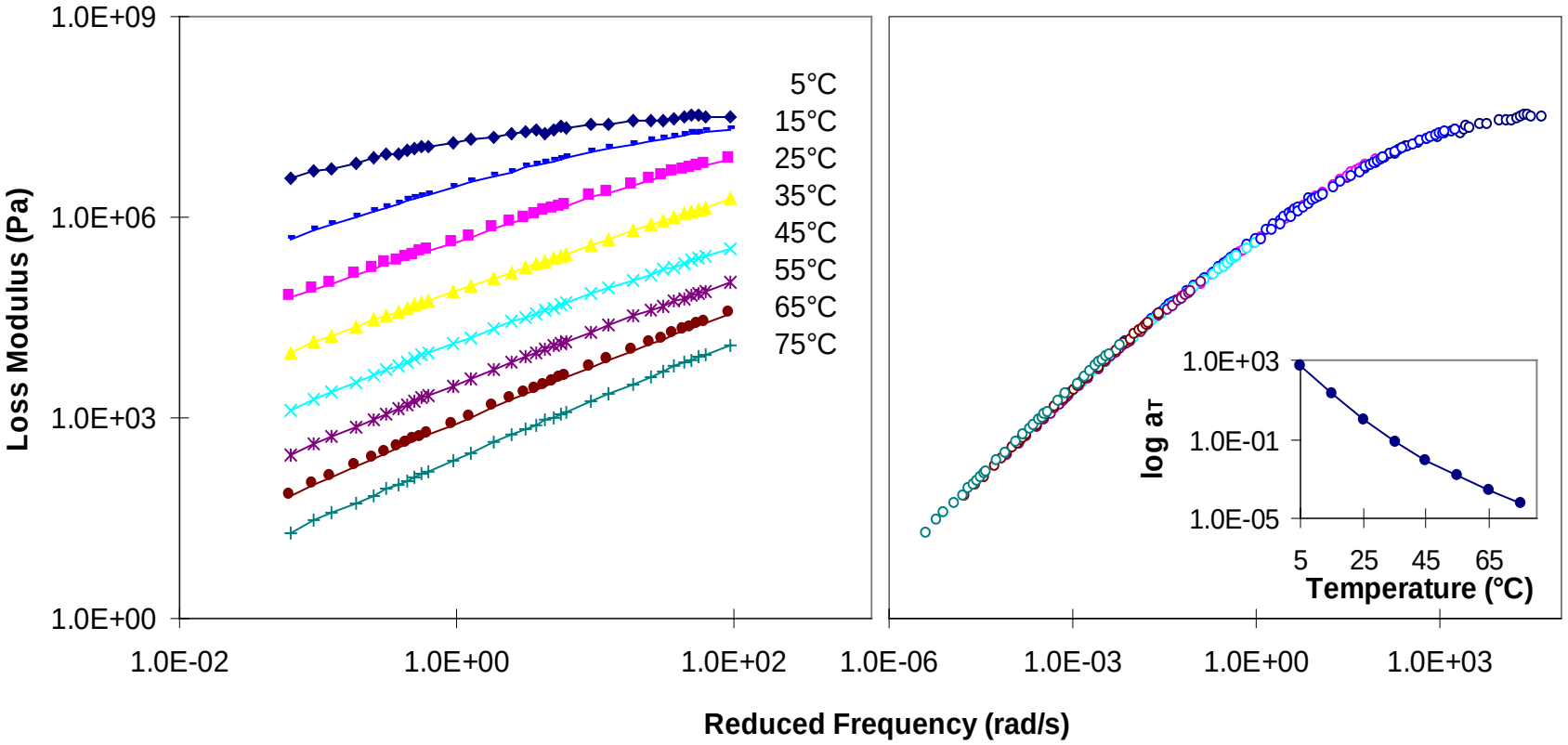

Figure A-52. Dynamic loss modulus isothermal, master curve (with reference temperature of 25°C), and shift factor, a_T, for AUX4.

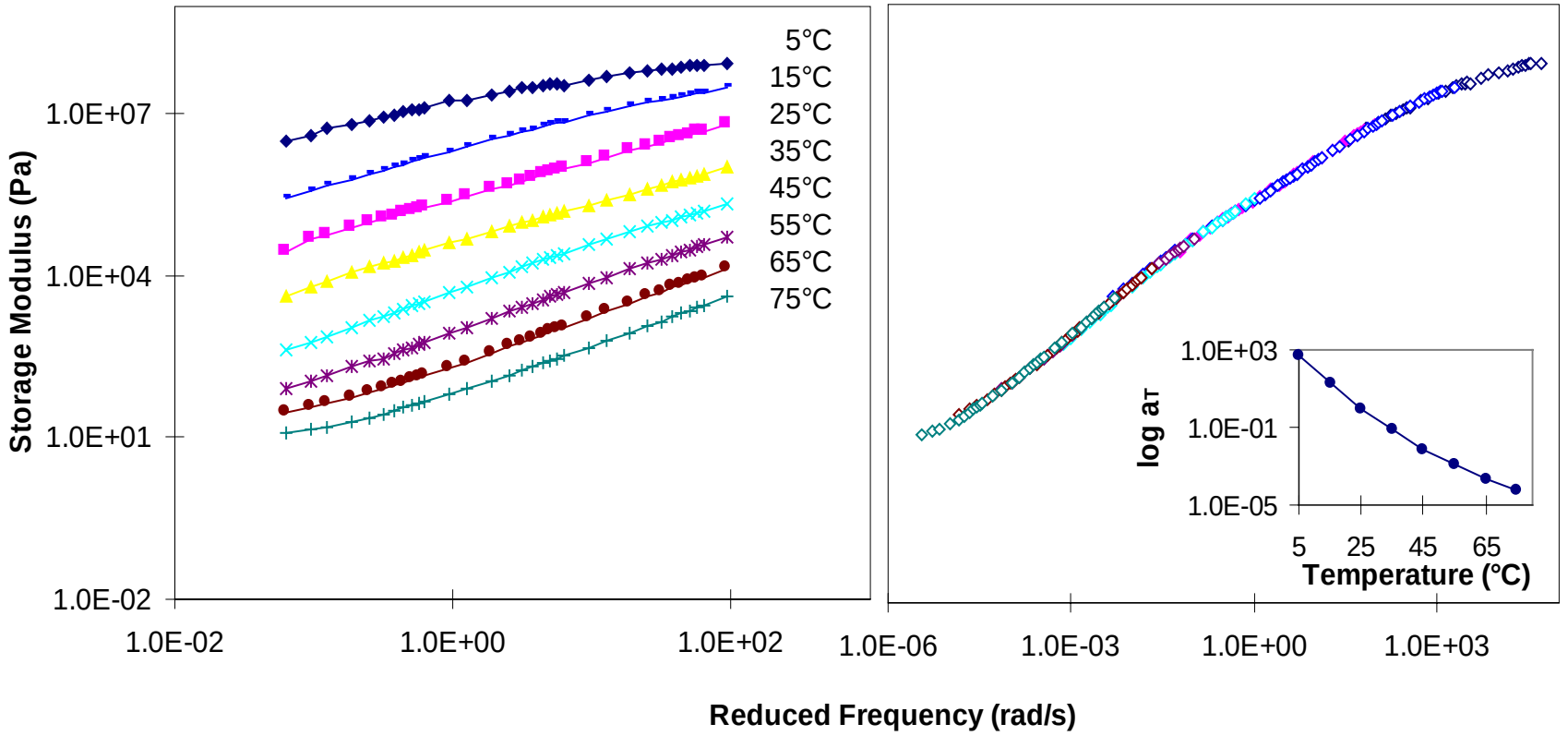

Figure A-53. Dynamic storage modulus isothermal, master curve (with reference temperature of 25°C), and shift factor, a_T, for AUX5.

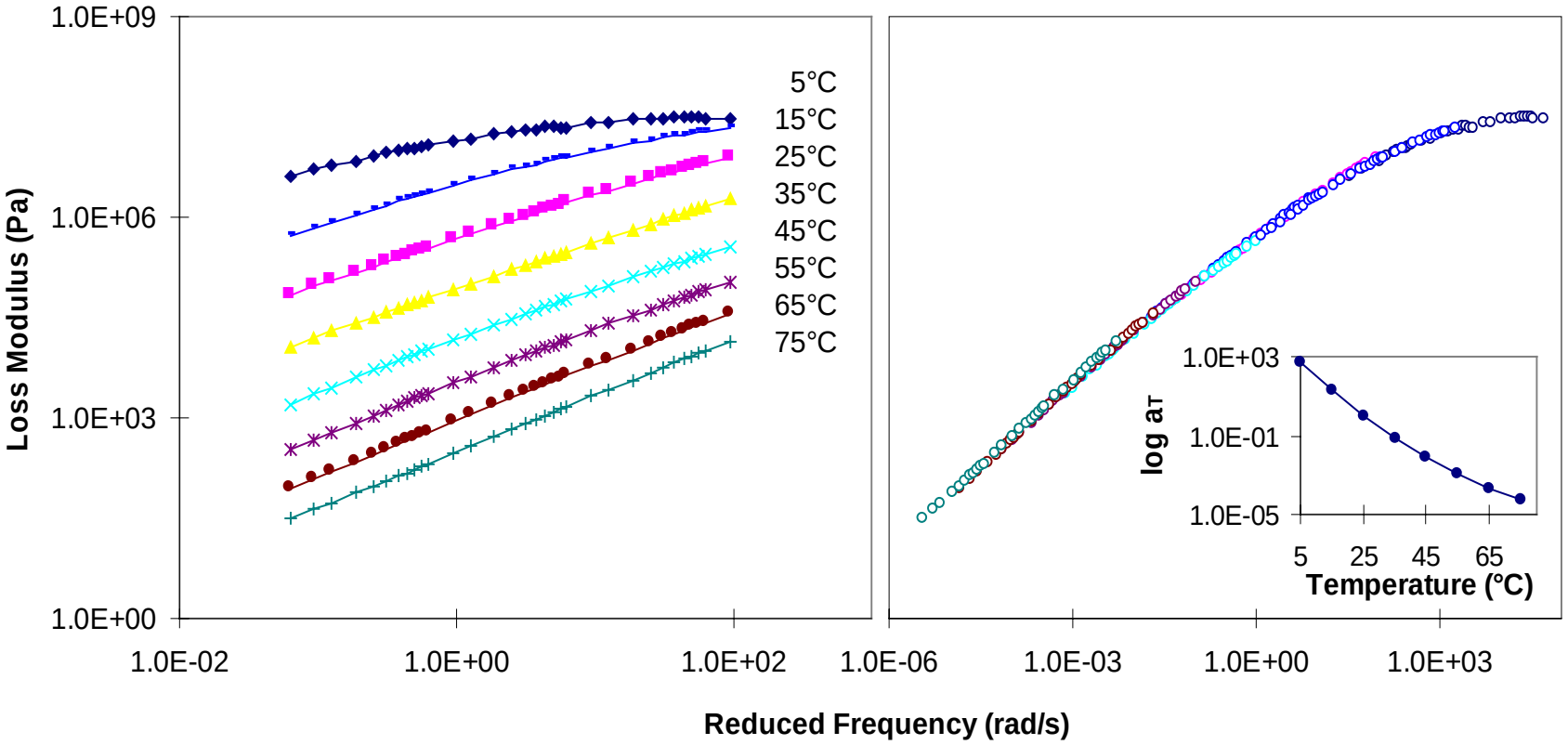

Figure A-54. Dynamic loss modulus isothermal, master curve (with reference temperature of 25°C), and shift factor, a_T, for AUX5.

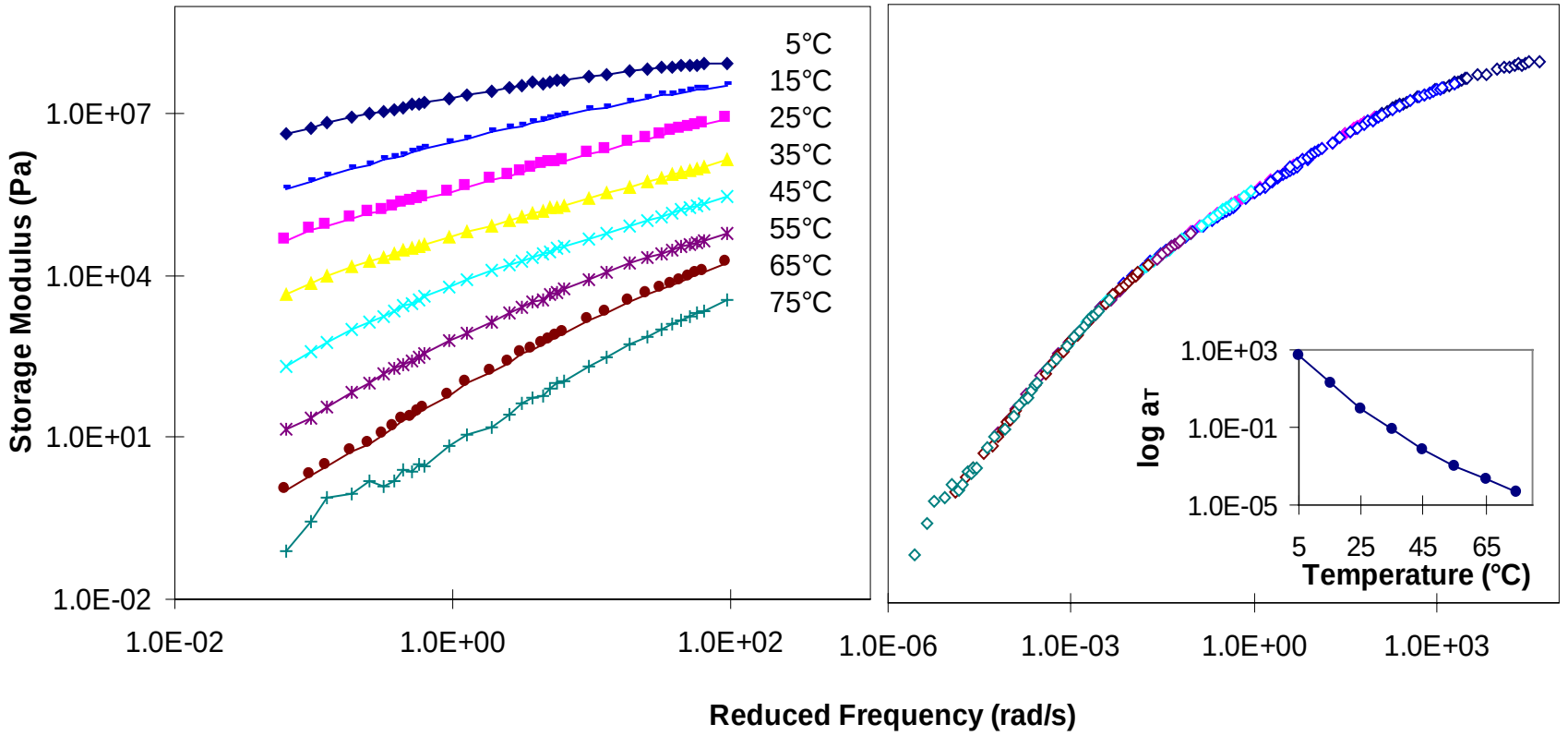

Figure A-55. Dynamic storage modulus isothermal, master curve (with reference temperature of 25°C), and shift factor, a_T, for ARX3.

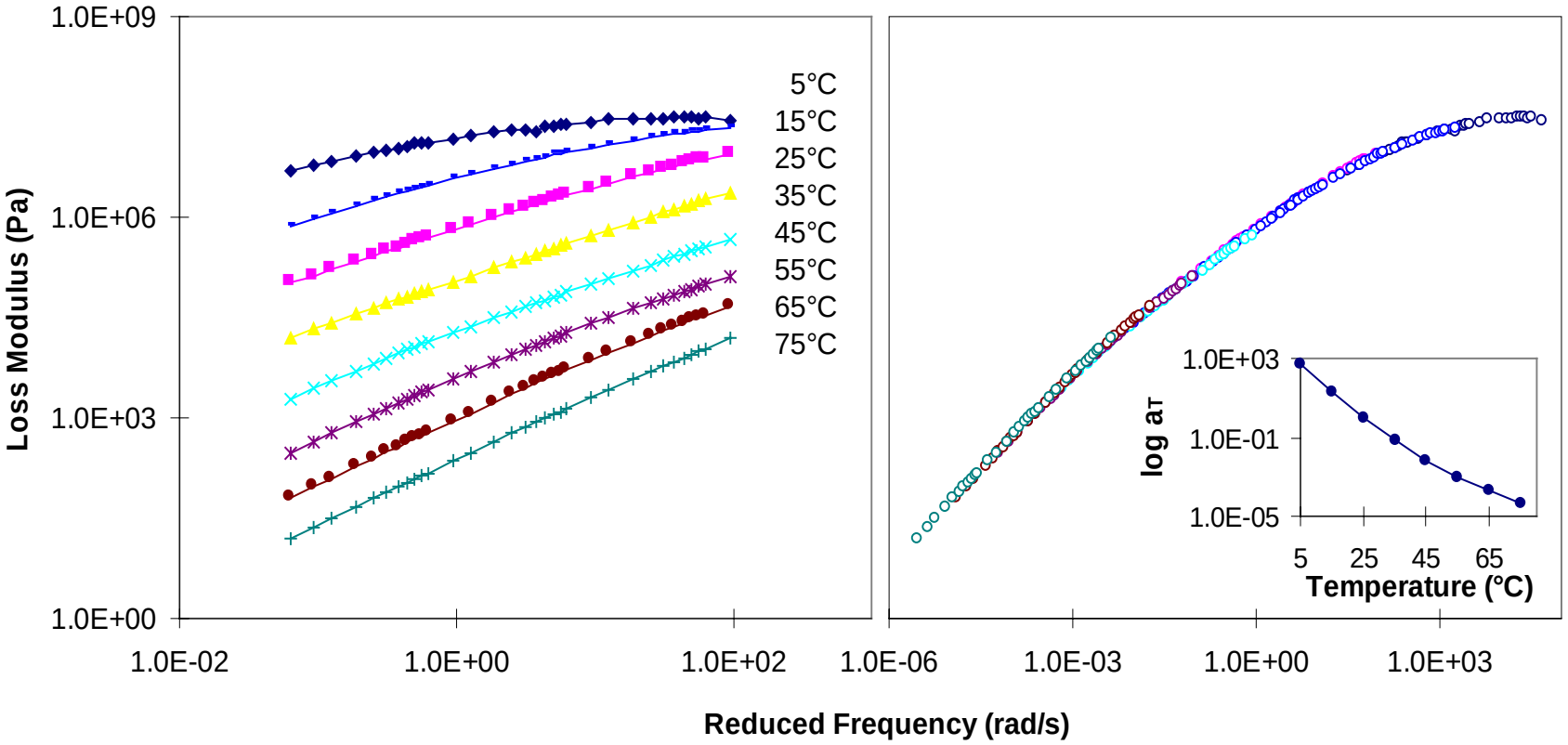

Figure A-56. Dynamic loss modulus isothermal, master curve (with reference temperature of 25°C), and shift factor, a_T, for ARX3.

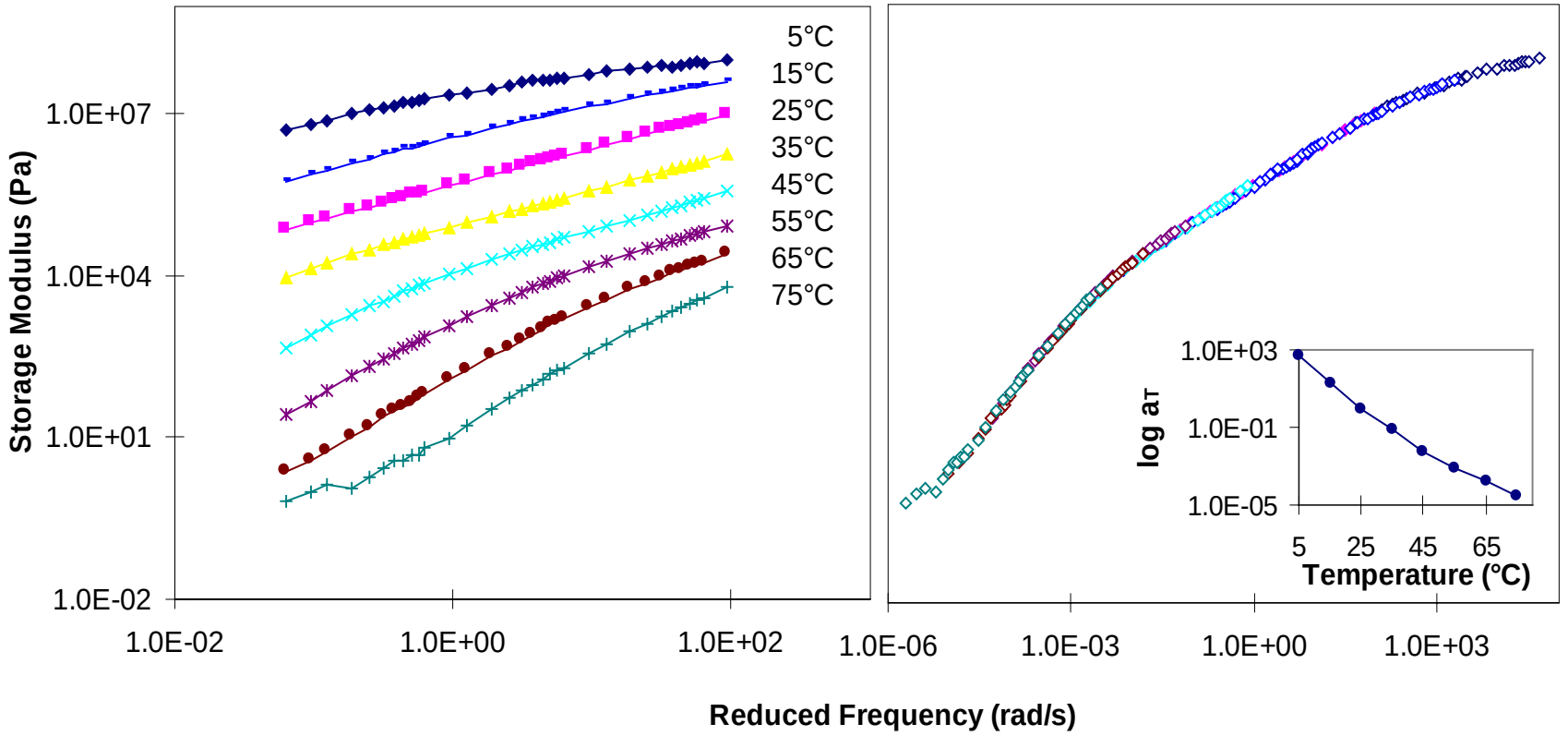

Figure A-57. Dynamic storage modulus isothermal, master curve (with reference temperature of 25°C), and shift factor, a_T, for ARX4.

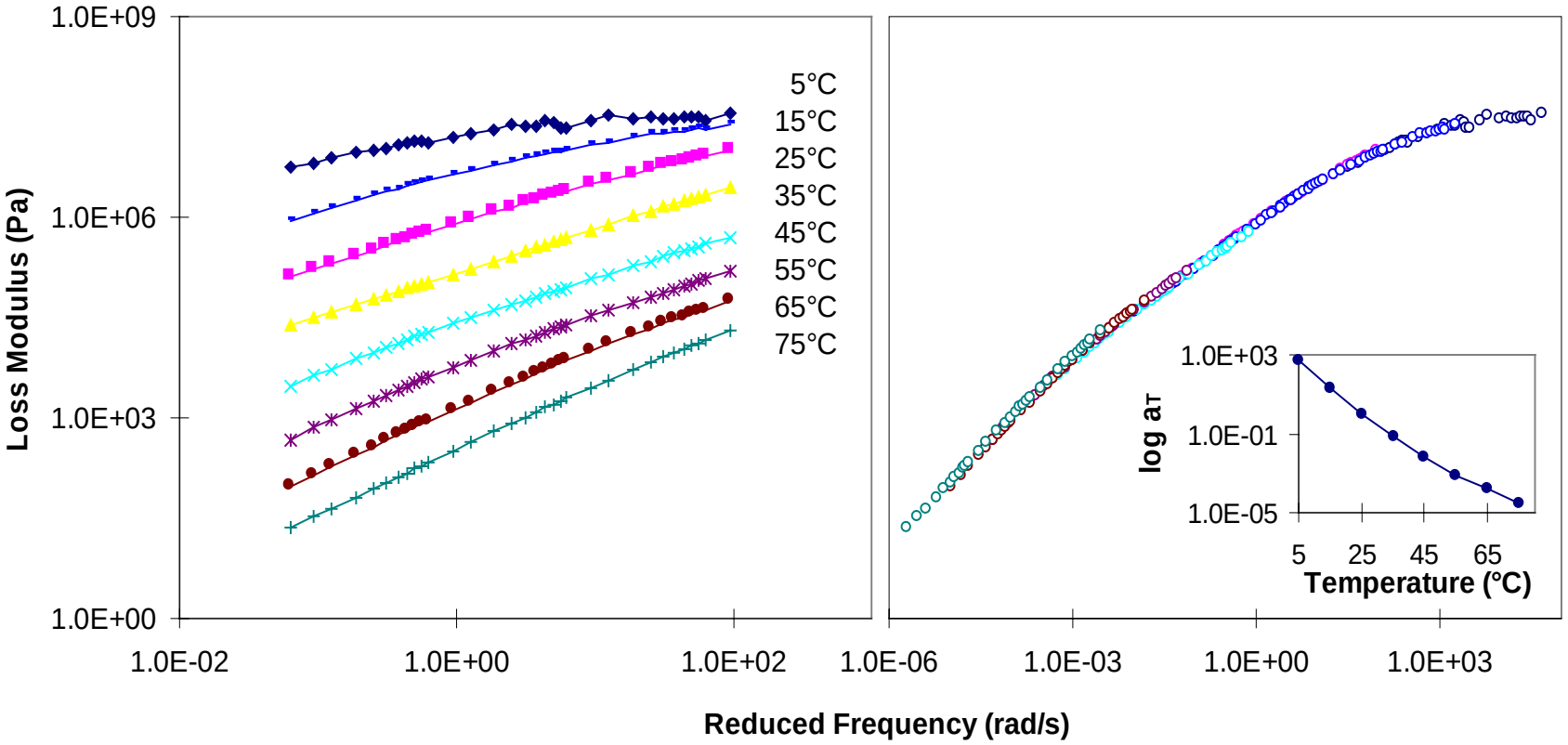

Figure A-58. Dynamic loss modulus isothermal, master curve (with reference temperature of 25°C), and shift factor, a_T, for ARX4.

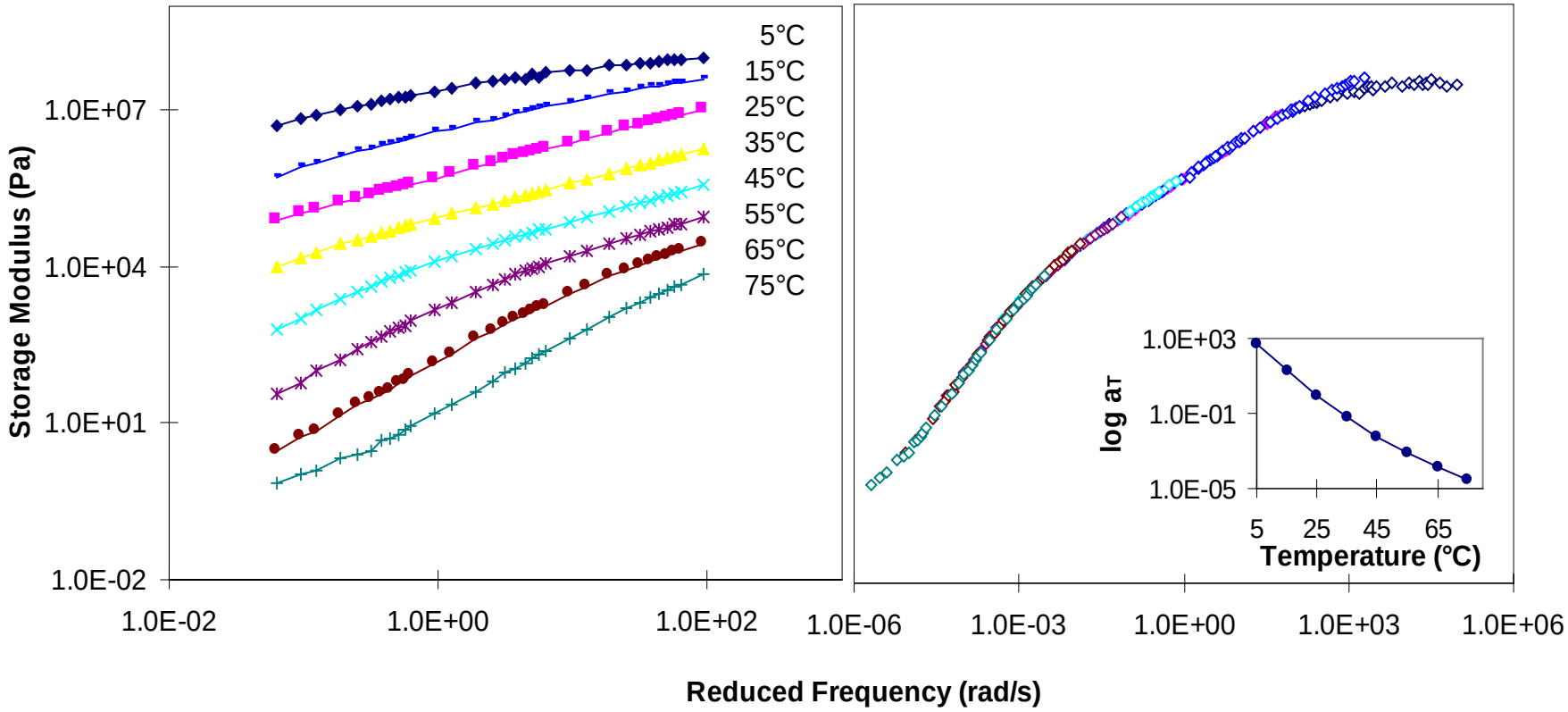

Figure A-59. Dynamic storage modulus isothermal master curve (with reference temperature of 25°C), and shift factor, a_T, for ARX5.

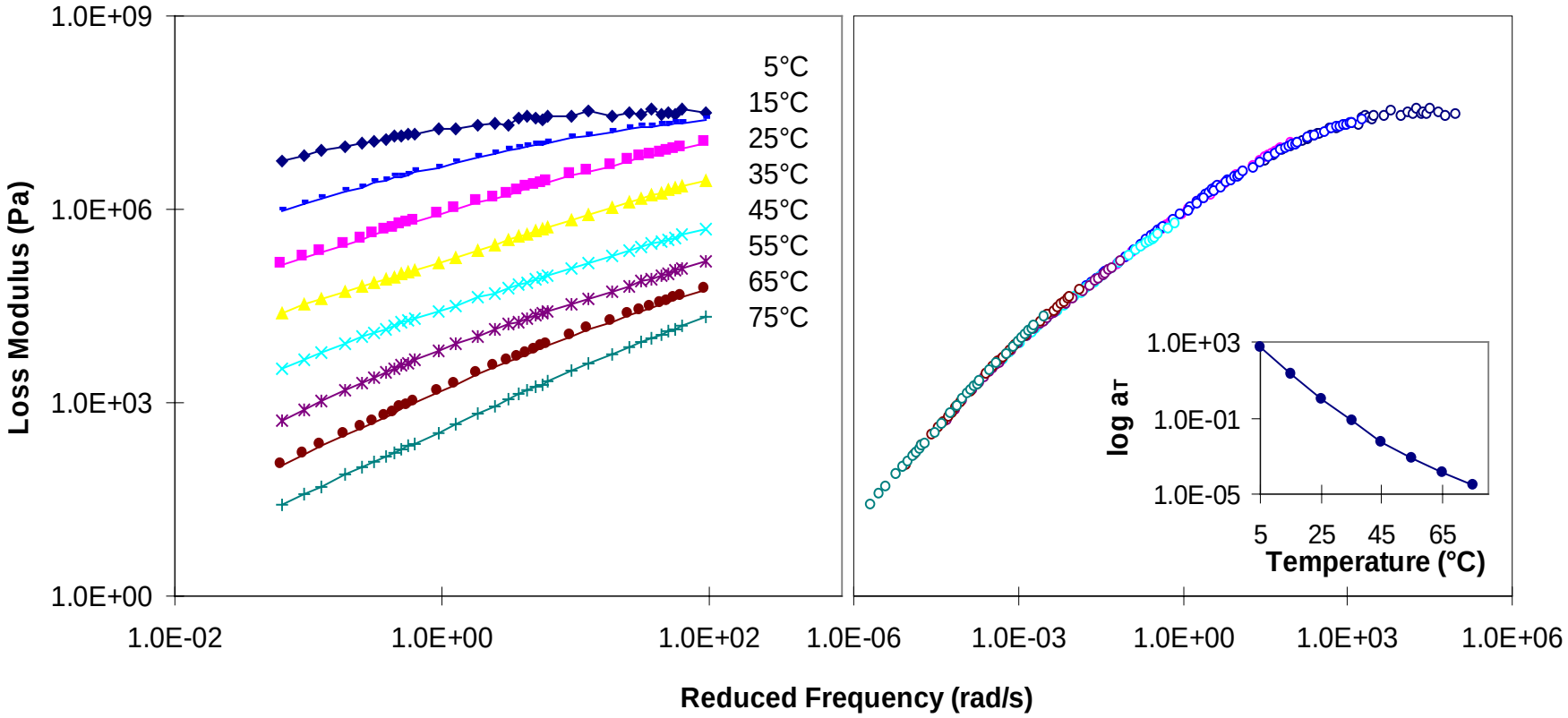

Figure A-60. Dynamic loss modulus isothermal, master curve (with reference temperature of 25°C), and shift factor, a_T, for ARX5.

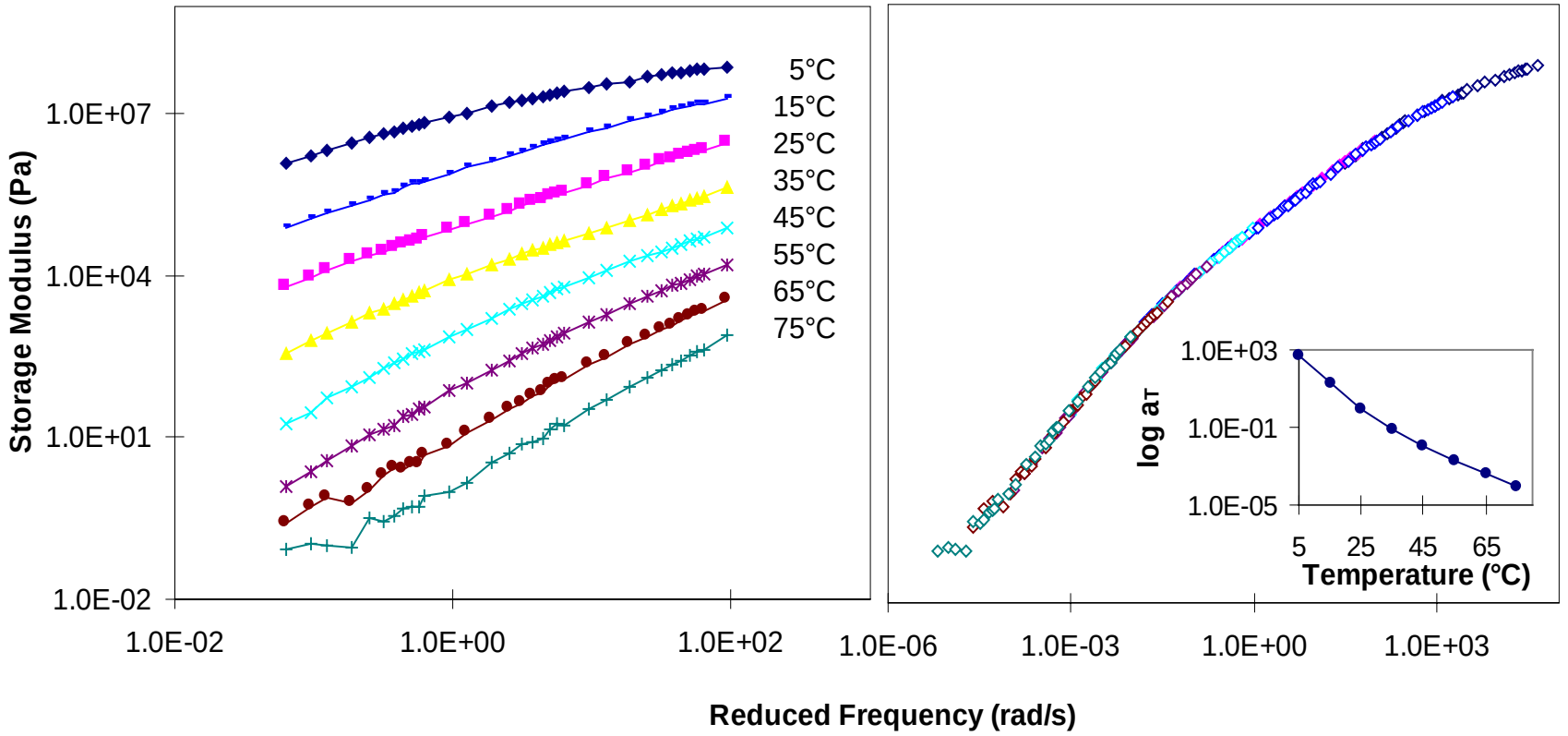

Figure A-61. Dynamic storage modulus isothermal, master curve (with reference temperature of 25°C), and shift factor, a_T, for AUD3.

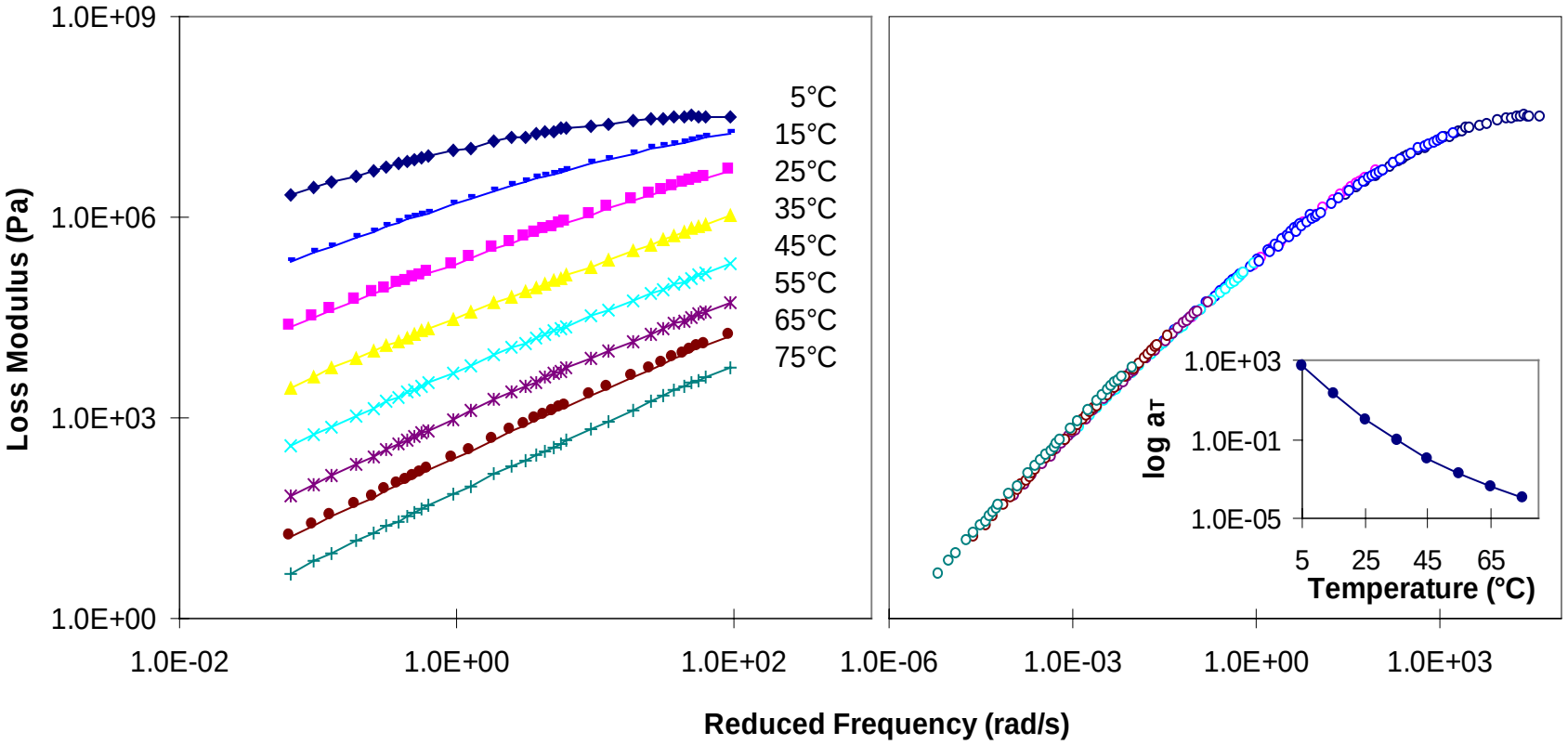

Figure A-62. Dynamic loss modulus isothermal, master curve (with reference temperature of 25°C), and shift factor, a_T, for AUD3.

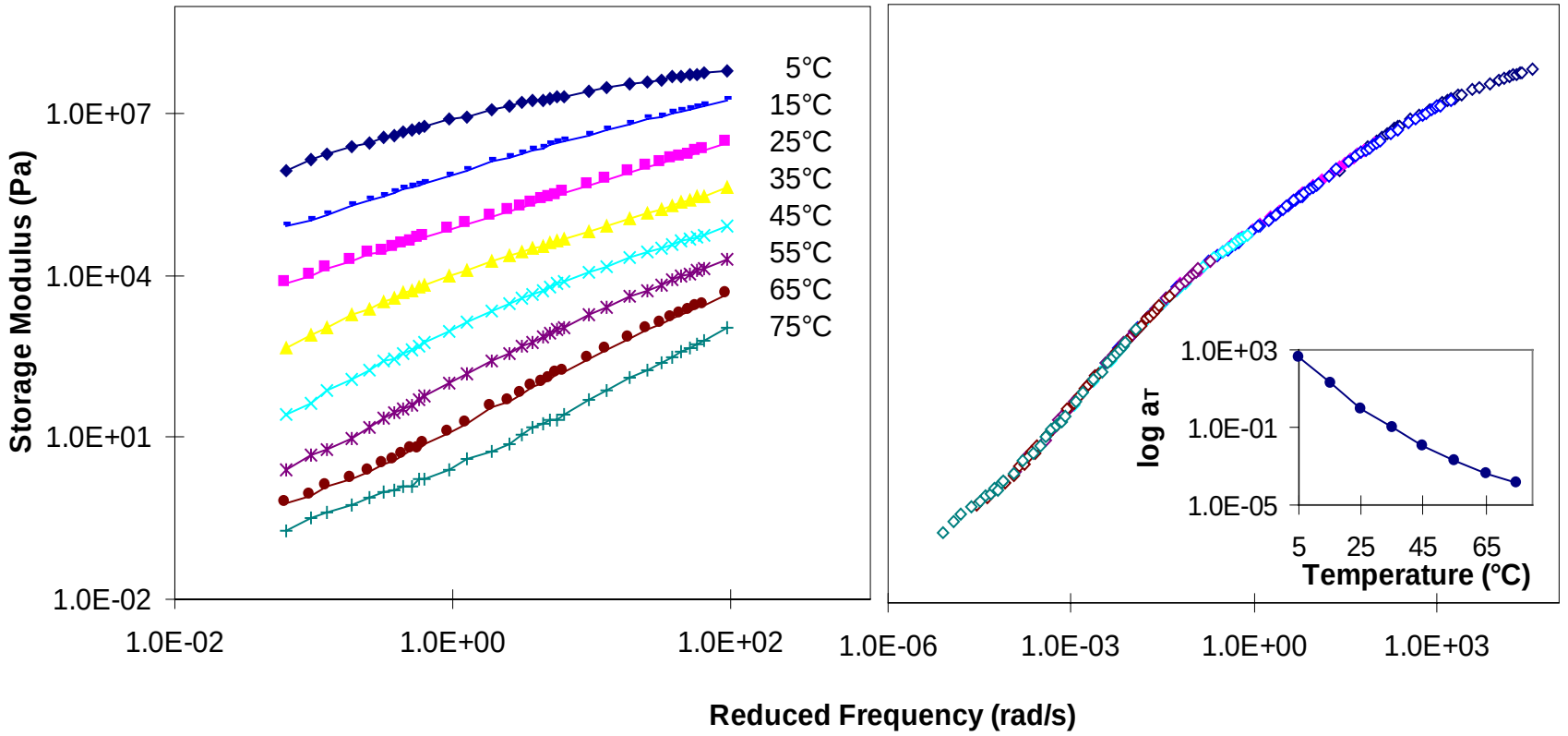

Figure A-63. Dynamic storage modulus isothermal, master curve (with reference temperature of 25°C), and shift factor, a_T, for AUD4.

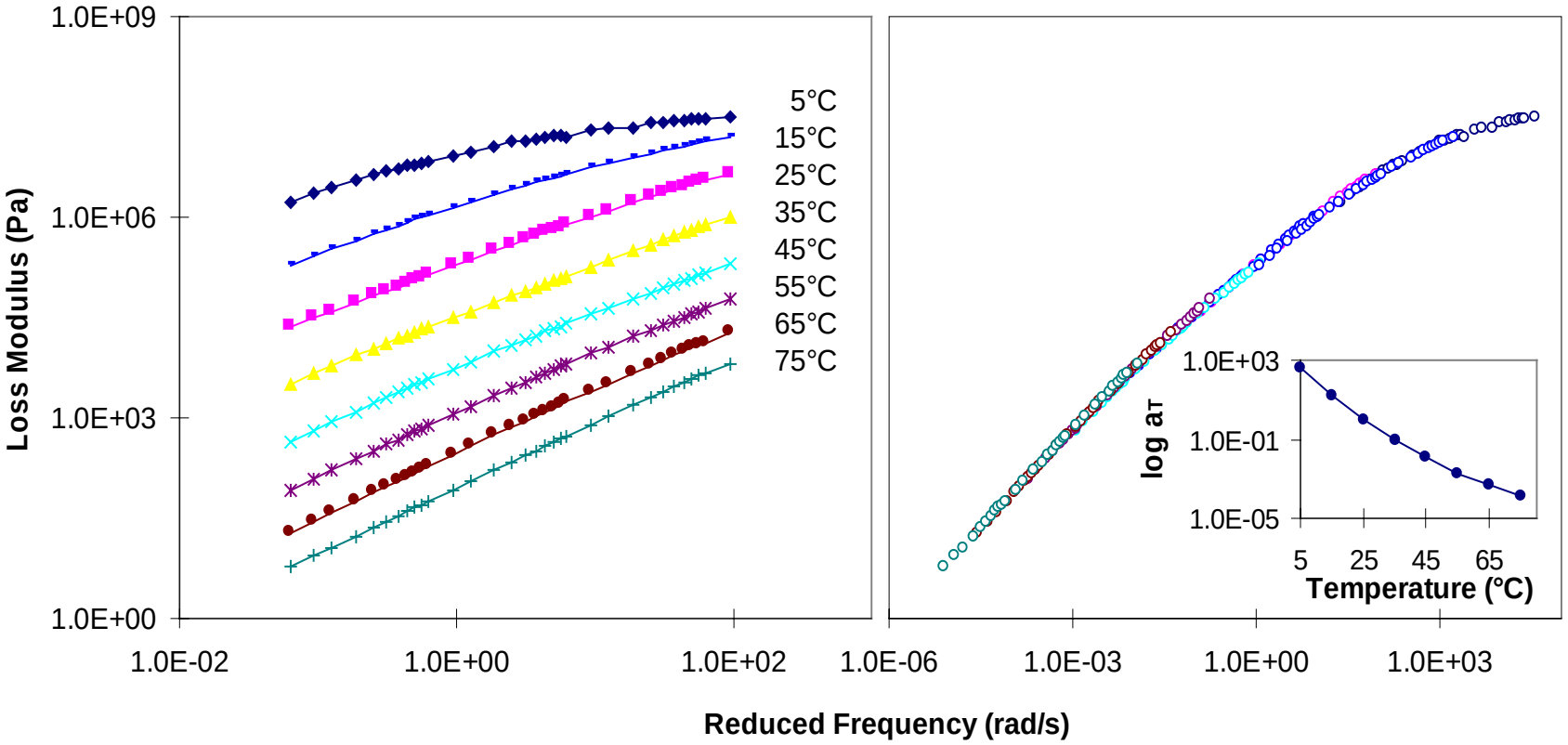

Figure A-64. Dynamic loss modulus isothermal, master curve (with reference temperature of 25°C), and shift factor, a_T, for AUD4.

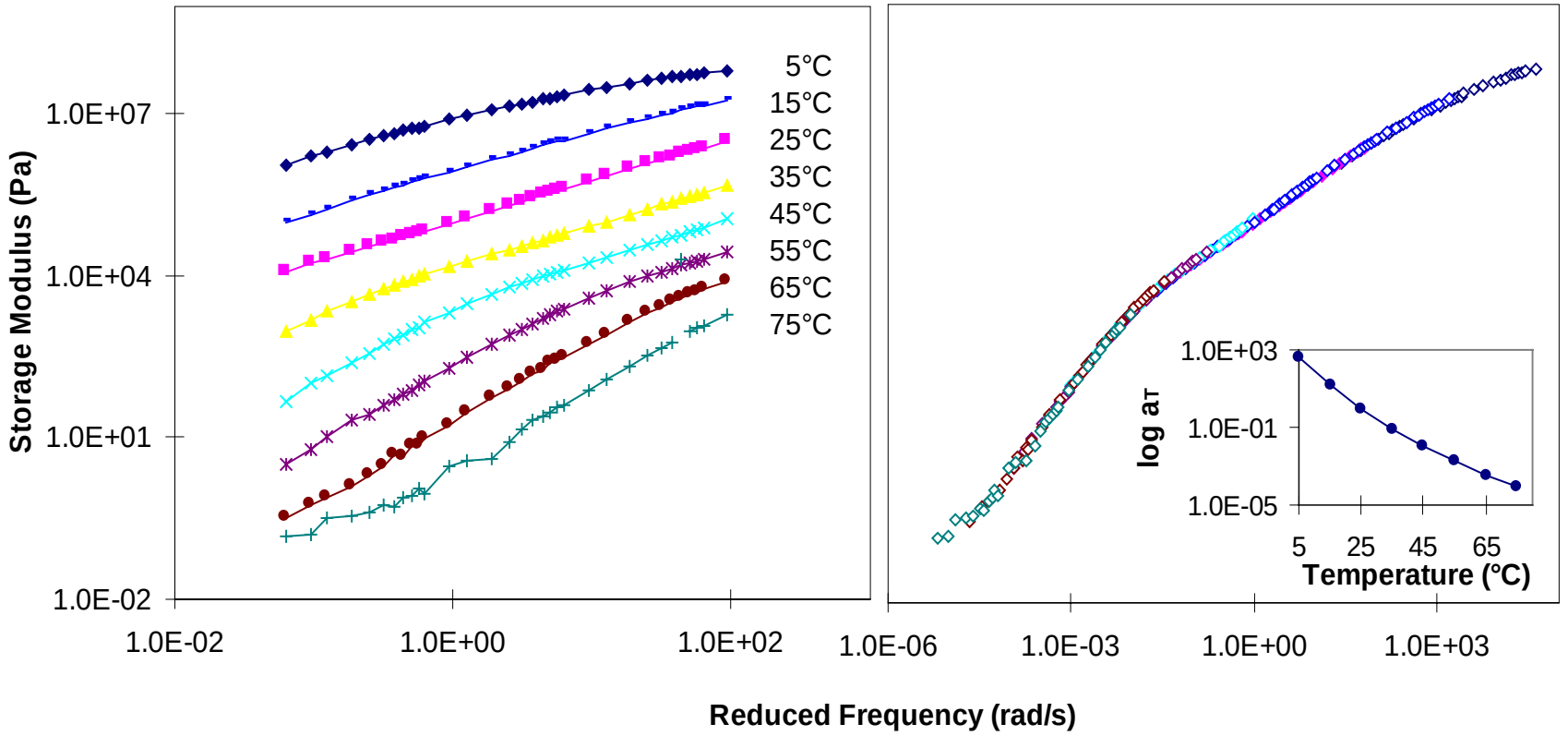

Figure A-65. Dynamic storage modulus isothermal, master curve (with reference temperature of 25°C), and shift factor, a_T, for AUD5.

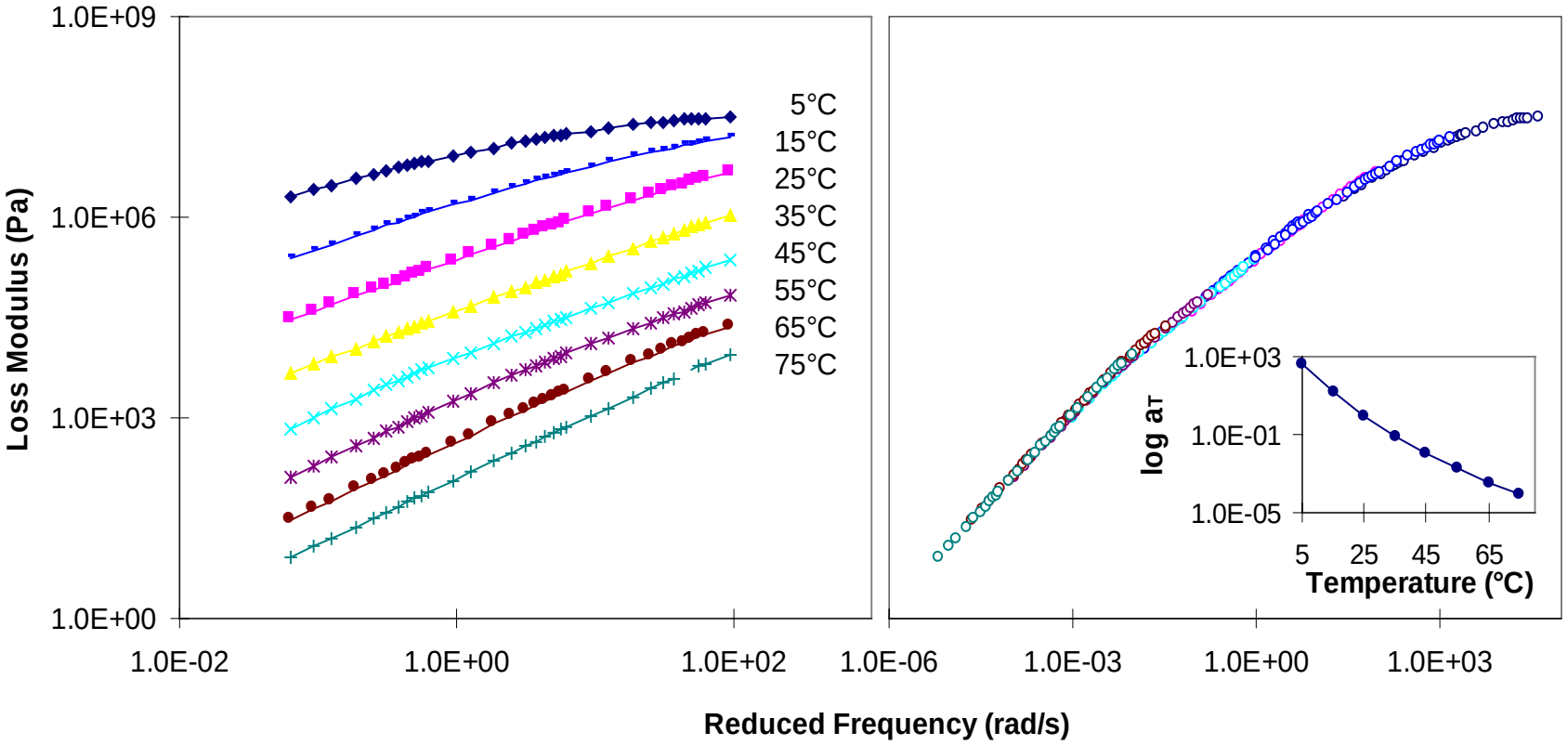

Figure A-66. Dynamic loss modulus isothermal, master curve (with reference temperature of 25°C), and shift factor, a_T, for AUD5.

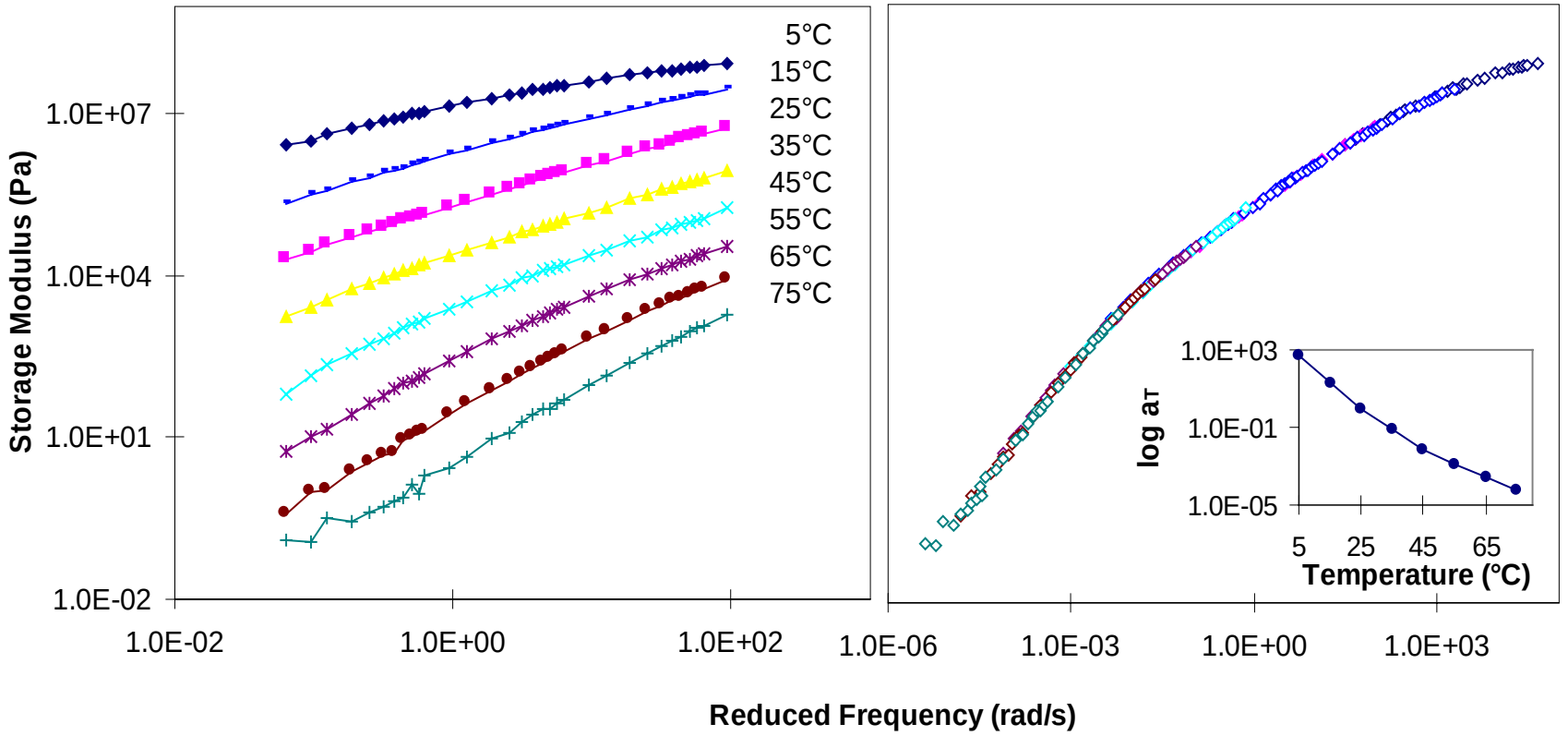

Figure A-67. Dynamic storage modulus isothermal, master curve (with reference temperature of 25°C), and shift factor, a_T, for ARD3.

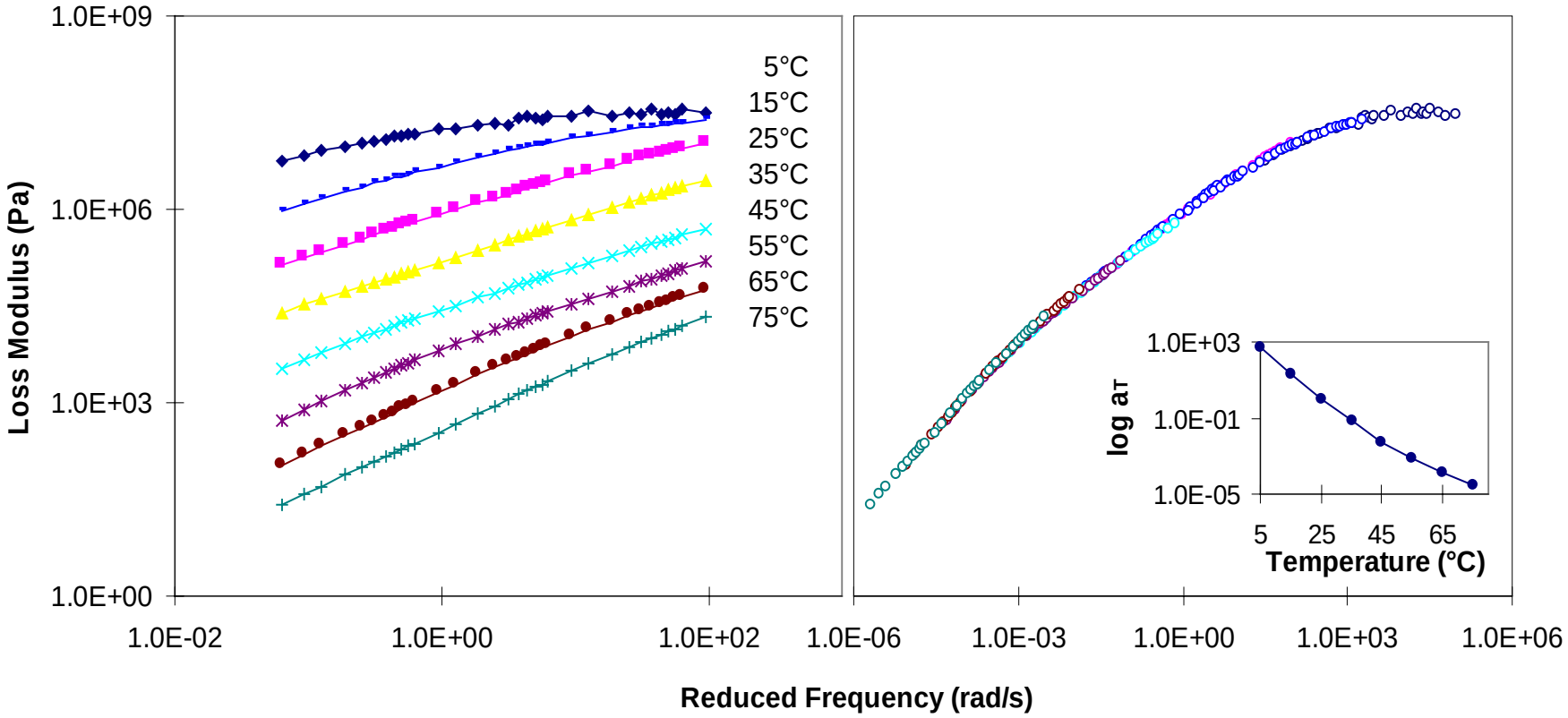

Figure A-68. Dynamic loss modulus isothermal master curve (with reference temperature of 25°C), and shift factor, a_T, for ARD3.

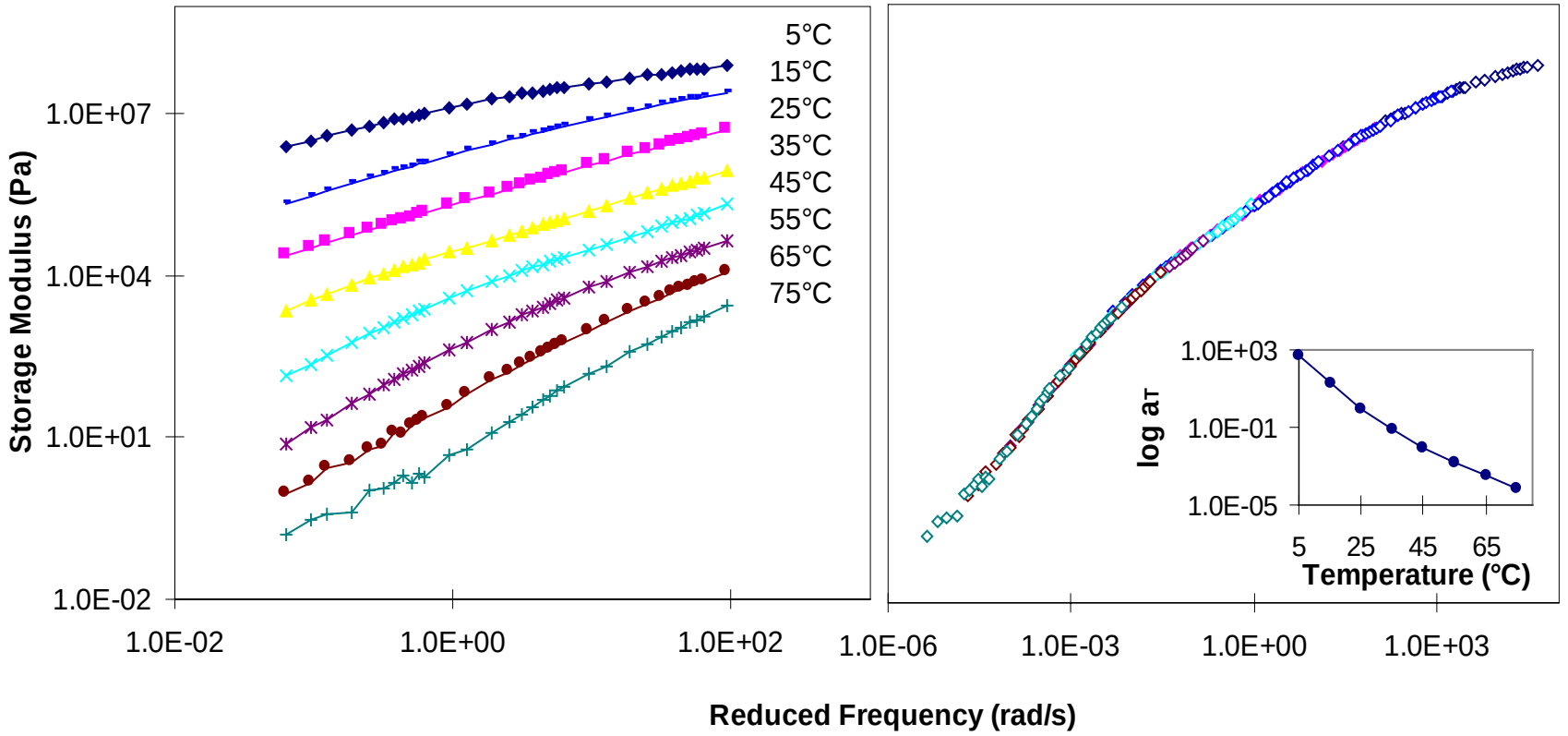

Figure A-69. Dynamic storage modulus isothermal master curve (with reference temperature of 25°C), and shift factor, a_T, for ARD4.

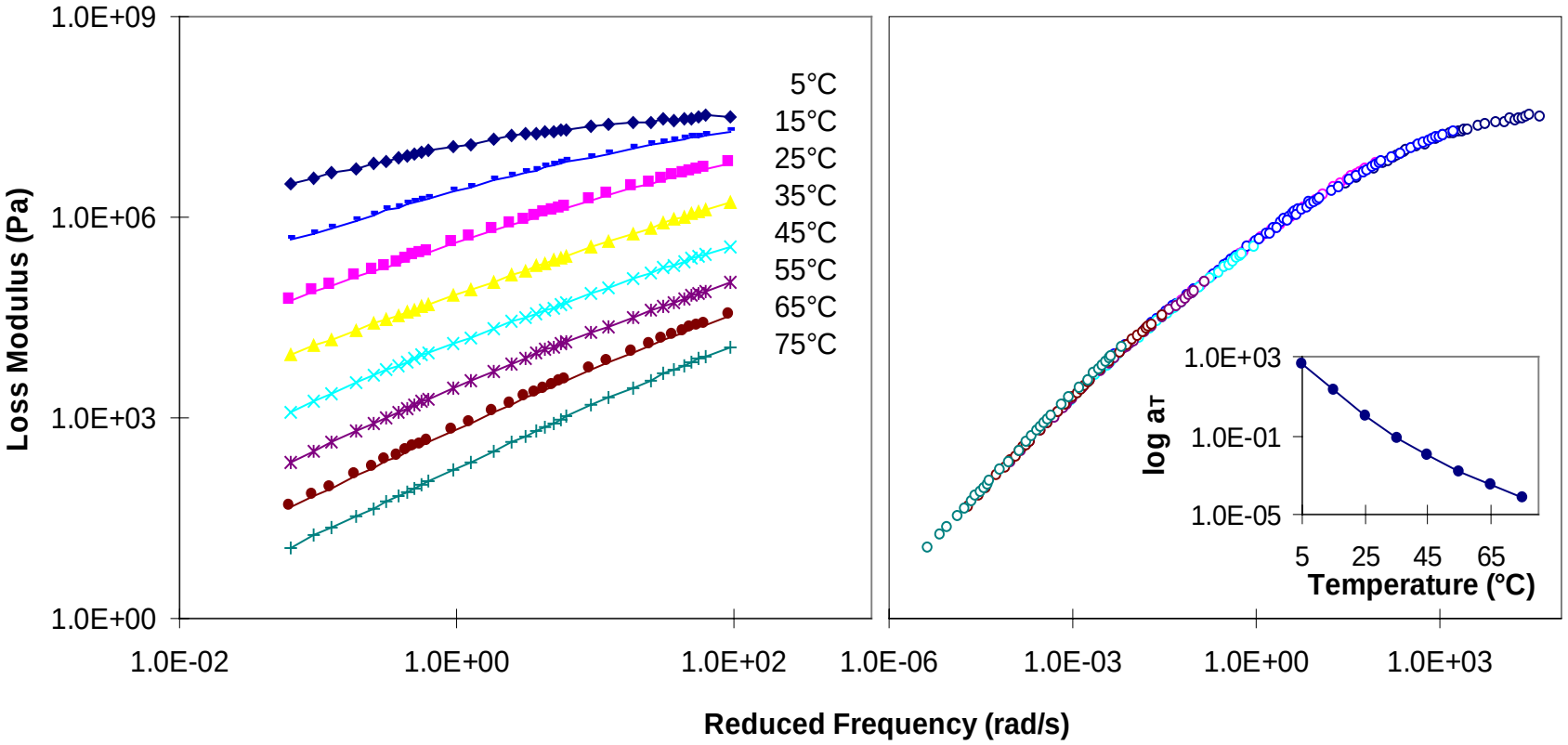

Figure A-70. Dynamic loss modulus isothermal master curve (with reference temperature of 25°C), and shift factor, a_T, for ARD4.

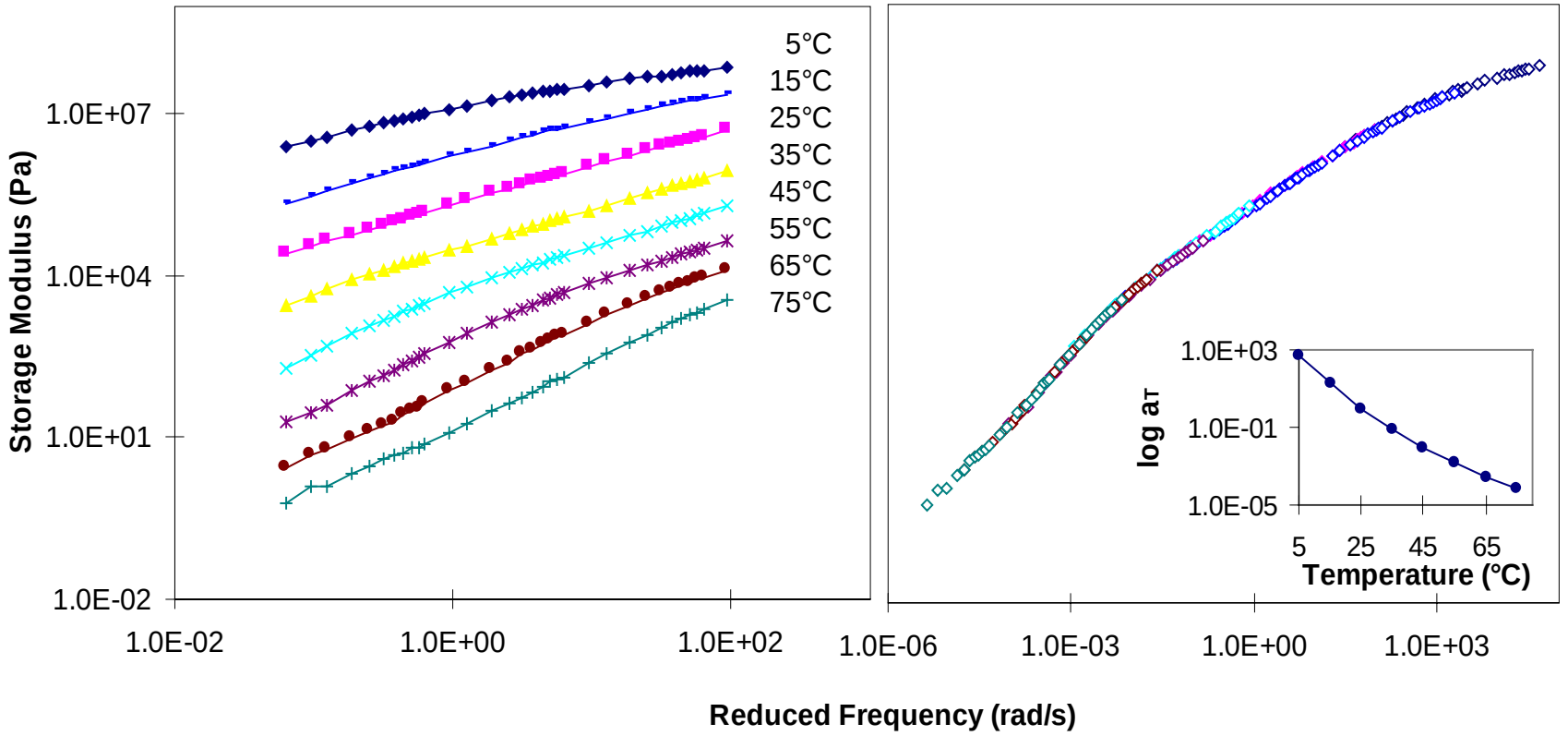

Figure A-71. Dynamic storage modulus isothermal master curve (with reference temperature of 25°C), and shift factor, a_T, for ARD5.

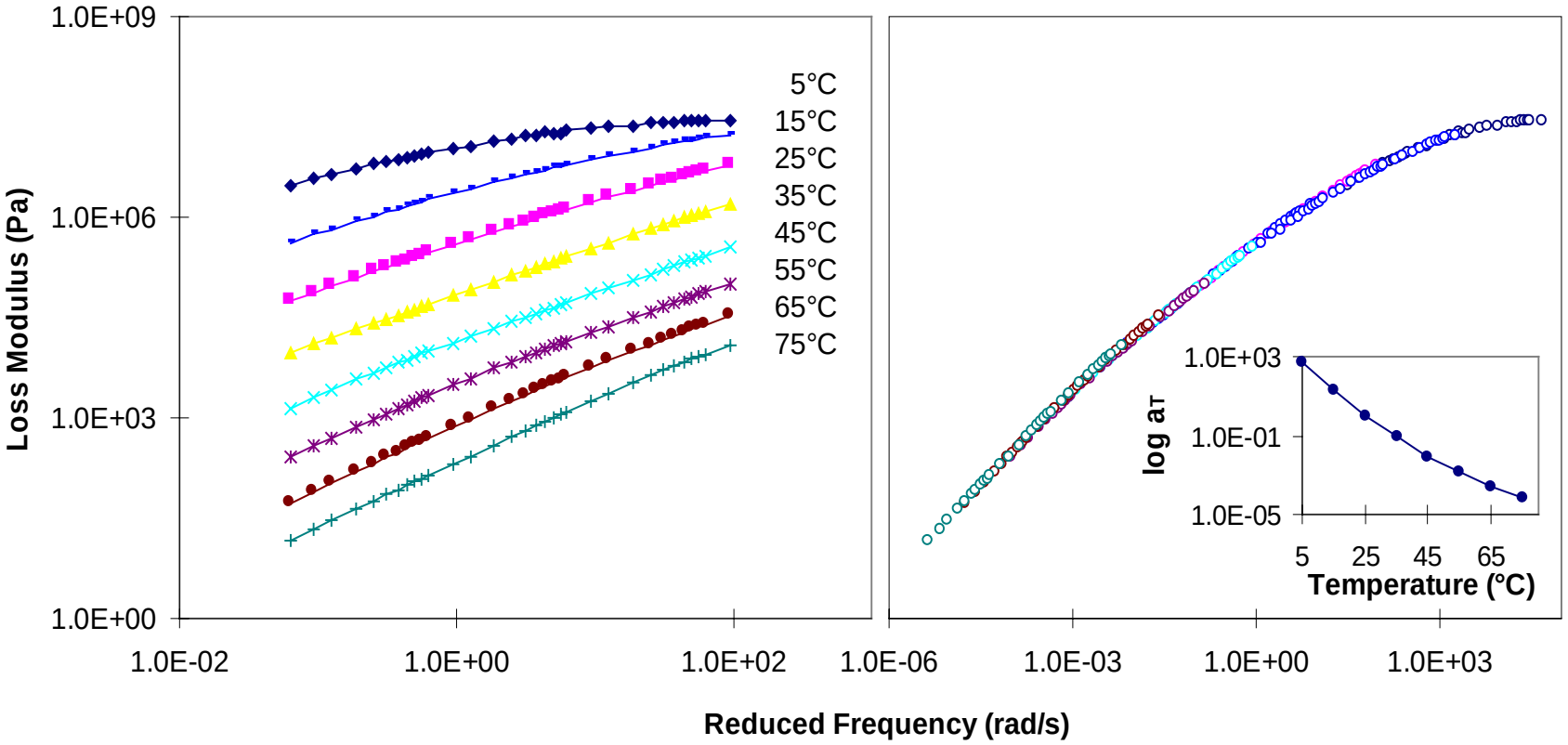

Figure A-72. Dynamic loss modulus isothermal, master curve (with reference temperature of 25°C), and shift factor, a_T, for ARD5.

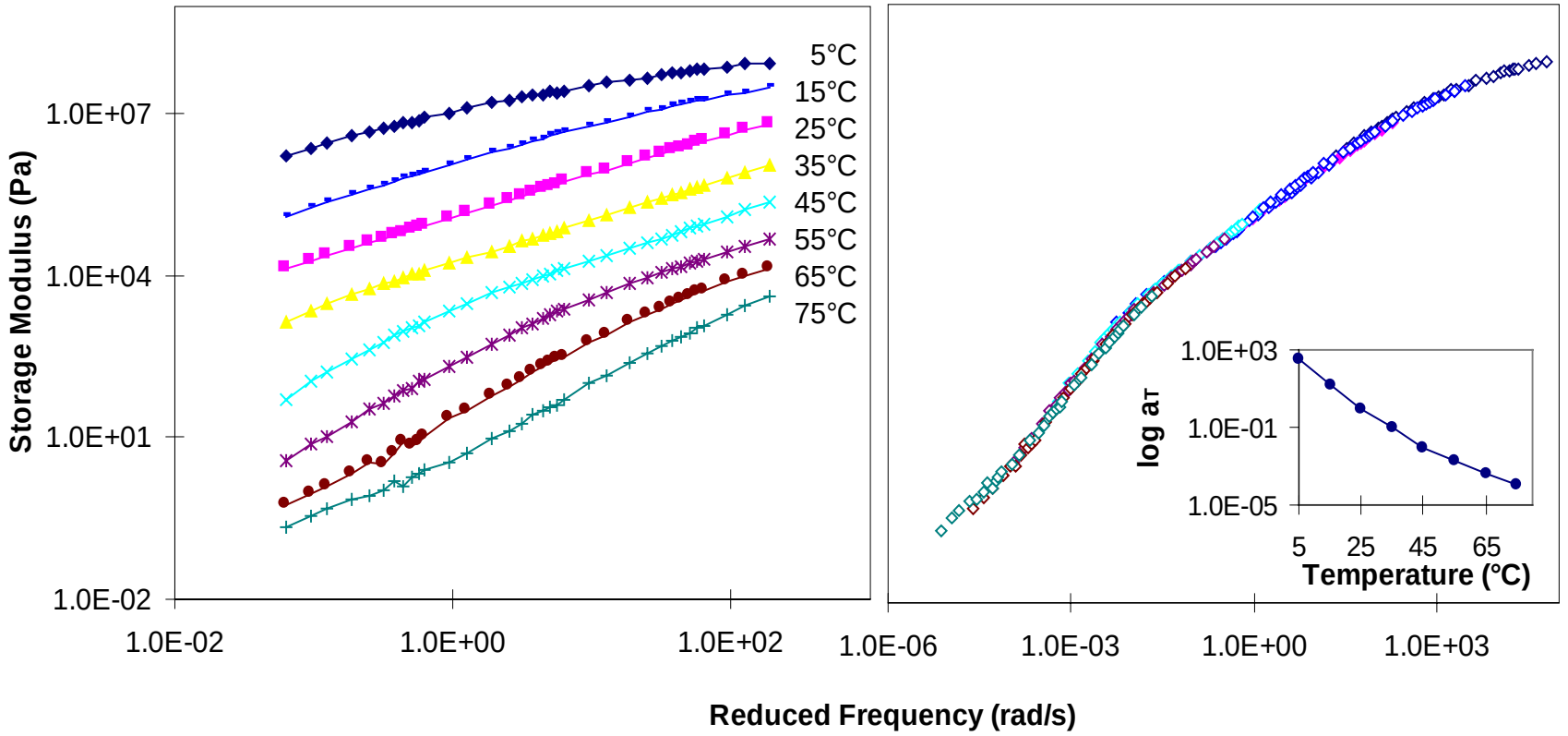

Figure A-73. Dynamic storage modulus isothermal master curve (with reference temperature of 25°C), and shift factor, a_T, for AUS3.

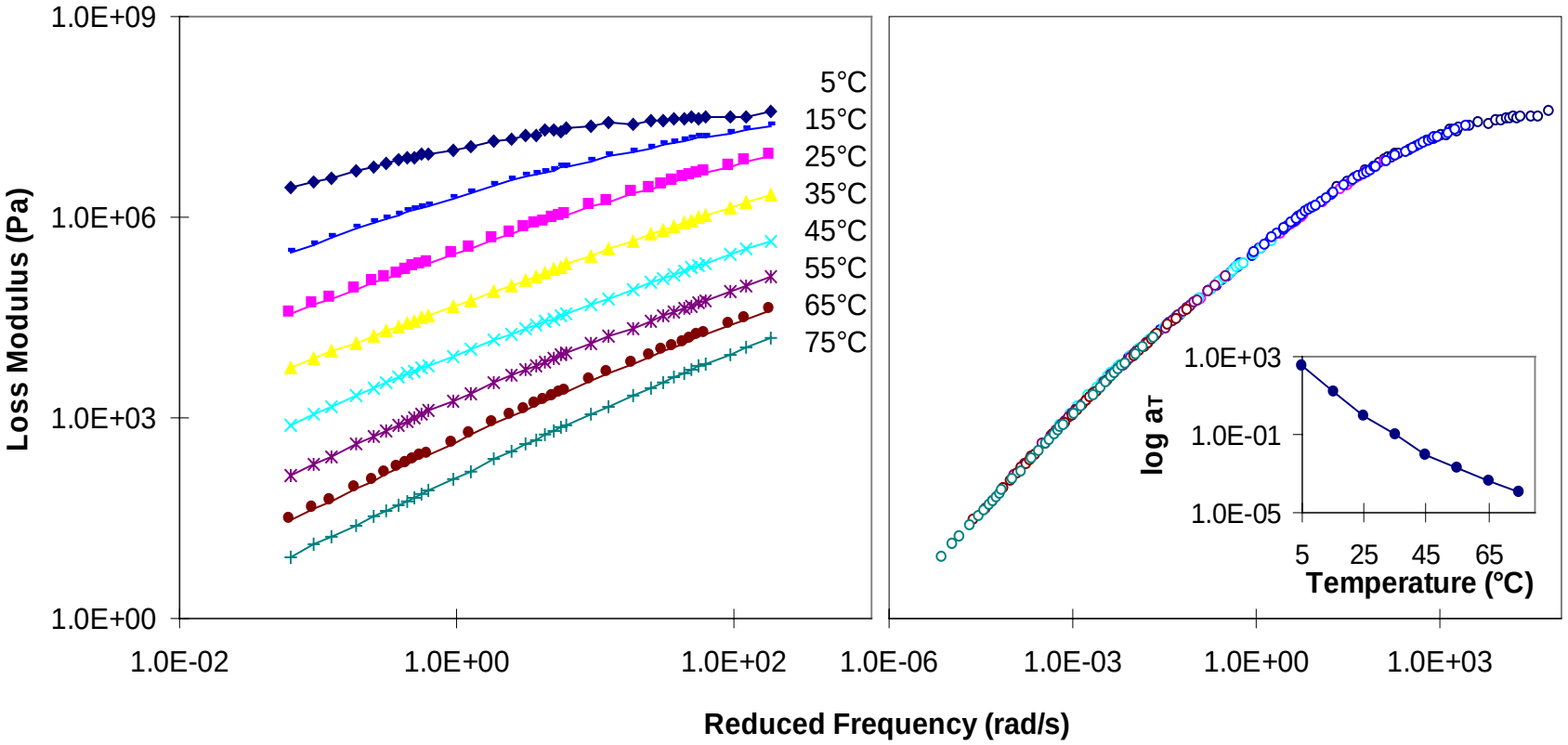

Figure A-74. Dynamic loss modulus isothermal, master curve (with reference temperature of 25°C), and shift factor, a_T, for AUS3.

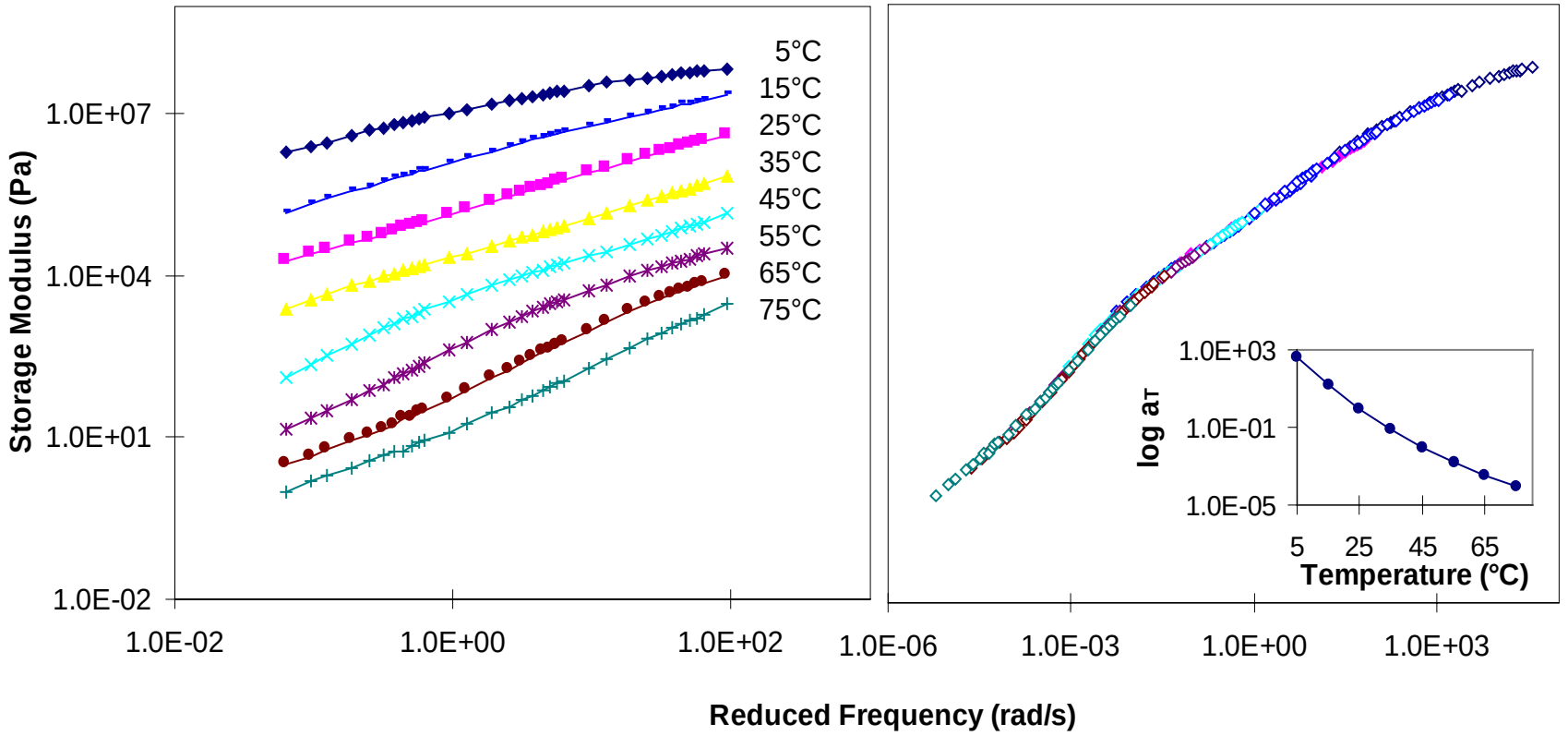

Figure A-75. Dynamic storage modulus isothermal, master curve (with reference temperature of 25°C), and shift factor, a_T, for AUS4.

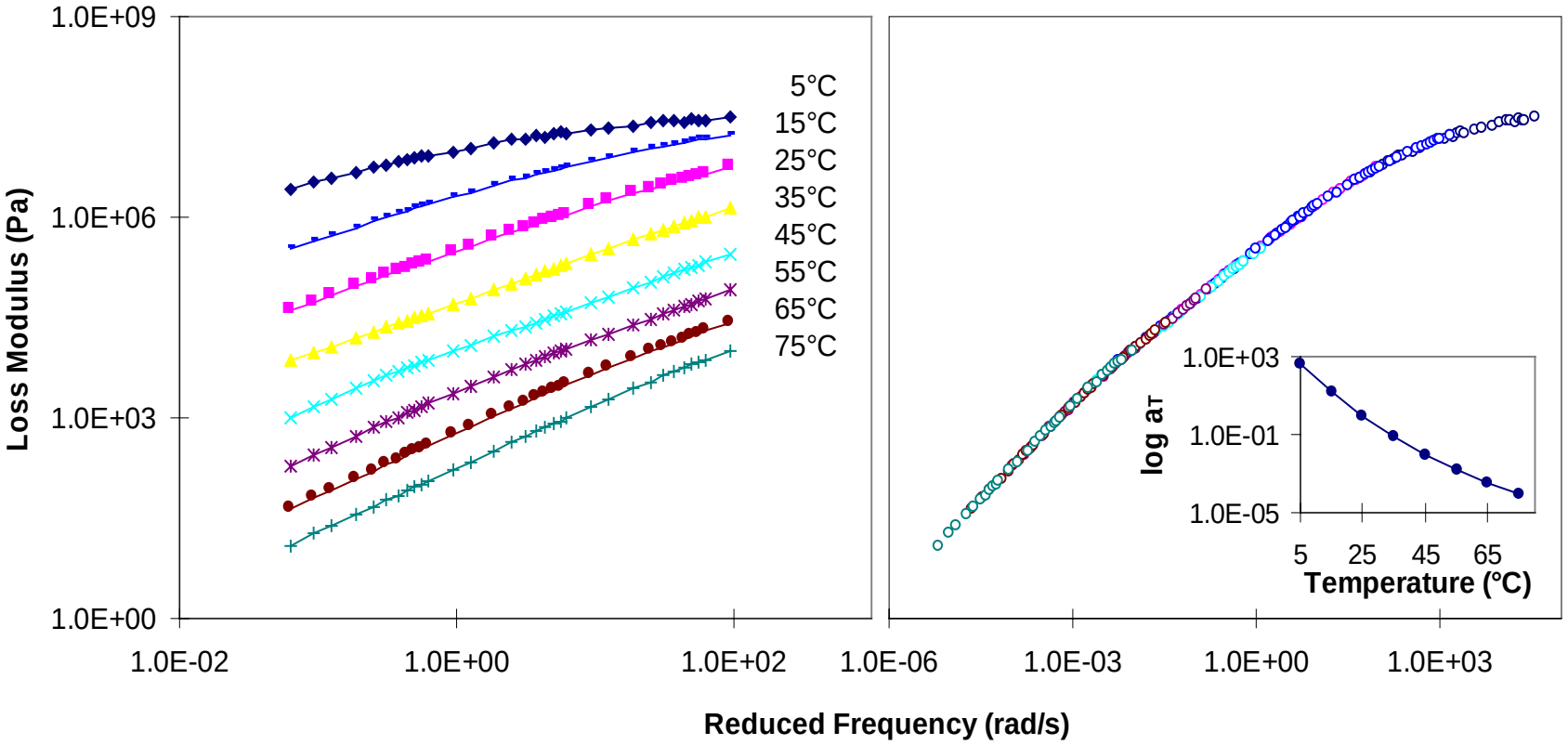

Figure A-76. Dynamic loss modulus isothermal, master curve (with reference temperature of 25°C), and shift factor, a_T, for AUS4.

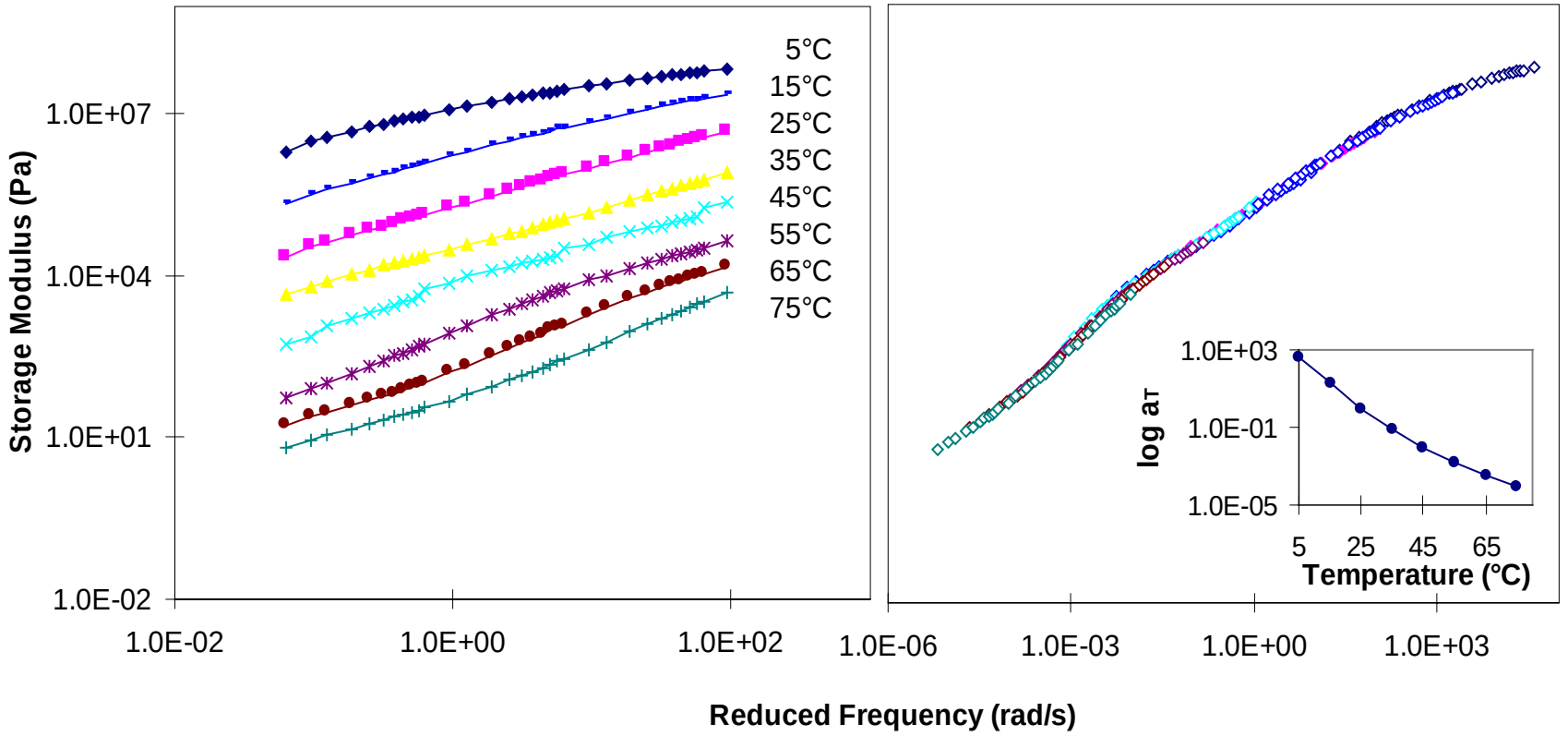

Figure A-77. Dynamic storage modulus isothermal master curve (with reference temperature of 25°C), and shift factor, a_T, for AUS5.

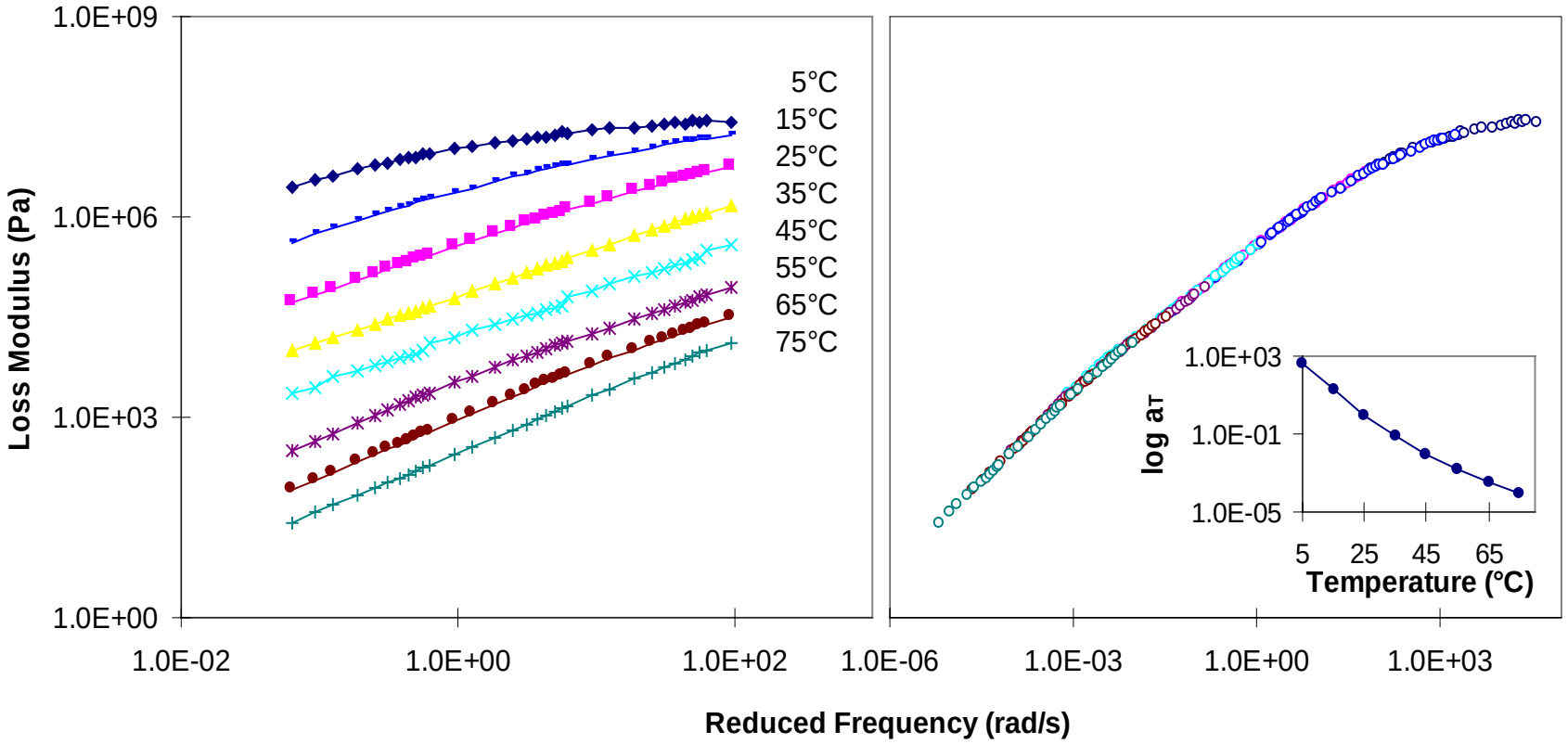

Figure A-78. Dynamic loss modulus isothermal master curve (with reference temperature of 25°C), and shift factor, a_T, for AUS5.

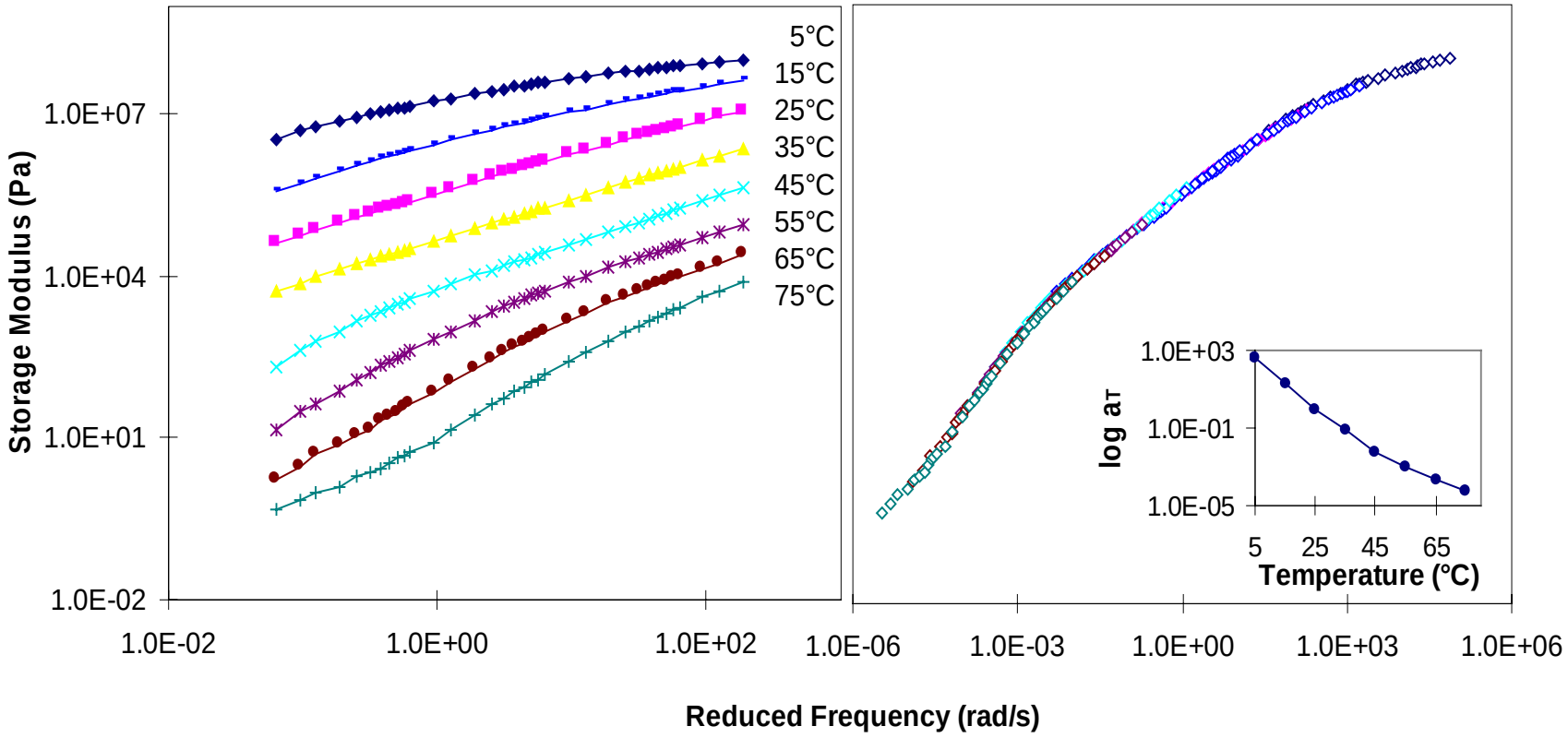

Figure A-79. Dynamic storage modulus isothermal master curve (with reference temperature of 25°C), and shift factor, a_T, for ARS3.

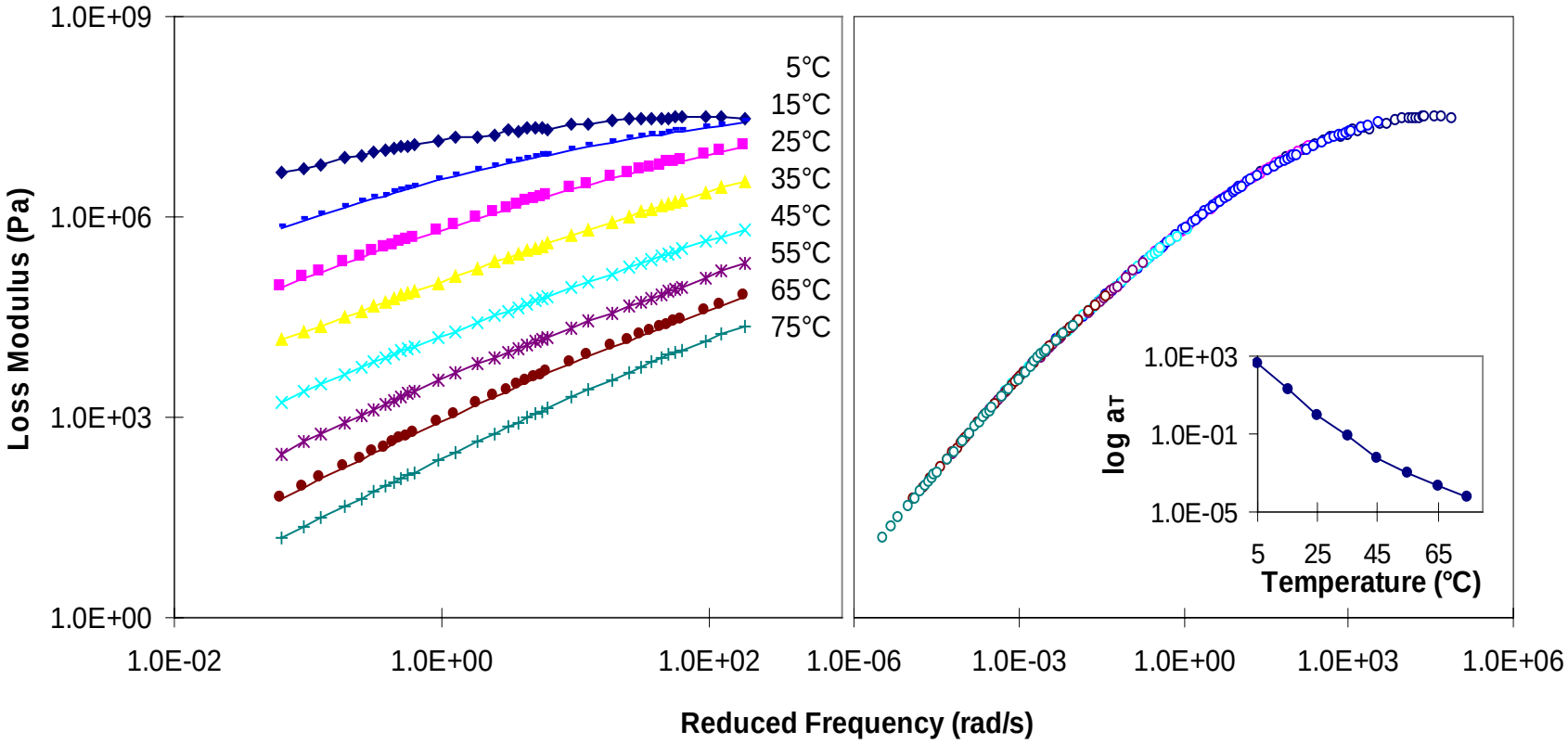

Figure A-80. Dynamic loss modulus isothermal, master curve (with reference temperature of 25°C), and shift factor, a_T, for ARS3.

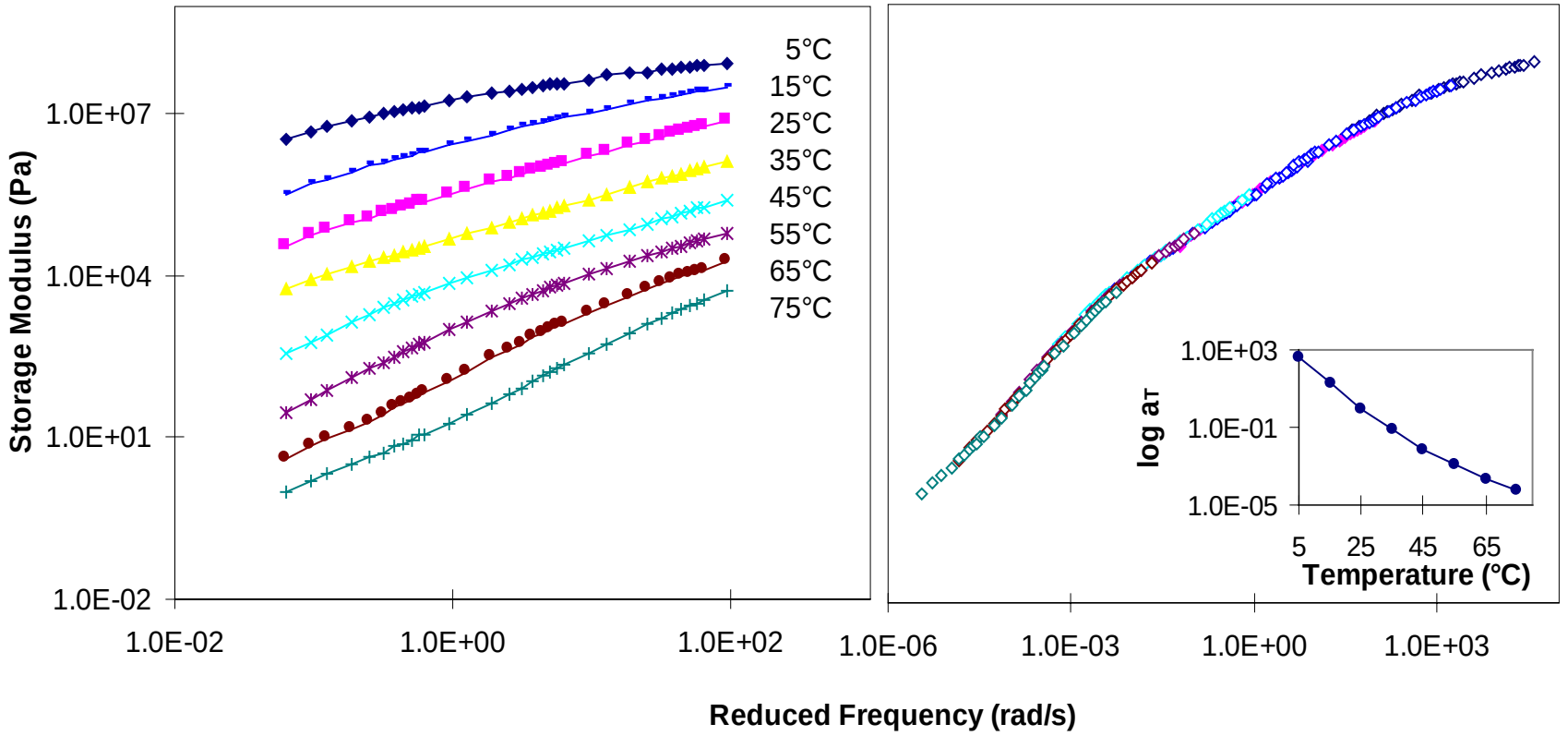

Figure A-81. Dynamic storage modulus isothermal, master curve (with reference temperature of 25°C), and shift factor, a_T, for ARS4.

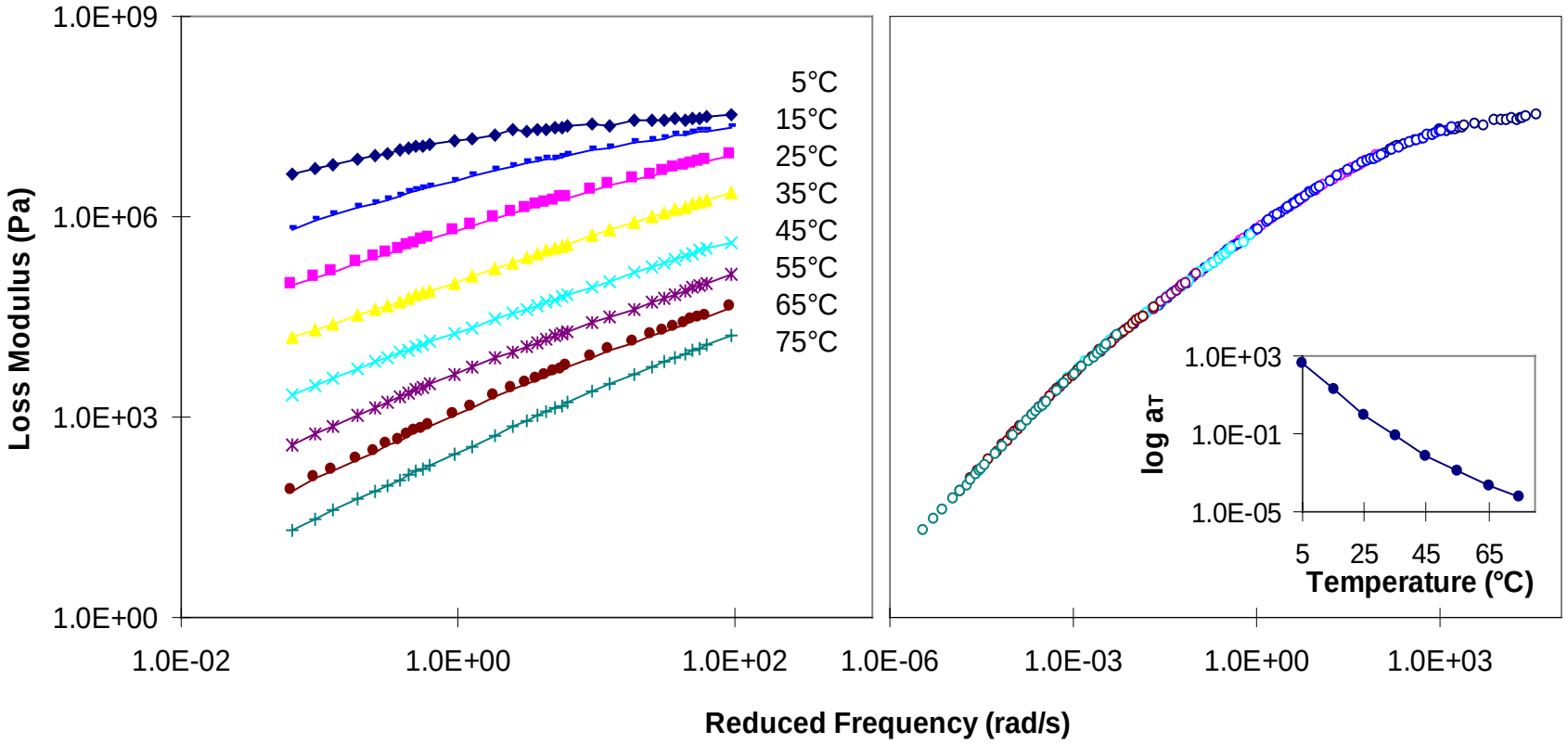

Figure A-82. Dynamic loss modulus isothermal, master curve (with reference temperature of 25°C), and shift factor, a_T, for ARS4.

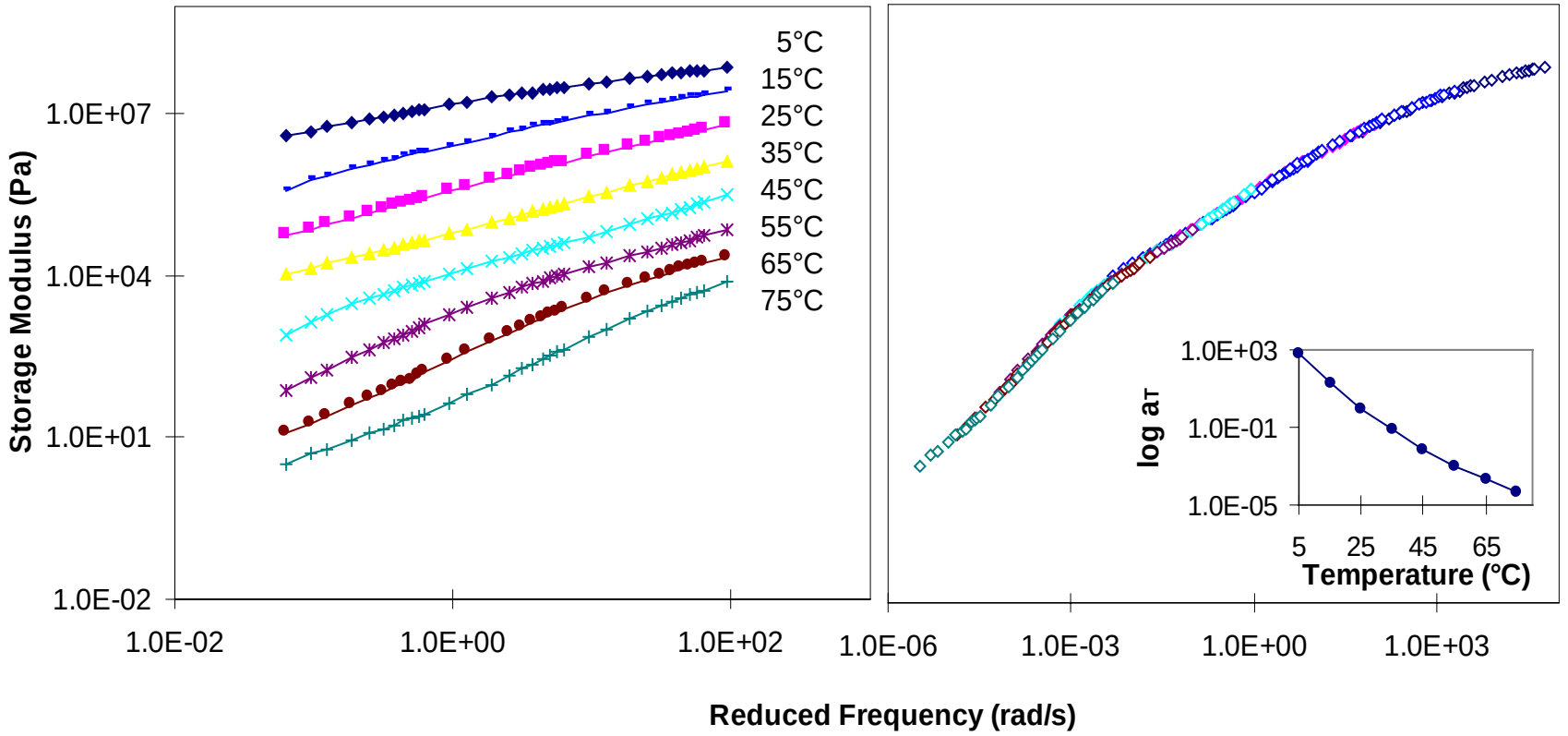

Figure A-83. Dynamic storage modulus isothermal master curve (with reference temperature of 25°C), and shift factor, a_T, for ARS5.

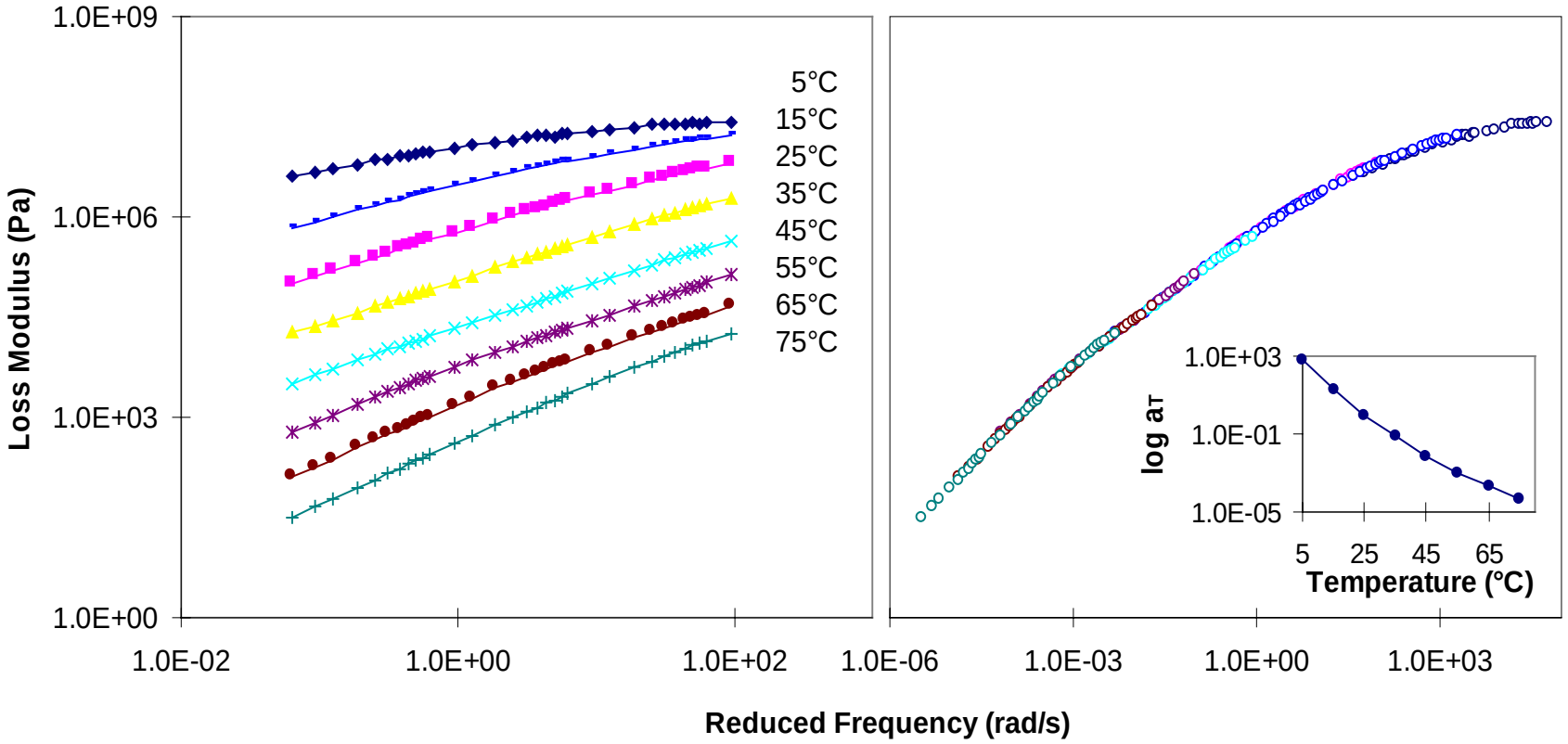

Figure A-84 Dynamic loss modulus isothermal, master curve (with reference temperature of 25°C), and shift factor, a_T, for ARS5.

Appendix B. SAS Input file

```
DATA;
INPUT X Y;
CARDS;
2.81E+01    2.43E+06
4.21E+01    3.07E+06
5.61E+01    3.63E+06
8.42E+01    4.52E+06
1.12E+02    5.45E+06
1.40E+02    5.92E+06
1.68E+02    6.58E+06
1.96E+02    6.96E+06
2.25E+02    7.65E+06
2.53E+02    8.18E+06
2.81E+02    8.64E+06
4.21E+02    1.04E+07
5.61E+02    1.15E+07
8.42E+02    1.34E+07
1.12E+03    1.48E+07
1.40E+03    1.70E+07
1.68E+03    1.69E+07
1.96E+03    1.78E+07
2.25E+03    1.97E+07
2.53E+03    1.81E+07
2.81E+03    1.90E+07
4.21E+03    2.24E+07
5.61E+03    2.26E+07
8.42E+03    2.43E+07
1.12E+04    2.82E+07
1.40E+04    2.75E+07
1.68E+04    2.90E+07
1.96E+04    2.92E+07
2.25E+04    2.98E+07
2.53E+04    2.93E+07
2.81E+04    3.14E+07
4.21E+04    3.27E+07
1.12E+00    2.66E+05
1.68E+00    3.62E+05
2.23E+00    4.53E+05
3.35E+00    6.11E+05
4.47E+00    7.47E+05
5.59E+00    8.80E+05
6.70E+00    1.00E+06
7.82E+00    1.11E+06
8.94E+00    1.20E+06
1.01E+01    1.31E+06
1.12E+01    1.39E+06
1.68E+01    1.79E+06
2.23E+01    2.16E+06
3.35E+01    2.82E+06
```

4.47E+01	3.32E+06
5.59E+01	3.80E+06
6.70E+01	4.31E+06
7.82E+01	4.56E+06
8.94E+01	4.87E+06
1.01E+02	5.24E+06
1.12E+02	5.54E+06
1.68E+02	6.86E+06
2.23E+02	7.90E+06
3.35E+02	9.64E+06
4.47E+02	1.08E+07
5.59E+02	1.19E+07
6.70E+02	1.29E+07
7.82E+02	1.37E+07
8.94E+02	1.44E+07
1.01E+03	1.50E+07
1.12E+03	1.55E+07
1.68E+03	1.80E+07
6.28E-02	3.30E+04
9.42E-02	4.48E+04
1.26E-01	5.55E+04
1.88E-01	7.46E+04
2.51E-01	9.44E+04
3.14E-01	1.11E+05
3.77E-01	1.28E+05
4.40E-01	1.43E+05
5.03E-01	1.57E+05
5.65E-01	1.72E+05
6.28E-01	1.87E+05
9.42E-01	2.54E+05
1.26E+00	3.16E+05
1.88E+00	4.25E+05
2.51E+00	5.22E+05
3.14E+00	6.14E+05
3.77E+00	7.04E+05
4.40E+00	7.74E+05
5.03E+00	8.50E+05
5.65E+00	9.26E+05
6.28E+00	9.93E+05
9.42E+00	1.31E+06
1.26E+01	1.58E+06
1.88E+01	2.06E+06
2.51E+01	2.47E+06
3.14E+01	2.86E+06
3.77E+01	3.18E+06
4.40E+01	3.48E+06
5.03E+01	3.79E+06
5.65E+01	4.07E+06
6.28E+01	4.32E+06
9.42E+01	5.49E+06
5.21E-03	5.12E+03
7.82E-03	7.17E+03
1.04E-02	9.09E+03
1.56E-02	1.24E+04

2.08E-02	1.55E+04
2.61E-02	1.83E+04
3.13E-02	2.10E+04
3.65E-02	2.34E+04
4.17E-02	2.59E+04
4.69E-02	2.82E+04
5.21E-02	3.05E+04
7.82E-02	4.07E+04
1.04E-01	5.03E+04
1.56E-01	6.79E+04
2.08E-01	8.51E+04
2.61E-01	1.00E+05
3.13E-01	1.16E+05
3.65E-01	1.30E+05
4.17E-01	1.43E+05
4.69E-01	1.57E+05
5.21E-01	1.70E+05
7.82E-01	2.31E+05
1.04E+00	2.86E+05
1.56E+00	3.86E+05
2.08E+00	4.79E+05
2.61E+00	5.65E+05
3.13E+00	6.48E+05
3.65E+00	7.20E+05
4.17E+00	7.98E+05
4.69E+00	8.73E+05
5.21E+00	9.33E+05
7.82E+00	1.24E+06
6.28E-04	7.60E+02
9.42E-04	1.10E+03
1.26E-03	1.43E+03
1.88E-03	2.07E+03
2.51E-03	2.67E+03
3.14E-03	3.24E+03
3.77E-03	3.78E+03
4.40E-03	4.28E+03
5.03E-03	4.79E+03
5.65E-03	5.31E+03
6.28E-03	5.74E+03
9.42E-03	7.99E+03
1.26E-02	1.01E+04
1.88E-02	1.37E+04
2.51E-02	1.71E+04
3.14E-02	2.01E+04
3.77E-02	2.29E+04
4.40E-02	2.55E+04
5.03E-02	2.83E+04
5.65E-02	3.11E+04
6.28E-02	3.33E+04
9.42E-02	4.49E+04
1.26E-01	5.60E+04
1.88E-01	7.57E+04
2.51E-01	9.44E+04
3.14E-01	1.12E+05

3.77E-01	1.29E+05
4.40E-01	1.45E+05
5.03E-01	1.61E+05
5.65E-01	1.76E+05
6.28E-01	1.89E+05
9.42E-01	2.55E+05
9.96E-05	1.30E+02
1.49E-04	1.93E+02
1.99E-04	2.54E+02
2.99E-04	3.74E+02
3.98E-04	4.90E+02
4.98E-04	6.05E+02
5.97E-04	7.20E+02
6.97E-04	8.30E+02
7.97E-04	9.37E+02
8.96E-04	1.05E+03
9.96E-04	1.15E+03
1.49E-03	1.68E+03
1.99E-03	2.18E+03
2.99E-03	3.10E+03
3.98E-03	4.00E+03
4.98E-03	4.83E+03
5.97E-03	5.62E+03
6.97E-03	6.40E+03
7.97E-03	7.14E+03
8.96E-03	7.88E+03
9.96E-03	8.55E+03
1.49E-02	1.17E+04
1.99E-02	1.46E+04
2.99E-02	1.98E+04
3.98E-02	2.46E+04
4.98E-02	2.90E+04
5.97E-02	3.31E+04
6.97E-02	3.71E+04
7.97E-02	4.10E+04
8.96E-02	4.52E+04
9.96E-02	4.86E+04
1.49E-01	6.56E+04
1.99E-05	3.12E+01
2.98E-05	4.56E+01
3.97E-05	6.01E+01
5.96E-05	8.89E+01
7.95E-05	1.17E+02
9.93E-05	1.45E+02
1.19E-04	1.75E+02
1.39E-04	2.03E+02
1.59E-04	2.28E+02
1.79E-04	2.56E+02
1.99E-04	2.81E+02
2.98E-04	4.15E+02
3.97E-04	5.43E+02
5.96E-04	8.01E+02
7.95E-04	1.05E+03
9.93E-04	1.28E+03

```
1.19E-03    1.52E+03
1.39E-03    1.74E+03
1.59E-03    1.98E+03
1.79E-03    2.19E+03
1.99E-03    2.40E+03
2.98E-03    3.45E+03
3.97E-03    4.45E+03
5.96E-03    6.23E+03
7.95E-03    7.92E+03
9.93E-03    9.48E+03
1.19E-02    1.10E+04
1.39E-02    1.24E+04
1.59E-02    1.38E+04
1.79E-02    1.52E+04
1.99E-02    1.63E+04
2.98E-02    2.21E+04
5.60E-06    8.92E+00
8.40E-06    1.30E+01
1.12E-05    1.70E+01
1.68E-05    2.56E+01
2.24E-05    3.36E+01
2.80E-05    4.23E+01
3.36E-05    4.99E+01
3.92E-05    5.80E+01
4.48E-05    6.56E+01
5.04E-05    7.50E+01
5.60E-05    8.19E+01
8.40E-05    1.21E+02
1.12E-04    1.59E+02
1.68E-04    2.35E+02
2.24E-04    3.10E+02
2.80E-04    3.84E+02
3.36E-04    4.55E+02
3.92E-04    5.26E+02
4.48E-04    5.95E+02
5.04E-04    6.66E+02
5.60E-04    7.38E+02
8.40E-04    1.09E+03
1.12E-03    1.42E+03
1.68E-03    2.05E+03
2.24E-03    2.65E+03
2.80E-03    3.22E+03
3.36E-03    3.75E+03
3.92E-03    4.28E+03
4.48E-03    4.83E+03
5.04E-03    5.40E+03
5.60E-03    5.85E+03
8.40E-03    8.25E+03
;
PROC NLIN METHOD=DUD;
PARMS A=-16 B=.6 C=-.15 D=8;
X1=LOG10(X);
Y1=LOG10(Y);
MODEL Y1=D+A*EXP(-EXP(B-C*X1));
```

Appendix C. SAS Output File

Aun3 DATA TO FIT PROPOSED MODEL FOR LOSS MODULUS EQUATION (Gompertz) 31
11:31 Wednesday, July 15, 1998

Non-Linear Least Squares DUD Initialization Dependent Variable Y1

DUD	A	B	C	D	Sum of Squares
-5	-16.000000	0.600000	-0.150000	8.000000	1.273081
-4	-17.600000	0.600000	-0.150000	8.000000	46.775128
-3	-16.000000	0.660000	-0.150000	8.000000	14.603843
-2	-16.000000	0.600000	-0.165000	8.000000	13.228944
-1	-16.000000	0.600000	-0.150000	8.800000	142.414997

Non-Linear Least Squares Iterative Phase Dependent Variable Y1 Method: DUD

Iter	A	B	C	D	Sum of Squares
0	-16.000000	0.600000	-0.150000	8.000000	1.273081
1	-17.633006	0.647809	-0.138716	8.101375	0.749556
2	-18.070492	0.652899	-0.136759	8.120654	0.466220
3	-18.118961	0.652976	-0.136809	8.123178	0.449691
4	-18.115538	0.652881	-0.136818	8.123160	0.449688
5	-18.115436	0.652881	-0.136818	8.123146	0.449688
6	-18.109765	0.653352	-0.136905	8.120295	0.449658
7	-18.108090	0.653319	-0.136915	8.120219	0.449658
8	-18.112729	0.653401	-0.136888	8.120461	0.449658
9	-18.112886	0.653403	-0.136887	8.120470	0.449658

NOTE: Convergence criterion met.

Non-Linear Least Squares Summary Statistics Dependent Variable Y1

Source	DF	Sum of Squares	Mean Square
Regression	4	6443.6527709	1610.9131927
Residual	252	0.4496577	0.0017844
Uncorrected Total	256	6444.1024286	
(Corrected Total)	255	732.0593630	

Parameter	Estimate	Asymptotic Std. Error	Asymptotic 95 % Confidence Interval Lower	Upper
A	-18.11288634	0.74956580667	-19.589117037	-16.636655647
B	0.65340336	0.01390870165	0.626010900	0.680795823
C	-0.13688688	0.00442487463	-0.145601438	-0.128172319
D	8.12047014	0.04616835056	8.029543989	8.211396298

Asymptotic Correlation Matrix

Corr	A	B	C	D
A	1	-0.94704092	-0.993903737	-0.895211244
B	-0.94704092	1	0.9095608914	0.706256159
C	-0.993903737	0.9095608914	1	0.9316998254
D	-0.895211244	0.706256159	0.9316998254	1

Non-Linear Least Squares DUD Initialization Dependent Variable Y1

DUD	D	LOGOMD	LOGMAX	Sum of Squares
-4	4.000000	4.000000	7.500000	32.825295
-3	4.400000	4.000000	7.500000	62.828457
-2	4.000000	4.400000	7.500000	1.890498
-1	4.000000	4.000000	8.250000	310.075860

Non-Linear Least Squares Iterative Phase Dependent Variable Y1 Method: DUD

Iter	D	LOGOMD	LOGMAX	Sum of Squares
0	4.000000	4.400000	7.500000	1.890498
1	4.528923	4.683059	7.461858	0.401490
2	4.592632	4.744405	7.476652	0.355744
3	4.655709	4.809046	7.494882	0.341555
4	4.654097	4.808087	7.494699	0.341551
5	4.654197	4.808392	7.494872	0.341548
6	4.655123	4.809781	7.495626	0.341541
7	4.654991	4.809688	7.495615	0.341541
8	4.654985	4.809683	7.495614	0.341541

NOTE: Convergence criterion met.

Non-Linear Least Squares Summary Statistics Dependent Variable Y1

Source	DF	Sum of Squares	Mean Square
Regression	3	6443.7608878	2147.9202959
Residual	253	0.3415408	0.0013500
Uncorrected Total	256	6444.1024286	
(Corrected Total)	255	732.0593630	

Parameter	Estimate	Asymptotic Std. Error	Asymptotic 95 % Confidence Interval Lower	Upper
D	4.654984996	0.05032393513	4.5558765229	4.7540934685
LOGOMD	4.809683388	0.04103372793	4.7288711439	4.8904956313
LOGMAX	7.495614302	0.01378174674	7.4684723888	7.5227562149

Asymptotic Correlation Matrix

Corr	D	LOGOMD	LOGMAX
D	1	0.9578747001	0.7795996731
LOGOMD	0.9578747001	1	0.9201349432
LOGMAX	0.7795996731	0.9201349432	1

Appendix D. Comparison between measured dynamic loss modului and results from the Gompertz

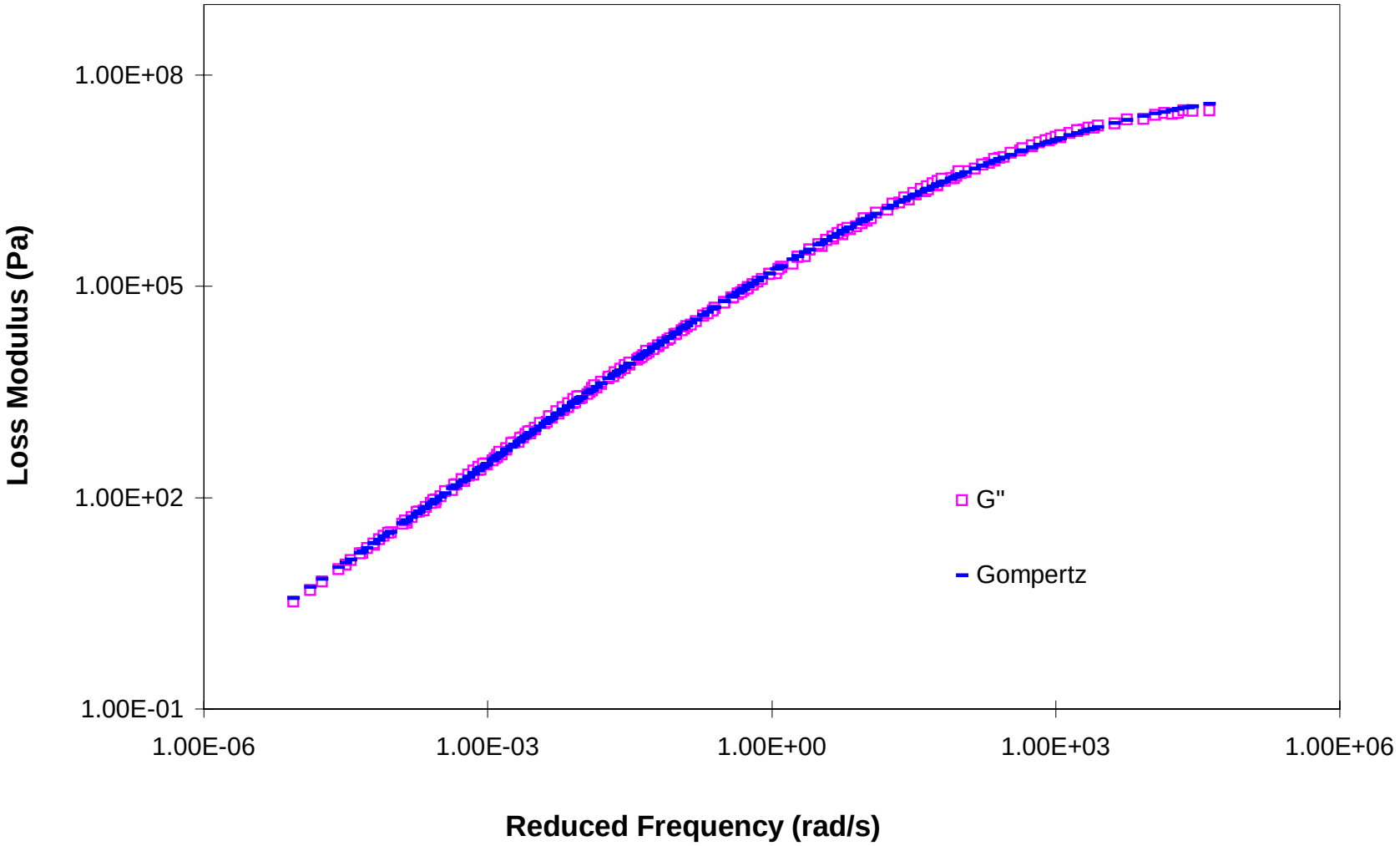

Figure D-1. Comparison between measured dynamic loss modulus for AUC2 and results from the Gompertz model.

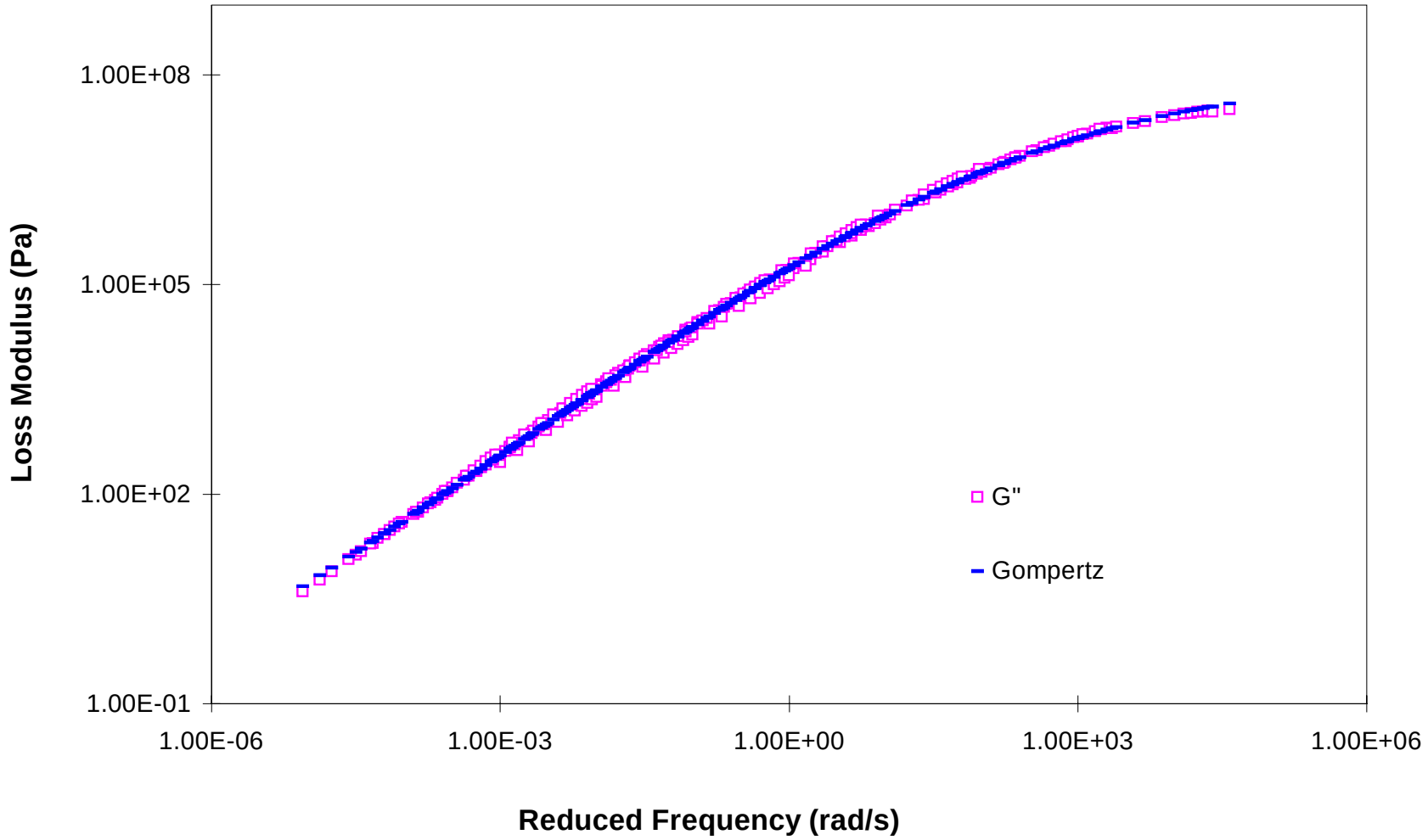

Figure D-2. Comparison between measured dynamic loss modulus for AUC3 and results from the Gompertz model.

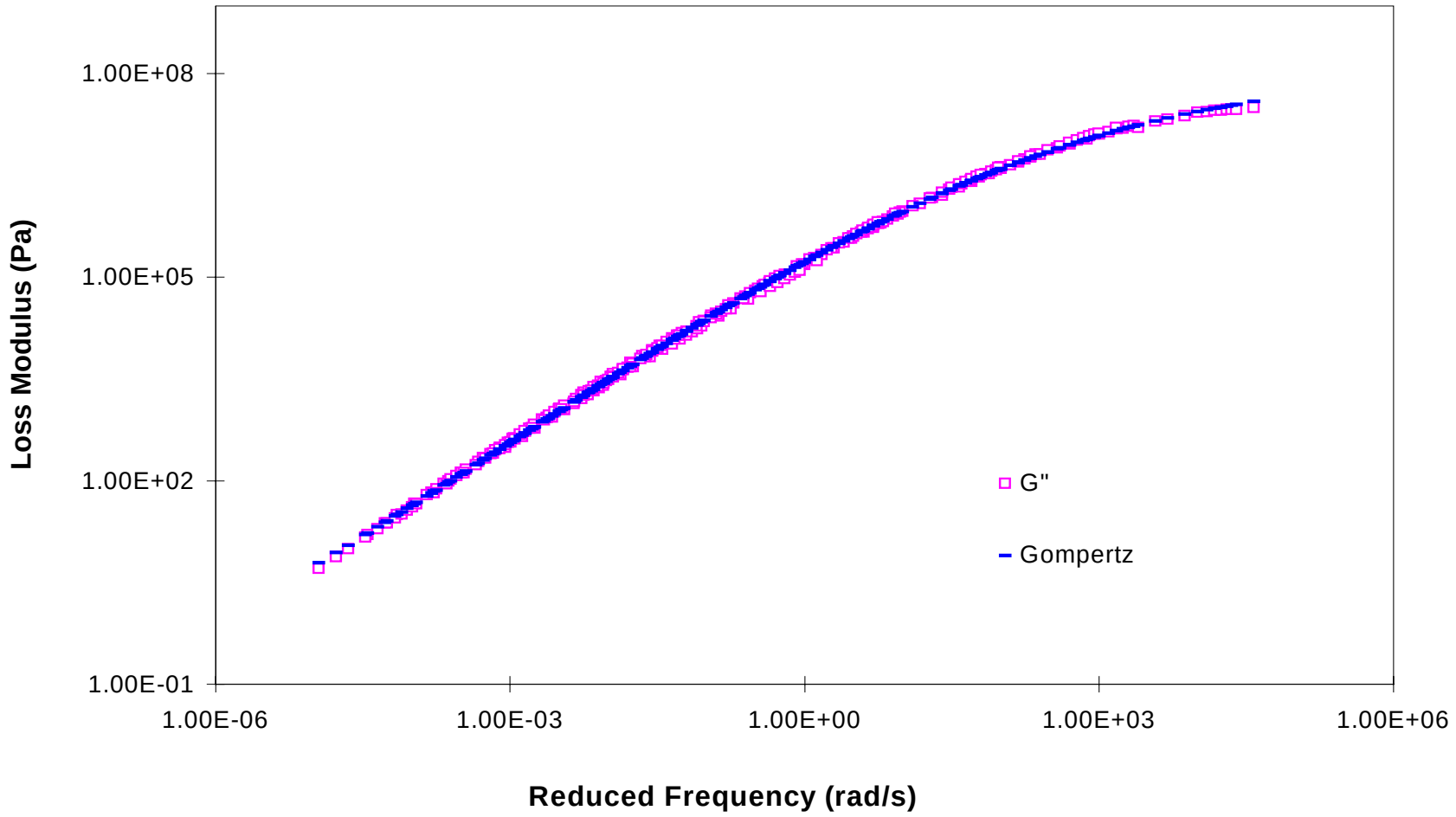

Figure D-3. Comparison between measured dynamic loss modulus for AUC4 and results from the Gompertz model.

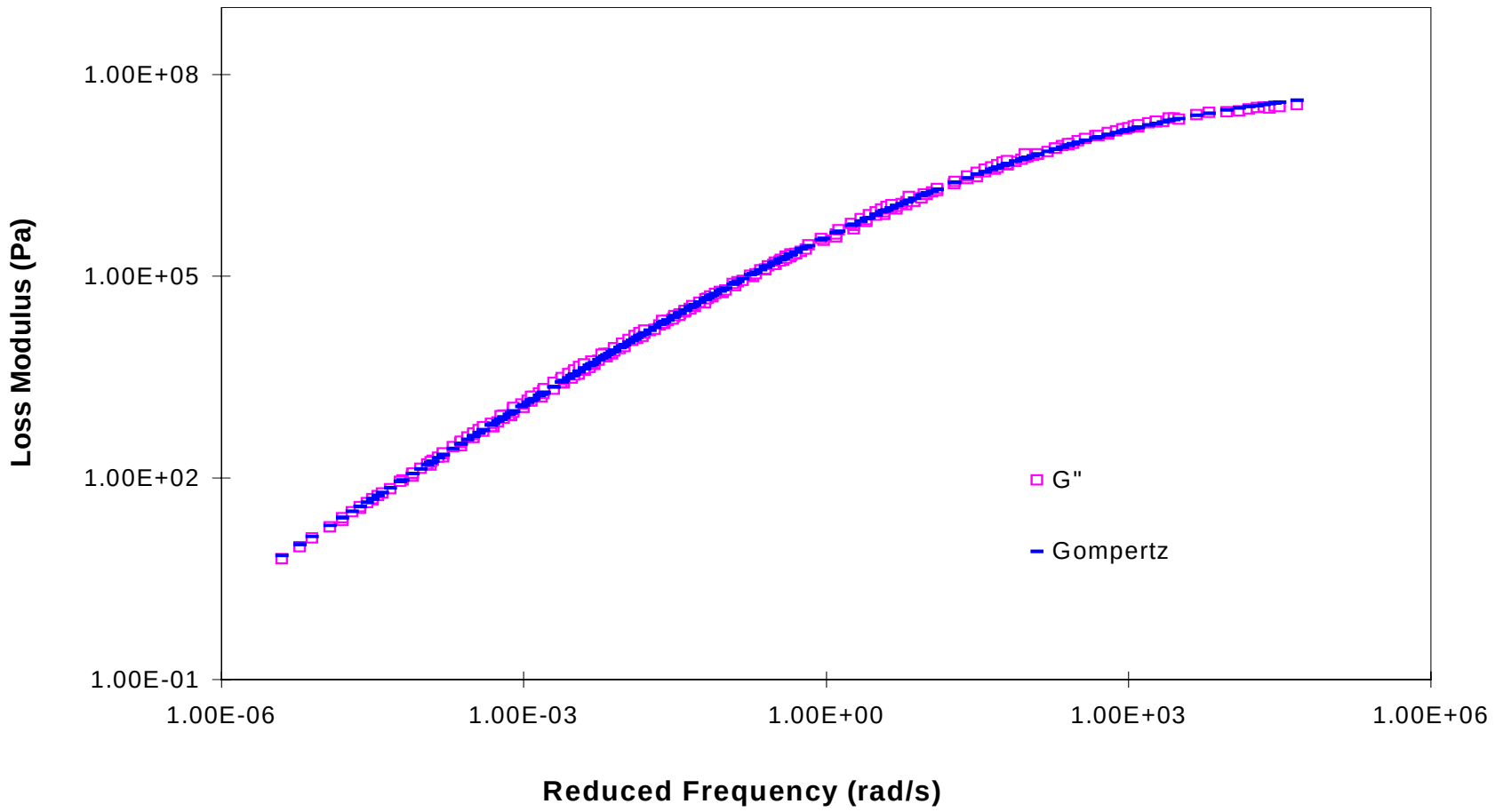

Figure D-4. Comparison between measured dynamic loss modulus for ARC2 and results from the Gompertz model.

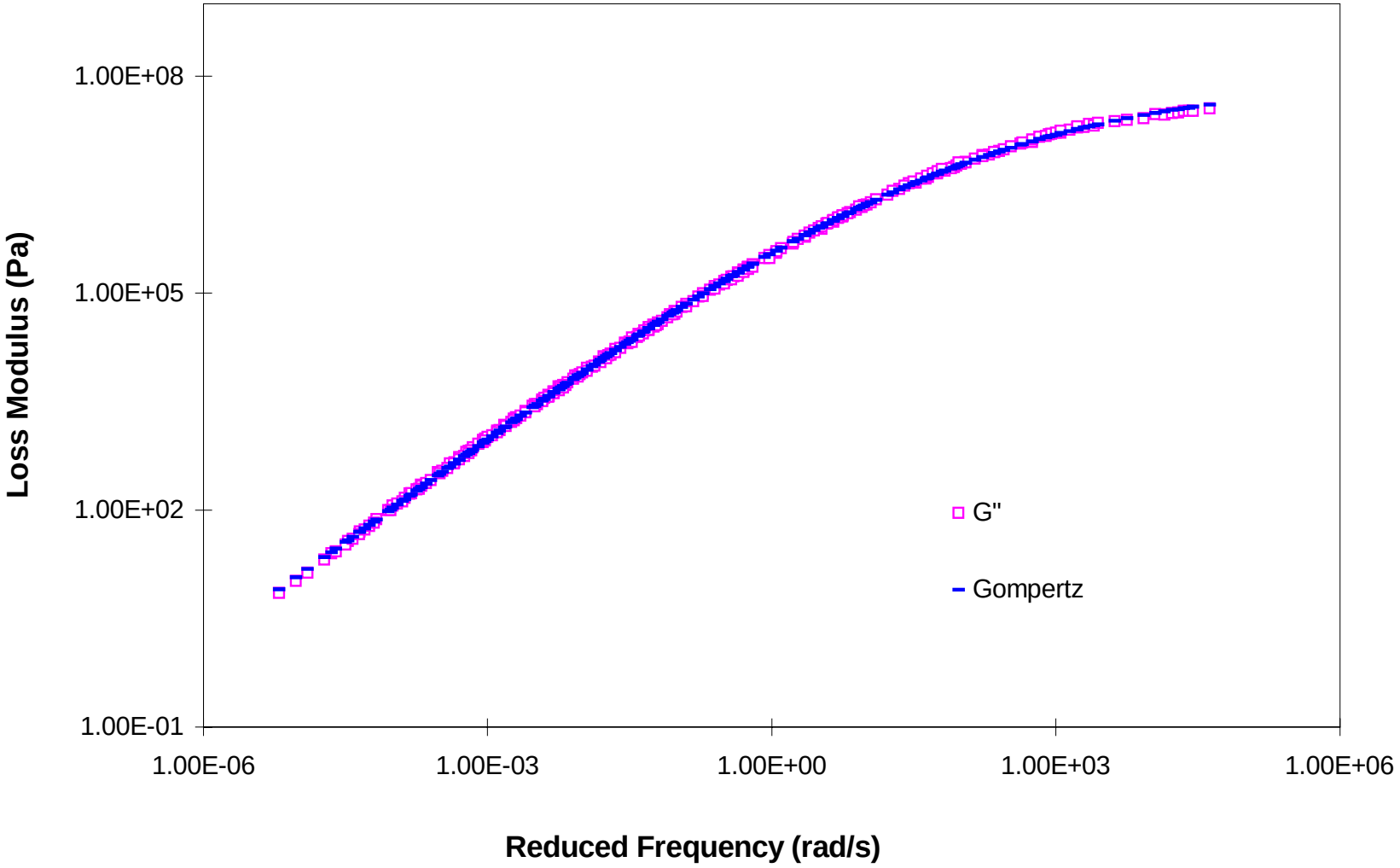

Figure D-5. Comparison between measured dynamic loss modulus for ARC3 and results from the Gompertz model.

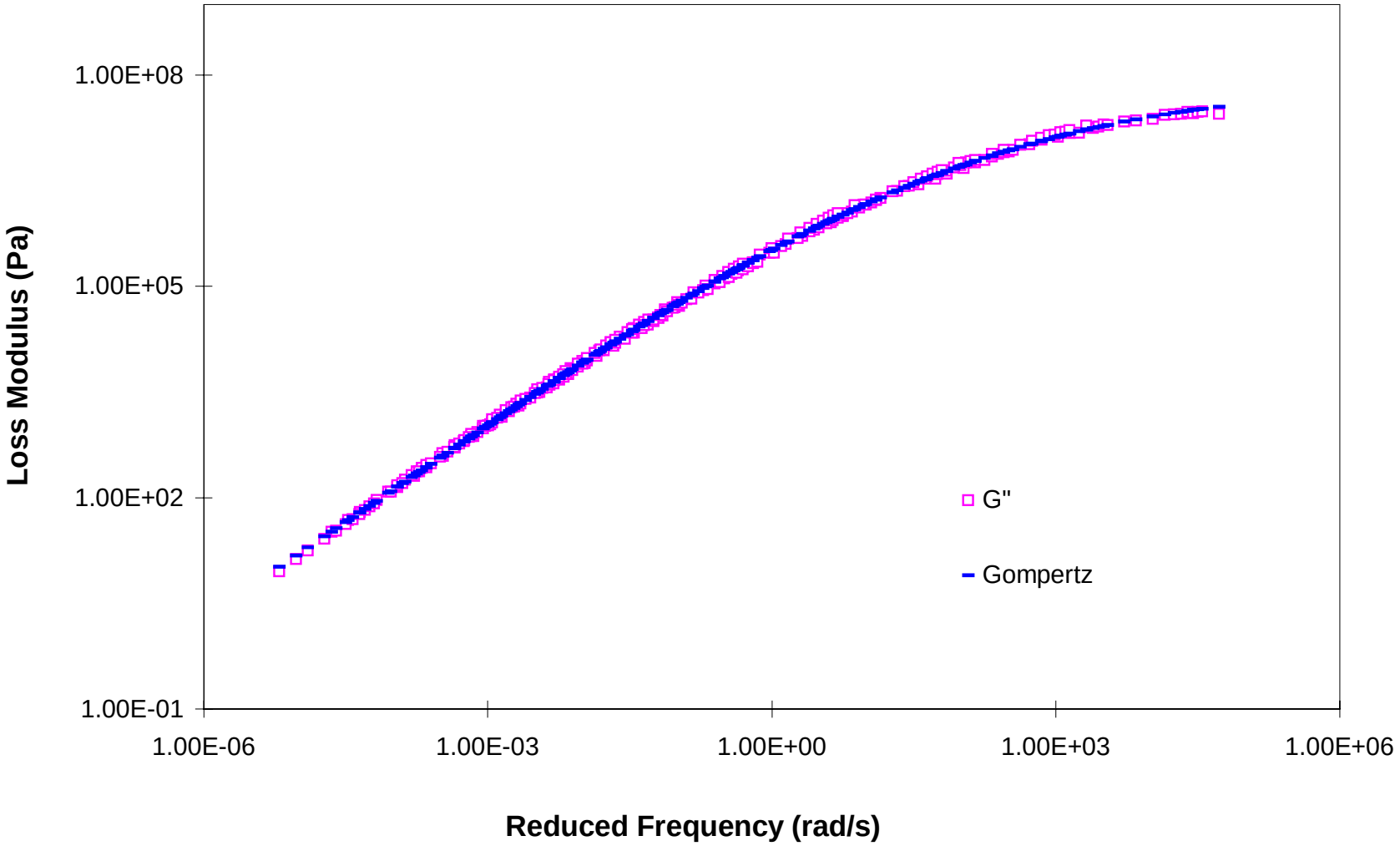

Figure D-6. Comparison between measured dynamic loss modulus for ARC4 and results from the Gompertz model.

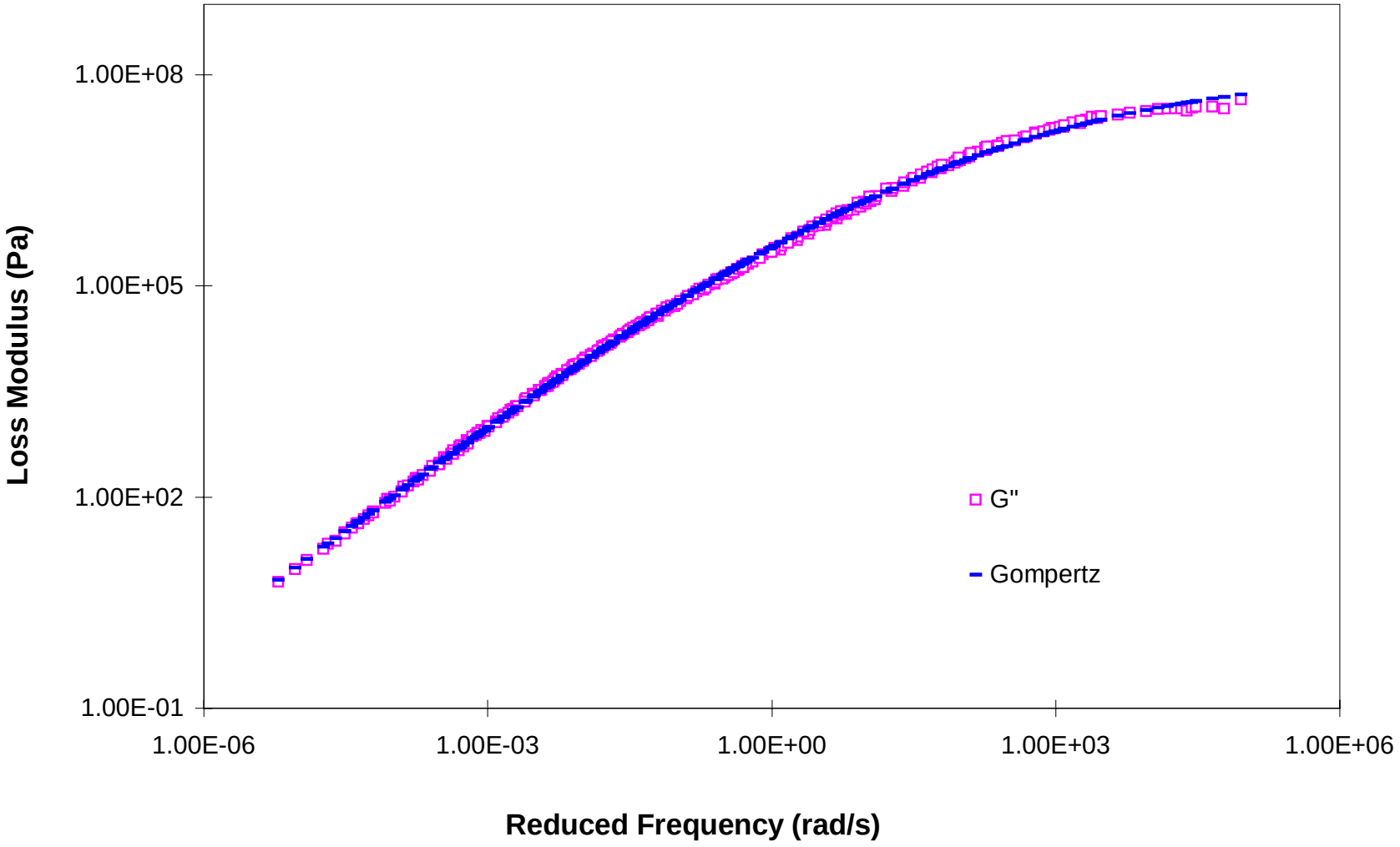

Figure D-7. Comparison between measured dynamic loss modulus for AUG3 and results from the Gompertz model.

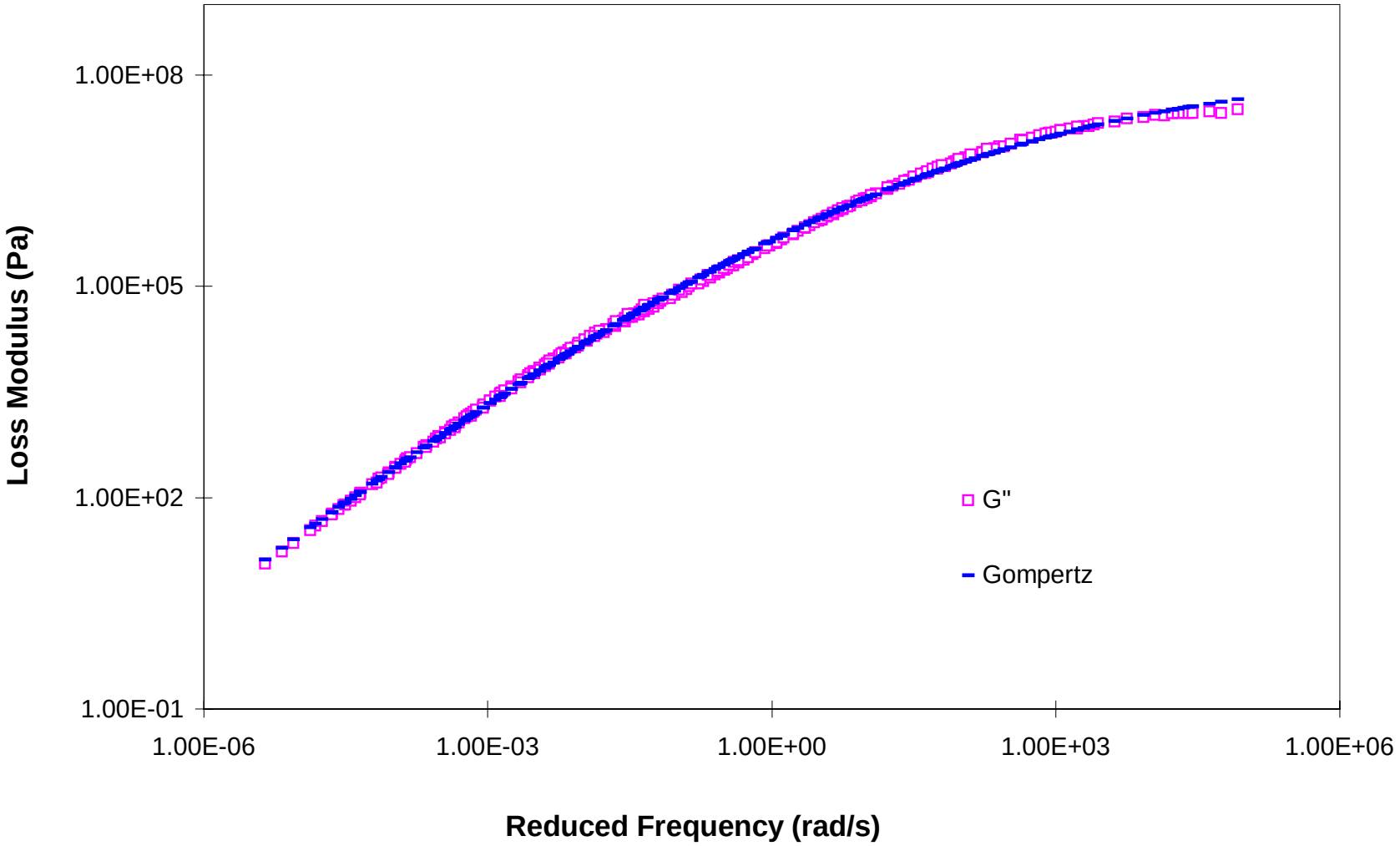

Figure D-8. Comparison between measured dynamic loss modulus for AUG4 and results from the Gompertz model.

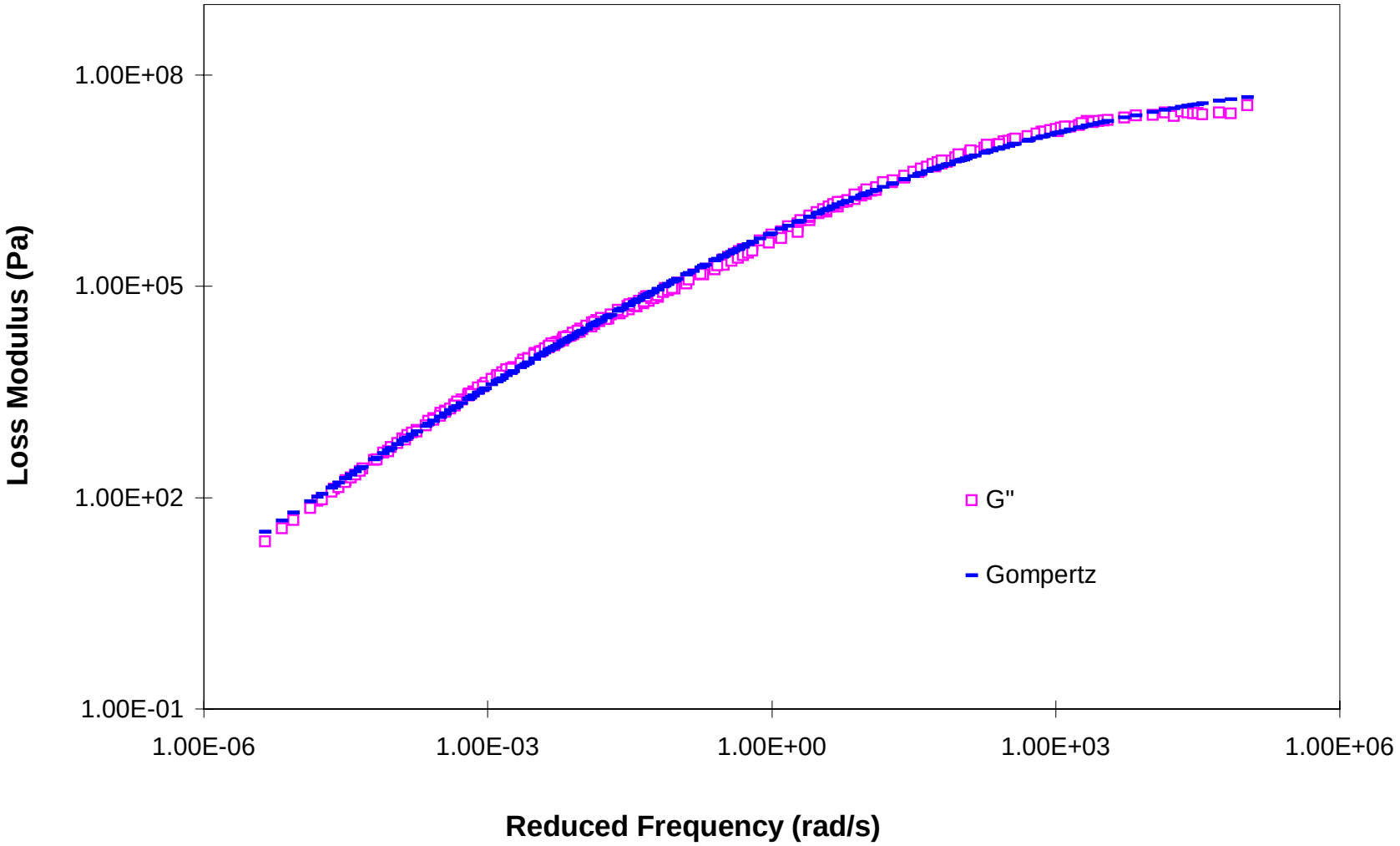

Figure D-9. Comparison between measured dynamic loss modulus for AUG5 and results from the Gompertz model.

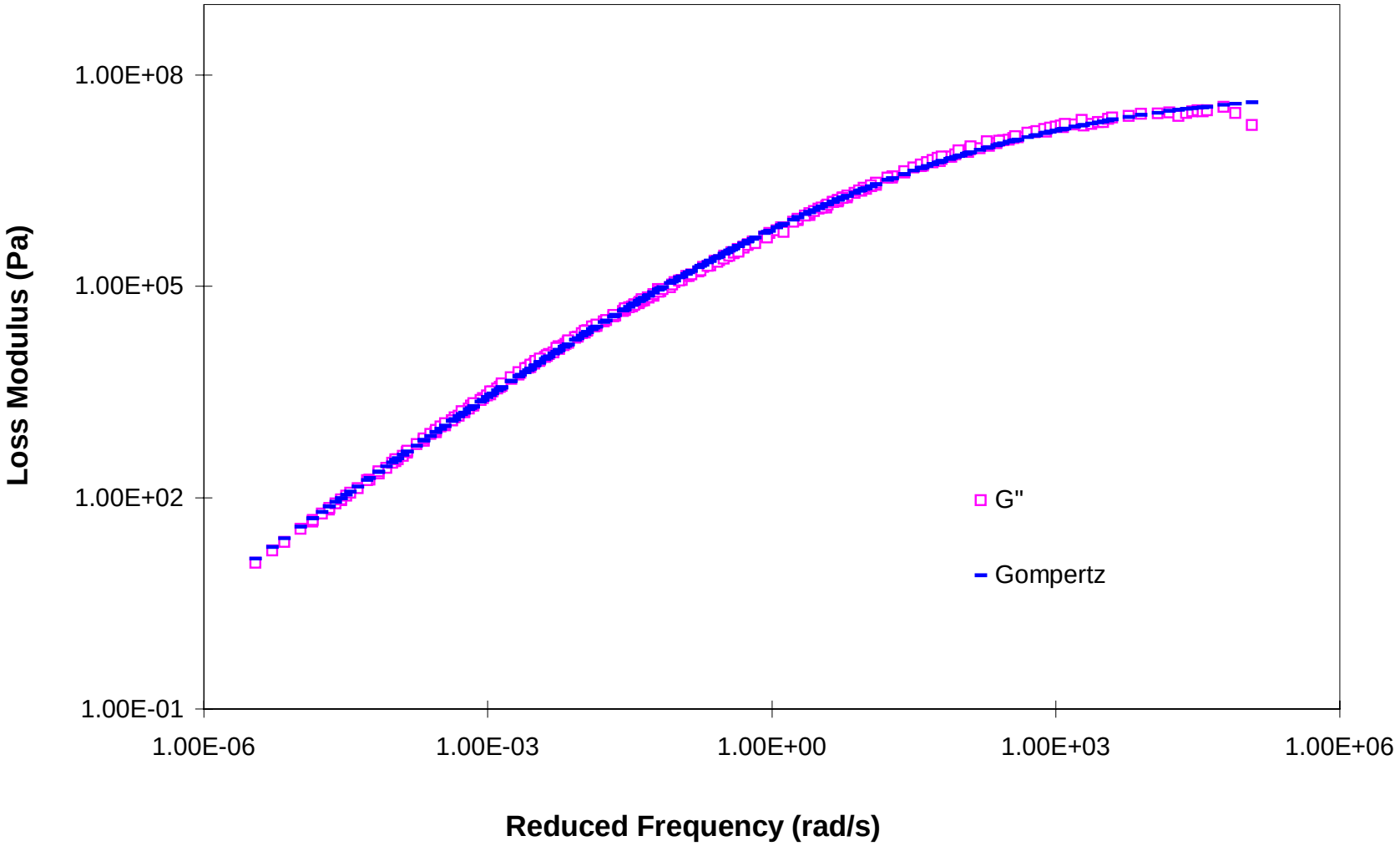

Figure D-10. Comparison between measured dynamic loss modulus for ARG3 and results from the Gompertz model.

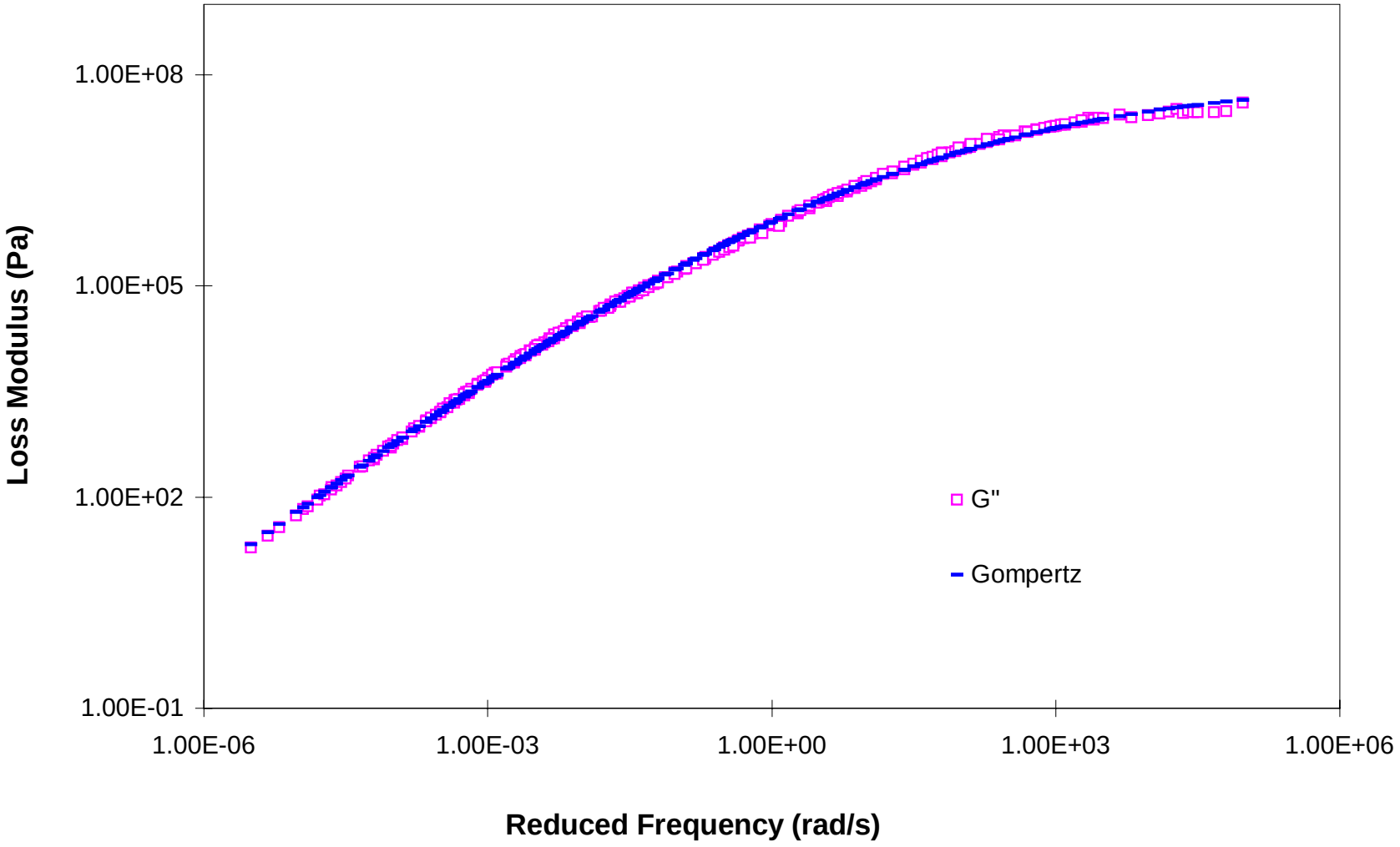

Figure D-11. Comparison between measured dynamic loss modulus for ARG4 and results from the Gompertz model.

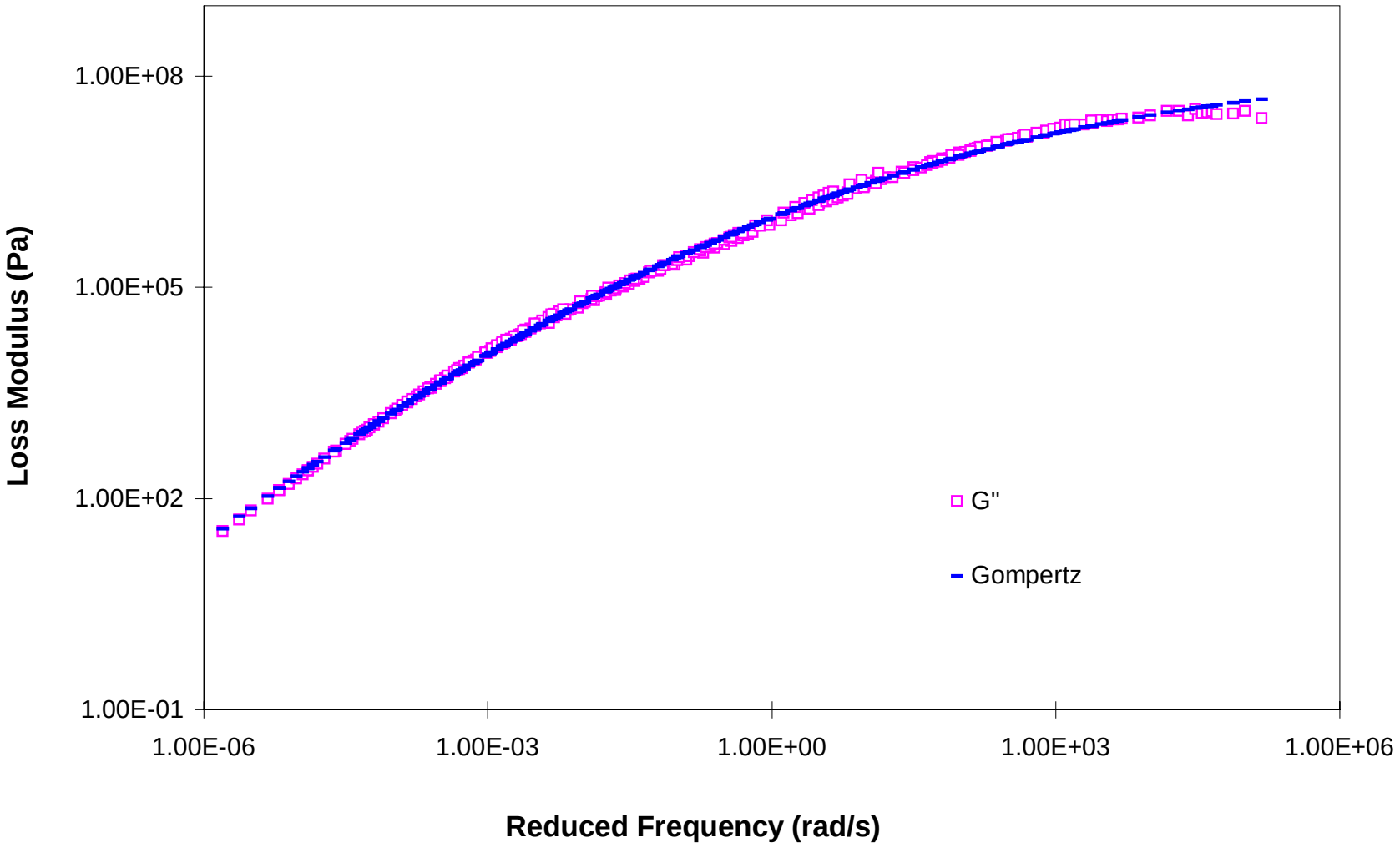

Figure D-12. Comparison between measured dynamic loss modulus for ARG5 and results from the Gompertz model.

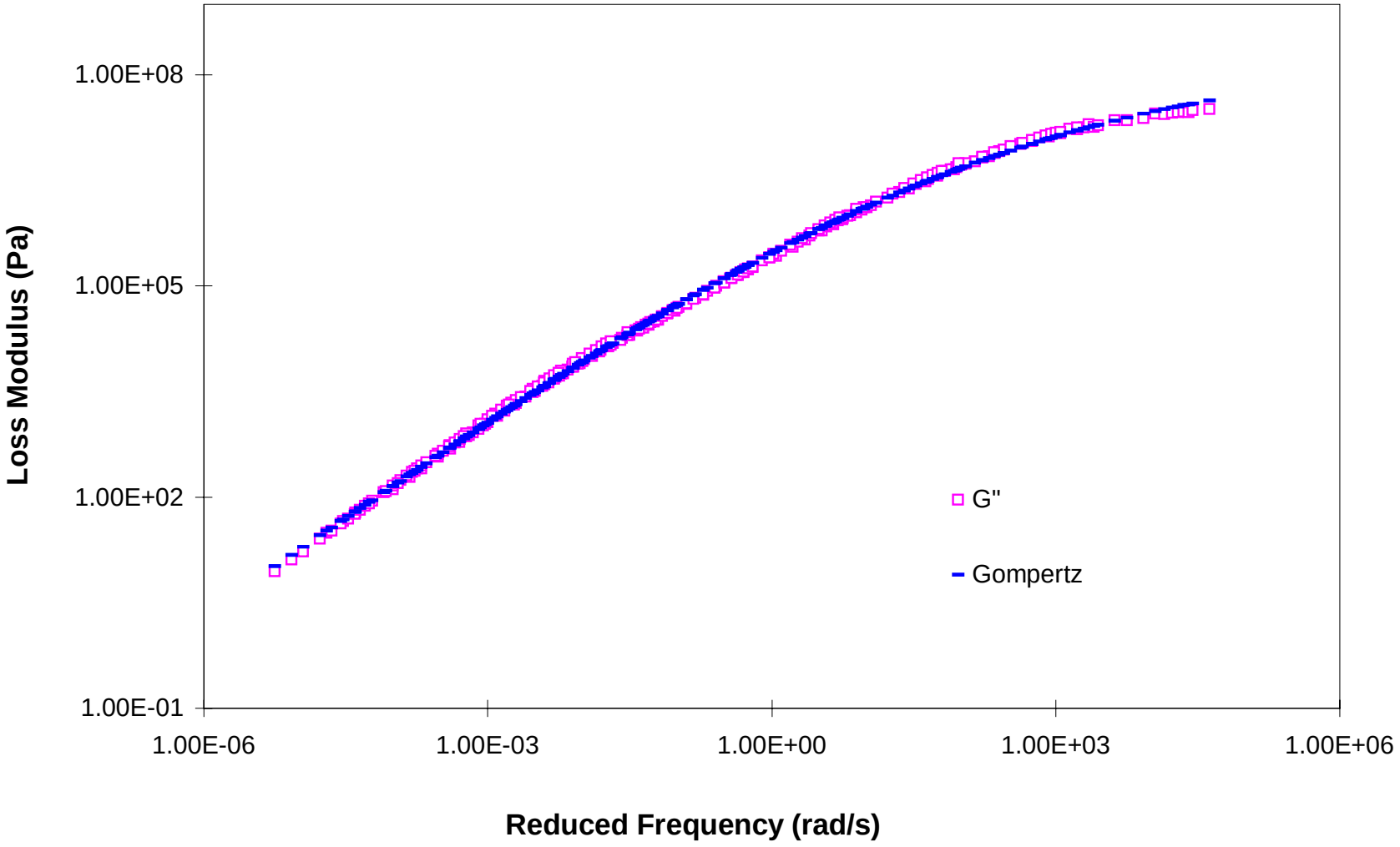

Figure D-13. Comparison between measured dynamic loss modulus for AUN3 and results from the Gompertz model.

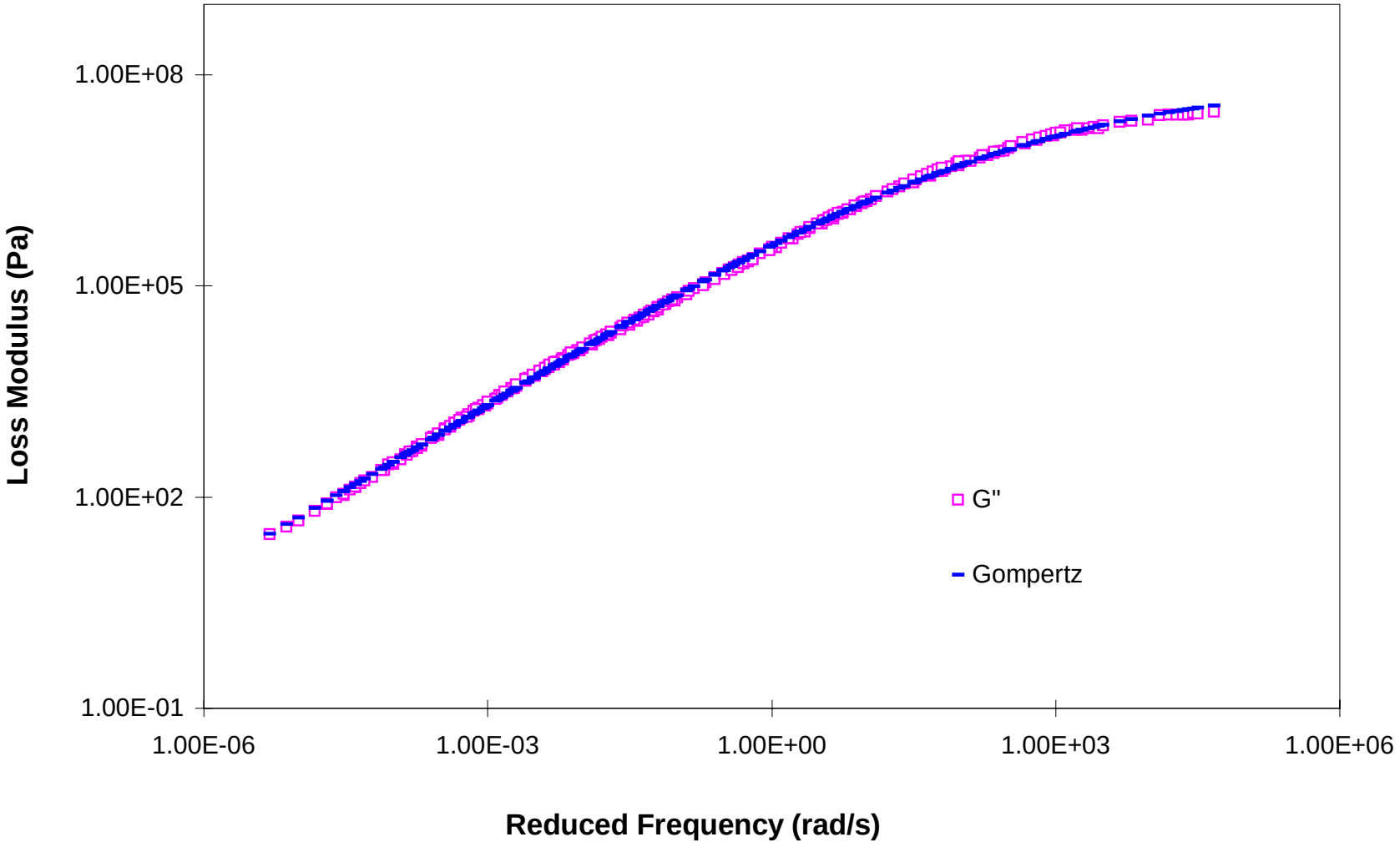

Figure D-14. Comparison between measured dynamic loss modulus for AUN4 and results from the Gompertz model.

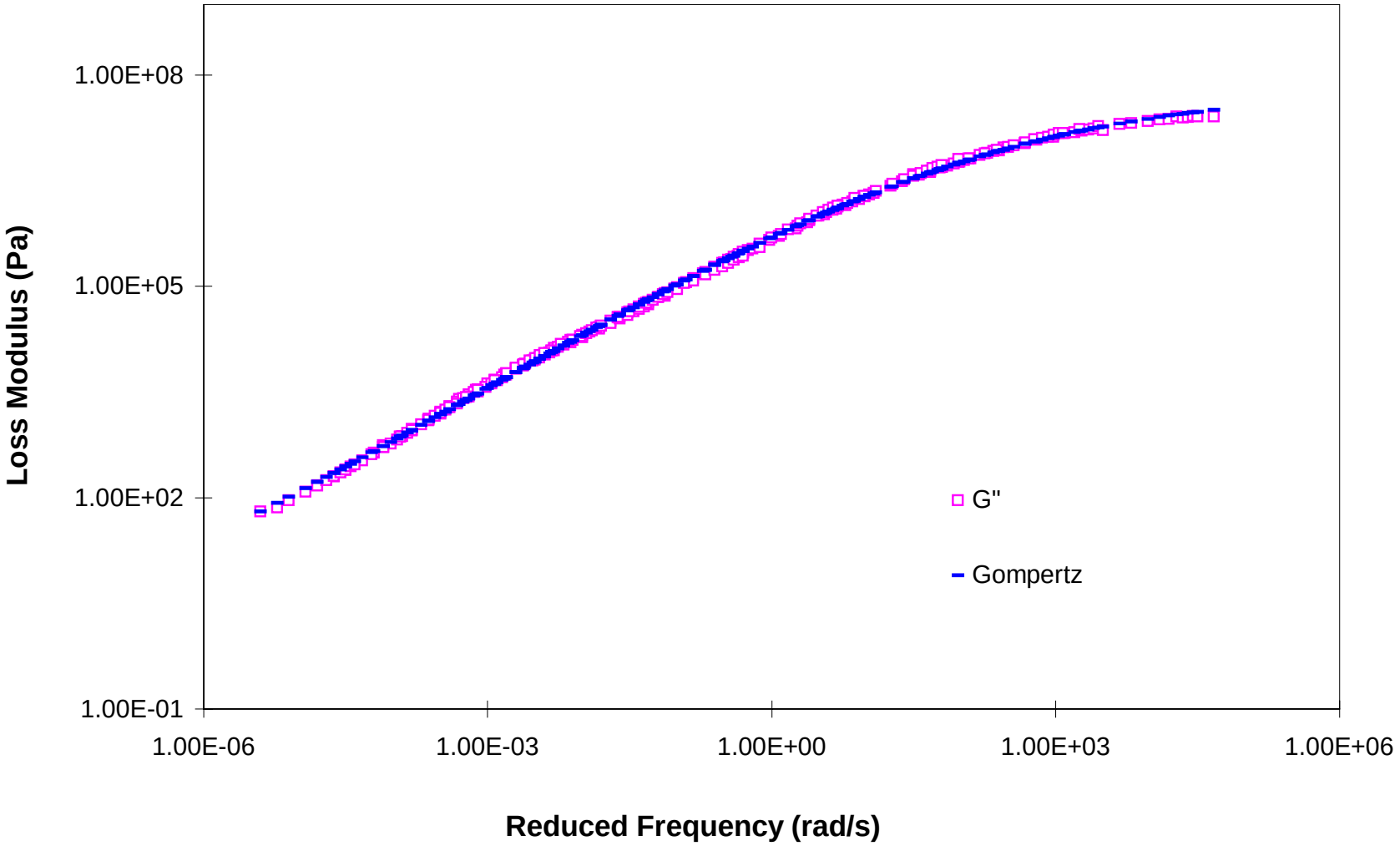

Figure D-15. Comparison between measured dynamic loss modulus for AUN5 and results from the Gompertz model.

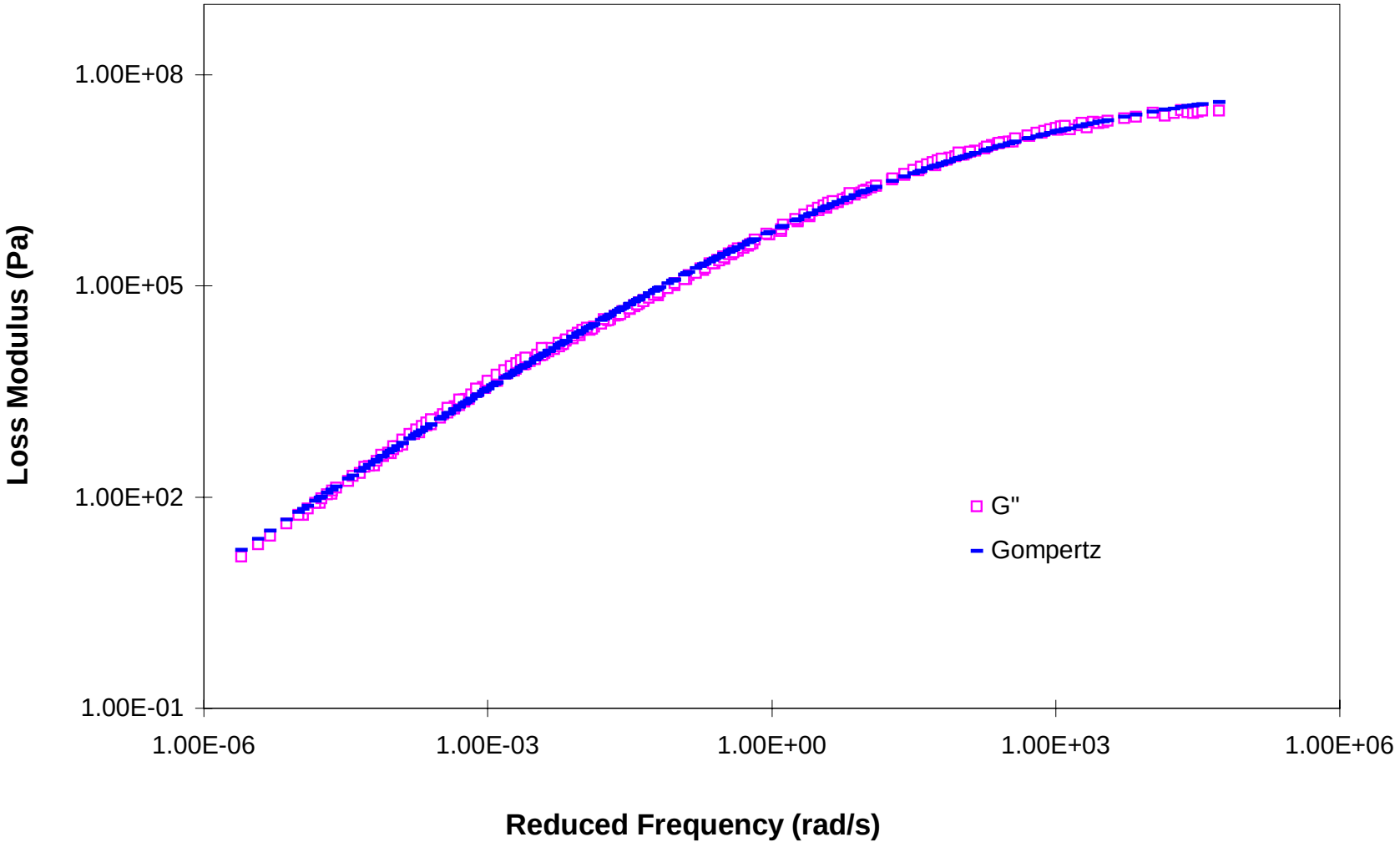

Figure D-16. Comparison between measured dynamic loss modulus for ARN3 and results from the Gompertz model.

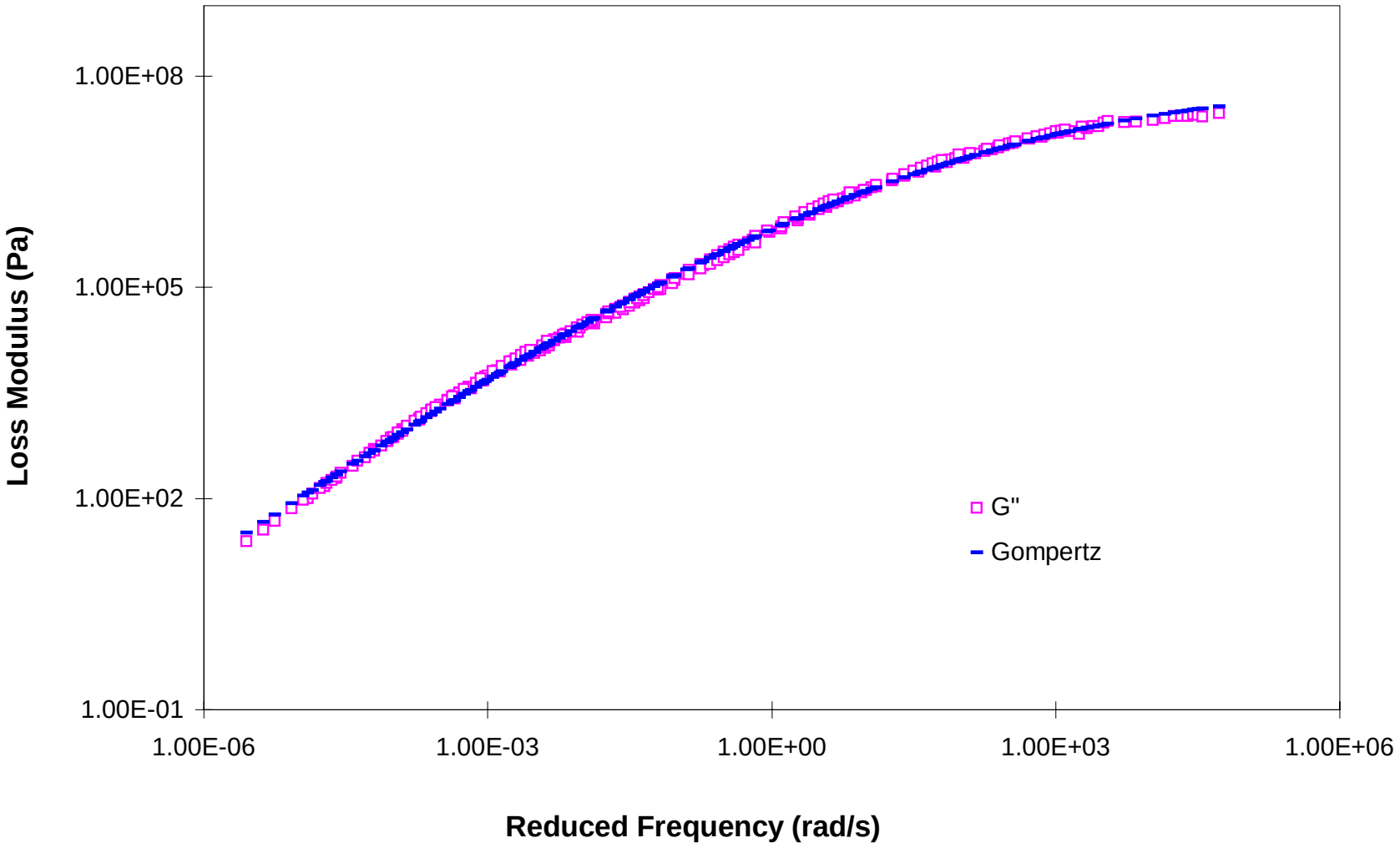

Figure D-17. Comparison between measured dynamic loss modulus for ARN4 and results from the Gompertz model.

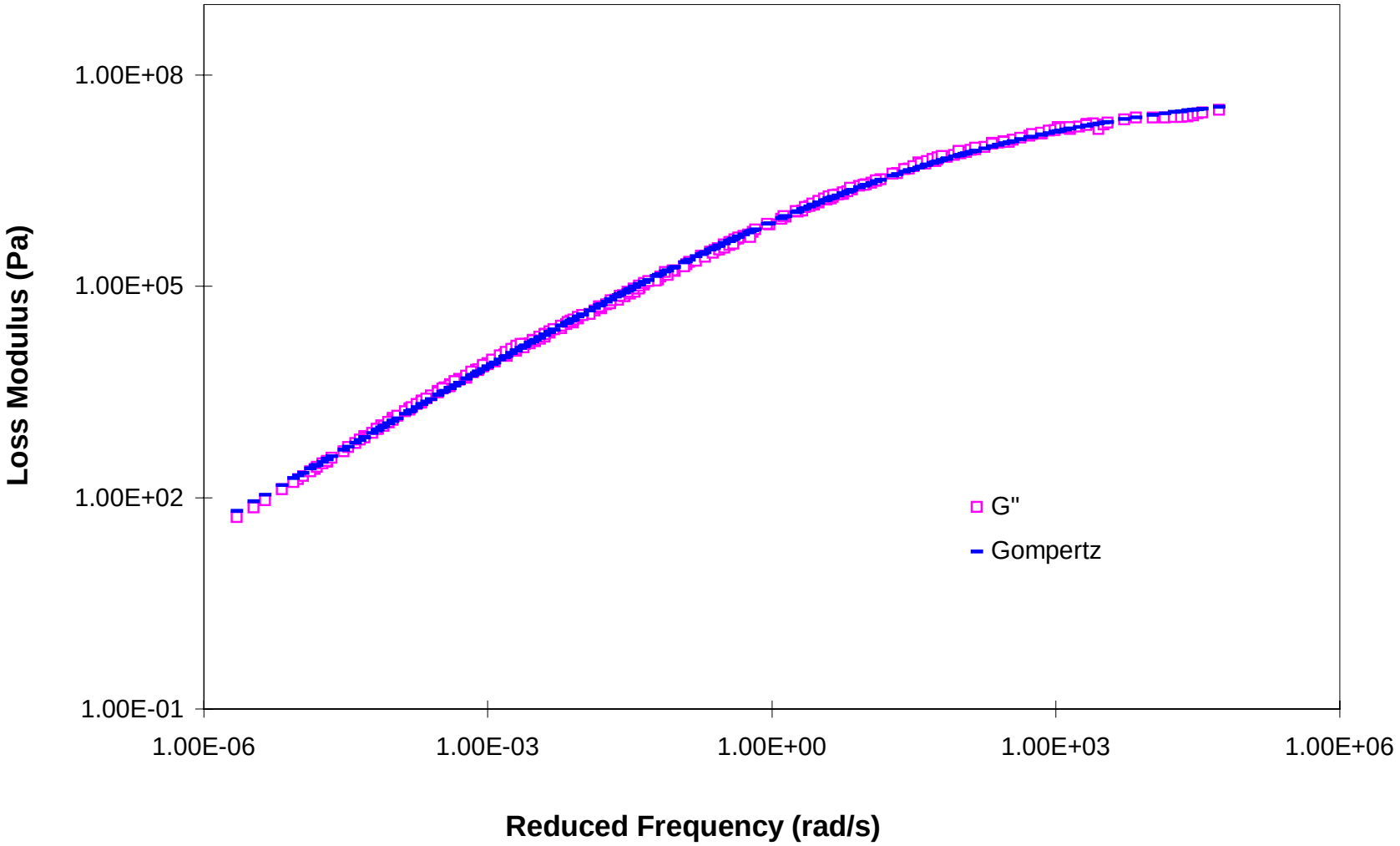

Figure D-18. Comparison between measured dynamic loss modulus for ARN5 and results from the Gompertz model.

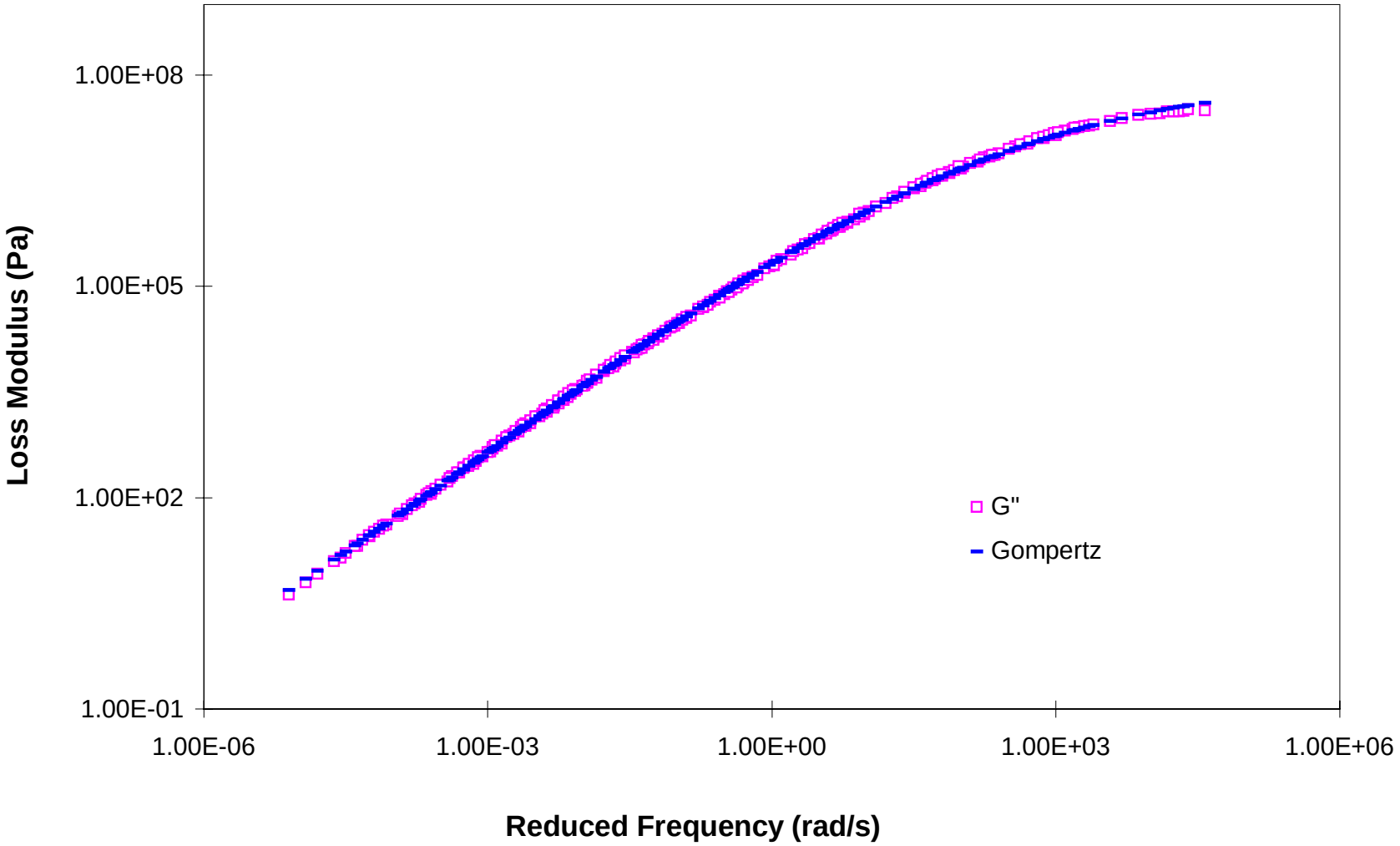

Figure D-19. Comparison between measured dynamic loss modulus for AUP3 and results from the Gompertz model.

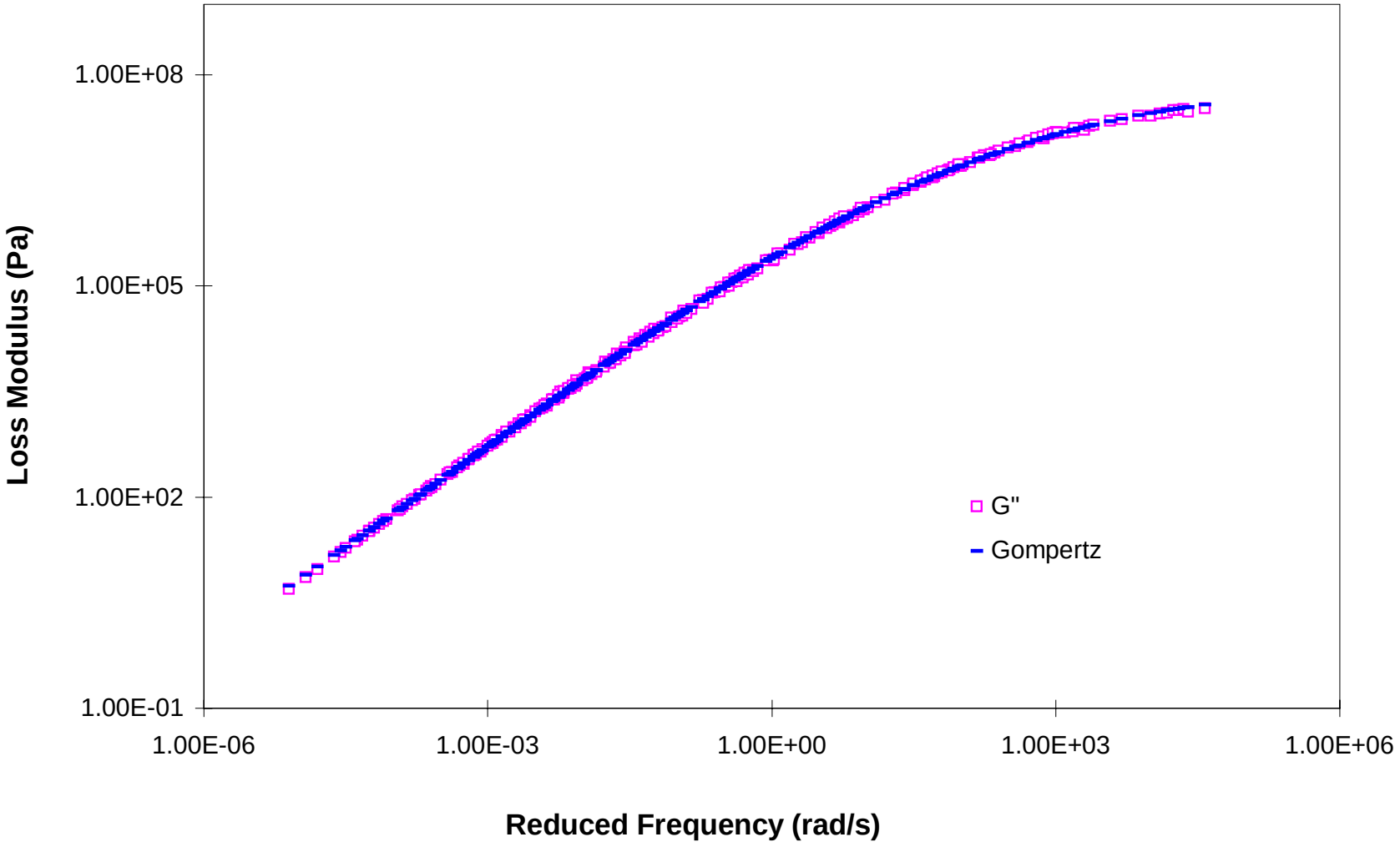

Figure D-20. Comparison between measured dynamic loss modulus for AUP4 and results from the Gompertz model.

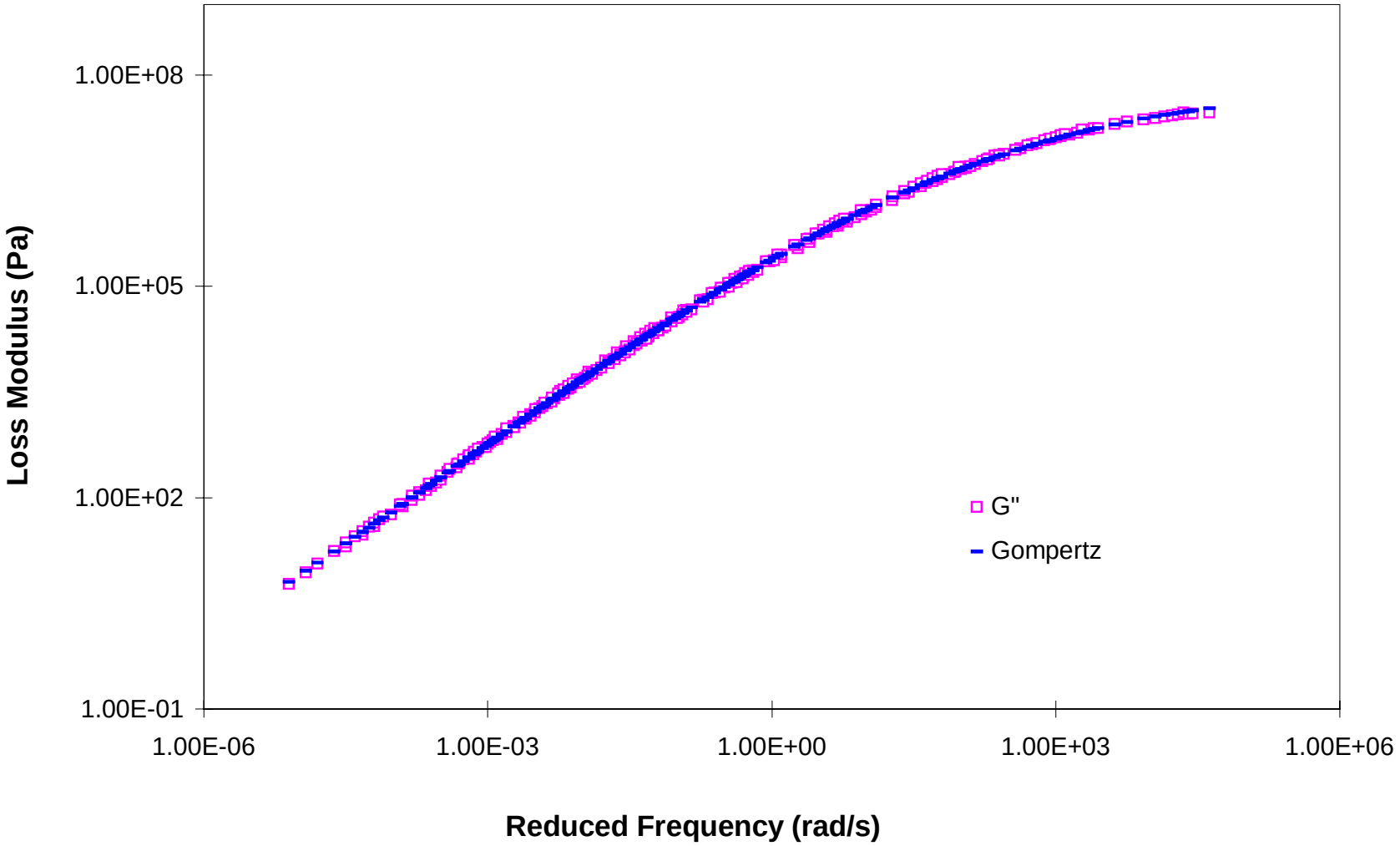

Figure D-21. Comparison between measured dynamic loss modulus for AUP5 and results from the Gompertz model.

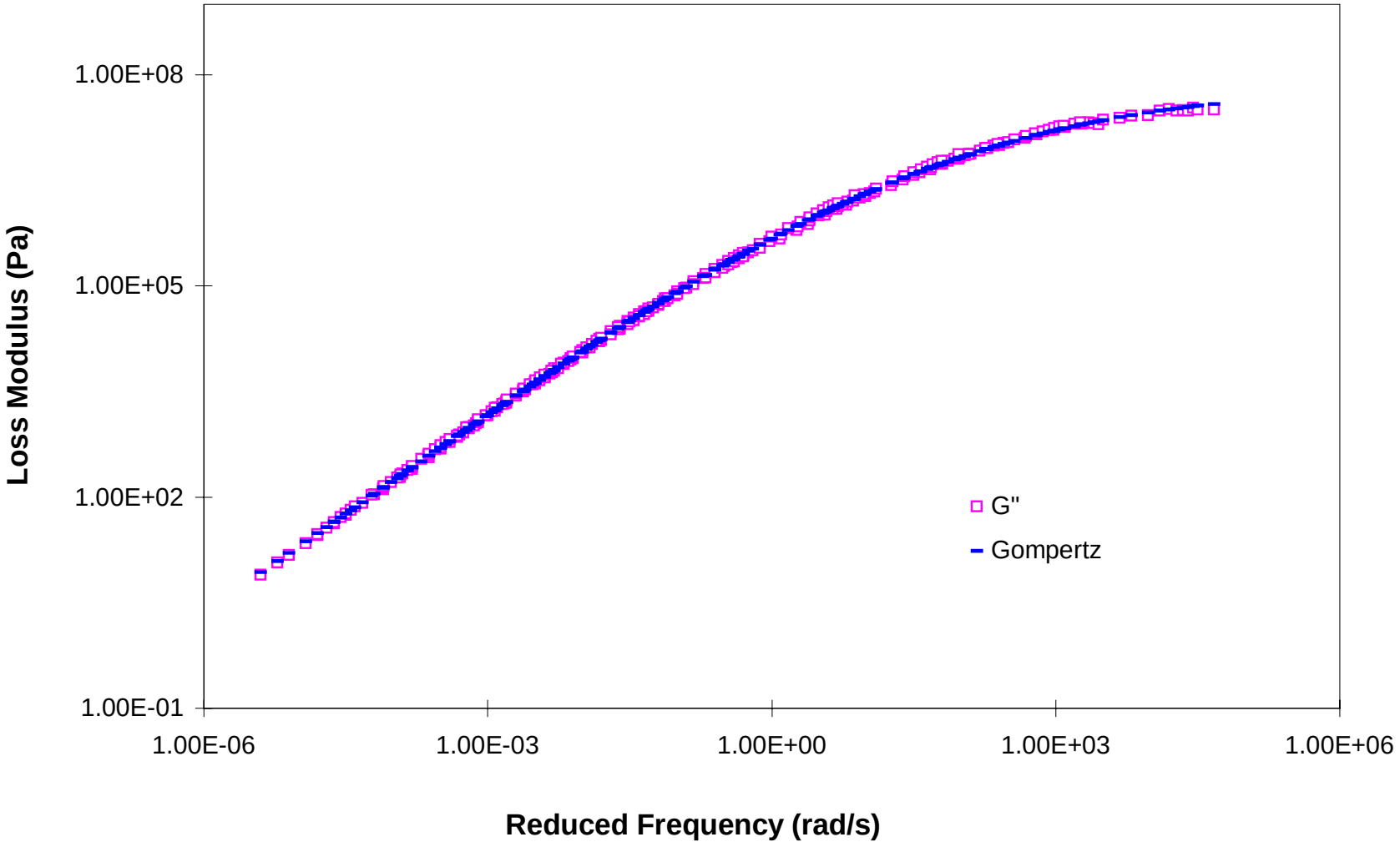

Figure D-22. Comparison between measured dynamic loss modulus for ARP3 and results from the Gompertz model.

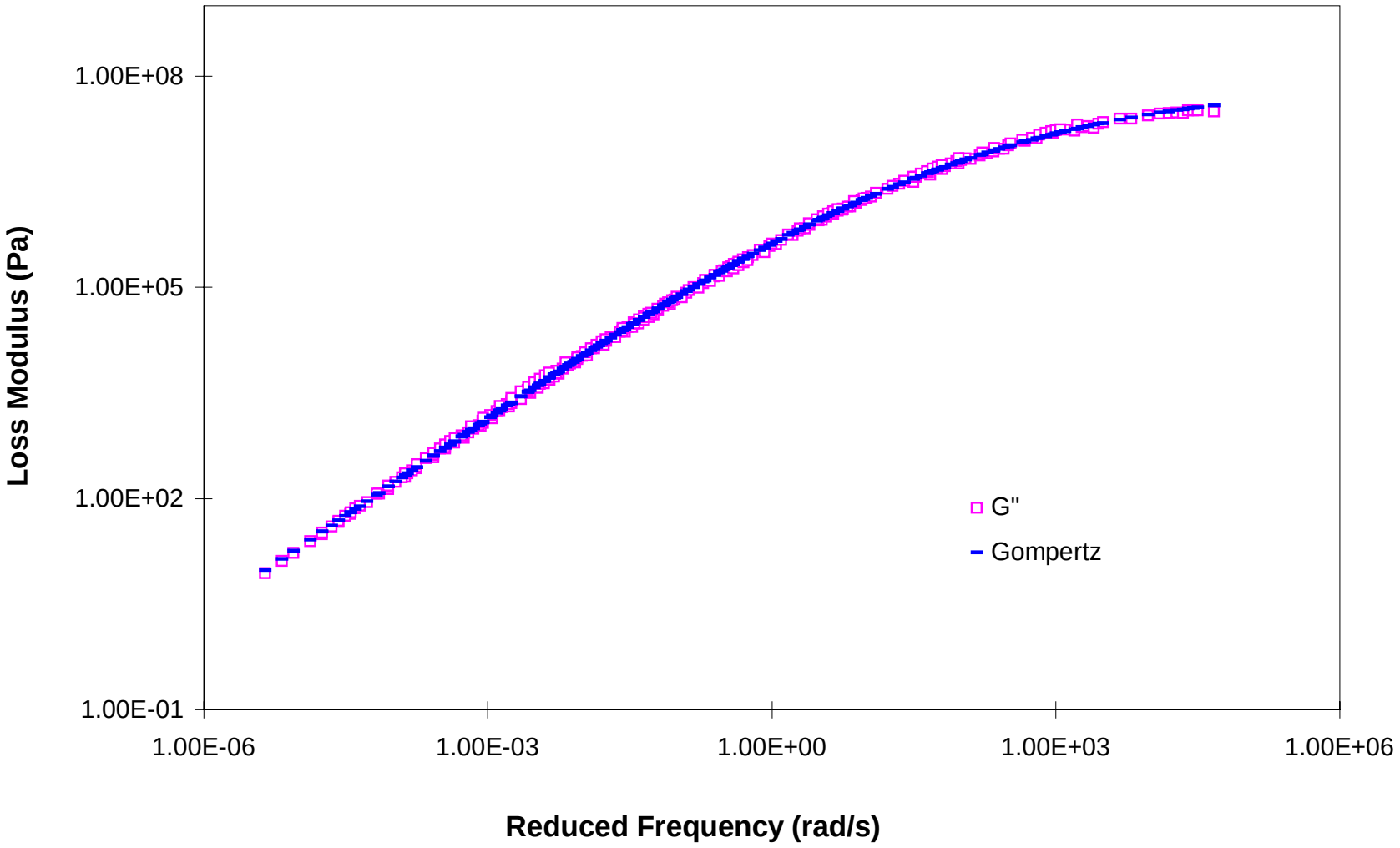

Figure D-23. Comparison between measured dynamic loss modulus for ARP4 and results from the Gompertz model.

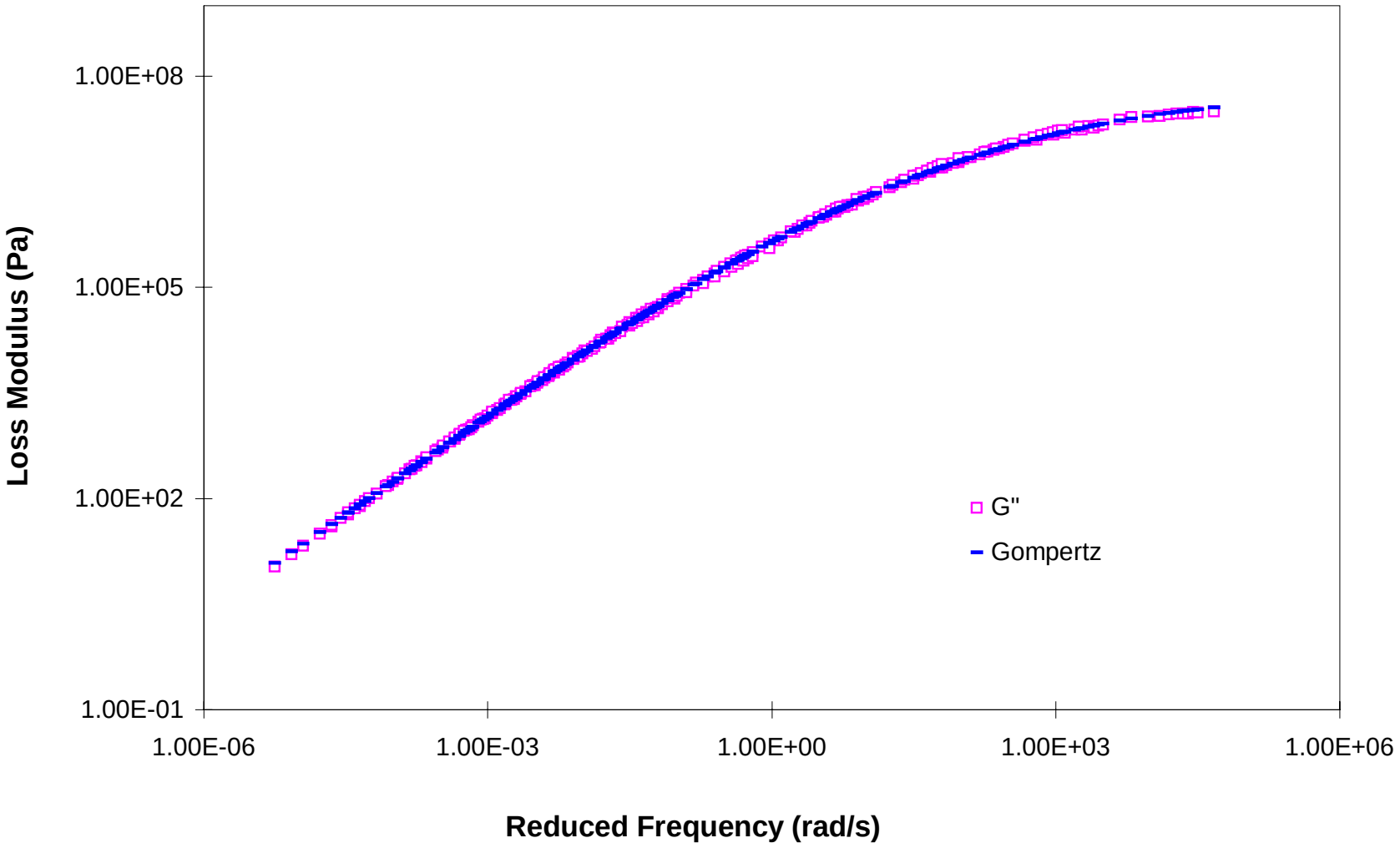

Figure D-24. Comparison between measured dynamic loss modulus for ARP5 and results from the Gompertz model.

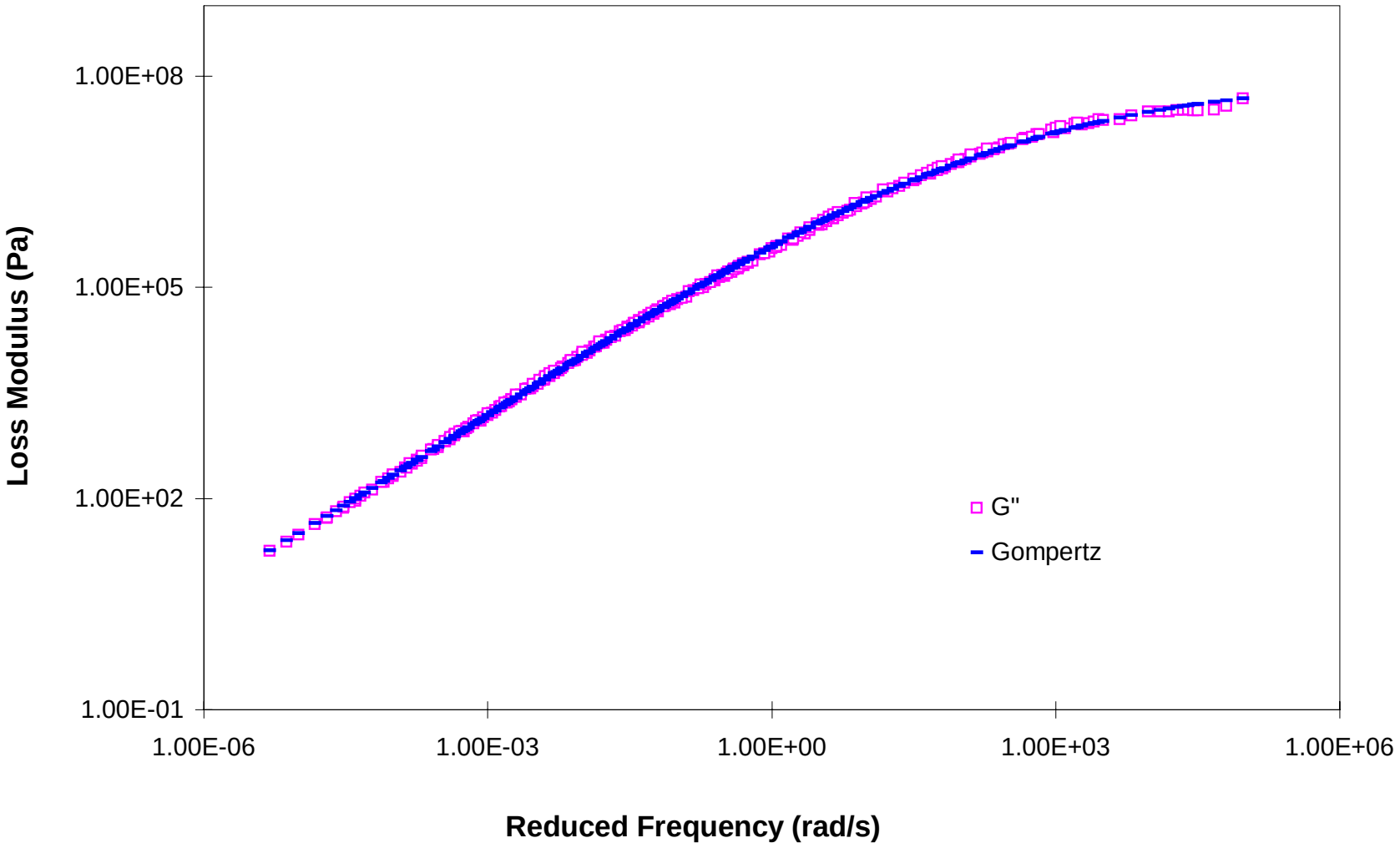

Figure D-25. Comparison between measured dynamic loss modulus for AUX3 and results from the Gompertz model.

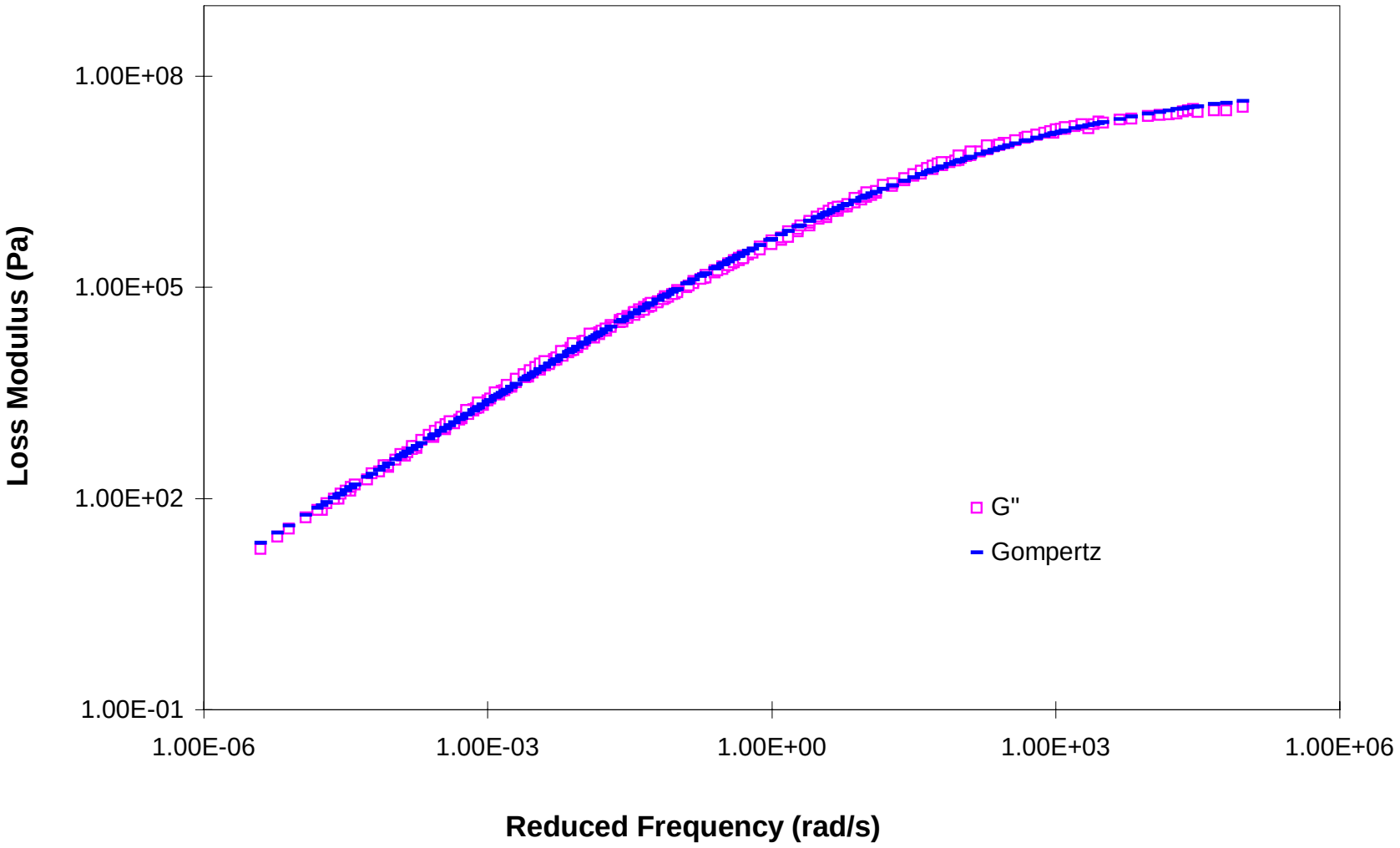

Figure D-26. Comparison between measured dynamic loss modulus for AUX4 and results from the Gompertz model.

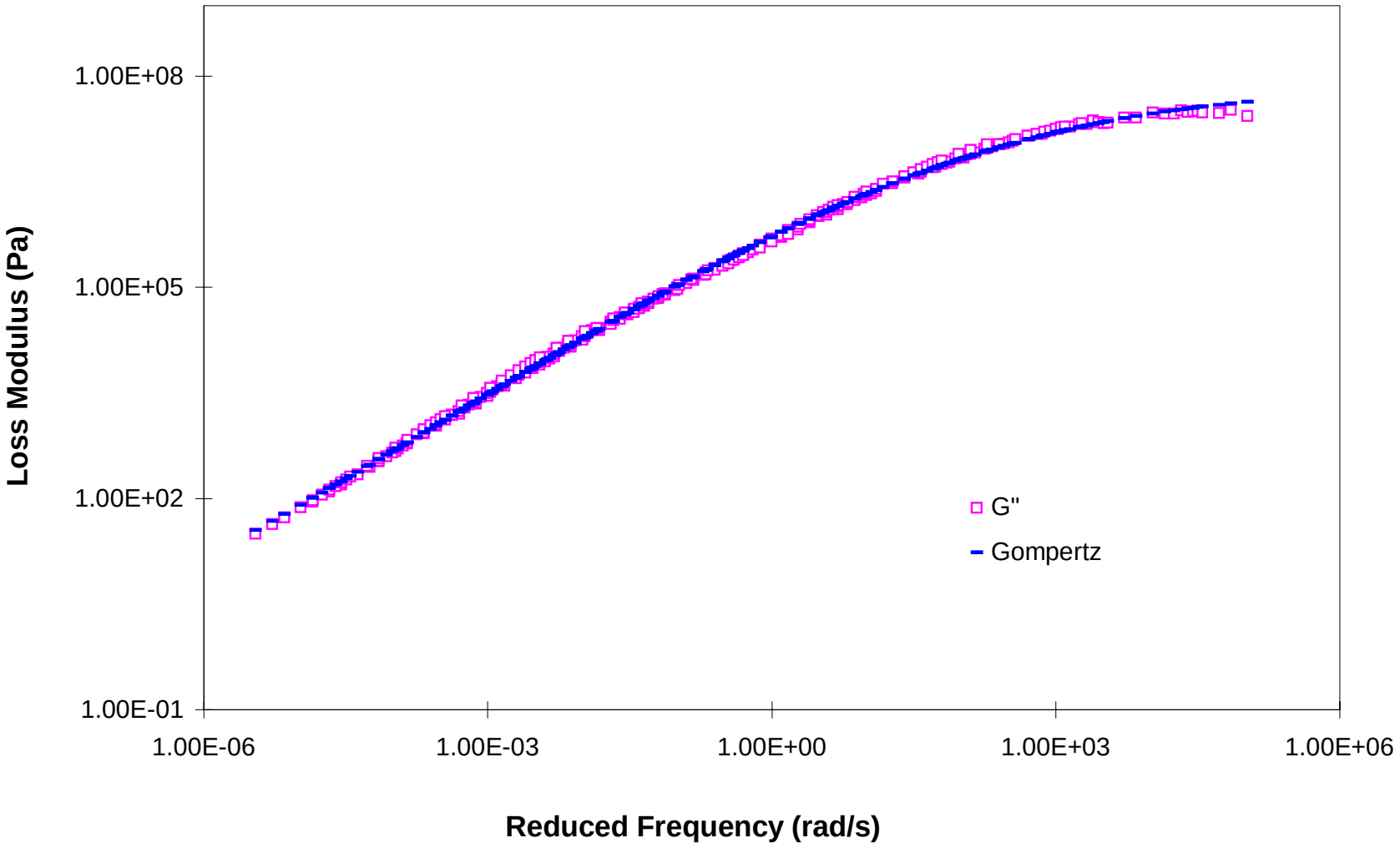

Figure D-27. Comparison between measured dynamic loss modulus for AUX5 and results from the Gompertz model.

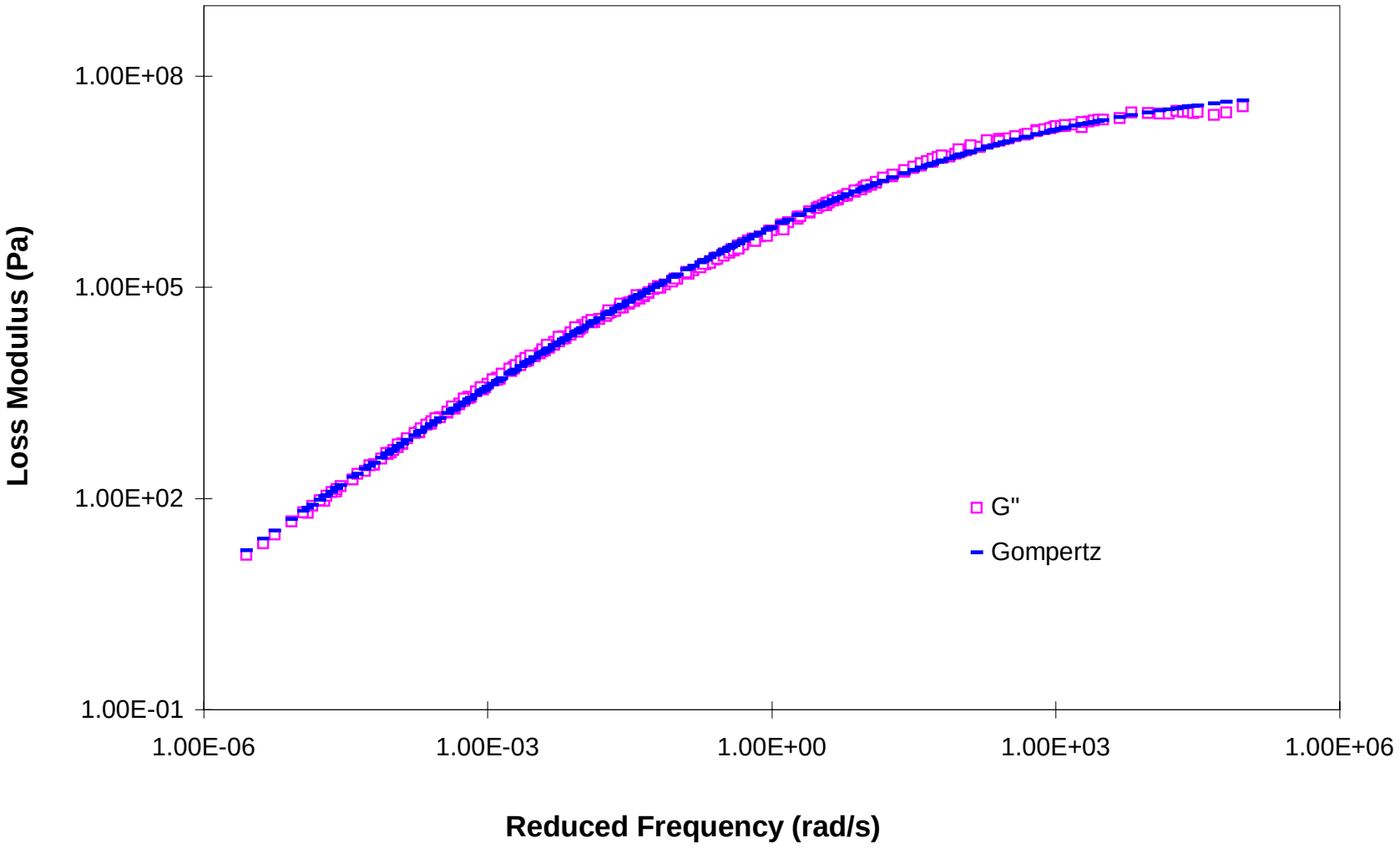

Figure D-28. Comparison between measured dynamic loss modulus for ARX3 and results from the Gompertz model.

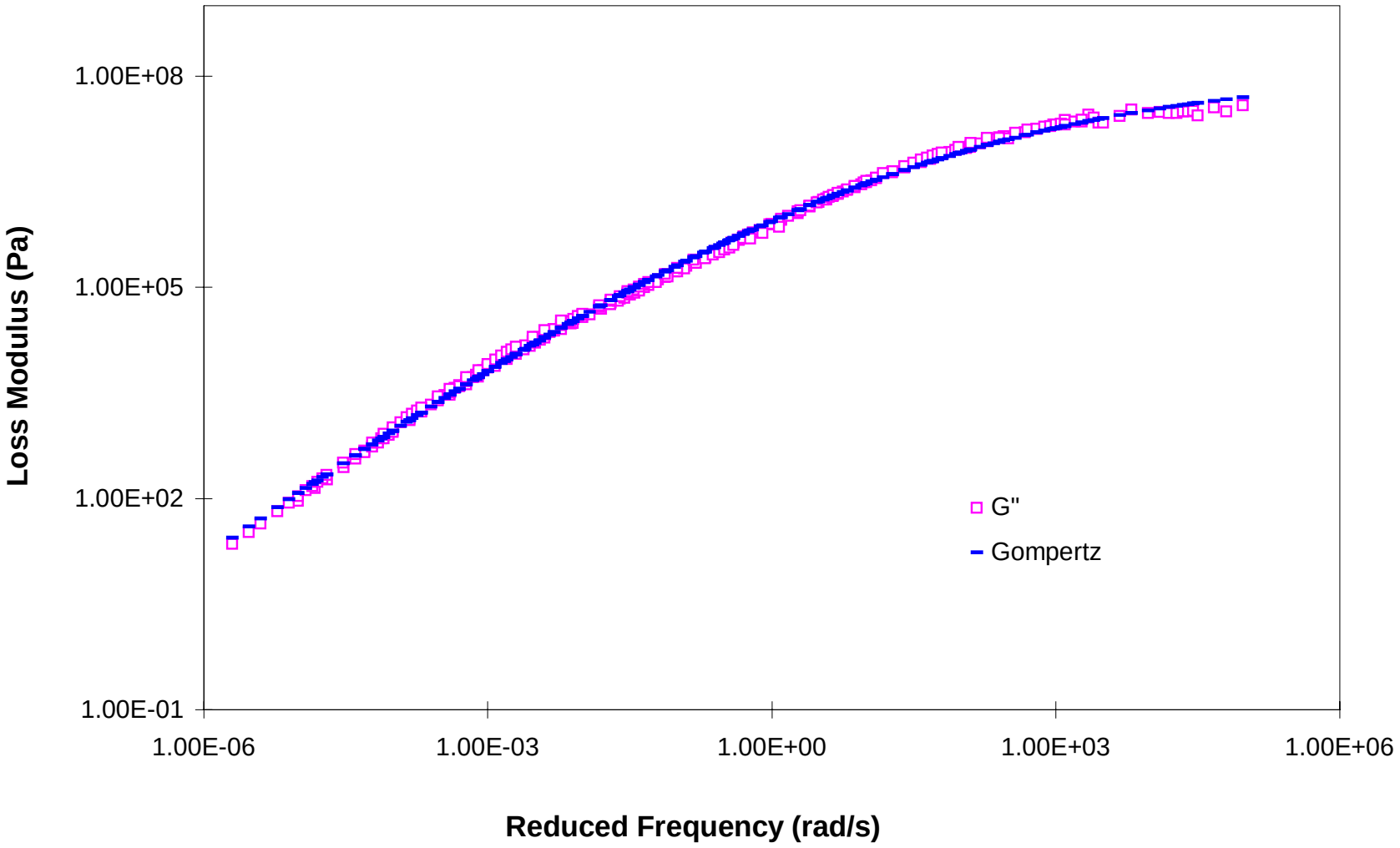

Figure D-29. Comparison between measured dynamic loss modulus for ARX4 and results from the Gompertz model.

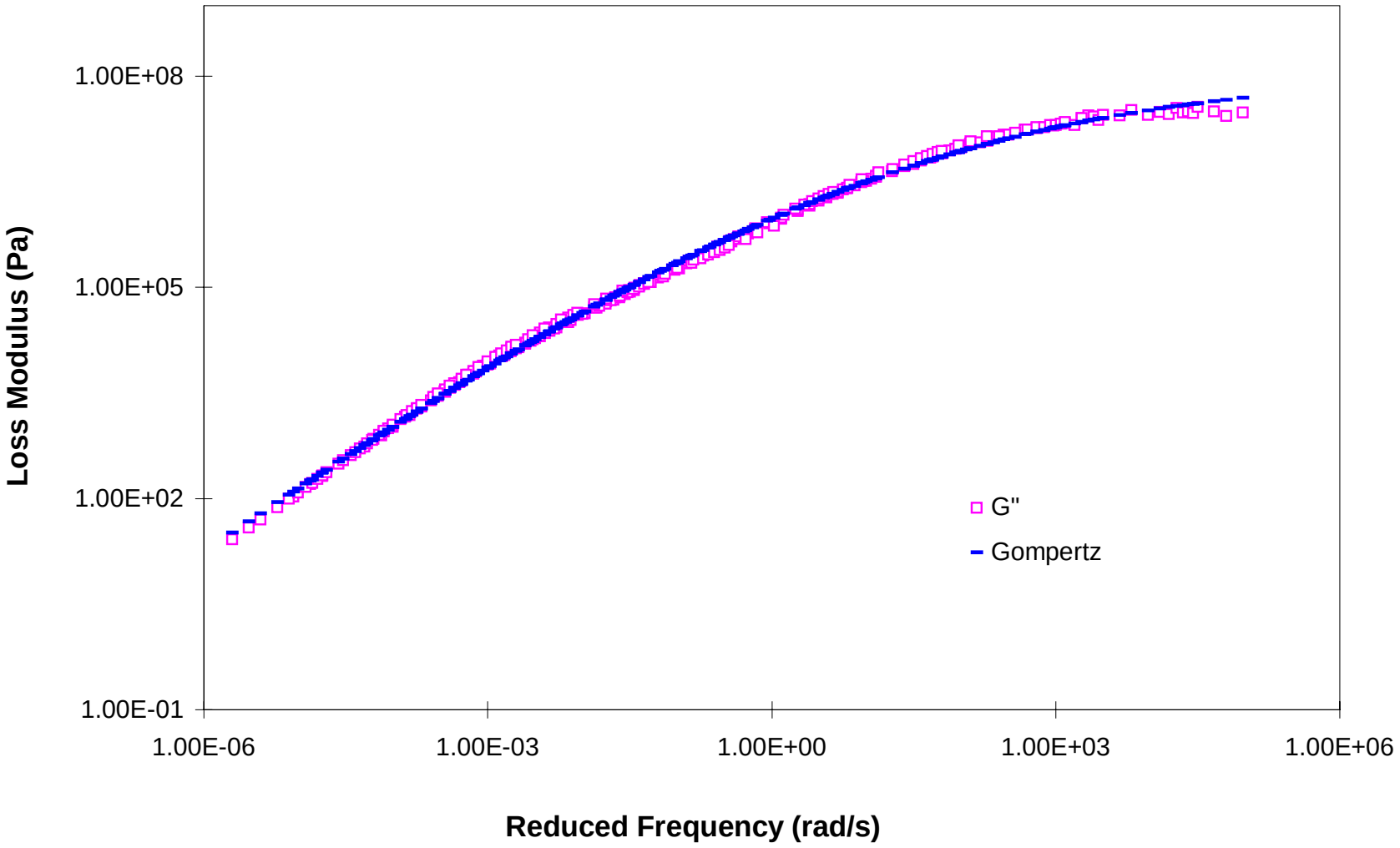

Figure D-30. Comparison between measured dynamic loss modulus for ARX5 and results from the Gompertz model.

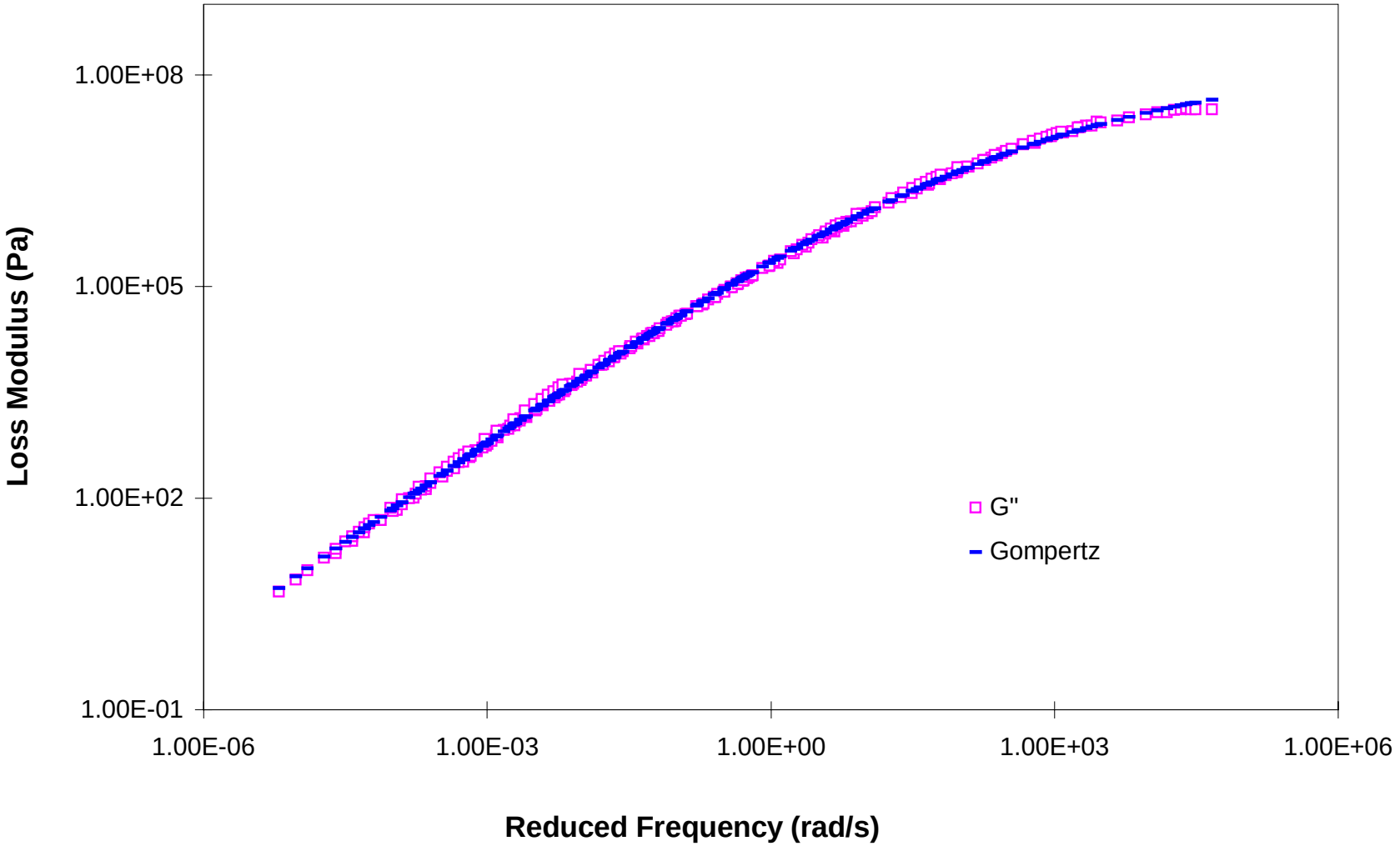

Figure D-31. Comparison between measured dynamic loss modulus for AUD3 and results from the Gompertz model.

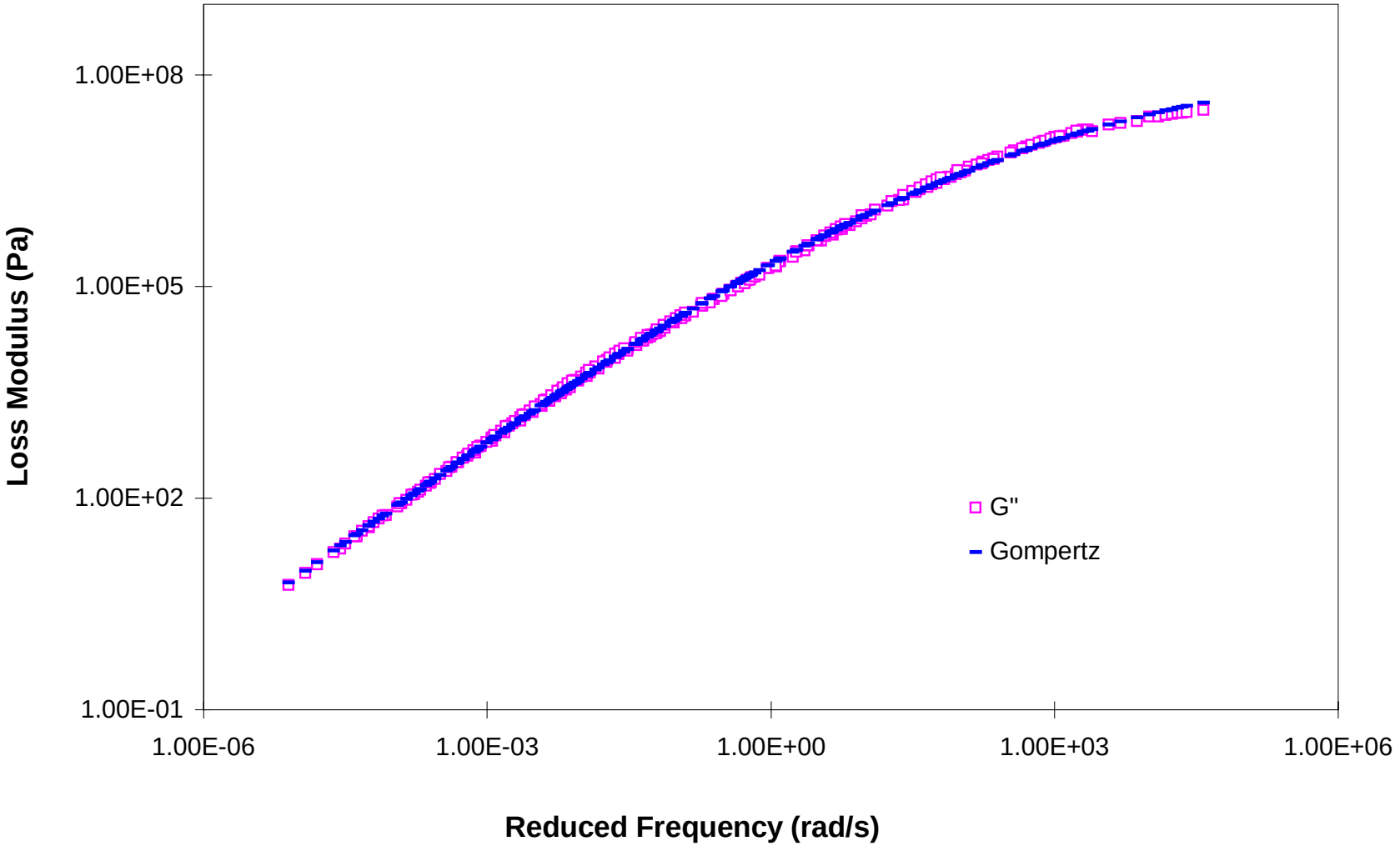

Figure D-32. Comparison between measured dynamic loss modulus for AUD4 and results from the Gompertz model.

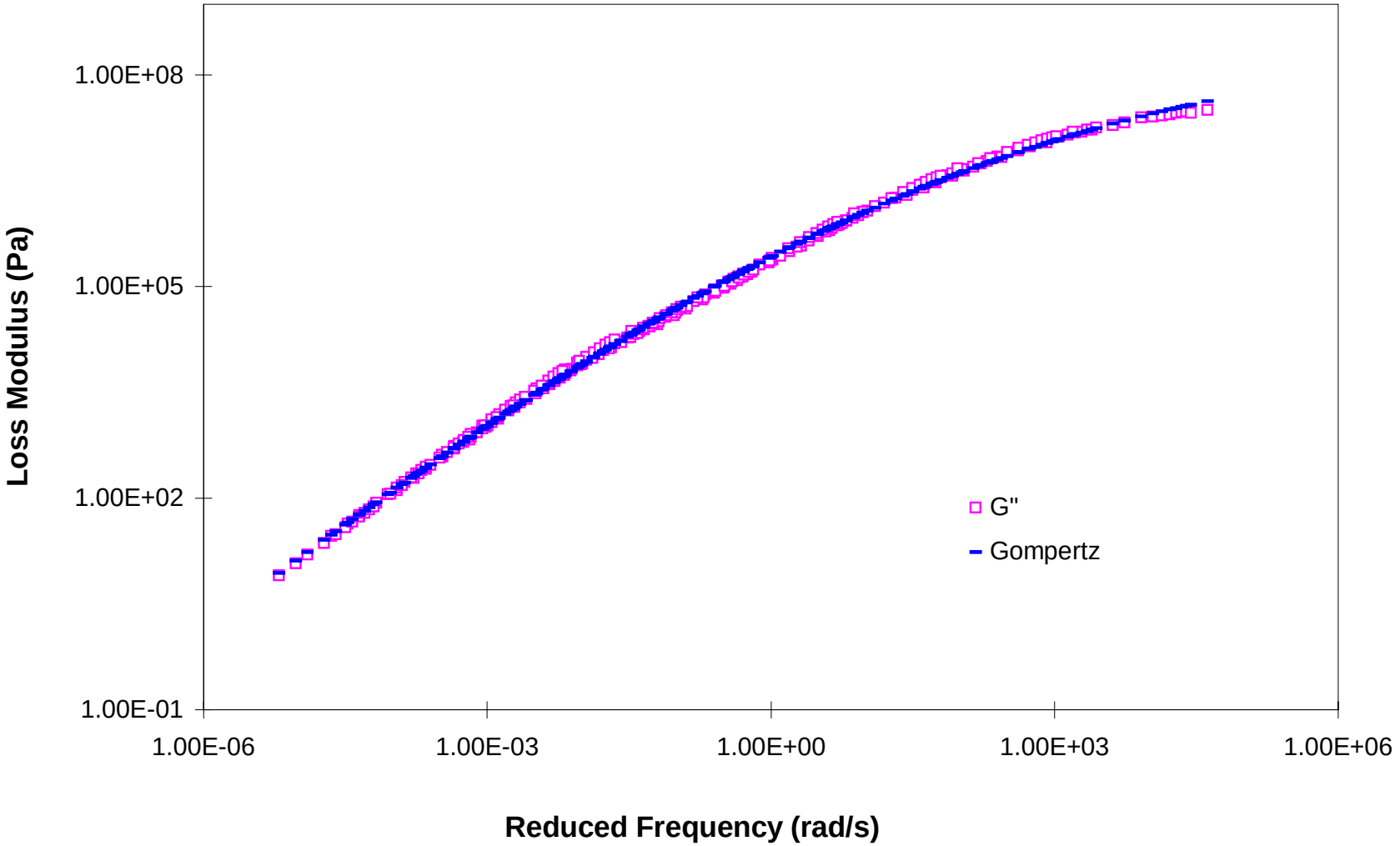

Figure D-33. Comparison between measured dynamic loss modulus for AUD5 and results from the Gompertz model.

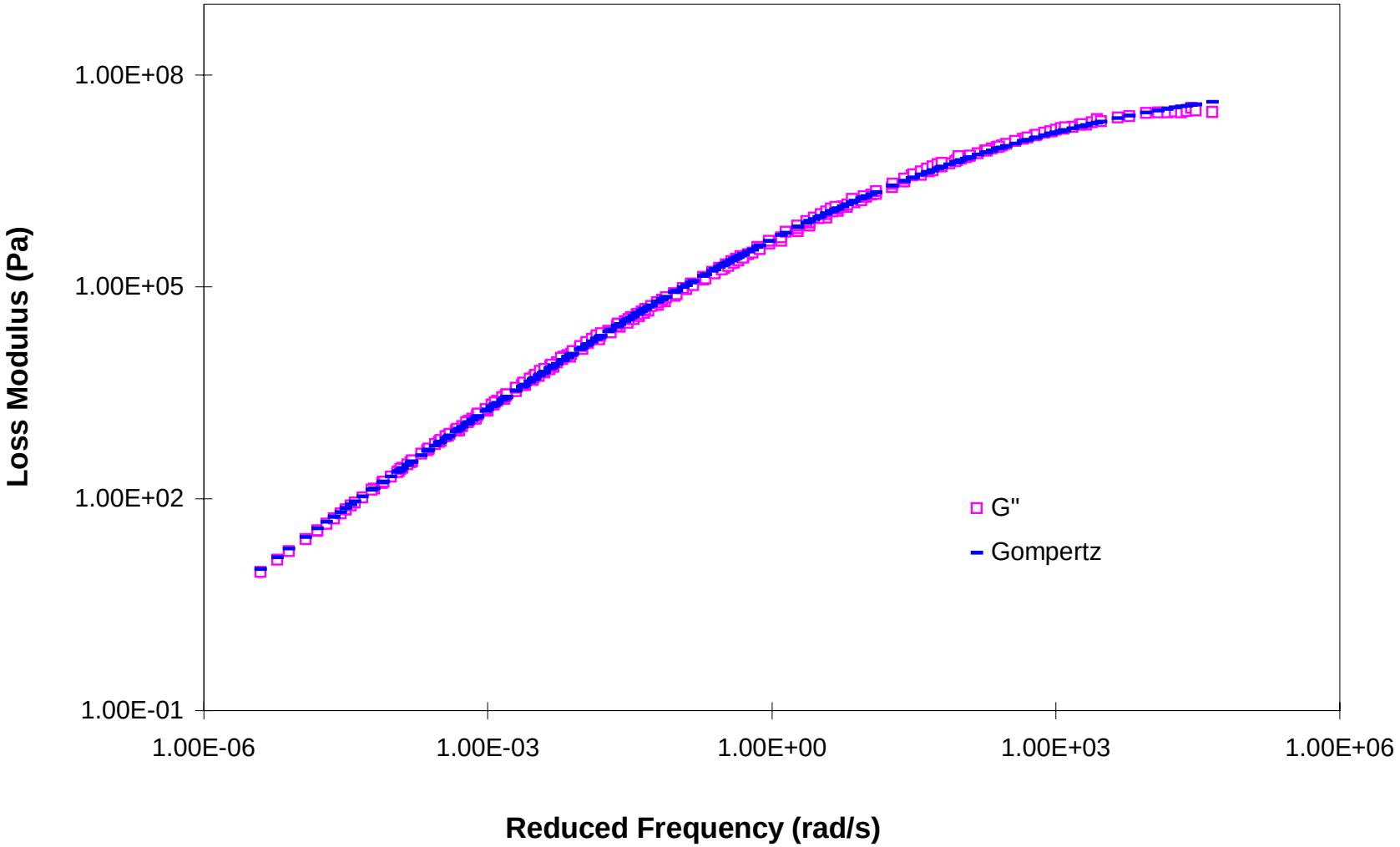

Figure D-34. Comparison between measured dynamic loss modulus for ARD3 and results from the Gompertz model.

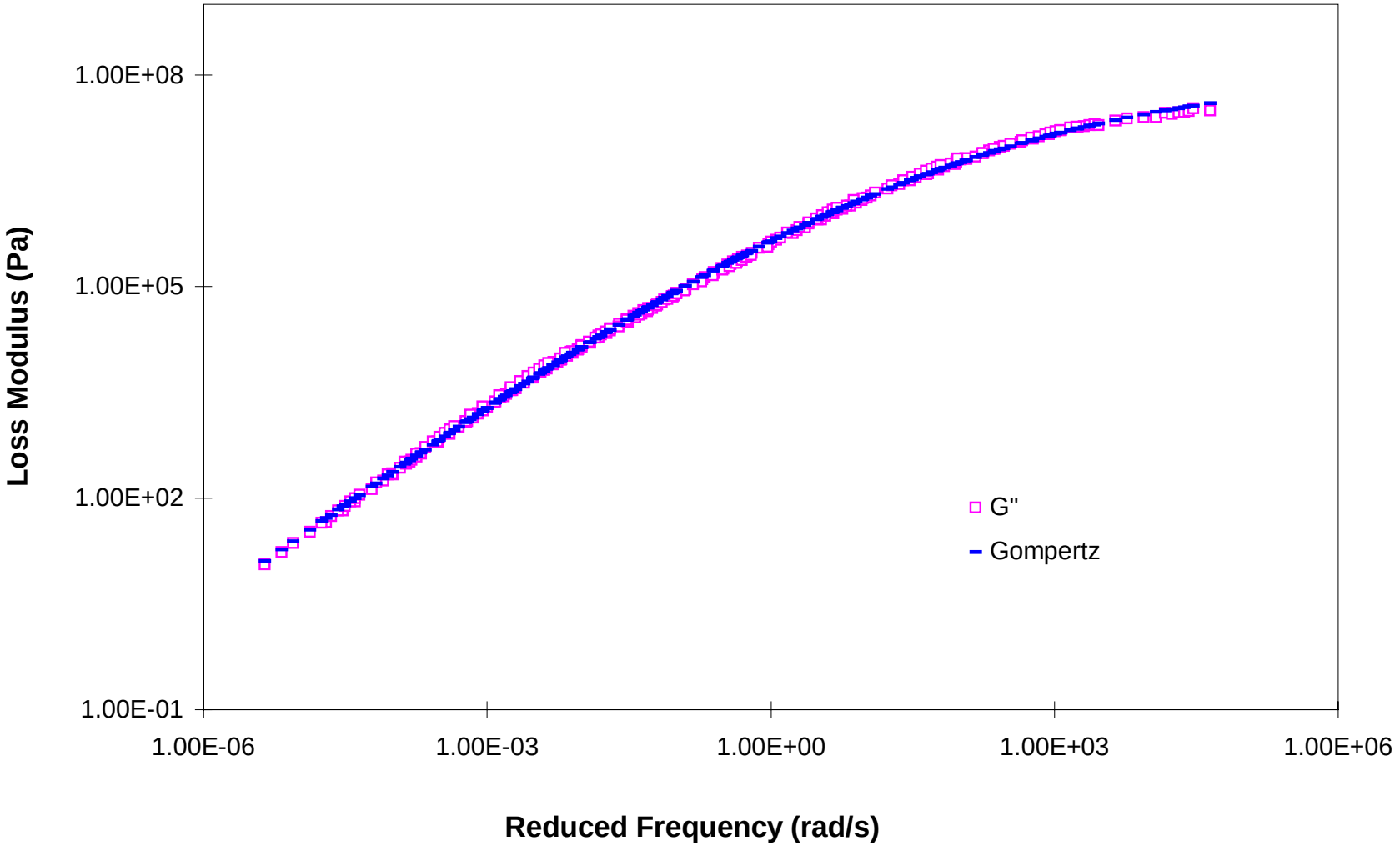

Figure D-35. Comparison between measured dynamic loss modulus for ARD4 and results from the Gompertz model.

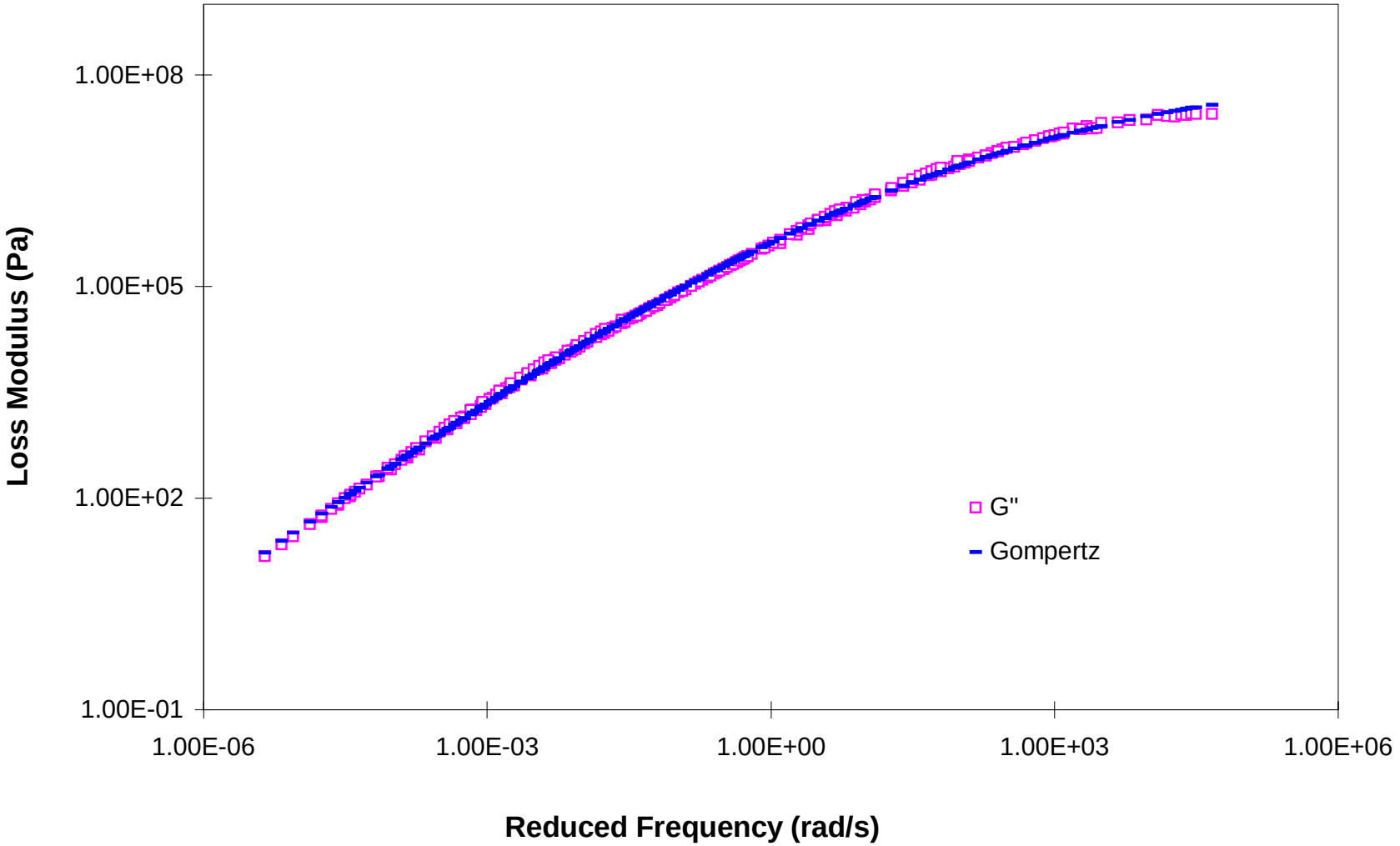

Figure D-36. Comparison between measured dynamic loss modulus for ARD5 and results from the Gompertz model.

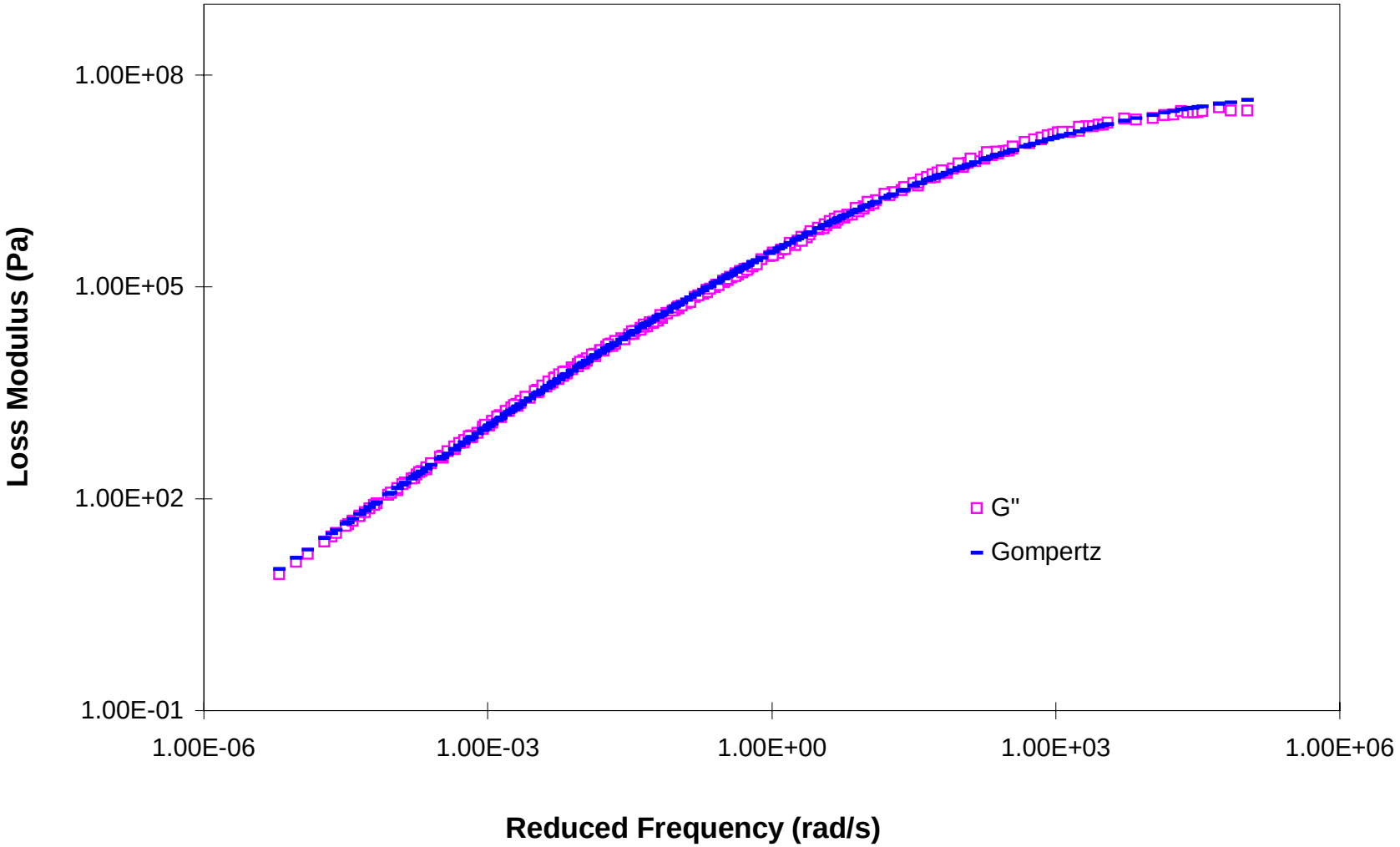

Figure D-37. Comparison between measured dynamic loss modulus for AUS3 and results from the Gompertz model.

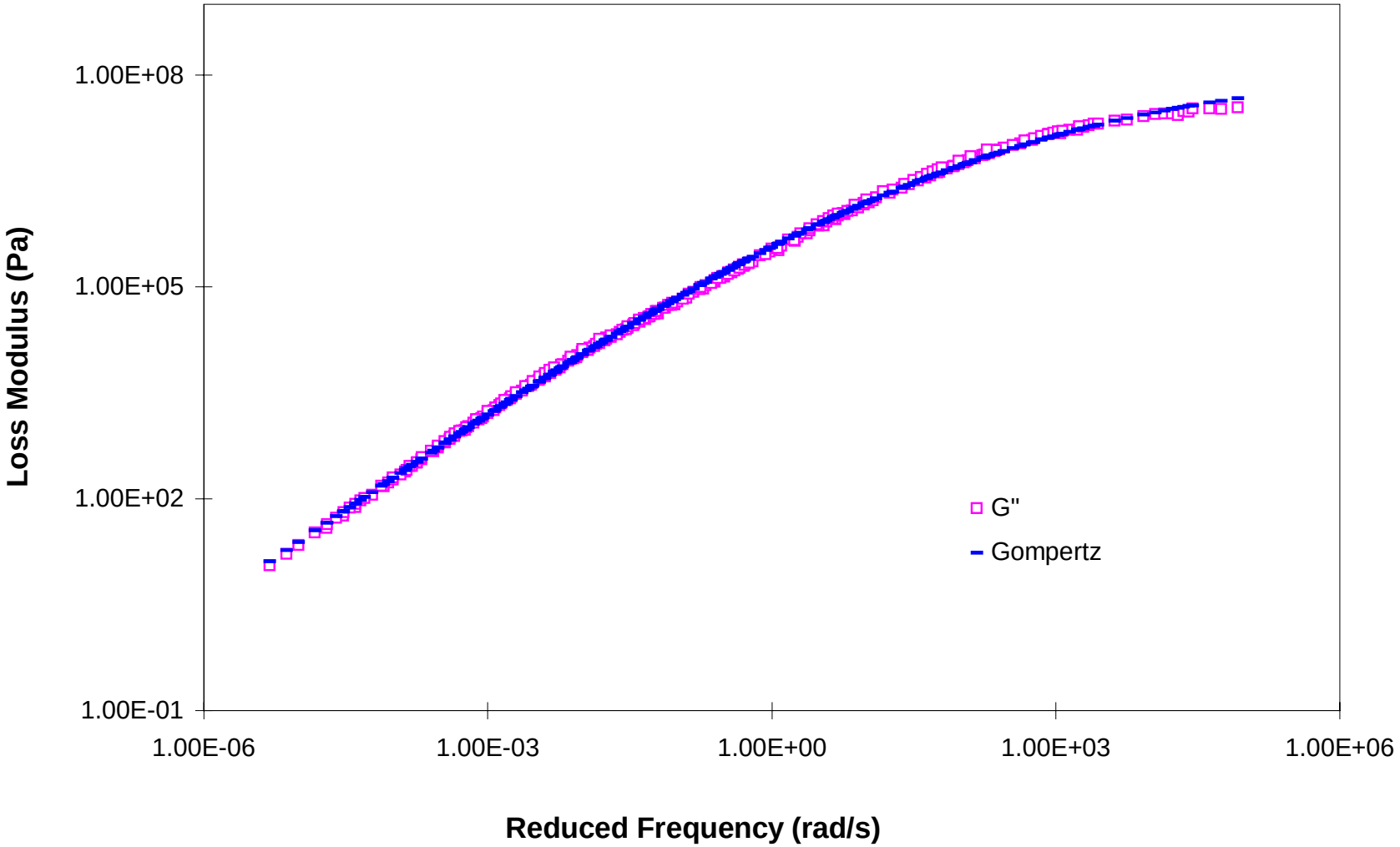

Figure D-38. Comparison between measured dynamic loss modulus for AUS4 and results from the Gompertz model.

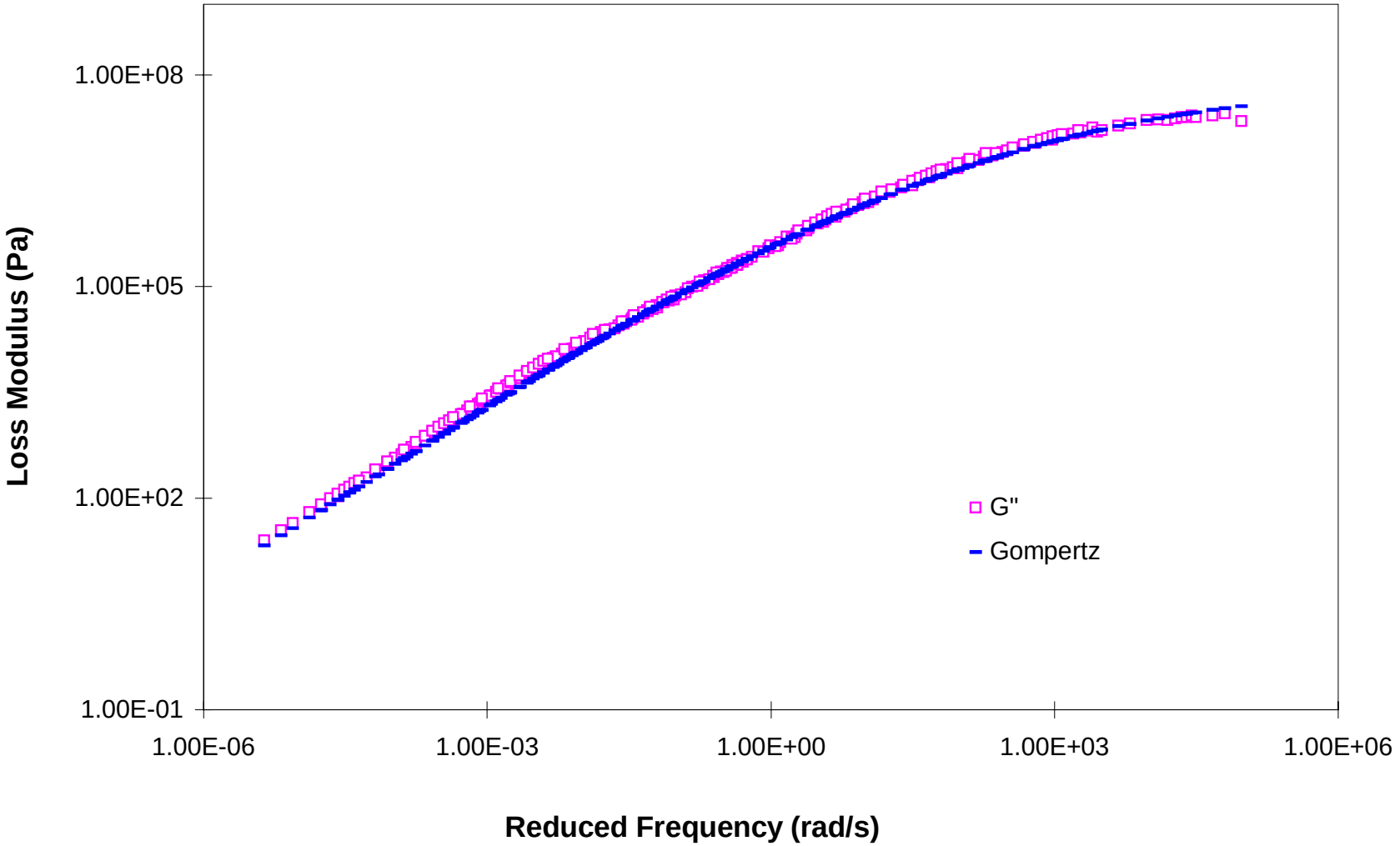

Figure D-39. Comparison between measured dynamic loss modulus for AUS5 and results from the Gompertz model.

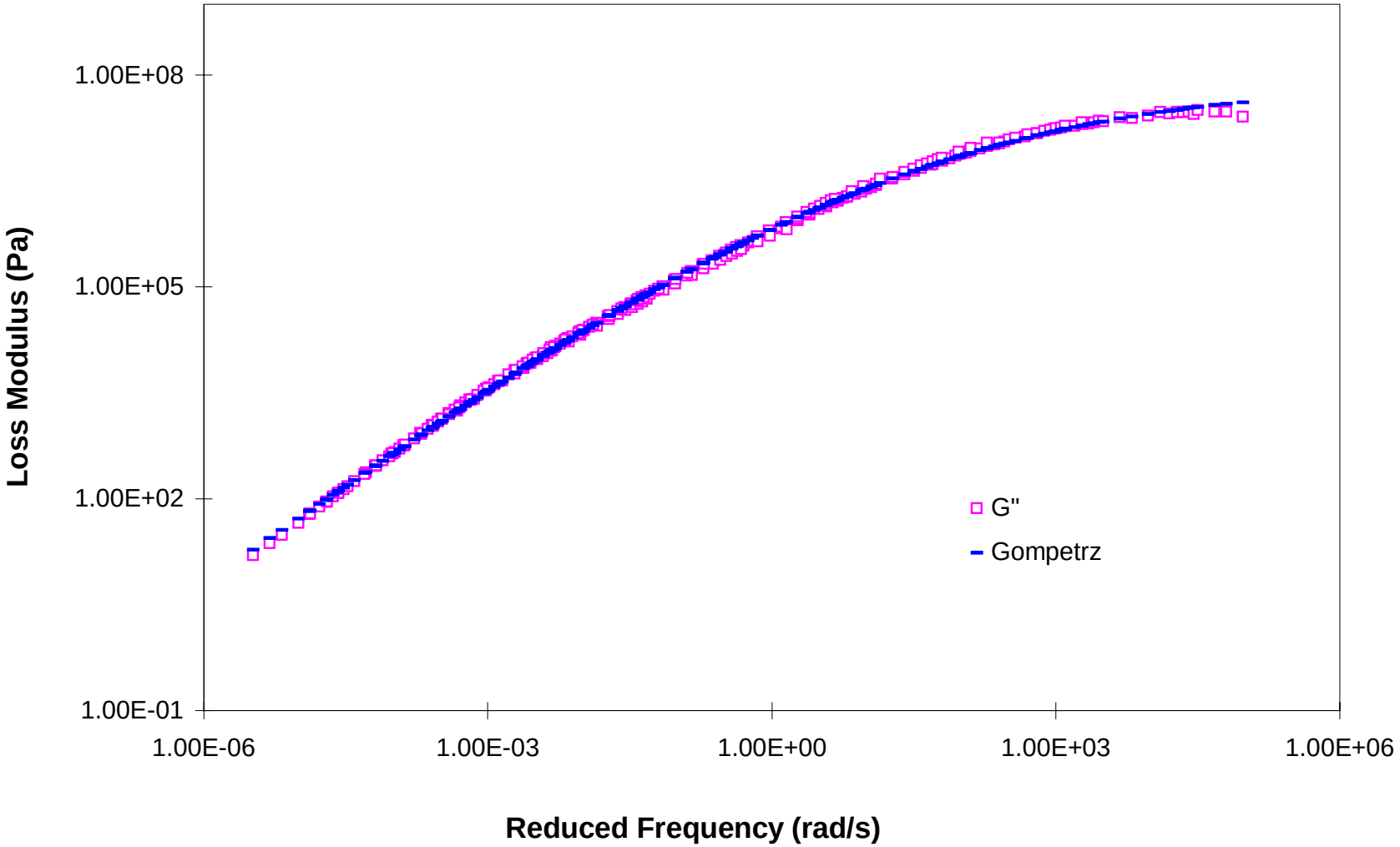

Figure D-40. Comparison between measured dynamic loss modulus for ARS3 and results from the Gompertz model.

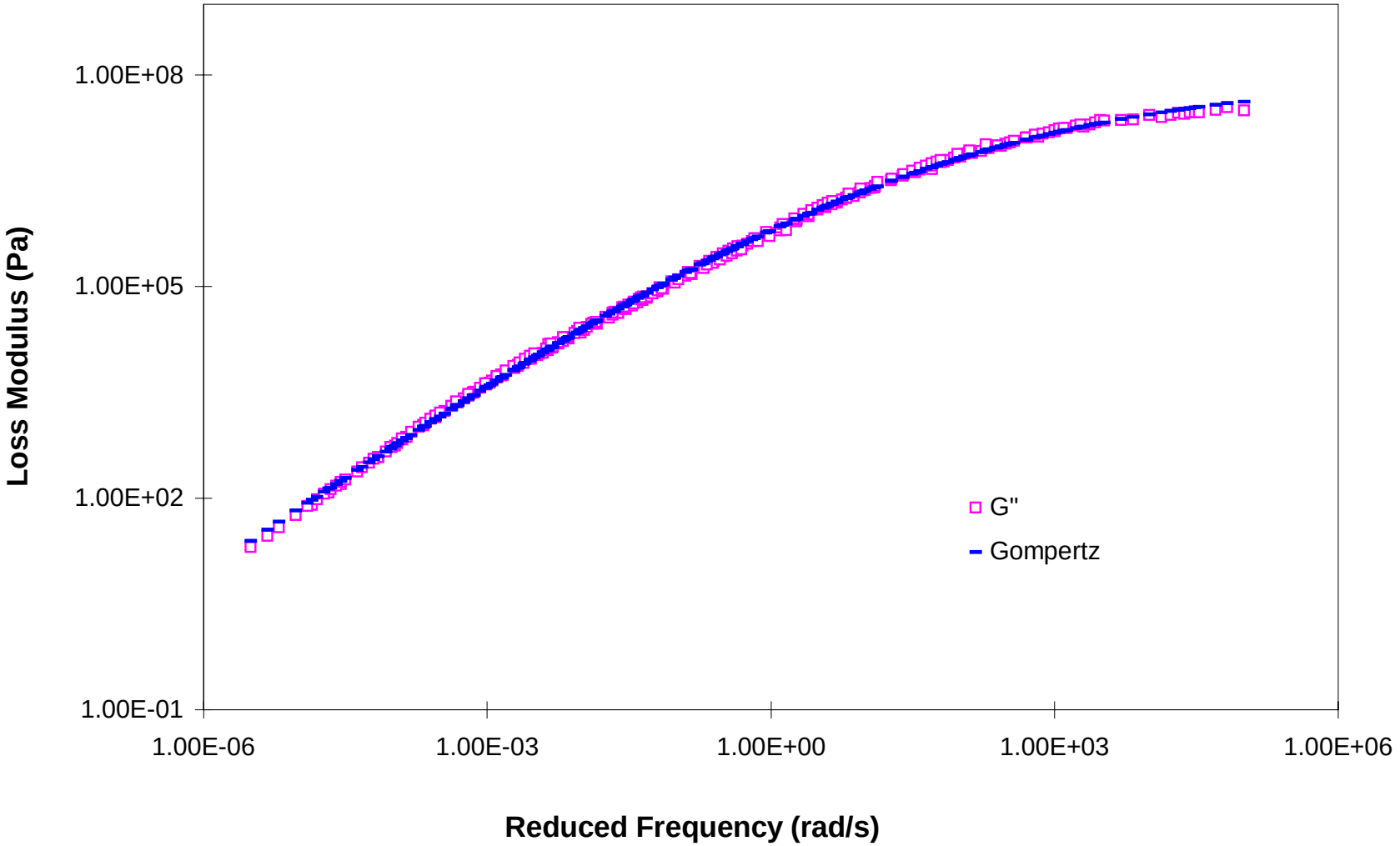

Figure D-41. Comparison between measured dynamic loss modulus for ARS4 and results from the Gompertz model.

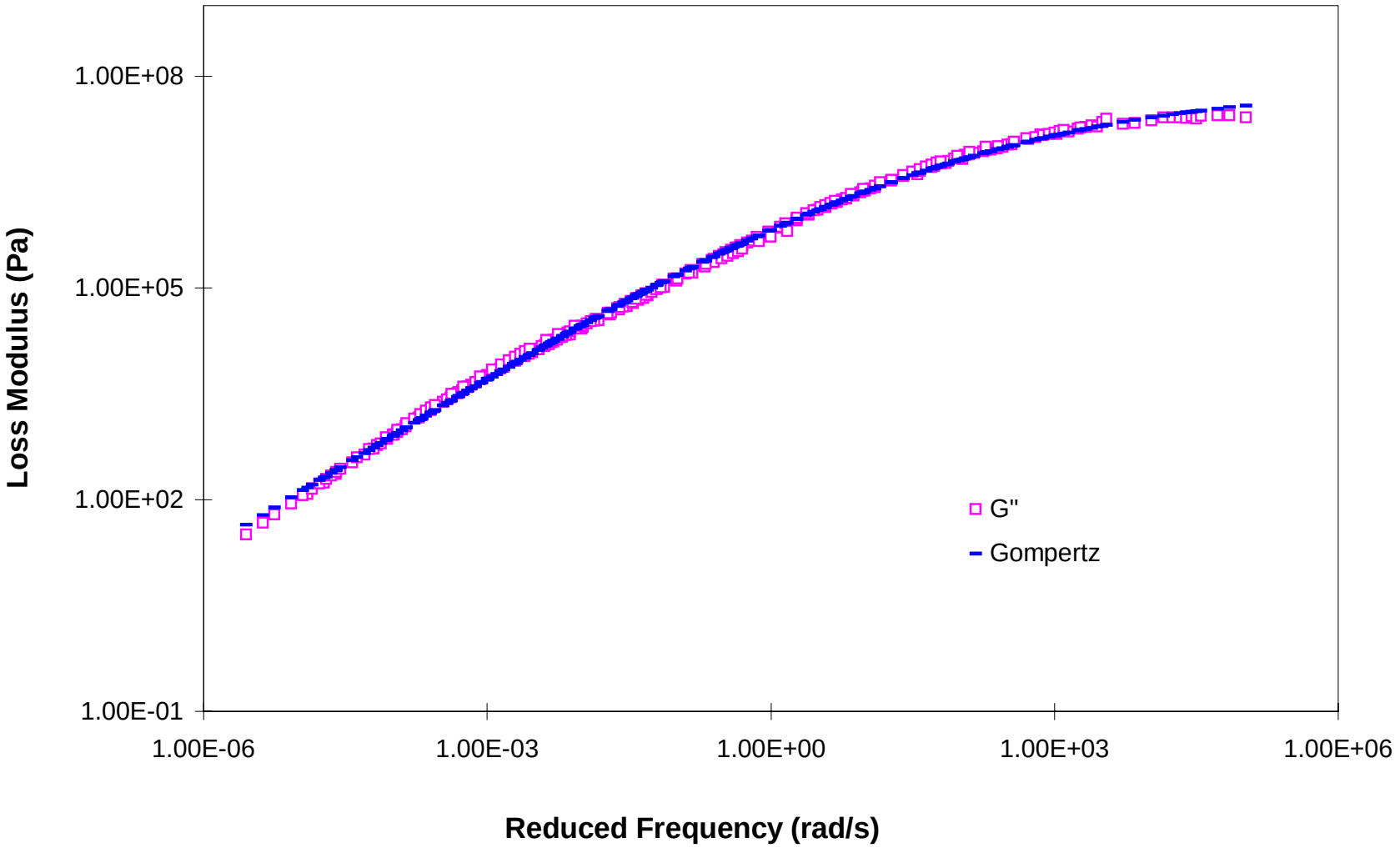

Figure D-42. Comparison between measured dynamic loss modulus for ARS5 and results from the Gompertz model.

Vita

James William Bryant, Jr. was born in Philadelphia, Pennsylvania in 1972. He attended Drexel University from 1990 to 1993 completing coursework toward a degree in Commerce and Engineering. In 1993 He transferred to North Carolina Agricultural and Technical State University, in Greensboro, NC, where he received a B. S. Degree in Civil Engineering. In 1996 he arrived at Virginia Tech where he plans to receive a M. S. Degree in Civil Infrastructure Engineering sometime in the spring of 1999. He is currently pursuing Ph. D. studies in Civil Engineering emphasizing construction engineering and management and structural materials. His areas of interest include application of new or non-traditional materials in civil engineering, the constructability concerns associated with them and rehabilitation of concrete structures.